Norges miljø- og biovitenskapelige universitet
Institutt for matematiske realfag og teknologi

Masteroppgave 2014
30 stp

Analysis of actual and forecasted power production for a solar energy system in Norway

Analyse av faktisk og prognosert energiproduksjon for et solenergisystem i Norge

Martin Andersen

Preface

This thesis is a result of an initiative taken by FUSen AS, a company projecting solar energy systems in Norway and the Institute for Energy Technology (IFE).

It was carried out to determine the existing discrepancy between forecasts made with simulation software used in the design of solar energy systems in Norway, as no such previous studies have been made until today.
Some other studies on the area does exist on a global basis, though most have been conducted in locations where sun is abundant and the weather conditions are less varied than in the northern hemisphere.

As such, the PV-industry, which is still in its early phase in Norway, can make good use of assessments of the validity of the tools being used for planning new solar energy systems. The knowledge about the accuracy of the forecasts of the yield such systems will provide, may lead to an improvement of pricing, reductions in cost and ultimately large scale implementation of solar energy.

I would like to thank my supervisor, Dr. Ing. Espen Olsen, for the support and motivation supplied for this thesis. His knowledge and insight has been highly valued during my time at the Norwegian University of Life Sciences (NULS).

Furthermore, I would like to give my appreciation to Dr. Erik Stensrud Marstein, co-supervisor and Centre Director at the Norwegian Centre for Solar Cell Technology. His general guidance, eternal motivation and support has made my stay at IFE a learning experience I always will remember.

I would also like to thank Thor Christian Tuv, for his initiative to this thesis and his enthusiastic and much valued work within the Norwegian solar energy sector.

Lastly, I give out thanks to my friends and family, for the invaluable mental support during the work with this thesis.

Kjeller, May 14th 2014

_____

Martin Andersen

Abstract

In this thesis, the uncertainty related to the forecasting of yield for a solar energy system in Norway has been evaluated. The system was a 2 kW_p PV-system located on the campus of the Norwegian University of Life Sciences (NULS).

The work conducted aimed at determining the existing discrepancy between forecasted and actual yield for the PV-system, comparing forecasts of annual yield, generated by the simulation software PVsyst, to inverter output data for one year.
Moreover, it investigated the different factors influencing this discrepancy, by evaluating forecasted system losses and their relation to the meteorological data used as input.
The effect of the diffuse-to-global ratio (DGR) in datasets has been investigated, along with the consequences induced in the simulation program used.
Also, the effect of missing diffuse data has been tied to high errors in forecasting, especially for months of low irradiance levels.

The economic consequences of the discrepancies between actual and forecasted yield have been evaluated by calculating the levelized cost of energy (LCOE) for the forecasted yield and comparing this to the actual LCOE.

The effect of soiling has been discussed and suggestions have been made as to appropriate soiling values for solar energy systems within a climatic distance of 20 km from the PV-system evaluated.

The results showed a mean bias error (MBE) of -8.1% and RMSE of 10.3% in an ideal scenario with only 2% degradation losses applied, when disregarding choice of source for meteorological data.
The most accurate forecasts of annual yield had a bias error (BE) of -0.2%, using meteorological data from the NASA SSE database.
The worst performing forecast in this scenario had a BE of -19.7%, using data from the PVGIS database.
Measured data from weather stations in the vicinity of the PV-system site, on best yielded a BE of -2.3%.

In a heavy soiling scenario, an MBE of -25.3% and RMSE of 26.5% were obtained when disregarding the choice of meteorological data source.
The best performing forecast had a BE of -20.2% and was obtained using meteorological data from the NASA SSE database.
The worst performing forecast in this scenario had a BE of -34.3%, using data from the PVGIS database.
Measured data from weather stations in the vicinity of the PV-system site at best yielded a BE of -23.6% in this scenario.

Of all the sources for meteorological data, the NASA SSE database showed to yield the most accurate forecasts and consistently proved to forecast accurately within an assumed investor risk tolerance of 6 - 7% when excluding heavy soiling.

Sammendrag

I denne oppgaven har usikkerheten forbundet med prognosering av produksjon for et solenergisystem i Norge blitt undersøkt. Systemet hadde en kapasitet på omtrent 2 kW_p og befant seg på området til Norges miljø- og biovitenskapelige universitet (NMBU).

Arbeidet som ble utført tok sikte på å bestemme det eksisterende avviket mellom prognosert og faktisk kraftproduksjon for solenergisystemet, ved å sammenligne prognoser for årlig kraftproduksjon, generert av simulasjonsprogrammet PVsyst, med omformerdata for ett år.
Videre ble de forskjellige faktorene som påvirker dette avviket etterforsket ved å undersøke de prognoserte system tapene og deres forbindelse til de meteorologiske dataene brukt i simuleringene.
I tillegg ble effekten av manglende data for diffus stråling knyttet til store avvik i prognosering, spesielt for måneder med lave nivåer av solinnstråling.

De økonomiske konsekvensene av avvikene mellom faktisk og prognosert kraftproduksjon har blitt undersøkt ved å regne ut elektrisitetskostnaden for den prognoserte kraftproduksjonen og sammenligne denne med elektrisitetskostnaden for solenergisystemet basert på faktisk produksjon.

Påvirkningen av tilsmussing av solkraftpaneler har blitt diskutert og forslag til passende verdier for tap som følge av tilsmussing har blitt foreslått for solenergisystemer innenfor en klimatisk radius på 20 km fra solenergisystemet som ble evaluert.

Resultatene viste et gjennomsnittlig avvik på -8.1% og et standardavvik på 10.3% i et ideelt scenario med kun 2% degradasjonstap implementert, uavhengig av valg av kilde for meteorologiske data.
Den mest nøyaktige prognosen for årlig kraftproduksjon hadde et avvik på 0.2% ved bruk av meteorologiske data fra NASA SSE databasen.
Den minst nøyaktige prognosen for årlig kraftproduksjon hadde et avvik på -19.7% ved bruk av meteorologiske data fra PVGIS databasen.
Målte data fra en værstasjon i nærheten av solenergisystemet ga i den mest nøyaktige prognosen et avvik på -2.3%.

I et scenario med høy grad av tilsmussing ble et gjennomsnittlig avvik på -25.3% og et standardavvik på 26.5% funnet, uavhengig av valg av kilde for meteorologiske data.
Den mest nøyaktige prognosen hadde et avvik på -20.2% ved bruk av meteorologiske data fra NASA SSE databasen.
Den minst nøyaktige prognosen i dette scenarioet hadde et avvik på -34.3% ved bruk av data fra PVGIS databasen.
Målte data fra en værstasjon i nærheten av solenergisystemet ga i den mest nøyaktige prognosen et avvik på -23.6% i dette scenarioet.

Av alle kilder for meteorologiske data evaluert ble de mest nøyaktige prognosene gitt ved bruk av NASA SSE databasen. Disse tilfredsstilte en investor risiko på 6 – 7%, når man ser vekk fra scenarioet med høy grad av tilsmussing.

Contents

List of figures

List of tables

Abbreviations

Abbreviation	Meaning
a-Si	Amorphous Silicon
AC	Alternating current
AM	Air mass
AMGD	Average meters above ground
AMSL	Average meters above sea level
BE	Bias error
BoS	Balance of system
c-Si	Crystalline silicon
CAD	Computer aided design
CdTe	Cadmium Telluride
CIGS	Copper Indium Gallium Selenite
DC	Direct current
DGR	Diffuse-to-global ratio
DH	Diffuse horizontal radiation
EoT	Equation of time
FAGKLIM	Field station for agro-climatic studies
FF	Fill factor
GaAs	Gallium Arsenide
GH	Global horizontal radiation
GIS	Geographic information system
GMT	Greenwich mean time
HRA	Hour angle
IAM	Incidence angle modifier
IFE	Institute for Energy Technology
INV	Inverter
IRT	Investor risk tolerance
KCL	Kirchhoff's current law
KVL	Kirchhoff’s voltage law
LCOE	Levelized cost of electricity
LID	Light induced degradation
LiDAR	Combination of light and radar
LMT	Norwegian agro-meteorological service
LST	Local solar time
LSTM	Local standard time meridian
LT	Local time
MAGL	Meters above ground level
MET	Norwegian meteorological institute
mono-Si	mono crystalline silicon
MPP	Maximum power point
MPPT	Maximum power point tracking
NASA SSE	National space energy - surface meteorology and solar energy

NOCT	Normal operating cell temperature
NULS	Norwegian university of life sciences
OC	Open circuit
p.u.	Per unit
PID	Potential induced degradation
poly-Si	Polycrystalline silicon
PR	Performance ratio
PV	Photovoltaic
PVGIS	Photovoltaic Geographical Information System
PWM	Pulse-width modulated
REC	Renewable energy corporation
RMSE	Root mean square error
RY	Reference year
SC	Short circuit
SCI	Self-commutated inverter
SD	Standard deviation
SDR	System degradation rate
STC	Standard test conditions
TC	Time correction factor
TID	Temperature induced degradation
TP	Transposition surplus
Wp	Watt peak

1. Introduction

1.1 Motivation

The implementation of renewable energy systems in Europe the last decade has been formidable due to broad political agreement that fossil fuel carriers should be phased out.

One branch in the renewable energy family is the solar energy sector.
Vast subsidy schemes have been implemented in order to assure a faster transition into a renewable energy era, with countries like Germany and Spain in the forefront of implementing large scale, grid-connected solar energy power plants.

However, in Norway the development of the solar industry is still in its early beginning. The challenges of rough weather conditions, heavy soiling scenarios, missing expertise and high installation costs all contribute to a halted pace of transition into large scale implementation schemes as the ones seen other places around the world.

Earlier studies conducted to map the solar resource in Norway have concluded that actual solar irradiance deviates as much as, and sometimes more than, 10 per cent from forecasted irradiance [**1**]. Consequently, the margins of error are larger in Norway than in other nations around the world where the end use of PV electricity has been higher, and the research has been conducted for longer

One of the great factors of uncertainty lies in the investors will to take risks in a sector still under development. Most investors in renewable energy operate with margins of error way below the mentioned 10 per cent. In this thesis the limit for economic viability, hereafter referred to as the IRT, is assumed to be in the range of 6 – 7 per cent [**2**]. The actual number will necessarily vary from case to case.

The missing knowledge about forecasting accuracy using simulation software is a great contribution to this uncertainty, and therefore should be investigated to supply much needed information.

With such information available, the hope remains that investors may be willing to place more resources in developing an energy sector bound for great shares of the energy production in the future.

1.2 Problem statements

This thesis aims at investigating the following problem statements:

- What is the existing discrepancy between actual and forecasted yield for a solar energy system using simulation software?
- Which factors may influence this discrepancy and to which extent?
- What is the most straightforward way to reduce the discrepancy?
- What are the economic consequences or implications of the discrepancy?

1.3 The PV-system

The PV-system used as basis for this analysis is located at the campus of the Norwegian University of Life Sciences (NULS) in Aas municipality, Akershus County, Norway.
The system is rated at 2 kW_p and operated as a free standing, roof mounted system. It was taken into operation in October/November 2013, but didn't start production before February 2014.

A picture of the PV-array is seen below in Figure 1:

Figure 1: The PV-array at the campus of NULS at Aas, including solar reference cell

1.4 Thesis outline

This thesis is divided into seven chapters. These are as follows:

- Chapter 1 gives an introduction to the motivation behind the thesis, the problem statements investigated and a brief description of the case used in the analysis.

- Chapter 2 provides all the necessary theory for the understanding of the methods and results in this thesis, along with some recommended literature.

- Chapter 3 explains the methodology used in the thesis, giving an introduction to the simulation software used (PVsyst), the selection of meteorological data and other relevant information related to the choice of analytic method.

- Chapter 4 presents all the results obtained in the thesis; the accuracy of the forecasts made, an analysis of the results related to the meteorological data, identification of loss factors and their relative extent and an economic calculation of the energy price based on the forecasted yield.

- Chapter 5 states the main conclusions drawn according to the problem statements

- Chapter 6 suggests further work that may be conducted to help feature analysis.

- Chapter 7 states references cited.

2. Theoretical prerequisites

In the following, the theoretical background required for understanding the work presented in this thesis will be given. The reader can through additional literature acquire the necessary theory for better comprehension of the nature of the photovoltaic (PV) generator. The underneath listed literature are a few of many sources that can give detailed information about the components of the PV system, solar geometry and meteorology, and other questions the reader might have that aren't directly relevant for the understanding of this thesis and thus are not answered here.

Recommended reading:

- Quaschning, Volker: Regenerative Energiesysteme (German only)
  Carl Hanser Verlag GmbH & Co. KG; Auflage: 7
  ISBN-13: 978-3446427327
- The German Energy Society: Planning and Installing Photovoltaic Systems
  Routledge; 2nd edition
  ISBN-13: 978-1844074426
- Honsberg, Christiana; Bowden, Stuart: PVeducation
  Photovoltaic Education Network; Online source available at:
  www.pveducation.org

2.1 The PV system

A grid connected PV system consists of many parts, of which some are more essential than others.
Balance of system (BoS) components are counted as all system components, except the PV generator itself [**3**].

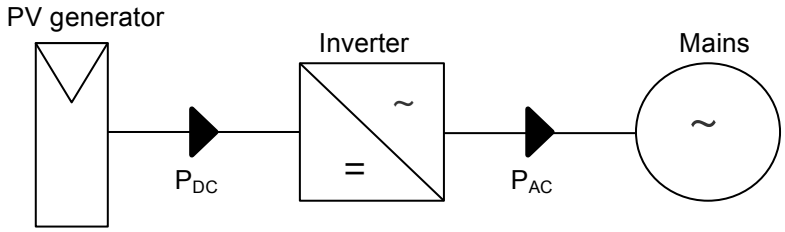

Figure 2: Flow diagram for a grid connected PV system

In the above figure P_{DC} is the direct current (DC) power delivered by the generator to the inverter, whereas P_{AC} is the alternating current (AC) power delivered from the inverter to the mains grid. Electricity meters are omitted for sake of simplicity, as only inverter data will be evaluated in this thesis.

Electrical safety measures include BoS-components like surge arresters, mains disconnection switches and circuit breakers, among others [**4**].
However, since these components are only of secondary importance to the operation of a PV system, and not directly relevant for this thesis, the information about them is omitted.

Most manufacturers of system components will print a spec-sheet or *datasheet*, containing some or indeed all parameters that might be of interest to the purchaser. Datasheets containing information about the inverter and modules incorporated into the system investigated in this thesis can be found in Appendix C: Datasheets.

2.1.1 The PV-generator

A PV-generator is a static current generator, converting electromagnetic radiation in the form of sunlight, to electricity.
The smallest PV-generator in existence is the *solar cell*, although it is customary to assemble more solar cells together, connecting them in either series or in parallel, to form a *module*. An assembly of modules may be called an *array*, and normally will contain one or more *strings*.

An illustration of a solar cell, a module and an array containing two strings (each string consisting of two modules in series) can be seen in Figure 3:

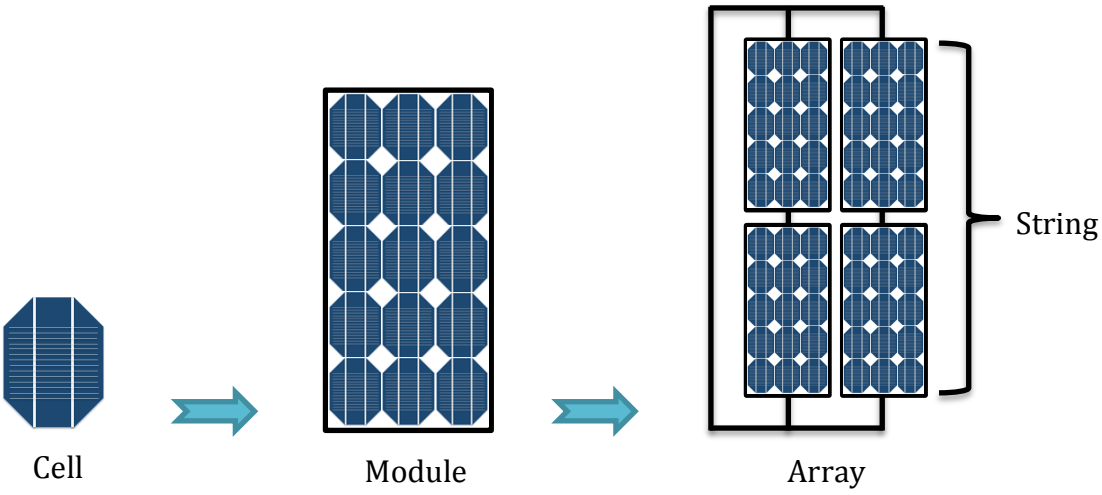

Figure 3: Illustration of a solar cell, a module and an array containing two strings.

2.1.2 Solar Cell Material

Different semiconductor material is used in solar cells, and the most used in modern cells is crystalline silicon with a market share in 2012 of 86% [**5**].
There are two forms of crystalline silicon: mono-crystalline silicon (c-Si) and poly-crystalline silicon (poly-Si).
In addition there exists non-crystalline silicon like the amorphous silicon (a-Si), which is a so-called thin film technology.
Some other types of solar cell material included in the thin film "family" are: Cadmium Telluride (CdTe), gallium arsenide (GaAs) and Copper Indium Gallium Selenite (CIGS).

2.1.3 Solar Cells

Solar cells work through the photovoltaic effect, first discovered by the French physicist A.E. Bequerel in 1839. It is an effect directly related to the photoelectric effect, first discovered by Albert Einstein in 1905 and known for the ability of a metal to emit electrons when light is induced on it.
In the photovoltaic effect, however, light induced on a semiconductor induces a current, which can be made available for electrical work.

Photons (energized light quanta) in sunlight incident on the semiconductor material of the solar cell can dislodge valence electrons, if they possess sufficient kinetic energy, leaving behind a positively charged hole.
These electrons are then free to move in the lattice structure of the material, potentially performing electrical work on the way, if led through an external circuit.

The photovoltaic principle is well illustrated in the band gap model (Figure 4), where the valence electron is said to be in the valence band before being excited (dislodged) into the conduction band (lattice structure) [**6**]:

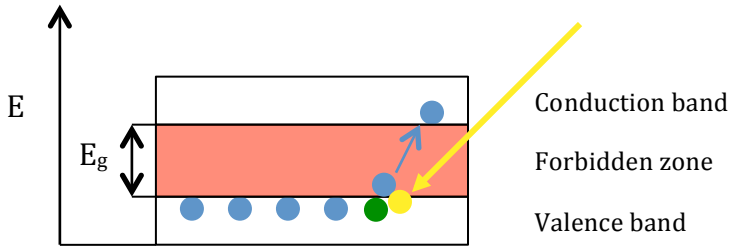

Figure 4: Illustration of the band gap model (photon in yellow, electrons in blue, holes in green)

The photon energy E_{photon} necessary to dislodge a valence electron and make it available for work through an external circuit is given by the band gap energy E_g, according to the formula:

$$E_{photon} = hf \geq E_g \tag{2.1}$$

Where h is the Planck constant and f is the frequency of the incoming light.
The forbidden zone is the energy gap between the valence band and the conduction band, and cannot be used for conduction.
For insulators, this band gap is too high for photon excitation, for metals, the forbidden zone is non-existent [**7**].

A solar cell is usually constructed through a process called doping, where elements from group II and VI or group III and V are combined with the semiconductor material by molecular diffusion to create a so-called pn-junction. By doing this, the different parts of the semiconductor material will contain a deficit (p-doped) or surplus (n-doped) of negative charges in the conduction band, giving rice to an electrical field E between the doped parts.

By electrical diffusion, electrons move from the n-doped to the p-doped side of the cell, until an electrostatic equilibrium is attained. The area with an active electrical field containing the pn-junction is then called the "depleted region". The depleted region gives rise to a potential, working as an electromotive force (EMF) for electrons dislodged by photons [**6**].
This voltage drop *V* (hence voltaic cell) and the resulting current of interaction between photons and electrons in the depleted region, is known as the photovoltaic effect.

The principle of a solar cell is illustrated in Figure 5:

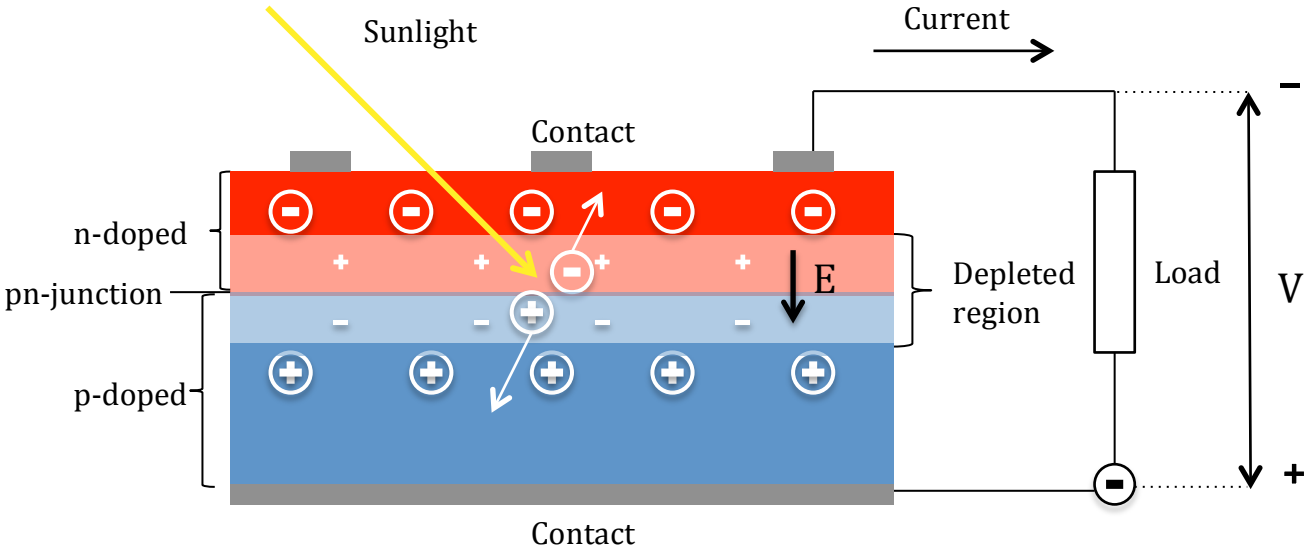

Figure 5: Illustration of a solar cell build and working principle

A solar cell is a form of diode, as the electrical field only allows current flow in one direction. An equivalent circuit diagram, known as the one-diode model, can be seen in Figure 6:

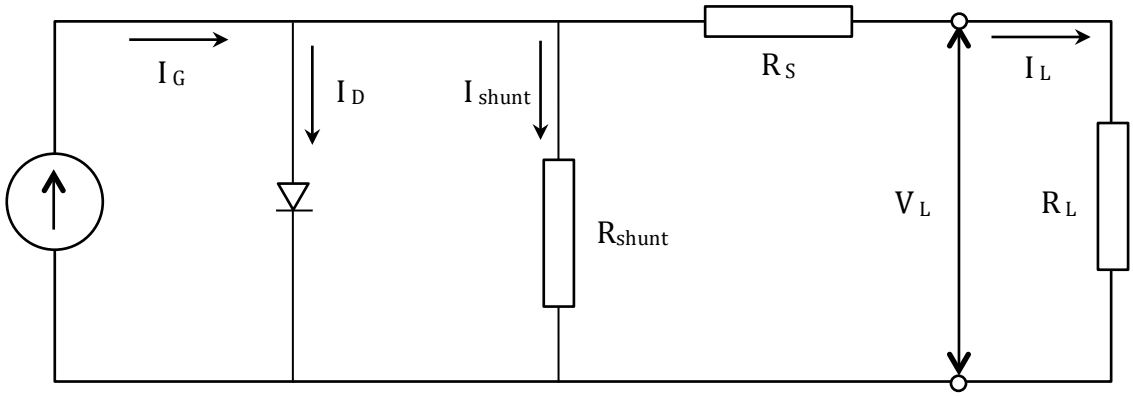

Figure 6: Equivalent circuit diagram of the solar cell; the one-diode model

The photo-generated current I_G is proportional to the number of incoming photons and therefore is a function of the radiation incident on the cell.

The diode current I_D is the charge flow through the pn-junction, and can be seen as current loss due to electron-hole recombination [**8**].

The cell has several parasitic resistances, leading to power loss and reduction in the energy conversion efficiency. Two of the most important parasitic resistances include the shunt resistance R_{shunt} and the series resistance R_S. R_{shunt} represents the power loss due to the leakage currents in the cell; given by I_{shunt}, whereas R_S represents power loss due to internal cell resistance, cell contact resistance and cell-contact surface resistance [**6**].
R_L represents the load, while V_L and I_L is the potential loss over it, and the current through it, respectively.

The power P_{cell} supplied by the cell to the load is given by the formula:

$$P_{cell} = I_L \cdot V_L \tag{2.2}$$

There are two situations at which the supplied power from the cell equals zero:

1. The voltage drop over the load equals zero; $V_L = 0$ V.
   In other words, when the load resistance R_L is negligible.
   Photo-generated electrons will move through the circuit without performing work, recombining at the other side of the pn-junction.
   The circuit is then said to be short-circuited and, instead of a load current I_L, there will flow a *short-circuit current* I_{SC}.

2. The current through the load equals zero; $I_L = 0$ A.
   This is the case when the load R_L is infinitely large, in which the circuit is said to be at open-circuit.
   The dislodged electrons and the holes will then accumulate in their respective regions within the cell, until the electric field is weak enough for the diode current I_D to equal the photo-generated current I_G.
   The accumulated charge in the cell necessary to cancel the electric field across the pn-junction leads to an increased voltage across the cell terminals, called the *open-circuit voltage* V_{OC}.

To be able to investigate the behavior of a solar cell under illumination, between these two operating points, the cell can be equipped with a variable shunt-resistor that acts as load, and tested under some standardized conditions.
This makes it possible to compare different cells to each other.

These standard test conditions (STC) are as follows:

- Irradiance of 1000 W/m^2
- Cell temperature 25 ± 2°C
- Light spectrum according to air mass (AM) 1.5

The behavior of the solar cell at STC is usually represented by something called the characteristic curve, or the IV-curve, of the solar cell [**4**].

An illustration of how such a curve is shown in Figure 7:

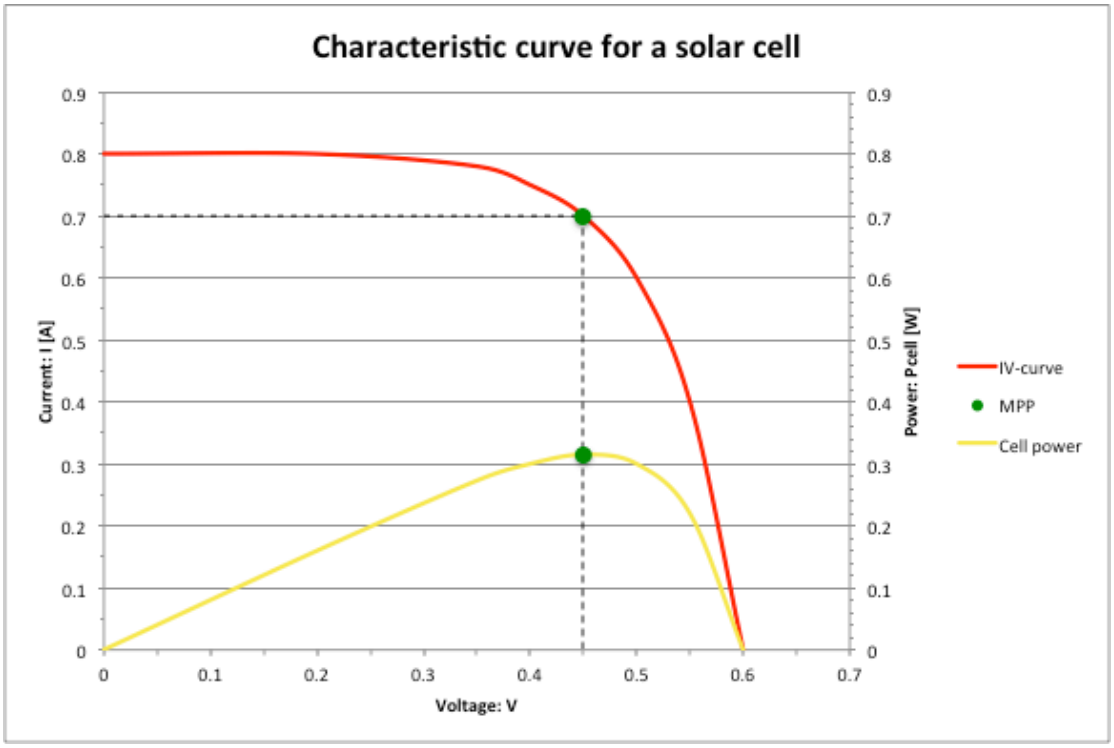

Figure 7: Illustration of the characteristic curve for a single solar cell

This curve displays how the current and voltage of the cell changes with respect to each other as the load changes. The delivered cell power is also shown.
The green dots marked on the graphs indicate the *maximum power point* (MPP), where the supplied cell power is at its maximum ($P_{cell} = P_{MPP}$).

This cell maximum power can be calculated from the following formula:

$$P_{MPP} = I_{MPP} \cdot V_{MPP} \tag{2.3}$$

V_{MPP} and I_{MPP} is the common denotation for the MPP-voltage and MPP-current, respectively.

Mathematically, the theoretical maximal power $P_{max\ theory}$ would be found in the point where the gridlines of V_{OC} and I_{SC} intersect in Figure 7.

The ratio of the real power supplied to the theoretical maximum, is a measure of the how square the curve is, and it is called the *Fill Factor* (FF).

The lower the FF, the rounder the IV-curve will look.
A value for the FF of 1 characterizes an ideal cell, and will never be achieved in reality.

The FF is calculated according to the following formula:

$$FF = \frac{I_{MPP} \cdot V_{MPP}}{I_{SC} \cdot V_{OC}} = \frac{P_{MPP}}{P_{max\ theory}} \quad (2.4)$$

Using formula (2.4) on the cell in Figure 7, with I_{MPP} = 0.7A, V_{MPP} = 0.45V, I_{SC} = 0.8A and V_{OC} = 0.6V, gives a FF = 0.66.

Crystalline solar cells usually have a FF in the range 0.75 - 0.85, whereas amorphous cells might have fill factors in the range 0.5 - 0.7 [**4**].

The effect of the parasitic resistances described in relation to the one-diode model is to reduce the fill factor.

With FF now defined, equation 2.3 may be rewritten in the form:

$$P_{MPP} = I_{SC} \cdot V_{OC} \cdot FF \quad (2.5)$$

The fill factor is closely related to the (maximum) *cell efficiency*, which can be calculated from the following formula [**6**]:

$$\eta_{cell} = \frac{P_{MPP}}{P_{in}} = \frac{I_{SC} \cdot V_{OC} \cdot FF}{P_{in}} \quad (2.6)$$

Where P_{in} is the power (irradiance) incident on the solar cell from the sun.

Because the MPP is defined at STC, and the FF is a function of this parameter, it should be noted that also the cell efficiency is defined at STC.

2.1.4 From cell to module

As mentioned in chapter In the above figure P_{DC} is the direct current (DC) power delivered by the generator to the inverter, whereas P_{AC} is the alternating current (AC) power delivered from the inverter to the mains grid. Electricity meters are omitted for sake of simplicity, as only inverter data will be evaluated in this thesis.

Electrical safety measures include BoS-components like surge arresters, mains disconnection switches and circuit breakers, among others.
However, since these components are only of secondary importance to the operation of a PV system, and not directly relevant for this thesis, the information about them is omitted.

Most manufacturers of system components will print a spec-sheet or *datasheet*, containing some or indeed all parameters that might be of interest to the purchaser. Datasheets containing information about the inverter and modules incorporated into the system investigated in this thesis can be found in Appendix C: Datasheets.
2.1.1 The PV-generator, a module consists of several solar cells connected together.

If stringing the cells in parallel would assemble the module, then the *current* of each individual cell would add up, according to Kirchhoff's Current Law (KCL).

The module voltage, however, would be approximately the same as that of the weakest cell.

If stringing the cells in series would assemble the module, the *voltage* of each individual cell would add up, according to Kirchhoff's Voltage Law (KVL).
The current, on the other hand, remains approximately the same as that of the weakest cell.

Because of this inherent influence of cell configuration on module behavior, cells are sorted according to their characteristics. This means that cells with similar properties (characteristic curves), are sorted together, the most important parameters being I_{SC} and V_{OC}.

Most modules today are assembled with a series-configuration of the cell.

The connected cells are usually encapsulated in a polymer or copolymer, laid upon an insulating layer and framed with a glass cover [**6**].

2.1.5 Module efficiency

A solar module is, like the single cell, tested according to the STC, in order to investigate the behavior under illumination and the module efficiency.
This makes it possible to compare modules of different technologies and from different manufacturers on equal terms.

As has been mentioned in earlier, connecting solar cells in series is most common in modules today.

The resulting module voltage can be calculated with the following formula:

$$V_{X\ module} = \sum_{n=1}^{N} V_{X\ cell\ n} \tag{2.7}$$

Where N is the total number of cells in series and X is the index of the wanted parameter (E.g. MPP, OC, etc.).

Hence, the module P_{MPP} may be calculated by replacing the V_{MPP} in eq. (2.3) by $V_{MPP\ module}$.

The Efficiency of the module can then be calculated according to eq. (2.6), substituting the index *cell* for *module*:

$$\eta_{module} = \frac{P_{MPP}}{P_{in}} = \frac{P_{MPP}}{G_{inc} \cdot A_m} \tag{2.8}$$

Where G_{inc} [W/m^2] is the irradiance incident in the collector plane and A_m is the module area.

2.1.6 Watt-class sorting

Modules are rated according to the power output at MPP, which is found at STC. This means that, if a given module has a 200W power output at MPP, it will have a nominal capacity of 200W and hence be rated in the 200W class.
Occasionally, the term Watt-peak (W_p) is used to signify that the rated power is the highest obtainable at STC.

Usually, with the statement of a watt-class, comes a so-called watt-class *tolerance*. Thus, a panel may be rated at 200W (± 5W), meaning that the accuracy is of 5W absolute, or 2.5% relative.

As a result, when buying a panel rated this way, the P_{MPP} may be as little as 195W, or as high as 205W.
If the panel would perform in the lower tolerance range (<200W) it may be called overrated, and in the opposite case (>200W) it may be called underrated.

Many manufacturers today only state positive tolerances, consistently underrating the panels.

2.1.7 Module characteristics

As a consequence of the series-connected cells, the characteristic curve of a module will be drawn with a proportionally larger power- and voltage-axis than that of a single cell.

Most modules will never be operated under STC out in the real world. Instead, they will experience alternating operating temperatures and irradiance levels. This leads to different characteristic curves, MPPs, filling factors and efficiencies.

The comparison of prediction and production rely on extensive use of the simulation software PVsyst. This program contains module characteristics for many modules, allowing the user to generate characteristic curves for a specified module, by utilizing the one diode model.

Although the equations used to do this are readily available, the exact method used by the program is difficult to comprehend, and thus to explain.
For the sake of brevity, the explanation will therefore be omitted, as it has no practical meaning for this thesis.
More about the calculations performed by the program and the use of the one-diode model can be found in the PVsyst help file [**9**][physical models used].

Figure 8 below shows the characteristic curves under different irradiance conditions and constant operating temperature, for a solar module Aas:

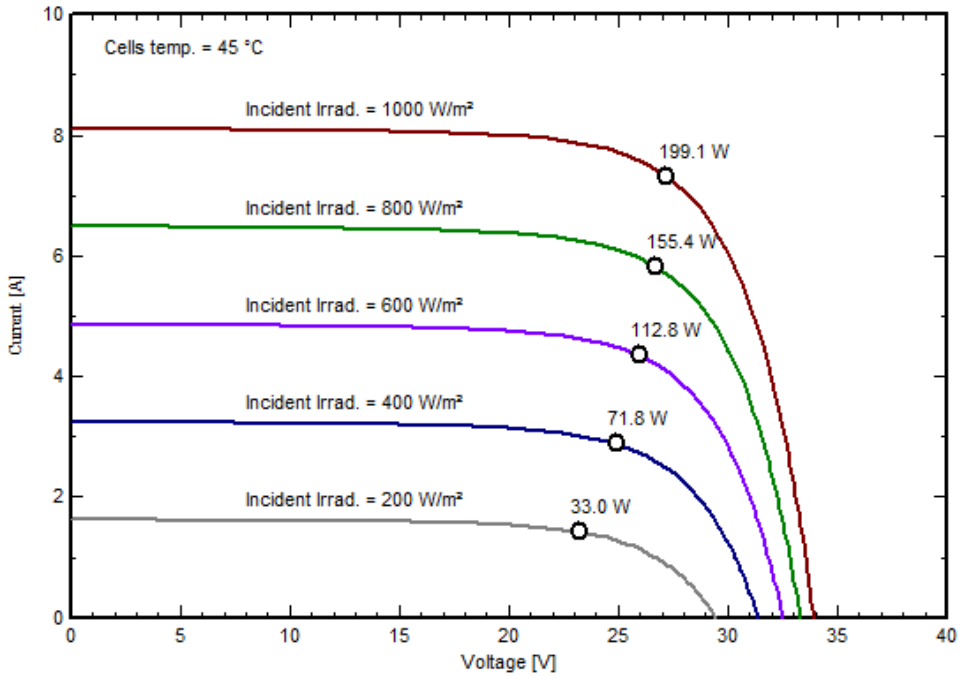

Figure 8: Characteristic curves under different irradiance conditions and constant temperature for one of the modules in the PV-system at Aas. PVsyst excerpt.

From the figure, it may be seen that the MPP of the module is at 199.1W at the elevated operating temperature (45°C). According to its datasheet, this module has a nominal capacity at STC of 220W, which means that the performance of the PV-cells decline with increasing temperature.

Indeed, such a behavior can be observed from Figure 9, where the characteristic curves of the same panel are shown, only this time with constant irradiance and alternating temperatures.

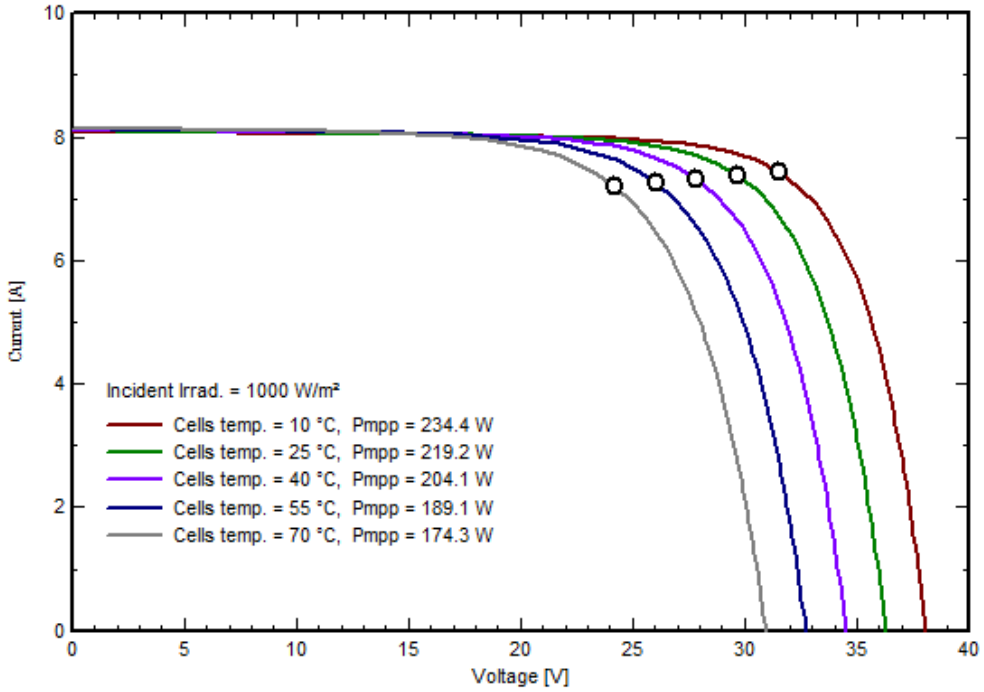

Figure 9: Characteristic curves under different temperatures and constant irradiance for one of the modules at Aas. PVsyst excerpt.

The discrepancy between the behaviors of the solar cells under STC and under real-world conditions, has led to the development of a second set of test conditions. They allow for the determination of the operating temperature of the cell under irradiance slightly more modest than at STC.

The *normal operating cell temperature* (NOCT) test conditions are [**6**]:

- Irradiance of 800 W/m²
- Ambient temperature 20°C
- Wind velocity 1 m/s

From the characteristic curve at NOCT and the characteristic curves that result from alternating the temperature in the range between ambient temperature and NOCT, temperature coefficients can be found for V_{OC}, I_{SC} and P_{MPP} [**10**] [**11**]. They are normally given on per unit (p.u.) basis (e.g. V/°C) or percentage basis (e.g. %/°C) and listed in module datasheets supplied by the manufacturer. Note that the coefficients are given relative to STC.

These coefficients can then be used to calculate the mentioned parameters at conditions that are site specific, when a PV-system is planned.

The equations used to do this are listed below [**12**]:

$$V_{OC} = V_{OC,STC} \cdot \frac{\ln G}{\ln 1000} \cdot \left(1 + \alpha(\theta - 25)\right) \tag{2.9}$$

$$V_{MPP} = V_{MPP,STC} \cdot \frac{\ln G}{\ln 1000} \cdot \left(1 + \alpha(\theta - 25)\right) \tag{2.10}$$

$$I_{SC} = I_{SC,STC} \cdot \frac{G}{1000} \cdot \left(1 + \beta(\theta - 25)\right) \tag{2.11}$$

$$I_{MPP} = I_{MPP,STC} \cdot \frac{G}{1000} \cdot \left(1 + \beta(\theta - 25)\right) \tag{2.12}$$

Where the following symbol definitions apply:

G - actual operating irradiance [W/m²]
θ - actual operating temperature [°C]
α - voltage temperature coefficient [V/°C]
β - current temperature coefficient [A/°C]

When the MPP temperature-coefficient (ϑ) is used, this formula applies:

$$P_{MPP} = P_{MPP,STC} \cdot \left(1 + \vartheta(\theta - 25)\right) \tag{2.13}$$

The irradiance dependence of the MPP is generally not considered.
When needed, this could be found by combining eq. (2.8), (2.10) and (2.12):

$$P_{MPP} = I_{MPP,\,STC} \cdot V_{MPP,\,STC} \cdot \frac{G}{1000} \frac{\ln G}{\ln 1000} \cdot \left(1 + (\alpha+\beta)(\theta\text{-}25) + \alpha\beta(\theta\text{-}25)^2\right) \quad (2.14)$$

Note that where the temperature-coefficients are given in percent, they have to be divided by a factor 100 and multiplied with the respective variable they're stated for, before being used in the formulas.

The efficiency of a solar module is normally stated according to STC, and called the *nominal* efficiency of the panel, denoted η_n.
Naturally, the efficiency will also change with alternating temperatures and/or irradiance, so that sometimes, temperature-coefficients for efficiency is used.

The general formula is as follows:

$$\eta_{module} = \eta_n - \Delta\eta \quad (2.15)$$

Where $\Delta\eta$ is the change in efficiency.

For a regime of constant temperature, but changing irradiance, the change in efficiency is approximated from eq. (2.16):

$$\Delta\eta \approx -0.04 \cdot \eta_n \cdot \ln s \quad (2.16)$$

Where *s* is the ratio of the actual operating irradiance, to the irradiance at STC.

For constant irradiance, but changing temperature, the following applies:

$$\Delta\eta = \zeta \cdot (\theta - 25) \cdot \eta_n \quad (2.17)$$

Where ζ is a material dependent temperature-coefficient.
For crystalline silicon, this coefficient is approximately 0.45 %/°C [**4**].

Temperature-coefficients of current and voltage are often used as input into simulation programs and other software intended to model the behavior of a PV-system. These programs can then use, for example the one-diode model, to simulate the behavior of the system under different temperature and irradiance conditions.

2.1.8 Inverters

An inverter is a device that first and foremost is developed to take the current and voltage from a source of electrical energy and transform it into the current and voltage needed for utilization by a consumer.
Both DC-DC and DC-AC inverters exist, although only the latter is used in grid-connected PV-systems.

An AC-DC inverter is normally called a grid-connected or grid-controlled inverter. Perhaps the latter expression reflects the function of the inverter better, as it inherently is dependent on the frequency of the grid to be able to perform its duty correctly. In short, this is [**4**]:

- To convert the DC-current of the PV-array into an AC-current and match the current frequency to the grid frequency.
- To maintain the PV-array at its MPP at all times – MPP-tracking (MPPT)

In addition, it should have some other functions:

- Record and alternatively transmit the operation data
- Safeguard the installation and grid with electrical protective devices

A grid-connected inverter is not necessarily protected from stand-alone operation, and therefore differs from the grid-controlled inverter.
In the event of a utility loss, the grid-controlled inverter will automatically disconnect itself from the grid, which is important to protect utility workers and grid components, among other things.

Grid-controlled inverters are sometimes also called square-wave inverters (SWI), referring to the output waveform of the AC-current. This means that a grid-controlled inverter has a relatively high harmonic component.
The advantage is a simple and inexpensive inverter.

Self-commutated inverters (SCI), or pulse-width modulated inverters (PWM), are another type of inverters not inherently grid-controlled. They usually apply complicated circuitry in the form of power electronics to construct pulses that imitate the sine wave of the grid AC-current. One of the features of these inverters is that they have low harmonic components, which increases power quality. The downside is often lack of galvanic isolation from the grid.

Modified SCI's feature either low or high frequency transformers.
These combine the advantages of both SWI and the SCI to offer an inverter with negligible harmonic components and galvanic isolation from the grid.
With one of these inverters, the grid is protected from DC-AC interference.
The inverter efficiency of these inverters is among the highest today.

Figure 10 shows typical efficiency curves for an inverter at different voltage levels. It can be observed that already from the beginning of feed-in at just above 0% of nominal inverter power; the efficiency is at 90%. Inverter efficiencies of most inverters today lie above 90% [**13**].

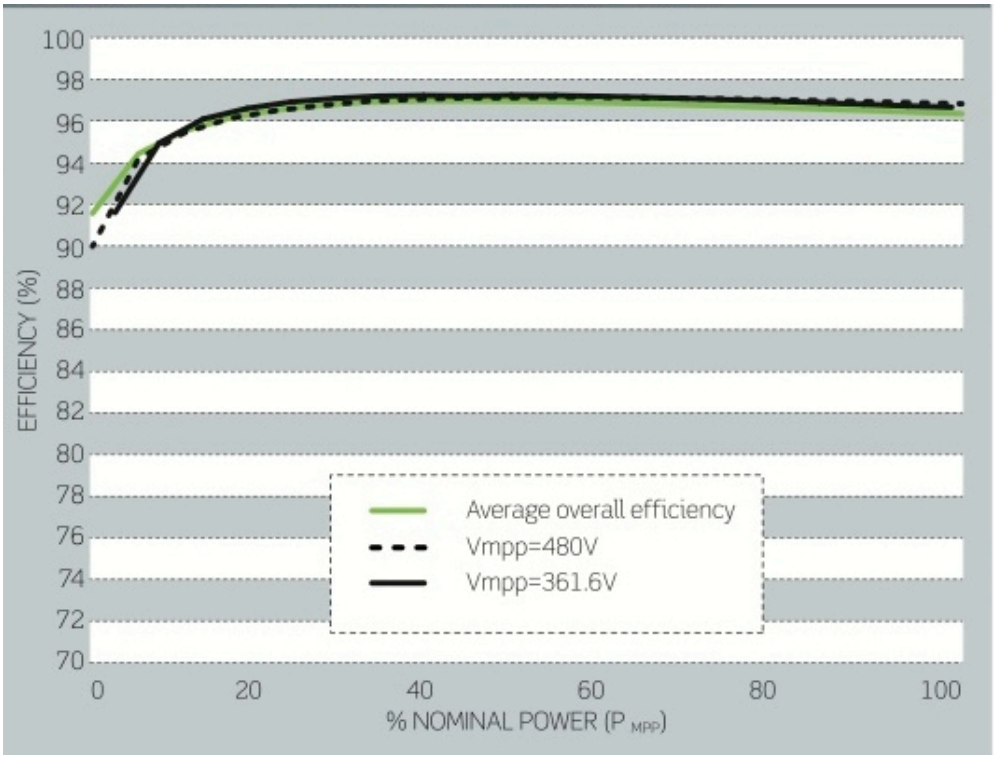

Figure 10: Efficiency curves for a Theia He-t 4.4 inverter for different voltages

Note that the inverter efficiency also is dependent on temperature. Thus, it will have different efficiency curves with changes in temperature.
The dependency is the same as for solar cells; high temperatures lead to low efficiency, and vice versa.

When implementing inverters into a PV-system, different configurations may be used, according to application [**4**]:

- Central inverter
- String inverter
- Module inverter

The central inverter configuration (Figure 11) is simple and only requires the purchase of one unit, which is cost efficient. On the other hand, the DC-cabling is usually significant enough to offset this cost-benefit.
The configuration has several important disadvantages; Shading will affect whole strings at a time, significantly reducing the output of the array. Furthermore, an inverter failure leaves the whole system unavailable, with a resulting loss in profitability. Also, the MPP-tracking can only follow the overall system, ignoring potential mismatching between modules.

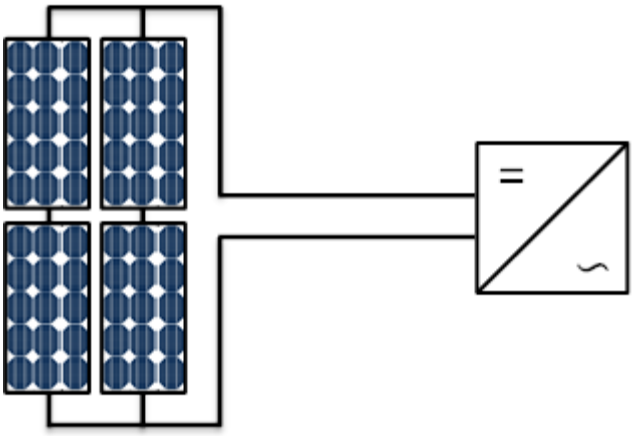

Figure 11: Central inverter configuration

The string inverter configuration (Figure 12) avoids some of the disadvantages experienced with the central inverter, one being a reduction in the DC-cabling. Another significant advantage is the isolation of strings affected by shading, or inverter failure. Another advantage may be the possibility of alternating string orientation, when necessary. The system might also be easier expandable to include more units, as strings can be added individually.
However, adding extra modules to an existing inverter may be difficult without overloading the inverter and the issue of mismatching modules still remains within the respective strings.

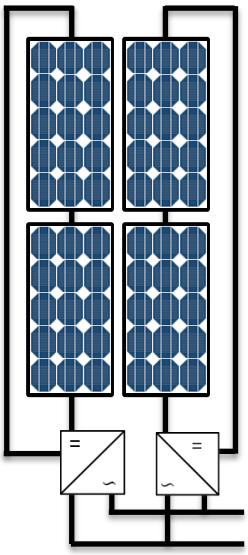

Figure 12: String inverter configuration

Module inverters (Figure 13) in a way are a continuation in the development of de-centralized inverters. They have all the advantages of the string inverters, and some additional as well.
For one, shading-effects only influence the shaded modules, so the system generally performs better in locations where shading is an issue.
Also, the MPP-tracking follows the individual modules, ruling out any loss due to mismatching of operating point.

Another thing is that the PV-system can easily be extended, one module at a time if desired. In addition, inverter failure only affects the coupled module, and allows for easy replacement.

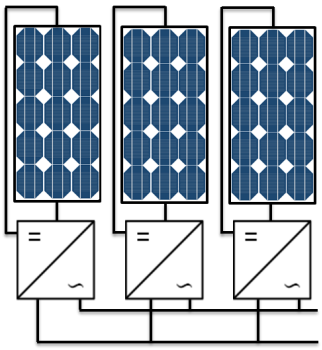

Figure 13: Module inverter configuration

Moreover, the module inverter is a small unit, most fit on the backside of the module, ridding the need for inverter rooms, auxiliary cooling, etc.
A significant shortfall attributed to this mentioned benefit, is that the inverter is exposed to the weather conditions of the site, which may shorten its lifetime drastically.

On the downside, the specific cost (price/W_p) of module inverters is somewhat higher than for centralized inverters.
Also, they have a slightly lower efficiency than centralized inverters, although this may be easily offset by the higher production due to accurate MPP-tracking.

In PVsyst, the inverter configuration may be chosen, along with the inverter type and size. The inverter efficiency curve for the chosen inverter is modeled according to information about the load behavior supplied in the datasheet or by the inverter manufacturer.

2.1.9 Cables

The cables in a PV-system represent vital BoS components, as they interconnect the PV-generators; conduct the produced energy from generator to inverter and from inverter to grid. They are usually water and UV-resistant and have good insulating and fire repelling capabilities.

Interconnection of PV-modules is usually done with DC-cables that follow the modules, hence their dimensions and quality is listed in the module datasheet. Connection of whole arrays to the inverter is done with a main DC-cable.

DC-cables are expensive because of the demand for overall robustness and large cable cross-sections, combined with high prices on copper. Recently, aluminum has become more used in PV-systems, as it is cheaper. The poor conductivity compared to copper, however, leads to even higher cable cross sections and thus imposes new challenges to the PV-industry [**14**].

2.2. System performance and loss factors

The meaning of system performance is directly deductible from the expression: "How well does the system perform?"

A common ways to measure how the system performs is by evaluating the **Annual yield [kWh/year]** of the system. It is the total amount of energy produced by the system within a given year.
This gives the opportunity of comparing the yield with that of other system. However, only comparisons made between systems of equal size, with different components, really make sense.

A more general, and useful, parameter used for evaluation of system performance is the **Specific yield [kWh/kW$_p$].** This is the amount of energy produced by the system per installed kW of PV-power.
It ignores the system size and allows for comparing all PV-systems based on their installed production capacity. The specific yield is found by dividing the annual yield by the total PV-system production capacity.
Despite being a useful parameter, often it is desired to know how the system as a whole is doing, and specify the amount of losses.

The **Performance Ratio (PR)** is a parameter that gives information about performance of the system relative to that of an ideal system, without losses.

The performance ratio can be found with the formula:

$$\mathrm{PR} = \frac{Y_R}{Y_i} \tag{2.17}$$

Y_R and Y_i is the actual or real system yield, and the ideal yield, respectively.
The ideal yield of a system is the theoretical yield, given that all the incident sunlight on the modules would be converted with the rated efficiency at STC, disregarding any other losses.

Formula (2.17) may be elaborated to yield a more specific formula, it is then written as a function of the different efficiencies that are included in a system:

$$\mathrm{PR} = \frac{Y_R}{Y_i} = \frac{G_G \cdot R \cdot \eta_{opt} \cdot \eta_{nom} \cdot \eta_{rel} \cdot \eta_{sys}}{G_G \cdot R \cdot \eta_{nom}} = \eta_{opt} \cdot \eta_{sys\ tot} \tag{2.17a}$$

Where G_G is the global horizontal radiation, R is the transposition factor, η_{nom} is the nominal module inverter efficiency at STC, η_{opt} is the pre-conversion efficiency, η_{rel} is the module efficiency relative to STC, η_{sys} is the efficiency of inverter and cables and $\eta_{sys\ tot}$ is a combined variable for the two latter mentioned efficiencies.

The pre-conversion efficiency is the efficiency of the transmittance of light to the actual semiconductor material in the cell, and represents the losses due to soiling and other factors that may be important in reducing incident light.

The relative efficiency is the efficiency of the module relative to that at STC, taking into account increase or decrease in conversion efficiency due to low irradiance, temperature, etc.

The system efficiency is the efficiency of the BoS components, namely inverter and cables. The total system efficiency is the combined efficiency of both the relative and system efficiency.

The PR will have a value between 0 and 1, the latter indicating that the system performs loss-free. This will never be achieved in reality; normal values for PR is 0.70 - 0.85, however well operated systems may do better. The PR values can alternatively be stated in percent, they are then multiplied by a factor 100.

A PV-system loses a lot of energy due to poor efficiency of the components. Although this loss is significant, the efficiency of the components may be reduced further due to unforeseen operating conditions.

However, not all of the energy lost in a PV-system is due to the components themselves. Often, there are other losses, too.
Some can be attributed to the access to the energy source, the sunlight, while others might be attributed to the nature of the light.

This subchapter deals with the different losses experienced in a PV-system, which are of significance to this thesis.

2.2.1 Module mismatching loss

As was mentioned in the previous subchapter (2.1.4 From cell to module), stringing cells in series when constructing a module, results in a module current corresponding to the current of the weakest cell.
In the same manner, stringing modules in series undoubtedly follows KVL too, leading to an elevated voltage level, but adopting the current level of the weakest module.

Because of the watt-class sorting tolerance, not all modules of the same model and stated rating will possess the same operating behavior.
According to the existing industry standards regarding rating, IEC61215 and IEC61646, the nominal rating of the panels at STC should be at least the same or higher than, the measured average power of the modules.
The power output of the module is not in any instance (at STC) allowed to differ from the nominal rating by more than 3% [**15**].
This means that modules with a power rating higher than the actual measured average, may be included in a string and lead to so-called mismatch losses.

Fortunately, many manufacturers today sort their modules only according to a positive tolerance, in which case mismatching losses are non-existent.
Instead, PV-systems implementing such modules occasionally will get smaller "mismatching-surges", which generally is considered to be positive.
Consequently, consideration should be taken, so that the inverter and system cabling isn't overloaded.

2.2.2 Module quality loss

The module quality loss is regarded as degradation of module P_{MPP} with time.

This degradation can be divided in two:

1. Initial degradation - also termed light induced degradation (LID)
2. Long term degradation - related to aging of the module

The LID of solar cells is degradation that passes within the first few days of operation by exposure to sunlight. A typical value is regarded as 3%, although values of 2.6% ± 1.3% have been reported in a field test.

According to the IEC61215 test standard, the LID degradation is never to exceed 5% between tests and 8% for a full test sequence, in order for the module to be approved. These values are certainly significant deviations in term of commercial viability of a PV-project.

The long-term degradation of modules has been studied ad several reports have been made; one stating that majority of the tested modules had degradation below 0.75% p.a. According to a collection of studies made on the subject, values of 0.3% - 0.8% p.a. have been suggested, although higher values have been reported in a few instances [**16**].

The module datasheets in the appendix section show values of 0.7% - 0.8% p.a.

In addition to the stated classes of degradation, there is also temperature-induced degradation (TID) and potential-induced degradation (PID).

The latter form of degradation is loss of module voltage due to ions wandering out of the solar cell. It is tested according to the IEC62804 standard, where a maximum of 5% degradation in P_{MPP} is accepted for the cell to pass.

The LID and long-term degradation losses will be specified for input in PVsyst before simulations are conducted.

2.2.3 Irradiance loss

As was explained in the previous subchapter (2.1.7 Module characteristics), the module characteristic curves change as the level of the incident radiation changes from that at STC.

One of the effects of lower irradiance levels in solar modules is a reduced efficiency, albeit the exact value depends on the cell technology.

The reduction in efficiency for different irradiance-levels, and at different operating temperatures, for a poly-crystalline module at Aas, can be seen in Figure 14:

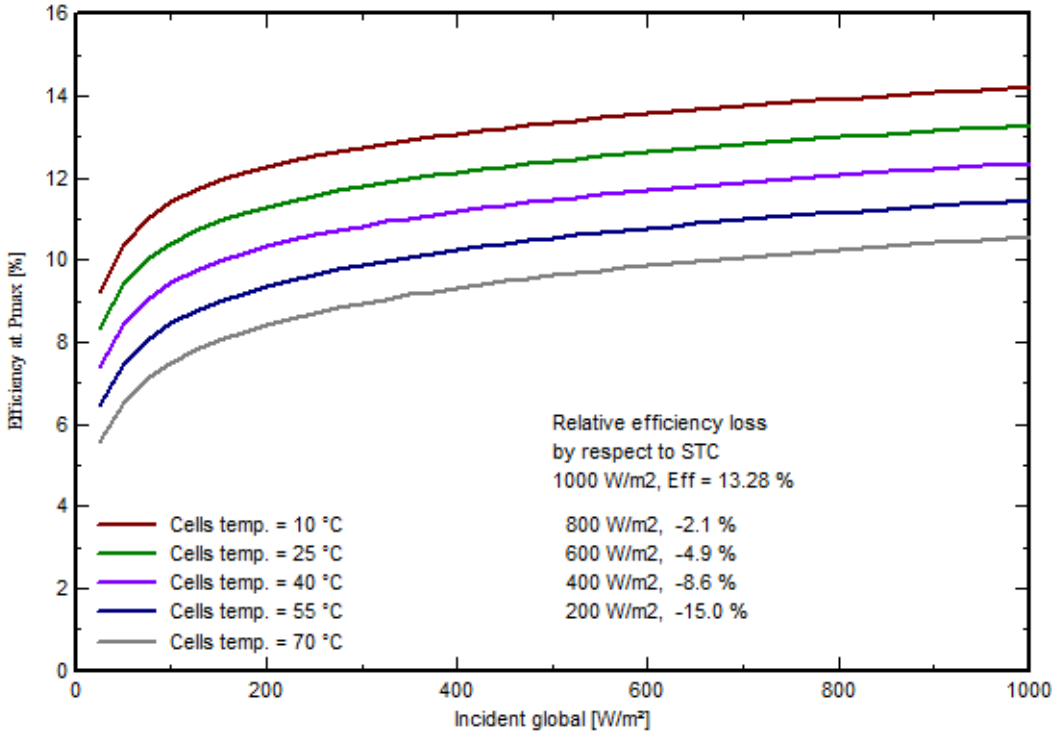

Figure 14: Efficiency curves for different irradiance levels, at different operating temperatures, for a poly-crystalline module at Aas. PVsyst excerpt.

The green curve shows the change in efficiency for changing irradiance-levels at the STC cell temperature.
The listed relative efficiency loss corresponds to this curve.

2.2.4 Temperature loss

Like in the previous section, the influence of temperature on characteristic curves has been explained in the previous subchapter.
Formula (2.15) used in combination with (2.17) shows that an increase in the solar cell-temperature leads to a decrease in module efficiency, and vice versa.

Indeed, this may be observed in Figure 15, which shows the change in efficiency with temperature, at different irradiance levels, for a poly-crystalline module from the system at Aas.

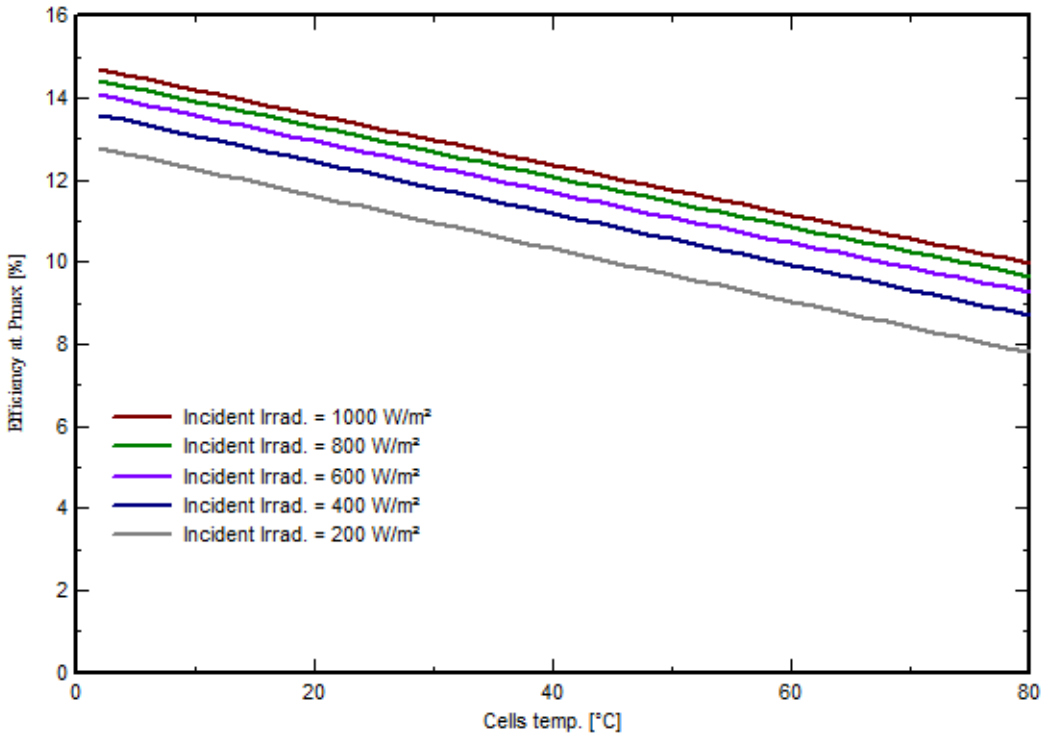

Figure 15: Efficiency for different operating temperatures, at different irradiance levels, for a poly-crystalline module at Aas. PVsyst excerpt.

To estimate the module temperature, the following formula may be used [**17**]:

$$T_{Cell} = T_{Air} + \frac{(NOCT - 20)}{800} \cdot G_{inc} \tag{2.18}$$

T_{Cell} *and* T_{Air} are defined as the cell, and air temperature, respectively.
G_{inc} [W/m^2] is defined as the global irradiance incident on the cell.

In the above formula it is assumed that the cell temperature is proportional to the incident irradiance relative to that under NOCT-conditions.
This is rarely the case; often, the temperature will be higher when the heat dissipation from the module is low, i.e. when the modules are well ventilated and wind speeds are higher than at NOCT, and vice versa.

This is why the cell temperature is often calculated by taking the thermal energy balance into account, and calculated with the following formula:

$$U \cdot (T_{Cell} - T_{Air}) = a \cdot G_{inc} \cdot (1 - \eta_{module}) \tag{2.19}$$

Where a is the module absorption coefficient, and η_{module} is the module efficiency.

The thermal loss factor U [W/m^2·K] in formula (2.19) can be referred to as the module U-value, and is calculated according to the following formula:

$$U = U_c + U_v \cdot v \tag{2.19}$$

Where U_c is the constant thermal loss factor and U_v is a thermal factor proportional to the site-specific wind velocity v.

Module U-values are highly site specific and vary with the module configuration. Modules with free front and backsides usually have higher U-values due to air circulation, whereas building integrated photovoltaic (BIPV) modules have lower values.

2.2.5. Inverter loss

The inverter efficiency curve was introduced in Figure 10 (2.1.8 Inverters). As can be observed, the inverter efficiency changes according to the amount of power being fed into it. If the inverter is working at loads outside the optimum working point, loss in inverter efficiency is unavoidable.

These losses are called inverter loss, and are most significant at working points way below the nominal capacity of the inverter. Thus, if an inverter is sized improperly, the PV-array will continuously experience efficiency losses, degrading the system performance. Sizing of the inverter is therefore of importance for the PR, and consequently, profitability of a PV-system.

The inverter sizing is normally expressed through the inverter-sizing factor (c_{INV}), which is calculated according to the following formula:

$$c_{INV} = \frac{P_{PV}}{P_{INV\ AC}} \tag{2.20}$$

Where P_{PV} *and* $P_{INV\,AC}$ is the PV-array nominal output, and the inverter nominal AC capacity, respectively.

An inverter is usually sized according to climate and meteorological conditions. If the irradiance levels generally are low, and irradiance peaks only are experienced occasionally, the inverter may be undersized ($c_{INV} > 1$). This way, the inverter works close to its nominal capacity at all times, at a higher efficiency, at the cost of losing production in the peak irradiance periods.

On the other hand, if the irradiance level is generally high, or consistent low temperatures are experienced which increase the array output above the nominal, the inverter might be oversized ($c_{INV} < 1$). Then, the inverter also works close to the nominal capacity at all times, though occasionally experiencing low efficiency at low irradiance.

The normal range for the inverter sizing factor is: $0.83 < c_{INV} < 1.25$ [**4**]. As a rule of thumb, inverters are sized with a $c_{INV} = 1$, which is the nominal sizing.

Other inverter losses are related to the inverter operating range.

All inverters have working voltage-ranges for the DC-input, i.e. 230V – 480V. Outside these ranges, the inverter generally stop working and feeding the grid. Consequently, if a system is improperly designed, the voltage input may be outside this range at certain operating conditions, which will result in additional production losses.

The implementation of inverter and the issue of inverter sizing in PVsyst will be addressed in chapter 3.

2.2.6 Cable resistance loss

Due to the relatively high DCs experienced on the DC-side of a PV-system, Ohmic resistance losses in the DC-cables are experienced.

The resistance power loss of the cables can be calculated from this equation:

$$P_{cable} = I_{cable} \cdot R_{cable}^2 \tag{2.21}$$

Where the resistance of the DC-cable can be calculated from eq. (2.22):

$$R_{cable} = \frac{l}{A_{ccs}} \cdot \rho_{cable} \tag{2.22}$$

Here, l [m] is the cable length; A_{ccs} [mm^2] is the cable cross-section and ρ_{cable} [Ω·mm^2/m] is the specific resistivity of the cable material.

As a rule of thumb, cable resistance losses shouldn't exceed 1% in a PV-system. In most cases it suffices to consider the DC-cable losses, as the AC-cable losses will be insignificant, unless the distance between grid injection point and the production site is significant [**4**].

2.2.7 Array incidence angle loss

The transmission of light in different media is governed by Fresnel's law, dividing light incident on a transparent surface into: one incident part, one reflected part and one refracted part (Figure 16).

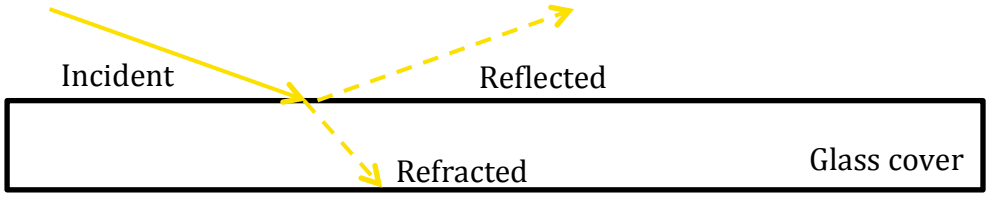

Figure 16: Illustration of how light divides when incident on a surface

As light is incident on a solar panel, some of the light will be reflected from the glass front covering the solar cells. The amount of reflected radiation would have been straightforward to calculate, if it wouldn't have been for the fact that both modules and cells are coated with anti-reflective coatings.

Thus, another method of evaluating this has been developed.
It works through so-called ASHRAE-parameterization, to calculate a parameter called the incidence angle modifier (IAM).
The IAM is supposed to give information about how much radiation the module receives, compared to an incidence angle of zero.

The general formula to calculate the IAM correction factor is:

$$F_{IAM} = 1 - b_0 \cdot \left(\frac{1}{\cos i} - 1\right) \tag{2.23}$$

Where F_{IAM} is the parameter representing the amount of radiation absorbed by the module, i is the incidence angle of the incoming sunlight, relative to the normal of the module surface.
The parameter b_0 is a module specific constant, measured to be approximately 0.05 for crystalline modules [**9**][array incidence loss].

When the incidence angle i is 0, the absorption parameter F_{IAM} is 1, indicating that the module is receiving the full power of the sun.
Thus, tilting the panel perpendicular to the sun will ensure better utilization of the sunlight incident on the module, minimizing reflection [**6**].

2.2.8 Shading loss

The current output of a solar module inherently is proportional to the amount of irradiance incident on the cell.
This means that when, the irradiance is lower, the produced current is lower, and when the irradiance is absent, the current production diminishes.

Thus, when a cell is shaded, the current production of the shaded cells is lowered and in worst case diminishes. If all the module cells are connected in series, this means that the module output current is lowered to that of the weakest cell, and in the worst case scenario becomes unproductive.

Because a load still exists, the current produced from the unshaded cells in a string still continues to flow. This makes the unproductive cells act as a resistive load, which in turn leads to power dissipating in the cell (Figure 17, right).
When this happens, the cell heats up. This is why the phenomenon is called hot-spot formation.

At his point if, for some reason, the module goes into short circuit, or the current produced from the unshaded cells is high enough, the power dissipated might damage the cell or even lead to a fire.

To circumvent such outfalls, the cell-strings in a module are usually equipped by bypass-diodes (Figure 17, left). These diodes allow the current of the unshaded cells to bypass the shaded cells, with the extra benefit of exploiting the power production of the unshaded cells [**6**][interconnection effects].

Figure 17: Illustration of hot-spot formation (left) and application of bypass-diodes (right).

2.2.9 Soiling loss

The meaning of soiling might seem obvious, stemming from the word soil.
In terms of PV-systems, soiling is regarded as dust, dirt, sediments, bird droppings and other impurities that might deposit on the modules.
Snowfall is of particular importance in the regions where it applies.

The natural result of this is a reduced transmission of sunlight through the module front (glass cover), consequently lowering the module efficiency.

The remedy is quite simple: washing or cleaning the module will redeem some, or all, of the efficiency lost.
Naturally, rainfall performs this job, so a sufficient tilt angle is required to for the module to be "self-cleaning". The suggested minimum required tilt angle to acquire this is 12° [**4**].

The arrangement of the module might be of importance.
Maintaining an upright position on the module might totally kill the current production of a module due to snow in the winter months (Figure 18).
This due to the effect of bypass-diodes explained in the previous section.
If a vertical arrangement is to be used, the snow should therefore be regularly removed. Using a horizontal arrangement limits the impact of the snow to concern only a few cell strings [**4**].

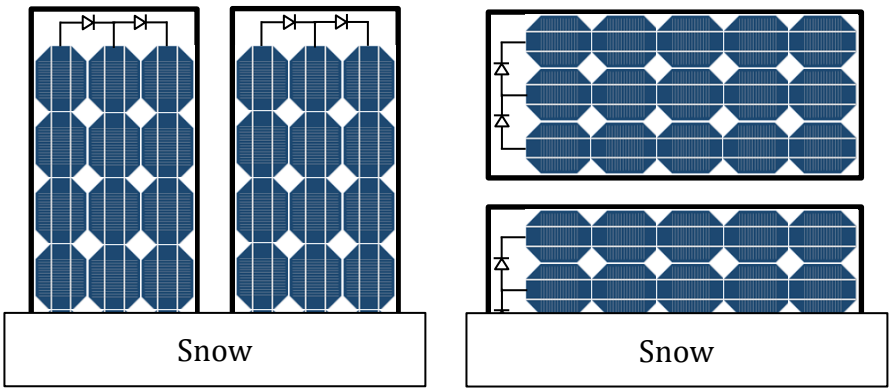

Figure 18: Arrangement of modules to minimize snow-soiling loss

Many studies have been conducted to investigate, and determine, not only the effects of soiling, but also the amount of it. Different regions, habitats, and indeed different topographies, might have different amounts of soiling - owing to the relative inconsistent frequency of rain, wind speed distribution, etc.
And this won't necessary translate between continents or countries, despite the similarities of the sites where studies have been conducted.

Suggested values for loss in forecasted yield due to overall soiling are in the range 2 - 5% [**4**], which is consistent with studies conducted. Other studies report values as high as 7%, though this might be lower in years with higher frequency of rain [**16**]. The PVsyst simulation software states that middle-European countries can assume an overall loss of 1% [**9**][soiling loss].

Soiling due to presence of snow is still not very well investigated, and the losses are therefore highly uncertain. A few studies conducted suggest annual values of around 2-3% for snow loss as appropriate [**16**].
One study conducted in Ontario, Canada - found that the soiling loss due to snow varies between 1 % and 3.5 %, for a tilt angle between 60° and 10°, respectively. This suggests that a tilt angle of at least 60° is required for automatic snow shed [**18**].

2.3 The solar resource and related parameters

Because a PV-generator converts electromagnetic radiation dispatched from the sun into electricity, the amount of radiation available for power generation, therefore, is of great importance when considering feasibility of a PV-system.

The amount of radiation available at the earth's surface, for utilization in a solar power plant, differs significantly from that outside the earth atmosphere.
At the edge of the earth's atmosphere, the irradiation received generally varies due to the elliptic path of the earth around the sun, and the average value is given by the *solar constant* (S_0):

$$S_0 = 1367\ W/m^2$$

This radiation usually suffers attenuation on its path towards the earth surface, resulting in an irradiance of varying intensity. This is due to atmospheric effects and weather, and the radiation will therefore vary with season and time of day, in addition to latitude [**4**].

2.3.1 Solar geometry: Heliocentrism

The heliocentric model of earth orbit dictates how perceive the motion of the sun relative to that of the earth. Our very own concept of time has been tied to this model, and the relations between our time-units and the motion of the sun has been found.

As such, the earth in our perception performs one revolution around its own polar axis in one earth day, consisting of 24 hours, and one revolution around the sun in one earth year, consisting of 365 earth days.

The heliocentric model is illustrated in Figure 19, showing the earth at different points in its elliptic path, corresponding to different times in the year.
March 21st and September 21st is the vernal-, and autumnal equinox, respectively. June 21st and December 21st corresponds to the summer-, and winter solstice, respectively.

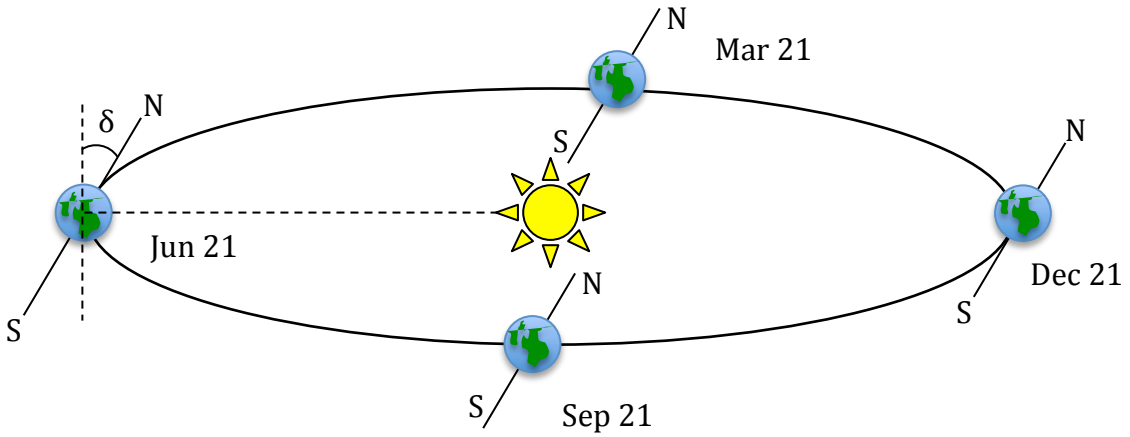

Figure 19: The heliocentric model showing the earth orbit around the sun at equinox and solstice dates

As can be seen from the figure, the earth polar axis is tilted away from the axis normal to the plane of the sun. This tilt is the reason the sun is high in the sky at summer and low in the winter, in the northern hemisphere.

The parameter δ is termed the earth declination angle; it is at its maximum of 23.45° at summer solstice and at minimum (- 23.45°) at winter solstice.
At the equinoxes, the declination is zero, meaning that the sun is directly above the equator [**13**].

The earth is divided into meridians, where the time is termed local time (LT). The LT changes according to the time zones, which are stated according to the prime meridian at Greenwich, Great Britain, where the LT is called Greenwich Mean Time (GMT). The prime meridian has longitude 0°.

Because one revolution (360°) of the earth around its polar axis takes 24 hours, one hour corresponds to 15° degrees of angular motion.
The concept of local standard time meridian (LSTM) is used to state the position of a meridian (time zone) relative to the prime meridian at Greenwich:

$$LSTM = 15° \cdot \Delta T_{GMT} \tag{2.24}$$

Where ΔT_{GMT} is the difference between LT and GMT in hours.

The LSTM is used to find the local solar time (LST) of a site in hours.
The LST differs from the LT due to the fact that a day length varies through the year, as a consequence of the elliptical orbit of earth around the sun.
The LST is calculated from eq. (2.25):

$$LST = LT + \frac{TC}{60} \tag{2.25}$$

The time-correction factor (TC) is measured in minutes and is calculated from formula (2.26) to account for the difference in longitude between a given site and the reference meridian of the time zone.

$$TC = 4(longditude - LSTM) + EoT \tag{2.26}$$

The equation of time (EoT) corrects for the eccentricity in earth's orbit and the axial tilt, it is given by the following formula:

$$EoT = 9.87 \sin 2B - 7.53 \cos B - 1.5 \sin B \tag{2.27}$$
$$B = \frac{360}{365}(d - 81)$$

Where *B* is stated in degrees and *d* is the day number of the year.

The hour angle (HRA) is defined as the discrepancy between the meridian of the sun, and the meridian of the respective site.

With the LST, the HRA can be calculated according to:

$$HRA = 15°(LST - 12) \tag{2.28}$$

The hour angle is negative in the morning, positive in the evening and exactly zero at solar noon [**6**].

2.3.2 Angles definition

Related to the motion of the sun relative to an observer on earth are several angles. If the PV-module is regarded as the observer, then the angles (in degrees) the sun makes with the position of the observer can be seen in Figure 20 [**4**]:

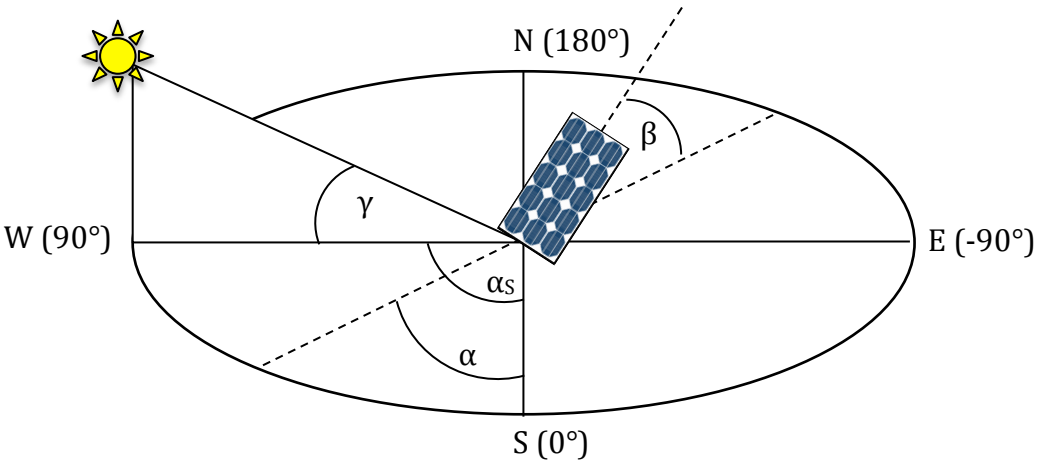

Figure 20: Illustration of the different angles the sun makes with an observer (module) on earth

In the figure, south is defined as 0°, north as 180°, west as 90° and east as - 90°. The azimuth angle (α) and the sun azimuth angle (α_S) are regarded as the angle the module, and the sun, is oriented with respect to the south, respectively. The module tilt angle (β) is regarded as the angle between the module plane and the horizontal plane. The solar elevation angle (γ), or sun height, is the angle between the sun in the sky and the horizontal plane.

The sun azimuth angle (α_S) is dependent on the latitude (φ), declination angle (δ), the HRA and the sun height (γ).
It can be calculated from the following relation [**6**]:

$$\cos\alpha_S = \frac{\sin\delta \cdot \sin\varphi + \cos\delta \cdot \sin\varphi \cdot \cos(HRA)}{\cos\gamma} \tag{2.29}$$

The sun height, in turn, is calculated from the following expression:

$$\sin\gamma = \sin\delta \cdot \sin\varphi + \cos\delta \cdot \cos\varphi \cdot \cos(HRA) \tag{2.30}$$

The declination angle changes throughout the year, so it must calculated from:

$$\delta = 23.45° \cdot \sin B \tag{2.31}$$

Where B has been defined in eq. (2.27).

With all the above-defined angles it will be possible to calculate the sun path throughout the year, and construct sun-path diagrams.
These will be explained in detail in chapter 3.

According to sun path diagrams, the sun is highest in the sky midday for an azimuth degree of zero degrees. Thus, this is the optimal module azimuth for fixed modules.

When considering the optimum fixed tilt angle of a module, there is an ambiguity related to its determination. Most literature found on the subject states optimum tilt angles for latitudes below 50°, here it seems that the relationship between latitude and optimal fixed tilt is rather well known.
However, above 50°, it seems that the relation is more complex and subject to calculation, a solar consultant firm stated [**19**]. This is mainly related to the longer sun path when the sun is lower in the horizon and the effects of clouds reflecting light, making the optimum tilt more site specific [**20**].

To obtain the maximum of incident radiation, it may be best to vary the tilt through the year, according to season. A fixed tilt of $\beta = 15° - \varphi$ may seem beneficial for optimal summer performance, whereas a tilt of $\beta = 15° + \varphi$ seems beneficial for optimal winter performance.
To assure the best average performance in spring, fall and/or over the year, an optimum fixed tilt of $\beta = 0.9\varphi$ is supposed to be necessary.
Obviously, to assure maximum at all times, a combination of the above tilt angles must be used

Incorporating trackers into a system allows for following the sun path over the course of the day. One-axis trackers are available for tracking both horizontally and vertically. However, two axis trackers are also available for tracking in both directions. The incorporation of such trackers is usually subject to evaluation of price vs. increased yield, as the components are costly. The components might suffer from breakdown, reducing system availability, and hence, yield. Also the added maintenance costs might drive up the price of LCOE.

2.3.3 Radiation; Quantization and atmospheric effects

Solar radiation is usually measured as either *irradiance* or *irradiation.*
Irradiation is a measure of the amount of collected energy in a given timespan, it can be stated in kWh/m^2/time, Wh/m^2/time or MJ/m^2/time.
Here, *time* may be day(s), month(s) or year(s). Thus, irradiation is the energy density of the solar resource.

Dividing a collected amount of energy (irradiation value), on the timespan in which it is collected, gives irradiance. It is usually stated in W/m^2.
Thus, irradiance is the power density of the solar resource [**13**].

The atmosphere consists of various gaseous components, including Ozone (O_3), Oxygen (O_2), Carbon dioxide (CO_2) and water vapor (H_2O).
These components will interfere with the incident electromagnetic radiation from the sun by either scattering it, reflecting it or even amplifying it.

The power density experienced at a given site will be dependent on the specific spectral irradiance of the light. The spectral irradiance is in turn dependent on the attenuation effects the light experiences on its way towards the ground.

Figure 21 [**21**] shows how the solar spectral irradiance is at the edge of the atmosphere (AM0), and at sea level (AM1), compared to that of a blackbody at a temperature close to that of the sun. Different atmospheric constituents are pinned to points where dips occur in the graph, indicating their influence on the spectral irradiance.

According to eq. (2.1), the photon energy necessary to dislodge an electron in a solar cell needs to be larger than the band gap energy. The photon energy is proportional to the frequency of the sunlight, which in turn is inversely proportional to the wavelength. The low spectral irradiance in the lower part (400 - 500 nm) of the visible spectrum due to attenuation means that few photons in this range can be utilized for current production.

The attenuation effects are more severe when the path length for the sunlight though the atmosphere is long. This path length is often defined using the concept of air mass (AM), which is calculated according to:

$$AM = \frac{1}{\cos\theta_Z} \tag{2.32}$$

Where θ_Z is the sun-zenith angle.

AM0 corresponds to zero atmospheres, like in the case of outer space, where no air is existent. AM1 is defined as one standard atmosphere, which is the case when the zenith angle is 0°.
Whenever the zenith angle deviates from 0°, the air mass will increase, lowering the amount of photons available for current production.

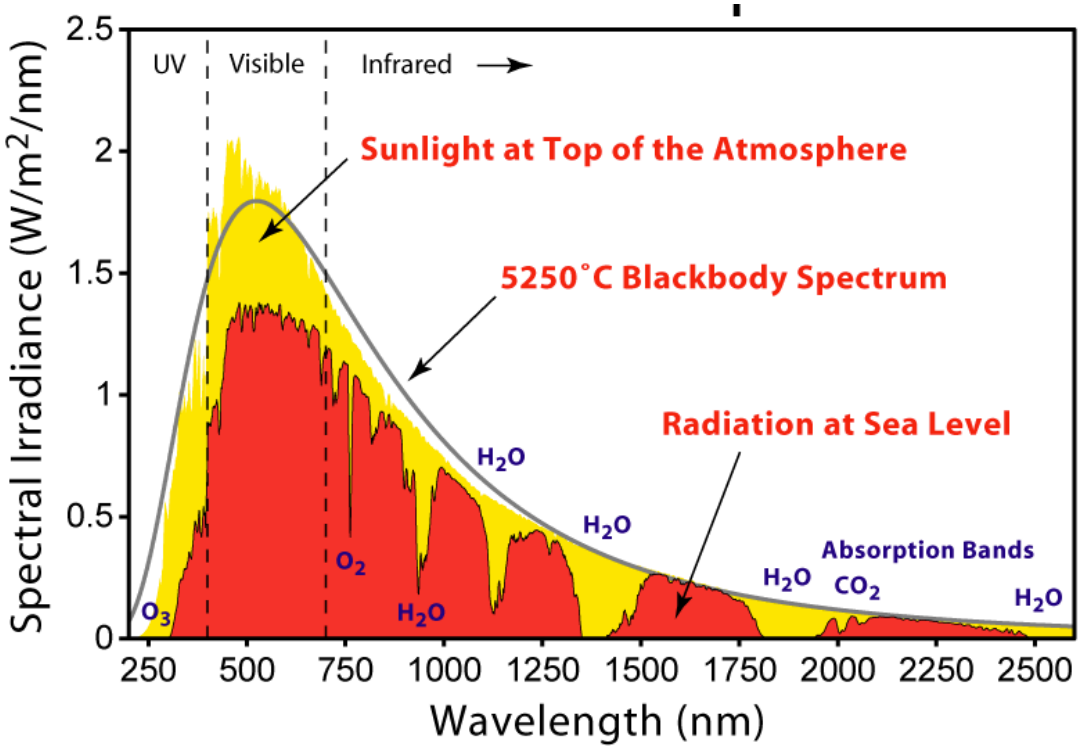

Figure 21: The solar irradiance spectrum at edge of the atmosphere and at the surface of the earth [21]

Figure 22 shows how sunlight divides into different components as it mediates in the earth atmosphere, as well as the zenith angle between the sun and the vertical. As it appears, direct radiation dispatched from the sun is partly scattered into *diffuse radiation* by for example aerosols, before it may reach a cloud. Here the radiation may be scattered again and/or *reflected*.
Direct radiation may also be reflected off the ground, in which case it is sometimes termed *albedo* radiation [**4**].

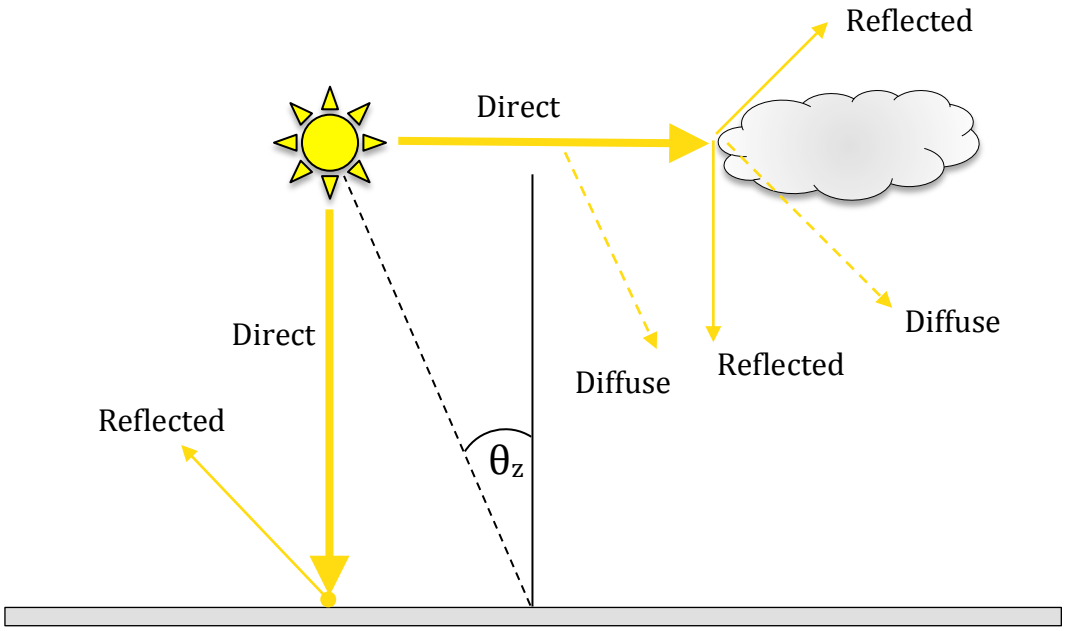

Figure 22: Illustration of the different radiation components from the sun and the zenith angle θ_z

The sum of direct-, diffuse- and ground-reflected radiation is termed *global radiation*.

Eq. (2.32) defines global horizontal radiation mathematically:

$$G_G = G_B + G_D + G_R \tag{2.32}$$

Where G_G is the global horizontal irradiance (GH), G_B direct beam horizontal irradiance (BH), G_D the diffuse irradiance (DH) and G_R the ground-reflected irradiance (GDR).

Normally, the ground-reflected irradiance is negligible for a horizontal surface, in which case eq. (2.32) can be revised:

$$G_G = G_B + G_D \cdot \cos\theta_Z \tag{2.33}$$

Where θ_Z is the zenith angle [**22**].

However, for a tilted surface, the ground-reflected irradiance makes a significant contribution to the global irradiance, and can't be ignored.
The formula for a tilted surface is:

$$G_G{}^T = G_B{}^T + G_D{}^T + G_R{}^T \tag{2.34}$$

Where the variable names are the same as in eq. (2.31), only indexed *T* for tilt.

The variables in eq. (2.34) are calculated with eq. (2.35), (2.36) and (2.37):

$$G_B{}^T = G_B \cdot R_B(\alpha, \beta, \delta, \varphi) \tag{2.35}$$

Where R_B is the ratio of average daily direct beam radiation on a tilted surface to that incident on a horizontal surface, called the *transposition factor*.
It is a function of azimuth angle, tilt angle, declination angle and latitude and should be as large as possible to maximize the incident energy.

$$G_D{}^T = G_D \cdot \left(\frac{1 + \cos\beta}{2}\right) \tag{2.36}$$

$$G_R{}^T = \rho_a \cdot (G_B + G_D) \cdot \left(\frac{1 - \cos\beta}{2}\right) \tag{2.37}$$

Where ρ_a is the albedo factor.

The albedo factor is defined as the ratio of reflected radiation to the initial radiation incident on <u>*a*</u> surface. It has a value between zero and one; zero meaning all radiation is absorbed, and vice versa.
For reference, asphalt has an albedo value of approx. 0.15, while fresh snow has a value of 0.85. [**23**]

From the above equations, it can be observed that the diffuse component will decrease with increasing tilt, whereas the reflective component increases. The reflective component vanishes totally for a tilt angle of zero, which is in accordance with the assumption that it is negligible for horizontal mounting.

It should be noted that occasionally, blue skies with dispersed clouds might actually help amplify the incident radiation at a site.
Radiation reflected off clouds may help to peak the global horizontal irradiance to values as high as 1400 W/m^2.

In the case of attenuation, by the time the solar radiation reaches the earth surface, the irradiance at AM1 has been reduced to approximately 1000 W/m^2. This value is regarded relatively independent on location [**4**].

2.4. Meteorological data and availability

Knowledge of where to find meteorological data and information about their accuracy is of key importance when conducting an investigation on the feasibility of a PV-system. Because the PV-generator is highly dependent on the solar resource in order to be able to convert energy, a miss-assessment of the solar resource could be decisive in determining the commercial viability for a potential project. Indeed, that is the background for this thesis.

Data is usually acquired from either a weather station close to the site location, when available, or from databases, when necessary.

2.4.1 Weather stations

Meteorological data used in feasibility studies should be, as far as possible, collected from weather stations within the proximity of the project site.
The definition of proximity might be tricky, but in the simulation program used for this thesis, the *climatic distance* shouldn't exceed 20 km.

The climatic distance takes the difference in altitude, and the horizontal distance between weather station and site, into consideration.

It is calculated according to the following formula [**6**][glossary]

$$D_{climatic} = \sqrt{((D_{horizontal})^2 + (\Delta H_{AMSL})^2)} \tag{2.37}$$

Where $D_{climatic}$ is the climatic distance, $D_{horizontal}$ is the horizontal distance and ΔH_{AMSL} is the difference in altitude between the weather station and project site. The altitude of a location is measured as average meters above sea level (AMSL).

The horizontal distance is calculated as the *great circle distance* (GCD) - the shortest path between two points on a sphere. If we assume the earth is a perfect sphere, the horizontal distance between any two points can be calculated mathematically:

$$D_{horizontal} = R_e \cdot \Delta\hat{\sigma} \tag{2.38}$$

Where R_e is the radius of the earth and $\Delta\hat{\sigma}$ is the *spherical central angle*.

The spherical central angle is the arc length between two points on a sphere in radians; it is calculated from the following formula:

$$\Delta\hat{\sigma} = 2\sin^{-1}\left(\sqrt{\sin^2\left(\frac{\Delta\varphi}{2}\right)} + \cos\varphi_1 \cdot \cos\varphi_2 \cdot \sin^2\left(\frac{\Delta\lambda}{2}\right)\right) \tag{2.39}$$

Where φ_1 and φ_2 is the latitude coordinate of location 1 and location 2, stated in decimal degrees. $\Delta\varphi$ and $\Delta\lambda$ is the change in latitude-, and longitude-degrees, respectively.

2.4.2 Databases

Often, few or none weather stations may be available within the proximity of the project location. Many times, also when nearby weather stations can be found, their data may be unreliable due to short time-series or missing data points.

In these cases, the use of databases may be necessary. Several databases are in use today; they usually hold collections of data measured by either satellite or larger weather stations. These data can then be transposed or interpolated to find representative data for the location in question.

It should be noted that, in many cases, these data might be highly inaccurate, depending on the latitude of the site location. Often, there are only a few reference weather stations available for interpolation, resulting in a large uncertainty in the interpolated data. The same goes for transposed satellite data.

2.4.3 Relevant parameters

The meteorological data collected doesn't only concern the solar resource, i.e. irradiance data, but also other parameters relevant for system performance (see 2.2 System performance and loss factors).

Usually, it may be relevant to collect data for the following parameters:

- Irradiance (Global and/or diffuse, occasionally reflected)
- Ambient temperature
- Wind speed
- Snow cover (where applicable)
- Albedo (where applicable)

Snow may not be present everywhere, and is thus not relevant for all locations. Albedo measurements don't always exist, and they are really only necessary at locations where the surroundings are either very absorbent or reflecting.

2.4.4 Measurement of meteorological data

The temporal resolution of the data depends on the source; standard resolutions are hourly, daily or monthly, but occasionally minute-resolution is also available.

The measurement of the available solar resource is usually done by a *pyranometer*. It is a device constructed to measure the total power available in any incident spectrum, and hence measures the global irradiance available.
It works by placing an absorbing surface within two concentric glass domes, and measuring the heating of the surface relative to the surroundings [**13**].

A type CMP3 pyranometer from the well-known manufacturer of solar radiation measurement instruments, Kipp & Zonen, is shown in Figure 23:

Figure 23: Picture of a CMP3 pyranometer from Kipp & Zonen [24].

To measure diffuse radiation, it is possible to equip the pyranometer with a shade screen in the shape of a bow.
This screen will allow casting a shade on the glass dome, covering the absorber surface, for the entire sun path of a specific day. The screen has to be readjusted every now and then to follow the sun height [**13**].

Reflected radiation may be measured by installing a pyranometer upside-down [**25**].

Because the pyranometer measures radiation thermally, it is inherently a little slow, and thus doesn't allow for measuring of irradiance peaks.
Consequently, if the sun disappears momentarily behind a cloud, this will normally not be reflected in the time-series, despite high temporal resolution [**4**].

The pyranometer usually measures horizontal radiation, but can be fastened in an arbitrary tilt angle to measure the irradiance on an inclined surface.

The ambient temperature of a location is usually measured with an electrical thermometer, a so-called thermocouple, or resistance thermometer. It is often stated at either 2 or 10 AMSL, in degrees Celsius.

Wind speed is often measured with an anemometer, either 2 or 10 AMSL. These are either electromechanical (cup or vane anemometer) or purely electric (ultrasonic). Cup anemometers measure only wind speed, while vane and ultrasonic anemometers measure direction as well.

Snow cover is measured by observation, and requires an observer.
The snow cover is stated according to a code in the range 0 – 4, where 0 means no snow and 4 means the ground is completely covered in snow.
Consequently, every non-zero code unit may be interpreted as 25% cover.
The stated code is valid within a radius of 1 km from the weather station [**26**].

Albedo is usually stated as the ratio of measured reflected to global irradiance. Thus, if both global and reflected radiation is measured, the ratio is calculated. This then allows for calculating the direct beam component of the radiation.

2.5. Deviation and uncertainty

Whenever evaluating collections of data, certain statistical definitions are used to state the uncertainty in the data. When possessing a collection of yearly irradiation data, there is generally no correct value for what the yearly irradiation should be. In this case, uncertainty is stated relative to the mean. On the other hand, whenever a correct value does exist, the uncertainty of the measured values is stated relative to this "true" value, and is called error [**27**].

2.5.1 Uncertainty related to the mean

Let the variable *x* define the measured value of something measurable, i.e. yearly irradiation. The collection of all yearly values measured ever would then be the population of measurements. A limited number of yearly values would be called a sample.

Dealing with meteorological data- and time-series is often related to defining a representative value for a typical day, month, year, etc. This involves finding so-called expected values for a data sample, e.g. yearly irradiation.

If we have a certain number of measured monthly values, let's say x_1, x_2, x_3, …, x_n, where *n* signifies the total amount of measurements, the *expected value* might be found by the arithmetic average, or mean:

$$\bar{x} = \frac{1}{n}\sum_{i=0}^{n} x_i \tag{2.40}$$

Where $\bar{x}$ is the expected value (mean) and x_i is the value of measurement *i* from a total of *n* measurements.

When a value for the mean is obtained, it is possible to investigate how the measured values deviate from the expected value. Deviation can be defined mathematically as:

$$d_i = x_i - \bar{x} \tag{2.41}$$

Where d_i is the calculated deviation of measured value *i* from the mean.

If the measured values are close to the mean, our measurements are relatively homogeneous. The mean can then be regarded as a more accurate representative for the expected value.
In the opposite case, the measured values are said to be heterogeneous, or spread, and the mean does not reflect an expected value.

One way to assess the homogeneity of the time series is by looking at the *absolute average deviance*. The formula used to calculate it is:

$$|\bar{d}| = \frac{1}{n}\sum_{i=0}^{n} |d_i| \tag{2.42}$$

Where $|\bar{d}|$ is the absolute average deviance and $|d_i|$ is the absolute deviance of measurement number *i* out of *n* total measurements.
To evaluate deviances as "small" or "large", it is necessary to have reference values for comparison. As such, the use of deviation for investigating homogeneity is only useful between data-samples. It is then possible to deduce if one data-sample has a large deviance, compared to another data-sample.

Another, perhaps more common way of looking at homogeneity of a data-sample is by evaluating the *standard deviation*. Standard deviation (SD) is sometimes also referred to as variability. It is calculated according to this equation:

$$\sigma = \sqrt{\frac{\sum_{i=0}^{n} d_i^2}{n-1}} \tag{2.43}$$

Where σ is the standard deviation [**27**].

According to the *central limit theorem,* i*f* the values of measurements are random in nature, their means can be said to follow a *normal (or Gaussian) distribution.* This means that the probability function for the means is shaped as a so-called bell curve [**28**]; an example is shown in Figure 24 [**29**]:

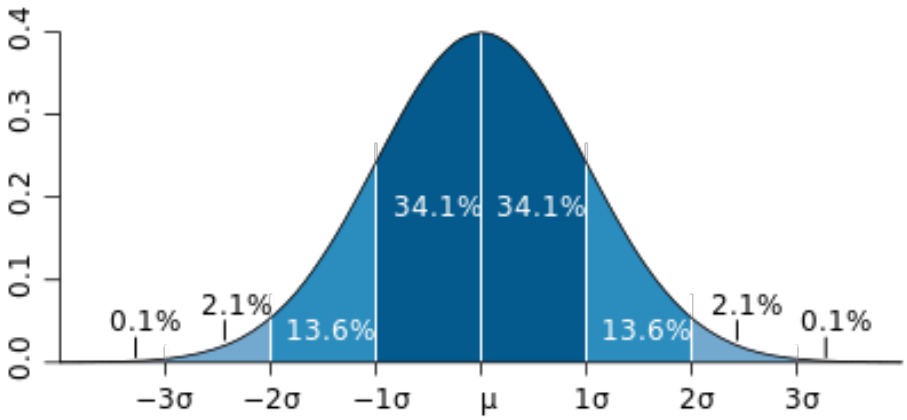

Figure 24: The probability function following the normal distribution [29].

In the above figure, the probability function is the solid curve. The horizontal axis shows the expected value (μ), with one, two and three standard deviations spread. The vertical axis shows the normalized probability of finding a value located on the curve. The sections of the area under the curve represent how much (in percent) of the total sample is located within the different ranges.
For example, 68.2% of all values in a sample will be located in the range μ ± σ.

In the case of irradiation, it is fair to assume that the irradiation measured one year, is no precursor of the irradiance the following year.
That is, the yearly mean irradiance is an independent variable, which is randomly distributed.

Hence, the yearly mean irradiation probability function follows the normal distribution. As such, any yearly mean irradiation calculated will be located somewhere on the probability function curve following a normal distribution. As the sample size increases, the expected value gets closer to its true value, and the spread gets smaller. Consequently, when evaluating data-samples, the smallest spread corresponds to a more precise value for the mean.

2.5.2 Uncertainty related to systematic error

Let the variable *x* remain the measured value of something measurable, like in the previous section, for example yearly irradiation.
Now, if a sample of these x's is acquired, and an expected value is known in advance, this value is termed *true value*.
The true value often exists when values are estimated from formulas or mathematical models, e.g. if the yearly irradiation for a specific year would already be known.

In this case, the deviation from the true (expected) value is termed *bias*, and eq. (2.41) can be modified to calculate this bias (b):

$$b = x_i - x_{true} \tag{2.44}$$

Where x_i is the measured value *i* of a total of *n* measurements and x_{true} is the true value of the measured parameter.

The ratio of the bias relative to the true value is called *bias error* (BE).
If the bias error is for all values is summed up and divided on the total number of measurements, the *mean bias error (MBE)* can be found:

$$MBE = \frac{1}{n}\sum_{i=0}^{n}\frac{x_i - x_{true}}{x_{true}} \tag{2.45}$$

The MBE is often multiplied by a factor 100 and stated in percent (%).

The MBE can be regarded as an analog to the (non-absolute) average deviation. It should be interpreted as the smallest deviation from the true value that can be found for a population of estimates and is considered better than RMSE in relating deviation [**30**].

The *root mean square error (RMSE)* is similar to the standard deviation. However, where the standard deviation is calculated using the mean, the RMSE is calculated using the true value, and using a different denominator:

$$RMSE = \sqrt{\frac{1}{n}\sum_{i=0}^{n}\left(\frac{x_i - x_{true}}{x_{true}}\right)^2} \tag{2.46}$$

The RMSE is often also multiplied by a factor 100 and stated in percent (%) [**27**].

The RMSE is used to disregard negative bias and to be able to state the deviation from the true value as a positive error. It is the largest value of error that can be found among a population of estimates, and is often less representative for error than MBE, but is stated to give grounds for comparing error [**30**].

2.6 Economical evaluation of PV-systems

To be able to evaluate a PV-system economically, it may be of use to introduce the principle of *specific cost*. It is generally defined as the price (in any currency) per installed watt-peak of PV-energy, but may just as well be used to define the price per produced watt-peak of solar cells.

Commercial viability of a PV-system is first and foremost decided by the price of the electricity produced. *Grid parity* is a term referring to the state where the price of power produced from a specific source, is low enough to compete with that of power produced from other sources.

As of today, the development of the PV-technology and increased production volumes continue to reduce the price of installed capacity.
This effect is termed the *learning rate* of the PV-industry. It says something about how much the specific cost of PV-power is reduced as accumulated production volume increases.

The learning rate of the PV-industry, together with the many existing support schemes in the world today, ensure that the PV-generated electricity may at some point in near future reach grid parity.

An analysis conducted has reported that by the end of 2010, of the countries in Europe, 80% have reached grid parity for residential PV-systems and 75% have reached grid parity for industrial PV-systems.
According to this analysis, Norway was not one of the countries to have reached grid parity in either sector.
However, the analysis forecasts that the residential PV-systems of Norway will have reached grid parity by 2015, and the industrial sector will follow in 2019 [**31**].

2.6.1 Levelized cost of energy (LCOE)

The levelized cost of energy/electricity (LCOE) is the usual way of comparing the price of produced energy. It is usually defined as the total lifecycle cost of the PV-system, divided by the total amount of energy produced during the entire lifecycle:

$$LCOE = \frac{Lifecycle\ cost}{Lifetime\ energy\ production} = \frac{C_{total}}{Q_{total}} \tag{2.47}$$

Where C_{total} and Q_{total} is the lifecycle cost, and lifetime energy production, respectively. Lifecycle costs includes all costs: Constructional, operational, maintenance and financial costs.

The LCOE can be calculated according to the following formula:

$$LCOE = \frac{C_{total}}{Q_{total}} = \frac{C_0 + \sum_{n=1}^{N} \frac{AO}{(1 + DR)^n} + \sum_{n=1}^{N} \frac{RV}{(1 + DR)^n}}{\sum_{n=1}^{N} \frac{Q_0 \cdot (1 - SDR)^n}{(1 + DR)^n}} \quad (2.48)$$

Where C_0 is the initial project cost, AO is the annual operating cost, RV is the residual value of the system and N is the system lifetime.
Q_0 is defined as the initial power output of the new system (year 1).
The system degradation rate (SDR) is the annual reduction the system output, resulting from degradation of system components [**32**].

3. Methodology: Data collection, simulation and analysis

In the following chapter, the methods utilized to collect necessary data for production of simulation forecasts are described, together with the setup for the analysis.

3.1 Chapter introduction

The process followed in this analysis is visualized in Figure 25:

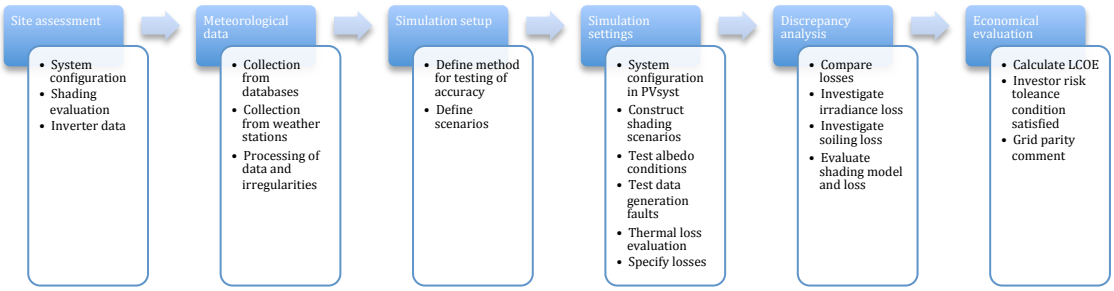

Figure 25: Work flow chart stating the steps of analysis

The chapter is divided in 9 subchapters:

3.1 Gives an overview over the methodology and chapters.

3.2 Gives an overview over the tools used in the thesis.

3.3 Gives an introduction to PVsyst and its user interface.

3.4 Explains the site assessment conducted and evaluation of shading.

3.5 Explains the collection and processing of meteorological data.

3.6 Explains the simulation setup and test conditions for forecast accuracy.

3.7 Specifies the simulation settings and the reasons the choices of them.

3.8 Specifies which sources of error were investigated after forecasting.

3.9 Specifies the conditions of the economical evaluation.

3.2 Tools

An overview of the tools used in this thesis can be found in
(Table A. 1), along with information about where to find them and which version was used. In order to better comprehend the methodology used, a brief description of these tools follow.

AutoCAD is software for *computer-aided design* (CAD).
It can be used for 2D and 3D design of just about anything, and as such is utilized by architects and draftsmen, among others.
The drawings displayed are often made in ratio 1:1, meaning that they have the same size as the object would in reality.
Thus, accurate measurements of object dimensions, distances between objects and angles can be conducted in the user interface. The precision is usually to four decimal places.

Global Mapper is a *geographic information system* (GIS) software package.
It is mainly used for viewing accurate digital maps, containing information about the topographical profile of a landscape. This includes elevation data and coordinates, which lets the user find exact statements of elevation for a given coordinate, among other things.
The program also can process so-called LiDAR data, which is a portmanteau (combination) of light and radar, reflecting the use of laser light and radar processing to make high-resolution 3D maps.
These maps contain accurate information on the spatial dimensions of every object found on the ground, which can be used for an arbitrary purpose.

Google Maps is online digital mapping software, allowing the user to search for addresses and find the coordinates of these addresses, or arbitrary points over the whole world. It features regular maps and satellite images, in addition to street viewing, which enables the user to grossly evaluate location surroundings without resorting to more advanced software like the global mapper.

Microsoft Excel is computer calculation software that utilizes tables in order to process datasets. It is able to perform regular arithmetics, as well as heavier mathematical operations, in addition to statistical calculations.
Excel is compatible with Microsoft Word, which lets the user transfer tabular data effortless between the two programs.

Microsoft Word is document-processing software, mainly used to write documents. Earlier versions have been regarded by many as inadequate for writing larger literary works as books and theses, although this perception changing. The program continuously offers increased graphic handling abilities with every update, rendering it a good all in one solution for documents like this thesis.

SunEarthTools is an online tool intended for use by solar professionals.
It utilizes a Google Maps plugin that allows the user to do the same as in Google Maps, although with higher coordinate accuracy. Also, it provides a way to convert between different coordinate formats, measure distances between

points on the map and the orientation of buildings and objects, among other functions related to astrological geometry.

The accuracy of the location finder in the program is related to the number of decimal places, the precision, of the location coordinates used as input.
This is due to the assumption that earth is a perfect sphere, and equal to all applications that handle coordinates.
When pinpointing a location, the coordinates are given with a precision of 5 decimal places.

Table 1 shows to which accuracy a location on the map is found, as a function of the longitude-coordinate precision choice. Stating longitude-coordinates to a precision of 5 decimal places results in an accuracy of ±1.11 m around the equator. The accuracy increases towards the poles.

Table 1: The accuracy of the distance measurements in Sun EarthTools

Places	Decimal deg.	Degrees	Distance
0	1	1°0’0"	111.319 km
1	0.1	0°6’0"	11.132 km
2	0.01	0°0’36"	1.113 km
3	0.001	0°0’3.6"	111.3 m
4	0.0001	0°0’0.36"	11.13 m
5	0.00001	0°0’0.036"	1.11 m
6	0.000001	0°0’0.0036"	11.1 cm
7	0.0000001	0°0’0.00036"	1.11 cm

The distance measurements are reported to have an error of 0.3% at the polar extremes, decreasing towards equator.
The orientation measurements presumably don't have any significant errors.

Theodolite Droid is a tool intended for use on mobile devices.
It allows the user to get approximate coordinates for the site where the device is located, orientation (azimuth) and horizon elevation angle.
In addition, it is possible to measure the height and distances to objects, by using the gyroscope built into the mobile device.

No information about the error of the application is found, but information about a very similar application developed for apple, states that the GPS coordinates are accurate to 10 feet under optimal conditions. The precision of coordinates is stated to the equivalent of 4 decimal places, giving an accuracy of ±11.13 m according to Table 1.
The accuracy of the gyroscope may be assumed to be 0.1 degrees, and accuracy of the azimuth measurements 2 – 5° according to the same source [**33**].

3.3 Introduction to the simulation software: PVsyst

Out of the many that exist, PVsyst is one of the most used simulation tools used in the PV industry today. It was authored and founded by Dr. André Mermoud, together with co-founder Michel Villoz.

The program was chosen because the supervisors of this thesis knew of it, in addition to the use by other authors in former reports. Studies conducted have described the software as one of the most detailed simulation programs available, used by engineers to verify production forecasts for investors.
Its main strengths are regarded as the shading evaluations [**34**].

The software version is continuously updated, in order to improve the software and correct faults. Therefore, future use of this software may yield other results than the ones obtained in this thesis. At the time of this thesis was printed, the most recent update was to version 6.2.2.

For the sake of brevity, only the basic information about the software is given. All fundamental information that may be of interest to the reader about the software, including models used and calculation methods may be found in the PVsyst help file online [**9**].

3.3.1 User interface

The user interface of PVsyst is shown underneath in Figure 26. It features four sections; of which the three lower are the most relevant for this thesis.

Figure 26: The user interface in PVsyst

Tools contain different choices for evaluating a PV-system. Functions here include the possibility of optimizing the system tilt- and azimuth-angle, investigating a solar module shading behavior as a result of different bypass-diode design, in addition to analysis tools for comparison of modeled and actual system behavior. In this thesis, this section was used to display the graphs for temperature and low irradiance behavior of the solar modules in chapter 2.

Databases contain a lot of useful information. It is divided into to sections:
The *component database* contains specifications for most BoS-components, like inverters, but also a module database exists.
The databases are linked to different online sources, Photon international solar energy magazine, being one of them.
This ensures that new module and inverter models are added to the software database as soon as they are released for sale.
Sometimes, when specifications for a system component is absent or incomplete, the user may specify a new component, using the component datasheet as input.

The *meteo database* contains different options related to meteorological data.

Under geographical sites, different predefined locations around the world are stored, together with meteorological data.
New sites are defined by coordinate and altitude (AMSL), and the meteorological data for the different locations can be hauled from one of the built in databases, like the NASA SSE database or Meteonorm.

If meteorological data is to be defined by the user, perhaps taken from a source close to the site, average monthly values are required for a whole year.

The necessary parameter input is:

- Global irradiance/irradiation (mandatory)
- Diffuse irradiance/irradiation (optional)
- Temperature (mandatory)
- Wind speed (optional)

The user must supply the mandatory input in any case. If the optional input is not available, it can be omitted. However, for the most accurate results, it is advisable to supply all the optional data when defining a site.

Regardless of the availability of input, under the synthetic hourly data generation tab, the user can let the program generate synthetic hourly data for both mandatory and optional parameters. For irradiance, this is done by constructing daily values first by probability models incorporating measured data from weather stations around the world. Then hourly values are constructed.
In short, a mathematical model is applied, which transposes the irradiance data to the tilted plane by calculating the transposition factor R shown in eq. (2.35). This transposition is independent for the diffuse factor, which is calculated by a so-called Perez model and then corrected using a so-called Liu-Jordan correlation. Finally the irradiance data are fit under a Gaussian curve representing a perfect clear sky sun path, for every day of the year.

An excerpt showing such a clear sky day and the generated hourly data is shown below in Figure 27:

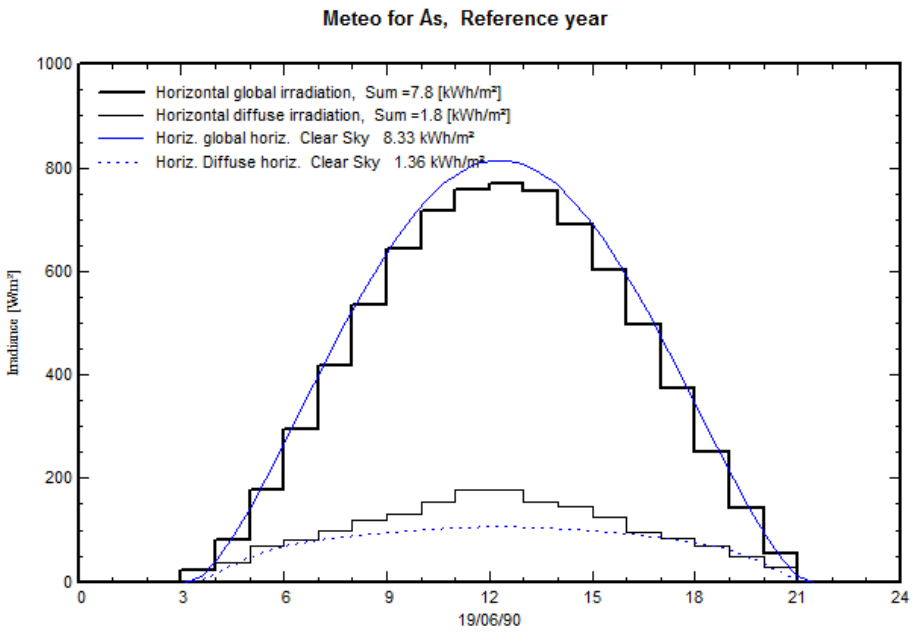

Figure 27: Excerpt of PVsyst showing generated hourly synthetic irradiance data

In the sun path diagram, the step-curve represents the synthetic hourly data, as their amplitude is constant in one-hour steps, with intermittent jumps.
The solid blue curve is calculated from the equations in chapter 2.3.2 and represents the sun path of a clear sky day.
Sometimes a time shift may appear, which means that the black curve is shifted either to the left (-) or right (+) of the clear sky curve. This implies that the sun rises earlier (-) or later (+) in the generated data, than in the sun path.
This may induce errors in the simulations or higher IAM losses, especially in the morning [**35**][meteodata/POA].

Temperature data are usually generated more random, but generally are assumed to correlate to the irradiance, as in eq. (2.18). The generated data are then adjusted according to Swiss region topology, as the program is Swiss.
The generality of the data can't be proven, but Switzerland and Norway indeed share many common traits in terms of climate.

Wind data are generally not converted to hourly values, as no algorithm for this exists in PVsyst.

Meteo tables and graphs is the name of the tab where the hourly irradiation data may be visualized or tabulated. The visualization is in the form of sun path diagrams. Under this tab, one might also find the time shift of generated or imported hourly data (done with another tab). An example of a sun path diagram is shown below:

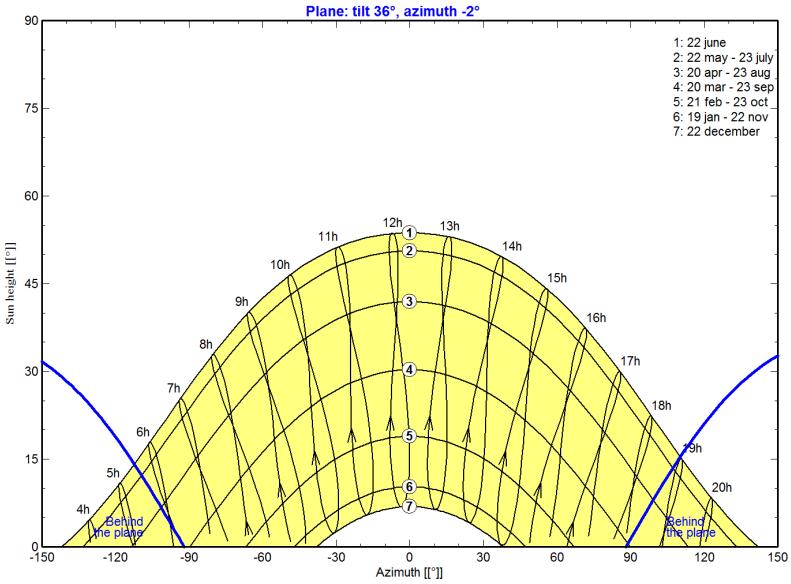

Figure 28: Sun path diagram from PVsyst

The figure above shows the sun path for the latitude and site at Aas, with the marked locations in the shortest day of the year (December 22nd) and the longest day of the year (June 22nd). The sun height on is the vertical axis and the azimuth angle is on the horizontal axis.

3.3.2 Project design

Under the project design tab (Figure 26), one may choose to define a grid-connected project, which is what was done for this thesis. An excerpt of the screen dialog is shown below in Figure 29:

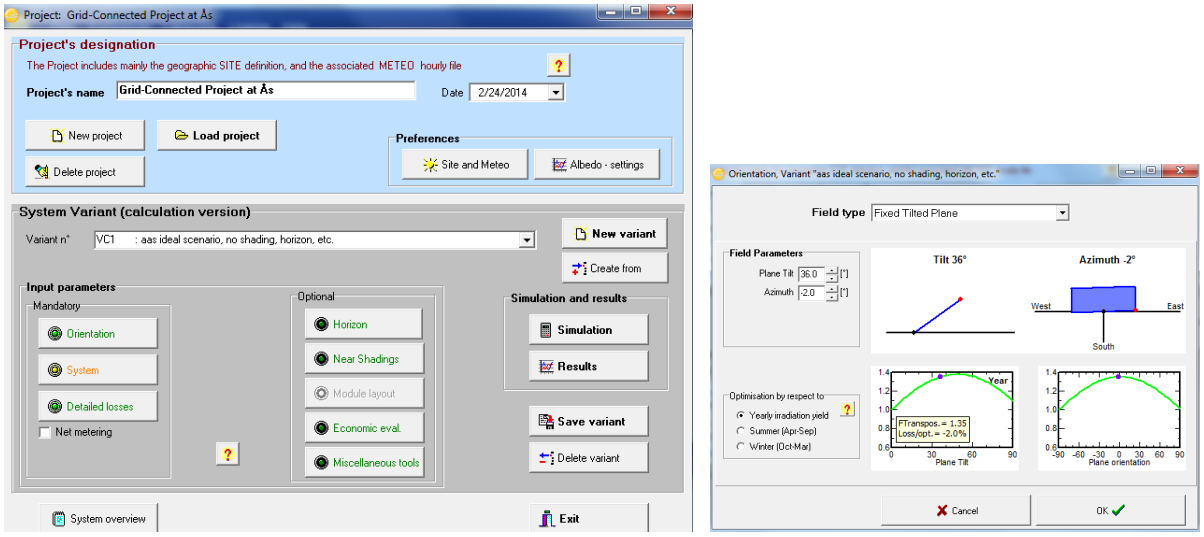

Figure 29: Project design dialog in PVsyst and module orientation

The *site and meteo* tab allows the user to specify the location of the site directly or choose another location specified in the *geographical sites* tab, explained in the last section. Also, one is allowed to specify the location meteorological parameters in monthly values. The corresponding synthetic hourly file may be chosen from a list or generated directly from the dialog window.

The *albedo - settings* tab allows for specifying the albedo value of the site on a monthly basis (eq. 2.37). Also, one may define the site-specific reference temperatures. This involves specifying the absolute lowest temperature of the site, ever recorded, the normal winter operating temperature, the usual operating temperature under an irradiance of 1000 W/m^2 and the summer operating temperature. One may also choose if the voltage temperature coefficient (2.1.7 Module characteristics) should be calculated from the one-diode model or specified by user.

The *variants* are used to define and store certain system configurations. These presets store information defined by the user for the mandatory and optional inputs. This allows making consecutive simulation runs for the same presets (settings) for different meteorological datasets.

Certain parameters are **Mandatory:**

The *orientation* tab is used to decide the settings for the plane orientation of the modules or arrays (right). It is possible to optimize according to season of the year or the year general. The assumed loss according to optimal tilt is shown for the selected orientation.

The *system* dialog is used to specify the system configuration, that is, the module type (s) and inverter type(s). Unfortunately, one can only specify one module type per string, which reduces application in this thesis, as will be seen briefly. However, it should be noted that in most cases only one type of module would be used, and that this feature is common among simulation programs.

When choosing an inverter, the program tells the recommended minimum number of modules of the selected type to connect in series. If the module number is below this number, the systems tab turns yellow, as seen in Figure 29. This indicates that the number of modules in certain conditions may fall below the voltage threshold of the inverter voltage operating range.
If this happens, the inverter cuts the array connection to grid, leaving it in open circuit. This induces inverter losses and is one of the risks of oversizing inverters too much (2.2.5. Inverter loss).
If the number of modules within a string is below a certain minimum required number, the program refuses to perform simulations altogether.

In the *detailed losses* section, one might specify the assumed constant loss factors in the system in percent:

- Thermal parameter: choice of U-values
- Ohmic losses: input of constant value or calculation from cable diameters and length of module interconnection and inverter connection cables.
- Module quality/LID/mismatch: Specification of module quality loss as a constant degrading factor, a constant LID and mismatch loss.

- Soiling loss: either input of constant overall factor for the year or specification of constant loss for individual months
- IAM losses: choice of the b_0 parameter (eq. 2.23)
- Unavailability loss: specification of system downtime

Other parameters are **Optional:**

The *horizon* tab allows one to specify a horizon profile for a specific site.
This is termed far shadings, and supposedly is defined as all objects located more than 10 times the system size away from the site [**36**].
Figure 28 shown earlier actually is how a flat horizon looks in PVsyst.

When making a profile, this can be done either by specifying it manually or importing one from for example the Solmetric SUNeye - It is a handheld shading analyzer incorporating a fisheye camera to graph shading elements.

An example of such a profile is shown below in Figure 30 [**37**]:

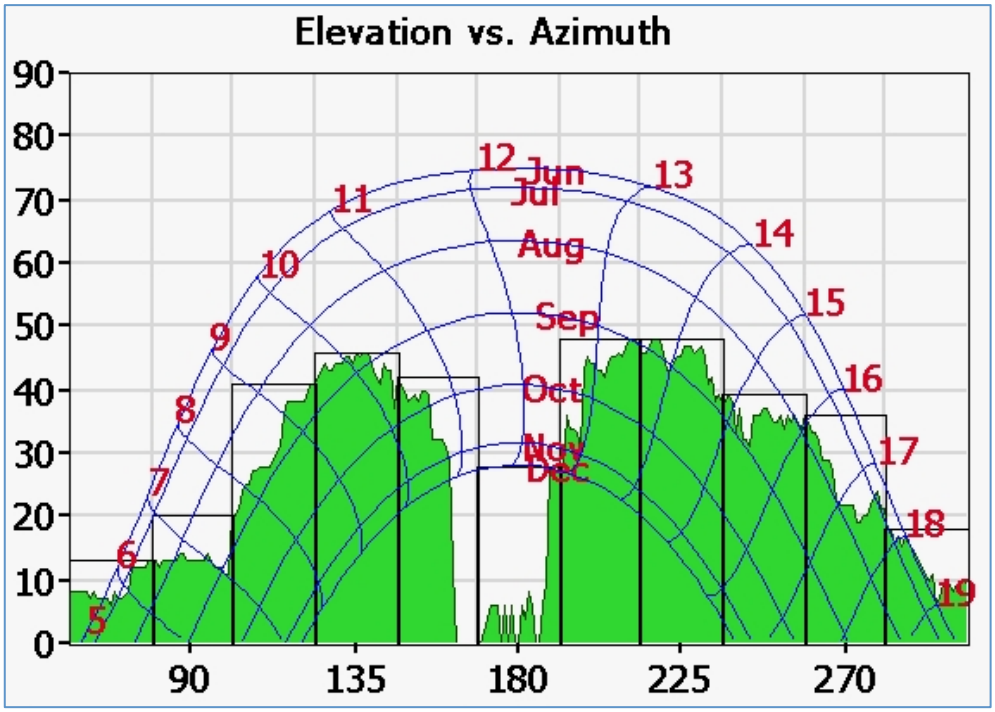

Figure 30: Horizon profile made with the Solmetric SUNeye.

In the above figure, the vertical axis labels sun height and the horizontal axis label the sun azimuth angle. Note that the definition of the azimuth is different from the angles definition used in this thesis and in PVsyst.
The figure shows how the horizon looks when a profile is drawn accurately.

The *near shading* tab is used to construct a 3D model of all near shading objects, which should be defined as the objects that fall outside the definition of far shading objects. This could be buildings, trees or other arbitrary objects.

The shading model construction relies on architect plans or similar documents to be accurate.

Figure 31 below shows the 3D model used in the combined shading scenario at Aas, for this thesis. This scenario will be explained in more detail in subsequent chapters.

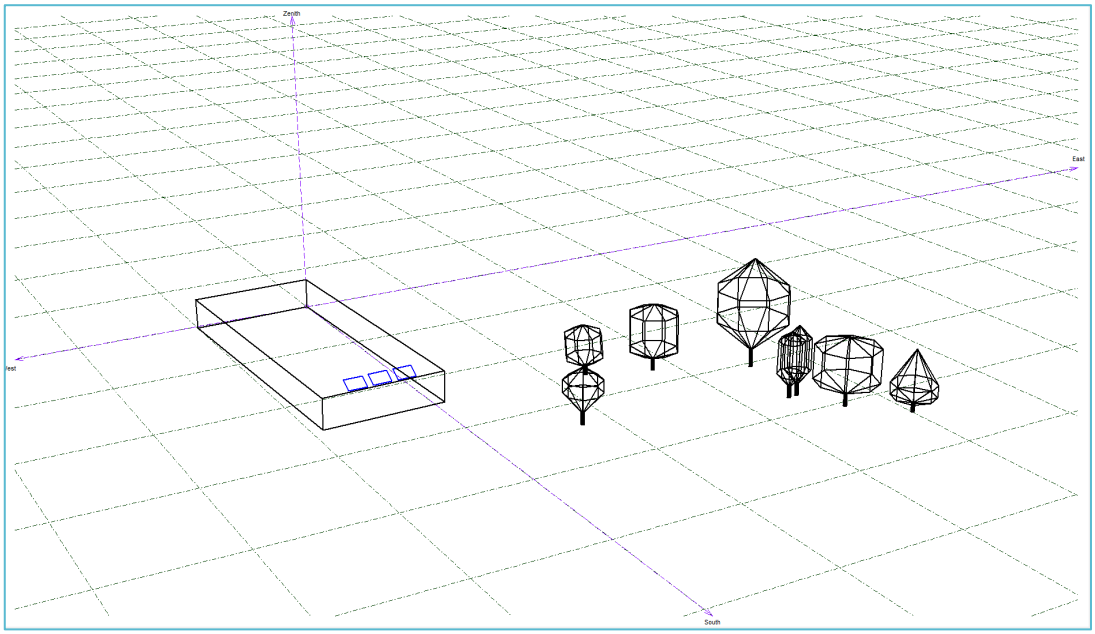

Figure 31: PVsyst except of the near shading 3D model for the combined shading scenario at Aas

When a 3D model is defined, the user may choose to construct a shading table. Three options are given for this (excluding no shading):

1) Linear shading: calculation of shading loss as the relative module area covered by shading. This is a lower bound for shading loss.

2) According to module strings: user defines a fraction of the module area that is considered covered by shading

3) According to module layout: Detailed computation related to how the modules are placed in the 3D model (see below).
   Takes into account the bypass-diode function in modules when shaded.

The *module layout* tab allows users to specify how modules are placed in the 3D scene defined under the near shading tab. The user can choose if the modules are placed in a horizontal or vertical arrangement, the string configuration, etc.

The *economical evaluation* tab lets the user define all costs of the system for automatic calculation of the LCOE. *Miscellaneous tools* contain different tools related to probabilistic forecasting of yield. These tabs weren't used in this thesis.

More information follows in subchapter 3.6 Simulations setup and forecast assessment and 3.7 Simulation settings.

3.3.3 Simulation results

Simulation results in PVsyst are generally presented in a simulation report, showing all forecasted parameters and generated meteo data.
An example of such a report has been included in Appendix G.8, along with a description.
For the sake of brevity, the report will not be explained here - it is left to the reader to become familiar with the contents of the forecast reports.

3.3.4 Accuracy of PVsyst

The synthetic hourly generation is reported by PVsyst to vary, and two consecutive simulations using the same meteorological data may not yield the same results. The variation is stated to be 0.5 – 1.0% [**9**][synthetic data generation].

The transposition of diffuse radiation in PVsyst is treated independently.
As such, the transposition factor, and the so-called transposition surplus (TP), is dependent on the diffuse-to-global ratio (DGR). The user can choose to use either the Hay model or the Perez model – the latter is set as default.
The validation of the software has shown that the Perez model yields an MBE 1.8 to 2.2 points-percent higher than the Hay model - for Swiss locations.
If diffuse radiation is omitted, the Perez model is stated to usually yield *annual* values for diffuse 0 – 2% higher than when diffuse radiation is supplied [**9**][Transposition model].

The correlation model for *monthly values* avoids synthetic hourly data generation and its uncertainty is stated to be about 5%. This supposedly may lead to errors in forecasted monthly diffuse of about 1 – 4% [**9**][Meteo monthly calculations].

The program help sites themselves state that the global uncertainty found inherent to modeling, excluding uncertainty related to measurements and parameter determination, is an MBE of 2 – 3% [**9**][old validations].
This is interpreted as if the program is using perfectly accurate measured data, one should expect a MBE of 2 – 3% in forecasting of system performance.

In recent validations performed of simulations of actual PV-power plants in Switzerland, the accuracy of the forecasts were supposedly accurate to ±5% when using default detailed loss vales and renormalizing results to measured meteorological data for the actual production year simulated [**9**][validations].

The earlier studies mentioned to assess the accuracy of simulation software has found PVsyst to be the most conservative simulation software in terms of yield forecasting. The software seems to rely on the expertise of the user to a higher degree than other software. It has been reported to be underestimating actual yield by 5 - 9% [**34**] [**38**]. However, as these tests have been conducted in sunny locations without significant soiling, they may not translate to heavy soiling scenarios.

3.4 Site assessment

In order to be able to correctly model the PV-system, a site assessment has to be conducted, where information about system components, orientation, shading elements, inverter output and other relevant information is collected.
This assessment, and the information in question, is presented below.

All datasheets used in this thesis may be found in Appendix C: Datasheets.

3.4.1 Location and surroundings - Aas

The PV-system to be evaluated is located on the campus of NULS (NMBU), situated in the municipality of Aas, in the county of Akershus, Norway.

It is administered by the Institute for mathematical sciences and technology (IMT), an administrational unit of the Faculty of environmental science and technology. The panels are mounted on the southernmost end of the roof on the building bearing the generic name *wing IV,* which is used interchangeably with the more specific *TF4 (technological faculty 4).*

The decimal coordinates of the system were found through the use of Google Maps, which states the coordinates to six decimal places.
The array is distributed along the southern roof side of the building, raising the question of what the correct coordinates are to represent the location.

When alternating the cursor position in the longitude direction, pinpointing the corners of the building, SunEarthTools shows that the coordinates can be stated to a precision of four decimal places.
According to the accuracy in coordinate measurement described in chapter two, this gives an accuracy of ±11.13 m around the equator, with the accuracy increasing with increasing latitude. Thus, the error in coordinate estimation is assumed insignificant and is regarded sufficient for an accurate calculation of climatic distance between site and weather station.

The coordinates for the location (*wing IV*) were found to be (Table 2):

Table 2: The coordinates of the PV-system at Aas

Decimal coordinates for Aas	
Latitude	59.6659
Longitude	10.7780

A screenshot from Google Maps showing the site location and surrounding buildings, with names, can be seen in Figure 32:

Figure 32: Satellite image showing the site location and surrounding buildings on the NULS campus

3.4.2 Initial Horizon- and shading analysis at Aas

One of the important aspects when performing a site assessment is mapping the horizon and evaluating the shading elements.
In order to do this, several tools and methods may be used, some of which may be more accurate than others.

The utilization of tools like the Solmetric SUNeye instrument will yield a horizon profile that includes the shading elements in the vicinity of the site (Figure 30), which can later be imported directly into the simulation software, PVsyst.
This may render a complex assessment of the shading elements superfluous.

However, because this instrument and the likes of it are costly, the evaluation of the site shading had to be performed by alternative methods.

In order to keep the shading evaluation as simple as possible, it was decided to make an attempt at a horizon profile bearing resemblance to those that would be constructed from the above-mentioned tool.
Such a horizon profile can by no means be assumed to be as accurate as the ones produced by a professional shading tool, and should be regarded as a rough model. However, this might give information about how accurate a forecast will be with a bare minimum of tools and information available.

To assess the horizon profile, a panoramic photograph was made from the position of the PV-array on the roof of *wing IV*. The photo is taken towards the south and shows a 180° view of the surroundings.

This photograph is shown in Figure 33:

Figure 33: Panoramic photo towards the south of the site surroundings at Aas

As have been mentioned in the last subchapter, the horizon (far shadings) in PVsyst is regarded as all elements located at a distance of approximately 10 times the system length or more.

From the panoramic photo, it was possible to deduce how the approximate horizon profile looked, and which elements constituted the horizon.
It was found that the *Student society*, *Aud Max* and the southernmost parts of *Wing II* were elementary horizon constituents.
The trees closest to *Wing IV* located towards the east were considered near shading elements, and would be modeled in the near shading section of PVsyst.

An enlarged version (Figure E. 1) of Figure 33 and an alternate version (Figure E. 2) marking the above mentioned elements is located in Appendix E: Location specifics: Aas.

In order to estimate the elevation (sun height) of the far shading elements in degrees, and to correctly model the near shadings, the objects height had to be estimated. This could be achieved by using Theodolite Droid.

The distance to the objects, used as input in the tool, was paced out from the object, where deemed possible (wing II, trees).
In the event that measuring by pacing couldn't be done, the distance was simply estimated by comparing known lengths of nearby infrastructure.
For example, knowing that the width of the Norwegian national road in front of Aud Max (Figure 32) is 6.7 m [**39**], the distance from the measuring point to the building could be estimated to be at least four times this.
Consequently, the distance was estimated to be 30 m in this case.

An excerpt from Theodolite Droid showing the measurement of Aud Max's height is shown in Figure 34:

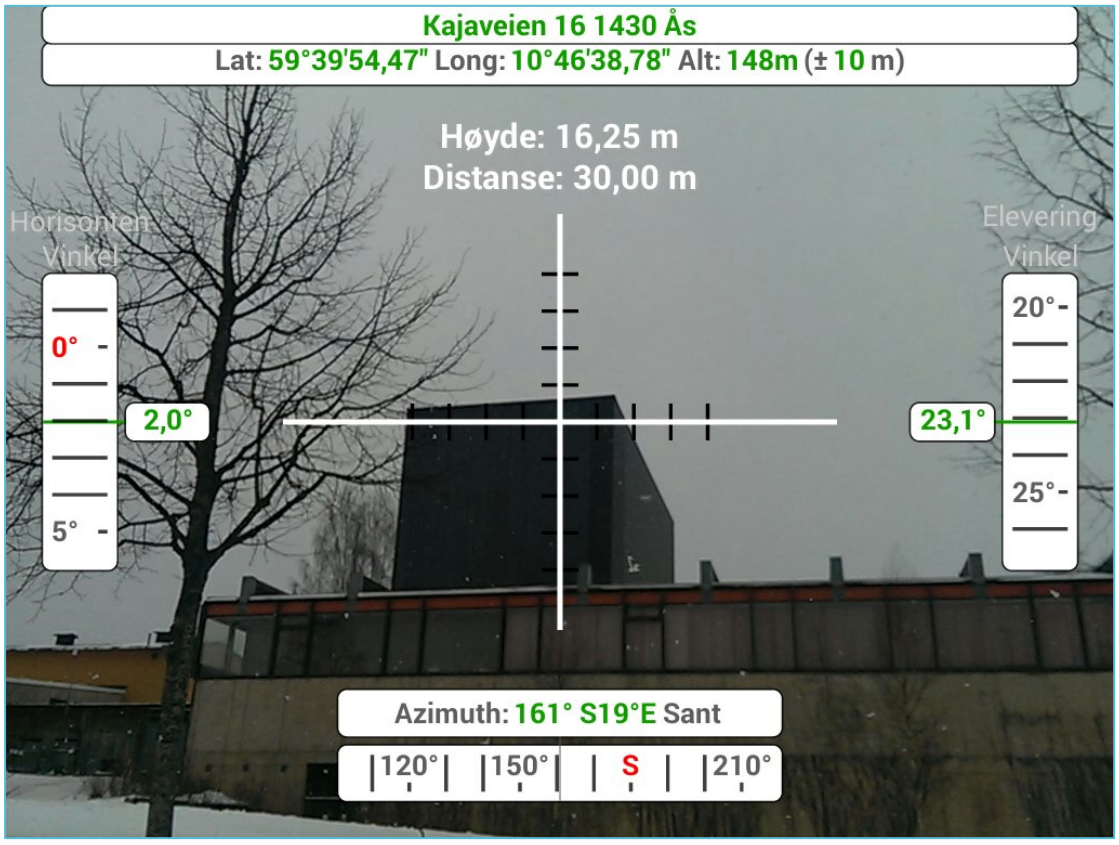

Figure 34: Excerpt from the app Theodolite Droid, showing the estimated height of Aud Max

3.4.3 Detailed shading analysis

The 3D scene made in PVsyst is supposed to incorporate only objects within the near shading definition, as explained in the last subchapter.
In constructing this 3D scene, the relative module placement above ground became an issue when aiming at combining the near shading and far shading scenario. The horizon is defined according to sun height, which in turn is related to height above ground. Thus, any difference in module height above ground level would make the sun height overestimated.

By correspondence with the technical advisor at PVsyst in the software related forum online, co-author of the PVsyst user manual Bruno Wittmer advised that, the far shading option was intended to be used for objects so far away that object height above ground didn't have any significance. This was a contradiction to what was stated in the user manual.

As such, it was decided to make an alternative, more detailed assessment of the surroundings at Aas – in order to complete a realistic 3D scene.
This scene would disregard the far shading altogether, and instead incorporate only the shading objects in the vicinity of the site. These were considered to be the ones marked in Figure 32 shown earlier.

To do this, architectural plans became necessary. Fortunately, they could be hauled from the draftsmen's office, located on NULS (NMBU) campus grounds. These drawings could then be assessed using AutoCAD, to measure all the buildings accurately in 1:1 ratio. AutoCAD excerpts are shown in Figure 35:

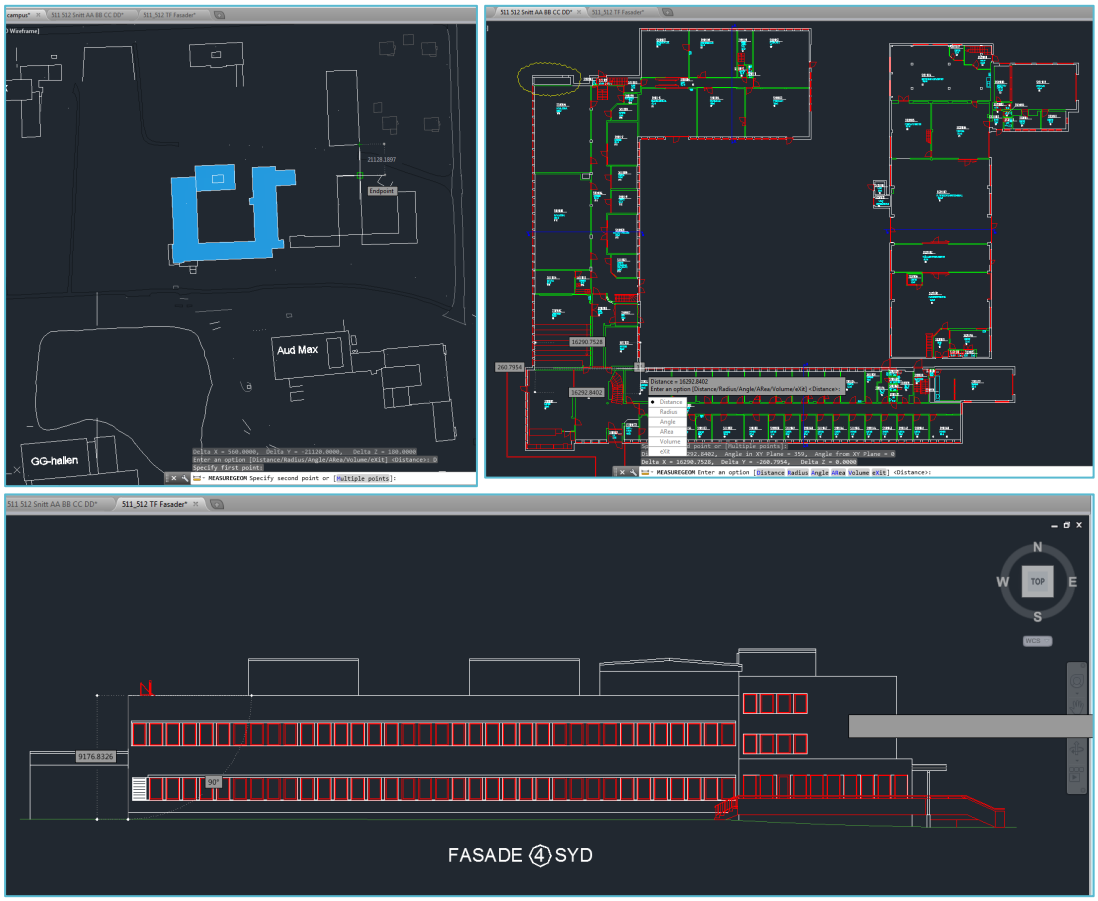

Figure 35: Excerpts from AutoCAD showing the PV site at Aas.

From the above figure, on may observe the equivalent of Figure 32 in the upper left corner, showing the site location with the different buildings.
The blue object marked is Wing I and II from the original figure.
In this mode, one can measure the outer dimensions, distances between and orientation of buildings.
The upper right corner shows Wing I and II when the detailed plans are considered. In this mode, one may measure the outer dimensions of a building more accurately, like length and width.
The lower picture shows the western facade at the site at Aas, allowing the user to measure height of the building and dimensions of roof shading objects.
Note that the façade notation says south – this is erroneous.
The two other pictures show that the real orientation is westwards.

Possessing dimensions for the buildings at Aas was a great advantage, as it ensured that a highly precise model could be made.
However, as can be seen from Figure 33, a large portion of the shading objects at Aas are trees – the dimensions of which are hard to obtain, and which may be sources of error. This could hardly justify making a detailed 3D scene.

The forestry service had in recent past conducted an economic assessment of the existing tree volume at Aas, which required accurate dimensions of the trees.
To supply such dimensions, LiDAR measurements were made.
These are really satellite measurements, using laser and radar to find the height of objects above ground within a defined area.

The LiDAR measurements from the forestry service were handed out on request. These could then be imported into Global Mapper, to show high-resolution 3D images of the surroundings at Aas.

Excerpts from Global Mapper are shown below in Figure 35:

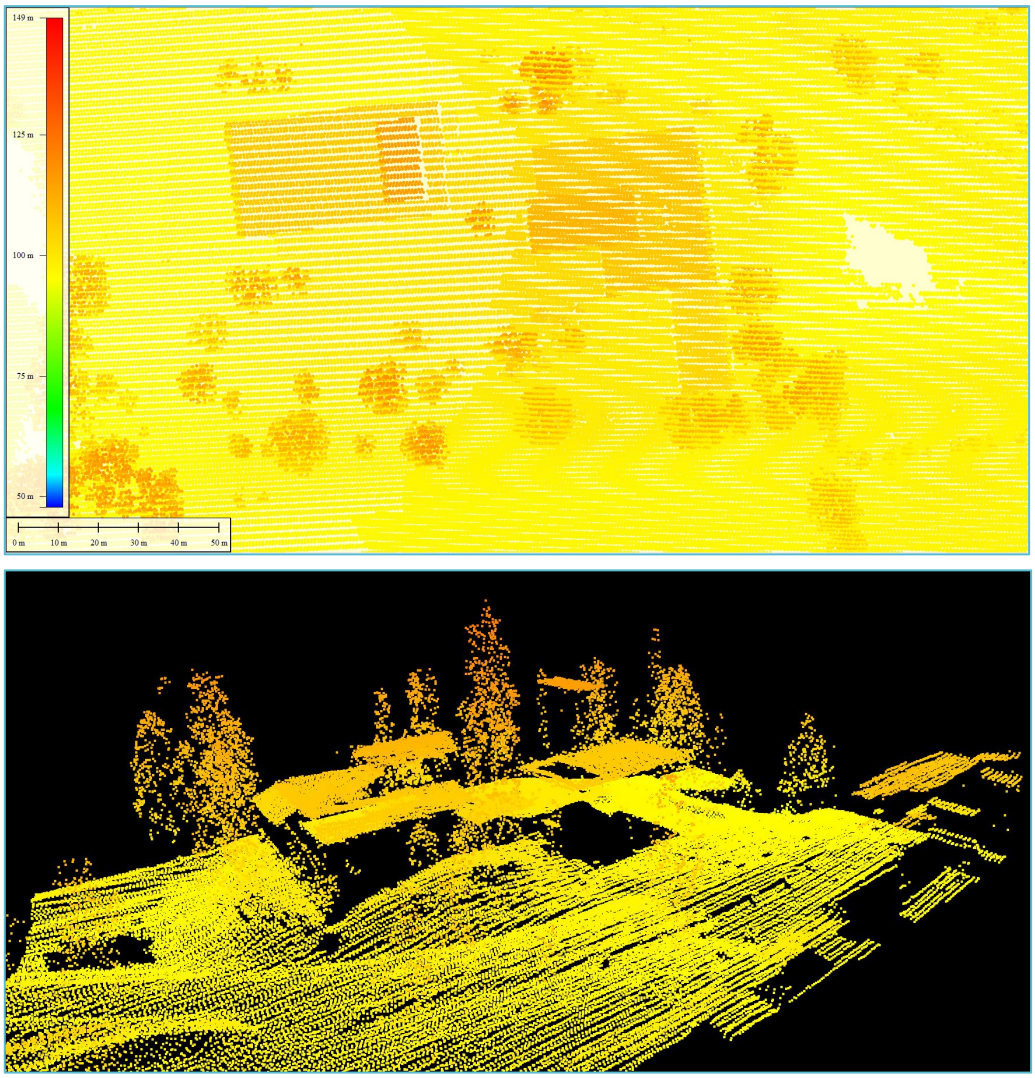

Figure 36: Excerpts from Global Mapper showing mapping of LiDAR measurements

The upper picture from figure above shows how LiDAR data map Aud Max and the student society from above, with the legend right indicating the height above sea level. From this mode, it is possible to place a marker over an arbitrary object (e.g. tree) and the program will state the height above sea level to four significant figures. Placing the marker next to the object, on ground level, allows the user to see ground level height above sea level. From the two values, the height of the object can be calculated.
The lower picture shows how the LiDAR measurements are mapped in 3D. This allows for deducing the shape of objects, particularly trees.

3.4.4 System at Aas

The PV-system in question was donated to NULS (NMBU), and the system configuration therefore differs from the customary configuration of a PV-system. This is reflected in mismatching of inverter and PV-array, and in mismatching of the PV-modules.

The relevant system components were primarily the panels, the inverter and conduction cables between the array and inverter.

The system information gathered about the site is summarized in Table 3:

Table 3: System overview Aas, listing necessary system information

Location	String no.	Number of panels	Panel type	Nom. Capacity [W]	Accum. Capacity [W]	Inverter type	Nom. Capacity [W]	Inverter no.
Aas	1	1	REC PE215A	220	220	Theia 4.4 He-t	4400	1
	1	3	REC PE220	220	660	Theia 4.4 He-t	4400	1
	1	1	REC PE230	230	230	Theia 4.4 He-t	4400	1
	1	1	REC PE235	235	235	Theia 4.4 He-t	4400	1
	1	3	REC PE240	240	720	Theia 4.4 He-t	4400	1
Total	**1**	**9**	**5 types**		**2065**	**1 type**	**4400**	**1**

As can be seen, the system features a total of nine panels, consisting of no less than five different types, all from manufacturer REC.
The modules were grouped in smaller arrays of three modules and connected in series, within the same string, and had an accumulated capacity of 2065 W.

A photo of the arrangement can be seen in Figure 37:

Figure 37: Photo towards the east of the PV-array at Aas

The module string was connected to a string inverter from Elkem Valere with a nominal capacity of 4400 W. Consequently, the inverter was grossly oversized, with an inverter-sizing factor (c_{inv}) of only 0.47.

All modules maintained a tilt angle of 36° and the orientation of the building they were situated on, which according to SunEarthTools had an azimuth of -3° (±1°). When using AutoCAD, this azimuth was found to be -2°, and consequently was fixed at this value.

There was no accurate information as to the model of the panels used, which made it necessary to collect the information from the module labels on the backside of the modules.

These labels can be found in Appendix A: Module labels Aas.

An example of one such label is shown in Figure 6:

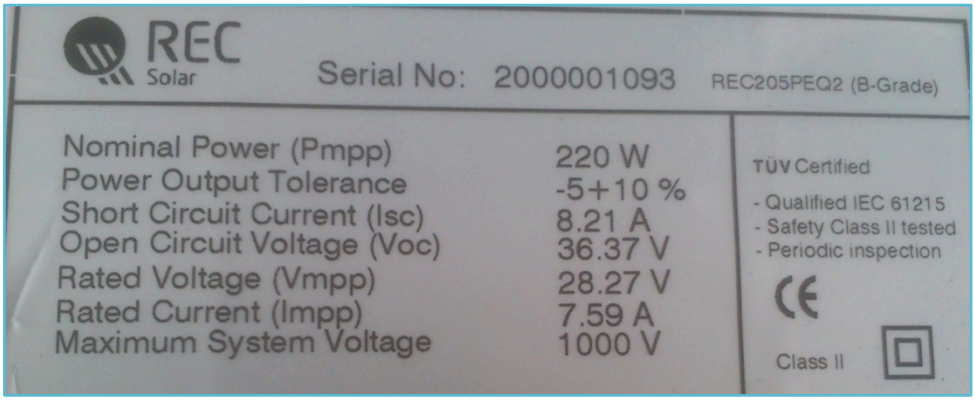

Figure 38: Module label for a PV-module (REC PE215AJM) at Aas.

Note that on the shown label, no production date is found.
Because of this, it was difficult to conclude when the panel was produced.

All the other panels at the site possessed labels with date stamps, allowing for finding the correct datasheet according to the respective panel model.
However, it soon appeared that for some panels, the values found in the datasheet corresponding to the production year differed from the labeled values.

Therefore, the general approach adopted when finding the appropriate datasheet for the panels, was to compare the labeled values with the values found in the datasheet for the year prior to, and after, the production year.
From these comparisons, the modules could be assigned the datasheets most similar to the labeled values.

A summary showing the relevant information about the PV-modules found in the spec sheets can be seen below (Table 4):

Table 4: Module overview for Aas

Location	Aas	Aas	Aas	Aas	Aas	Aas	Aas
Producer	REC	REC	REC	REC	REC	REC	REC
Model	PE215A	PE220	PE220	PE220	PE230	PE235	PE240
Prod. Year	2008	2008	2010	2007*	2010	2010	2011
Pmpp [W]	220	220	220	220	230	235	240
Tolerance Pmpp [%]	± 5 (1)	± 5 (1)	± 5 (1)	-5/+10 (1)	± 5 (3)	± 6 (2)	± 6 (2)
Isc [A]	8.1	8.2	8.2	8.32	8.43	8.75	8.75
Impp [A]	7.6	7.7	7.7	7.71	7.88	8.17	8.17
Vmpp [V]	28.6	28.7	28.7	28.33	29.2	29.7	29.7
Voc [V]	36.3	36.6	36.6	36.51	36.5	36.8	36.8
Efficiency η [%]	13.0	13.3	13.3	13.33	13.9	14.5	14.5
Temp. coefficient, Pmpp/Voc/Isc [%/°C]	-0.46/-0.32/0.011	-0.46/-0.32/0.011	-0.46/-0.32/0.011	-0.43/-0.28/0.048	-0.43/-0.33/0.074	-0.40/0.27/0.024	-0.40/0.27/0.024
Weight [kg]	18	18	18	22	18	18	18
Dimension (L x W x T) [mm]	1665 x 991 x 38	1665 x 991 x 38	1665 x 991 x 38	1665 x 991 x 38	1665 x 991 x 38	1665 x 991 x 38	1665 x 991 x 38
Area [m^2]	1.65	1.65	1.65	1.65	1.65	1.65	1.65
No. Cells parallel	1	1	1	1	1	1	1
No. Cells series	60	60	60	60	60	60	60
No. Bypass diodes	3	3	3	3	3	3	3
Max sys volt [V]	1000	1000	1000	1000	1000	1000	1000
Max sys current [A]	15	15	15	10	25	25	25
Interconnection cable cross section [mm^2]	4	4	4	4	4	4	4
Interconnection cable length [m]	2.1	2.1	2.1	1.9	2.1	2.1	2.1
Datasheet	2009	2009	2009	2007	2010	2011	2011
Power tolerance stated according to:	1. Nameplate	2. Spec sheet	3. Assumption	* No data found, assumed year			

From the above table, it becomes clear that the modules not only are of different models, but some are even from different years.

There are two PE220 modules bearing similar characteristics that have been assigned the same datasheet, the same is true for the three PE240 modules. Apparently, among the nine panels, there are six different panel characteristics. This further complicates any possible mismatch effects originally thought to be present.

The responsible engineer at the site gave information about the array-inverter conduction cable dimensions.
The dimensions of the interconnection cables following the modules would be found in the module datasheets and are listed in the above table.

The cable dimensions are listed below in Table 5:

Table 5: Cable dimensions for the PV-system at Aas.

Cable dimensions		
	Interconnection cable	Conduction cable
Length [m]	47	19
Cross section [mm^2]	5	4

3.4.5 Inverter production data at Aas

The extraction of data giving information about inverter output was necessary to be able to evaluate system performance and analyze what the discrepancies are between forecasts and actual production.

The log-files from the inverter are written weekly, and consequently there are 52 files for a calendar year. The data are logged according to the TDMS file-format; this can be displayed by installing an add-in to Microsoft Excel.

According to the existing log-files, the inverter at Aas and the PV-system was fully operational from week 7, 2013 – beginning 20th of February 2013.
For sake of simplicity, therefore, it was decided to define the production reference year (RY) as the period 01.03.2013 – 28.02.2014.

A complete description of the methodology related to the assessment of inverter output, and an example of one of the weekly-generated inverter files, is located in Appendix D: Inverter production data.

A graphical representation of the monthly inverter output and accumulated yearly output can be seen in Figure 39. Please note that monthly and yearly output is graphed according to the, left (primary) vertical axis and the right (secondary) vertical axis, respectively.

For reference, the yearly-accumulated output was 2034 kWh, for a system with 2065 W_p installed capacity, giving a specific yield of 985 kWh/kW_p.

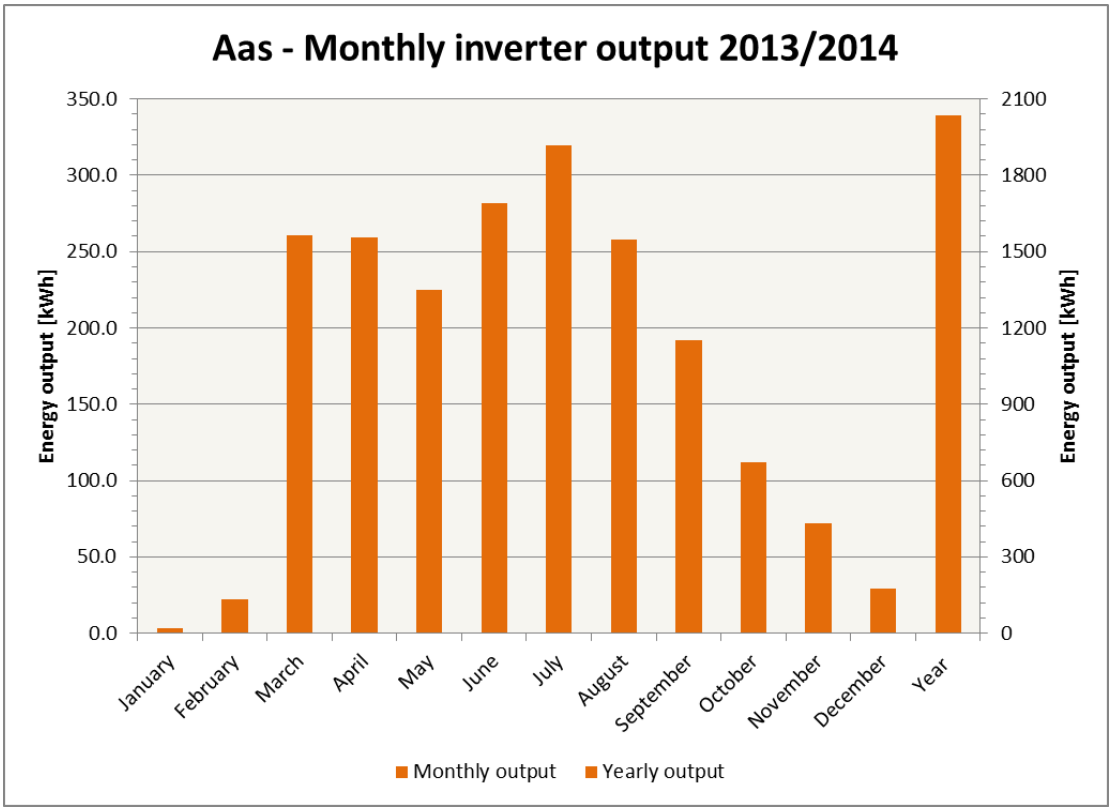

Figure 39: Graphical representation of the inverter output at Aas for the production year 2013/2014.

From the above figure, it is clear that the inverter output was low in January and February; this generally reflects that January and February were bad in terms of production, maybe due to low irradiance levels or soiling from snow.
The spring and summer months generally saw high output, with an exception in May. July seems to have been a good month, and from this month onwards the inverter output generally falls towards the end of the year, where weather conditions again impose restrictions in production.

3.5 Meteorological data

The meteorological data are the highest sources of uncertainty in any simulation as these are the fundament of the forecasts being made.
Therefore, the data used should be as accurate as possible and investigated for flaws or irregularities. The use of several sources is therefore advised to avail of data allowing for the control of homogeneity between sources.

The meteorological data used in this thesis were collected mainly from two sources: databases and weather stations.

All raw data collected has been made available at the following online location:

www.dropbox.com/sh/gg7c01u5zvlssr2/AAAQra3LL9QEPwxOwtB8_-n9a

3.5.1 Databases

Databases are useful, as they contain large amounts of information and are readily available for use in planning. However, some caution should be bestowed when consulting them, as they may be highly inaccurate.

In this thesis, databases well known from other studies and from the solar community were evaluated.

The databases in question would include:

- Photovoltaic Geographical Information System (PVGIS)
- Meteonorm
- NASA SSE 6.0

Two of these databases use a limited number of weather stations to collect time series for locations in Norway.

The PVGIS database contains data for global- and diffuse irradiation and temperature; the chosen resolution is monthly averages.
According to one resource mapping of Norway conducted in 2013, the PVGIS database consists of data from one weather station alone, and data from other locations are created by interpolating between this one station and other European stations [**40**].

The reported accuracy of the model used for interpolation is stated according to *cross-validation* with ground data, and is 0.3 % and 4.7 – 11.2 %, for the mean-bias-error (MBE) and the root-mean-square-error (RMSE), respectively [**41**].
As such, the discrepancy between forecasted and actual yield is expected to be significant for the simulation based on these data.

In comparison, 3 weather stations seem to be the fundament of the Meteonorm, according to the same report just mentioned.
The reported accuracy of the models used in Meteonorm version 6.0, according to the corporation itself, is 7 % for spatial interpolation and the beam radiation RMSE is 5.4 % [**42**].

The accuracy of the newest version of Meteonorm is not known, but is assumed not to differ significantly from the reported values.
Although this is an improvement over the PVGIS database, the interpolated data created for other locations with Meteonorm still give rise to the possibility of a significant discrepancy between forecasted and actual yield.

The NASA database contains satellite data measured as a time series over a period of 22 years over the time interval 1983 – 2005.
These data are used to assimilate the surface irradiation through the application of an algorithm that estimates cloud coverage and other relevant atmospheric phenomena. The produced surface radiation data are verified through comparison with measured terrestrial data.
The accuracy of the data contained in this database varies much according to the latitude of the site in question and the type of parameter [**43**].
The largest amount of uncertainty lies in the insolation data, with a RMSE ranging somewhere between 33 and 54 per cent for latitude 60 degrees pole ward and between 10 and 29 per cent globally.
The MBE lies at 0 - 7.5 per cent and 1 – 11 per cent, globally and for 60 degrees latitude pole wards, respectively [**44**].

Hence, simulations based on input from this database also have a significant potential for discrepancy.

Figure 40 below shows the annual global irradiance in the horizontal plane for the different databases consulted in this thesis. As can be seen, NASA SSE generally estimates highest irradiance, but also with higher error (see above). The Meteonorm is the least erroneous, but has intermediate irradiance values. PVGIS has second highest errors, but the lowest irradiance data.

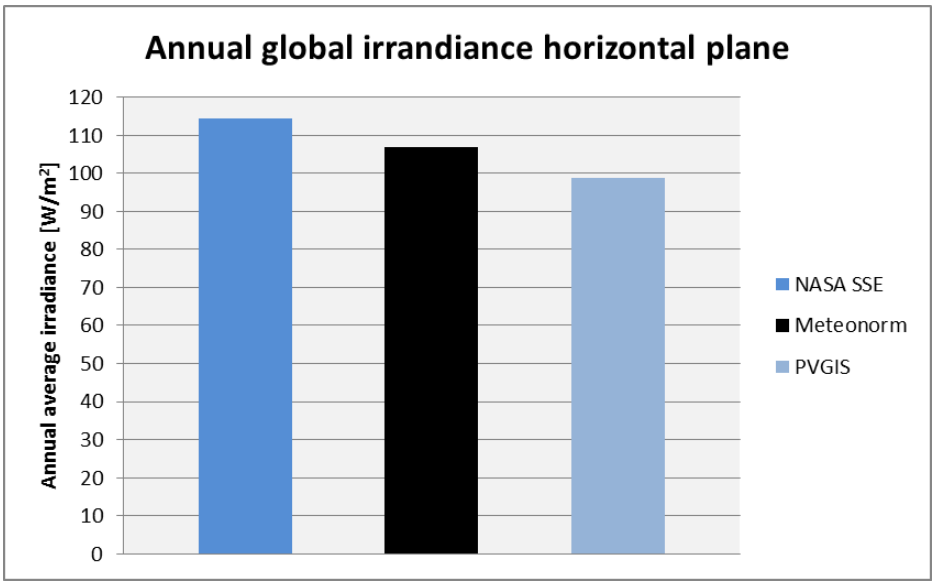

Figure 40: Annual global irradiance in the horizontal plane for databases consulted in the thesis

Tabular values for the above graph is located in Appendix F.1: Meteorological data from databases.

3.5.2 Weather stations - selection

Meteorological data from weather stations are the preferred choice of data, since they have been measured on site and represent the real conditions at project site. However, one has to use caution also when consulting sources of real data.

Where the database uses collections of data and interpolate values by applying mathematical algorithms, weather stations only possess the raw data.
The interpretation of the usefulness of these data relies on the person extracting the data and the liability in erroneous choice of data, which lead to errors in forecasting, cannot be owed to a faulty database.

Information about the weather stations considered in this thesis is located in Appendix F.2: Meteorological data from weather stations (Table F. 7).

An excerpt from this table can be seen in Table 6 below:

Table 6: Table showing the most relevant information about the weather stations at Aas

Overview over available weather stations and data at Aas						
Data for site	Station	**Data source**	**Climatic distance**	**Relevant parameter**	**Temporal resolution**	**Time interval**
Aas	Aas	Bioforsk	1	Air temperature	Hourly/Daily/Monthly	9 years, 4 months, 5 days
				Albedo	Hourly/Daily/Monthly	9 years, 4 months, 5 days
				Global radiation	Hourly/Daily/Monthly	9 years, 4 months, 4 days
				Wind speed (2 MAGL)	Hourly/Daily/Monthly	9 years, 4 months, 5 days
Aas	Aas	NMBU/NULS	1	Air temperature	Hourly/Daily/Monthly	24 years, 4 months, 5 days
				Albedo	Hourly/Daily/Monthly	24 years, 4 months, 5 days
				Diffuse radiation	Hourly/Daily/Monthly	24 years, 4 months, 5 days
				Global radiation	Hourly/Daily/Monthly	24 years, 4 months, 5 days
				Wind speed (10 MAGL)	Hourly/Daily/Monthly	24 years, 4 months, 5 days
Aas	Aas	MET	1	Air temperature	Hourly/Daily/Monthly	25 years, 10 months, 19 days
				Diffuse radiation	Hourly	18 years, 11 months, 30 days
				Global radiation	Hourly	18 years, 11 months, 30 days
				Snow cover	Hourly/Daily/Monthly	91 years, 3 months, 27 days
				Wind speed (10 MAGL)	Hourly/Daily/Monthly	20 years, 6 months, 14 days

In the table, green writing signifies secondary chosen data and red primary chosen data.
The available measured parameters are listed; together with the temporal resolution available and the time interval the parameters have been measured.
The time intervals were last updated May 12th, 2014.

All stations were located in the vicinity of the PV-system site, within a climatic distance of 1 km, at Søråsfeltet weather station.
All the institutions cooperate to some degree in exchanging data, although there is no apparent indication of which data is generally exchanged.
As such, all sources were treated separately.

NULS (NMBU) maintains the weather station FAGKLIM, which is a field station for agro-climatic studies. This source was generally considered sufficient for use in this thesis, and supplied the primary data. The dataset was supplied in hourly resolution, one file for every year in the period 1986 – 2013, in addition to data for the three first months of 2014.
The data chosen was from the period 1996 – 2013 (due to irregularities in data), for the inverter reference year (RY) of 2013/2014 and the year 2013 (See the next section, 3.5.3 Weather stations – processing of data and irregularities).
Staff engineer Signe Kroken at NMBU (NULS) supplied the data.

Bioforsk is a research institution belonging to the Norwegian agricultural meteorological service, in Norwegian: Norsk landbruksmeteorologisk tjeneste (LMT). This institution holds its own grid of independent stations.
The data were collected from their online portal [**45**] as monthly values, and consisted of the average from the period 2005 - 2013.
These data were chosen for comparison to the NULS (NBMU) data on grounds of data irregularities (See the next section, 3.5.3 Weather stations – processing of data and irregularities). They were considered secondary due to the fact that diffuse radiation measurements didn't exist.

The Norwegian meteorological institute (MET) held much data too, however, seeing that the data from NULS (NMBU) were sufficient, only snow cover data were chosen to obtain information about snow soiling. Snow cover data were chosen over snow depth data, as even the smallest amount of snow may lead to halted or even ceased production in the modules.
The data were collected from the eKlima website online [**46**] for the period 1897 - 1987 and consisted of monthly values.

A table showing all the meteorological data from weather stations is located in in numerical form is located in Appendix F.2: Meteorological data from weather stations (Appendix F.2: Meteorological data from weather stations)

The chosen data will be displayed in Ch. 3.5.4 Chosen meteorological data together with data from databases.

3.5.3 Weather stations – processing of data and irregularities

The data from NMBU was processed using Microsoft Excel, and the file format supplied was CSV.
Examining the data, it soon became clear that there were a number of missing data points in the hourly files for the first four years 1986 – 1989.
These were so many, that the data for this period were considered unusable.
The remaining period of 1990 – 2013 was then processed by taking monthly averages of all months within a given year. During the processing, a number of data points were found missing also in the remaining period.

A summary of the missing data points is shown below in Table 7:

Table 7: Table showing the missing data points in the original dataset chosen from NULS (NMBU)

Missing data points 1990 – 2013 in weather data from NULS (NMBU)
1990 missing 1062 data points 22.12-31.12
1991 missing 1343 data points
1992 missing 2708 data points 24.06-02.07, 27.08-06.09, 20.09-28.09, 10.10-31.10, 10.11-30.11, 10.12-31.12
1993 missing 297 data points
1994 missing 108 data points
1995 missing one (1) data point
2003 missing three (3) data points
2007 missing December values
2008 missing first quarter values
2010 based on diurnal values, temperature and wind speed values are averaged daily median

As can be seen from the above table, a significant number of data points were missing from several years. This induced a high degree of uncertainty as to how representable the data were.

This generally led to the choice of analyzing the differences between the period of 1990 – 2013 and 1996 – 2013, by calculating the averages of the extracted parameters for every calendar month from each period. When these were obtained, the standard deviation was calculated for the same averages.
The results were then compared.

A graph showing the comparison of monthly global irradiance for the two periods is shown below in Figure 41:

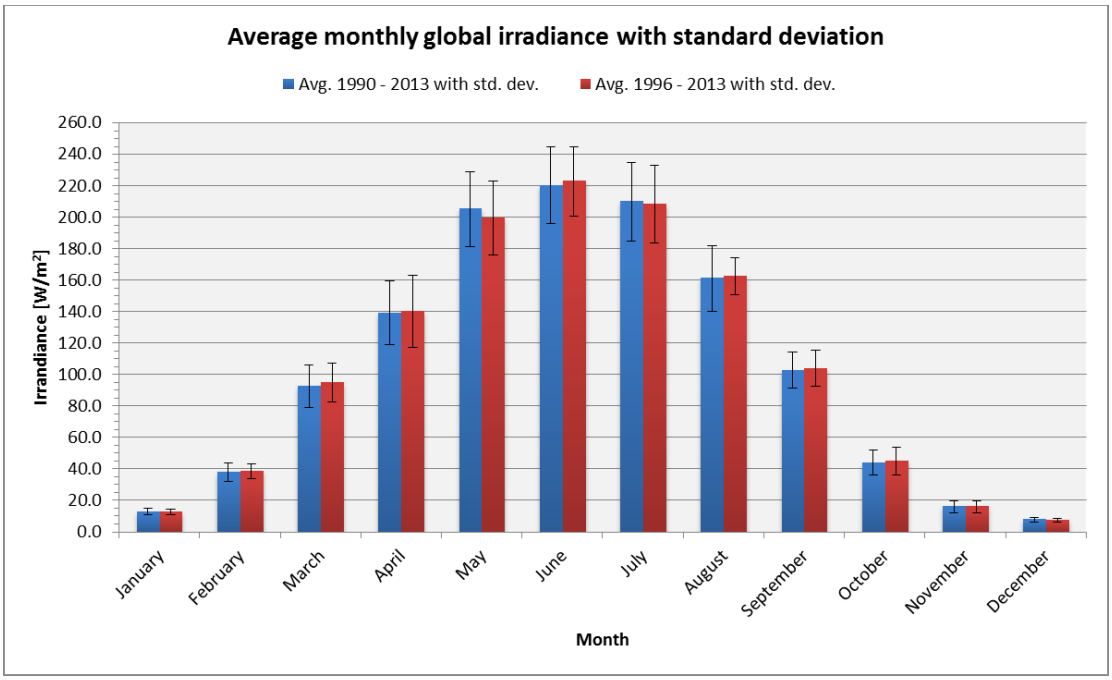

Figure 41: Comparison of average monthly global irradiance for two periods of data from NULS (NMBU) - with corrected diffuse

The comparison above showed some minor differences between the series, though the 1996 – 2013 average generally showed a lower standard deviation, and was therefore chosen. Comparisons were done for temperature, wind data and albedo as well, with the same results as for the global irradiance.

However, the irregularities experienced in missing data points weren't the only ones. Well into the process of working with this thesis, the responsible persons for the FAGKLIM weather service noticed that some sensor measuring error had been induced in the pyrometer used for measuring global radiation.
This had happened due to insufficient calibration over some time periods.

One of the professors at NULS (NMBU), Arne Auen Grimenes, is responsible for co-authoring the yearly report of weather data for the FAKLIM service.
To his understanding, there were two periods of four years each that had experienced a linear degradation in pyrometer accuracy; the years 2004 - 2007 and the years 2010 - 2013. As such, the global irradiance data of all these years would have to be corrected.

Table 8 below shows the correction factor that would have to be applied for each at the years at Aas:

Table 8: Correction factor for the monthly average global irradiance at Aas

Correction factor - Global irradiance at Aas								
Year	**2004**	**2005**	**2006**	**2007**	**2010**	**2011**	**2012**	**2013**
Degradation	0.0075	0.0150	0.0225	0.0300	0.0100	0.0200	0.0300	0.0400
Correction	1.0076	1.0152	1.0230	1.0309	1.0101	1.0204	1.0309	1.0417

There was also a problem with the diffuse radiation measurements, due to the use of a static screen when the diffuse component is measured. Apparently, this static screen induced an error of up to 31%, which is higher than for other available methods used to measure diffuse radiation.

Normally, a complex algorithm taking into account the clear sky index in measurement data would have to be applied for the correction of this error to be exact. Though, as this would require a considerable amount of labor to correct, considering 18 years of data in hourly resolution, correcting was therefore done by multiplying in a correction factor of 1.31 with the monthly diffuse values calculated from the raw data.
This would lead to an overestimation of the diffuse component in months with low irradiance levels. These months could be considered to be in the winter - most likely January, February and maybe November and December.

To assess the resulting values for diffuse component, the discrepancy between publication values found for an arbitrary year (2012) was compared to the original and corrected values calculated from FAGKLIM raw data. The result is shown in Table F. 12 (Appendix F.2: Meteorological data from weather stations). It indicated that the corrected values were more accurate than the original values.

The RY data seemed to be significantly influenced by the diffuse correction applied to the measured data at Aas. In the month of January the diffuse radiation ended up making out almost all of the radiation, giving a diffuse-to-global ratio (DGR) of 1. In December, the diffuse radiation ended up being higher than the global, and thus had to be reduced by 0.1 W/m^2 in order to allow simulation in PVsyst.

On grounds of all these irregularities, additional data were chosen to have grounds for comparison after forecasts were completed.
A 2013 data series was made from the already processed calculation of monthly averages, to yield grounds for comparison to the RY and the average 1996 - 2013 data. This could reveal if the RY was particularly good or bad in terms of irradiance, compared to the "normal".

The Bioforsk source was chosen as a second alternative source to the average 1996 - 2013 source. However, this source also wasn't optimal, due to the fact that diffuse data was lacking. The diffuse data therefore had to be generated synthetically in PVsyst. This could have lead to errors in forecasting as a result of the diffuse modeling in PVsyst, as explained in 3.3.4 Accuracy of PVsyst.

The snow cover data collected from the MET website online was analyzed by averaging as in the case of irradiance and temperature data. Though, because snow cover is contained in code, the average contained decimal places.
This had to be rounded to the nearest integer.
The result is shown in the next section.

3.5.4 Chosen meteorological data - all sources

Now that the proper understanding of the chosen meteorological datasets is in place, the chosen sets can be displayed for the reader to assess.

Figure 42 below shows the monthly distribution of irradiance for all sources evaluated in this thesis.

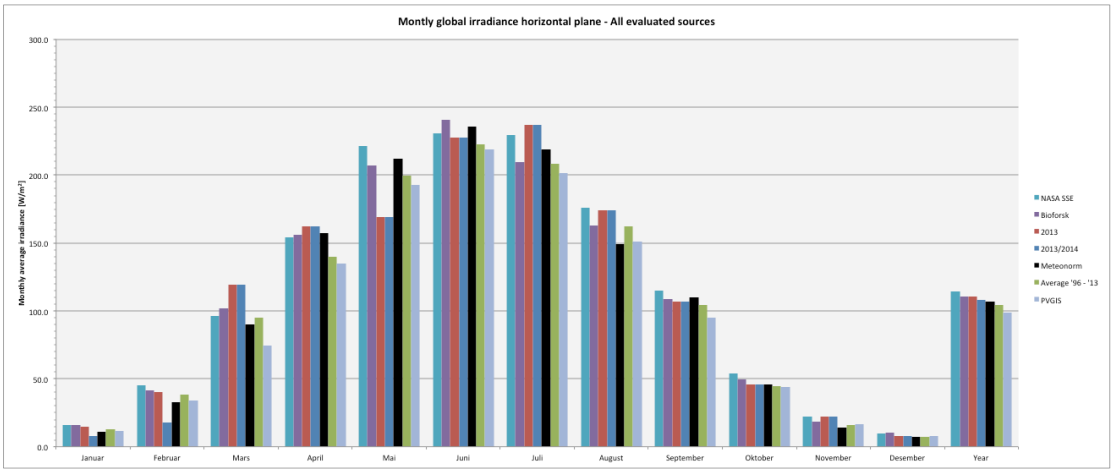

Figure 42: Monthly distribution of global irradiance in the horizontal plane for all evaluated sources

From the above figure, one may observe that the months of January, February and May indeed were months of poor irradiance in the RY, compared to that in other sources, in accordance with what is shown in the inverter production data. March, April and July look like good months when compared to the two averages of irradiance, Bioforsk and 1996 – 2013 series, which implicated that these months were better than "normal".

Over the year, NASA SSE and Bioforsk datasets seem to have the highest irradiance values. The Bioforsk average is from the nine most recent years of the last 18 years going back to 1996 and the average 1996 - 2013 generally shows very low irradiance values over the year. This implicates that irradiance may have risen the last decade. PVGIS clearly underestimates the irradiance in all months.

Note that the values don't take the diffuse radiation into account; this may lead one to believe there is good overall correspondence between the observed production and RY values.

A large version of Figure 42 is located in Appendix F.2: Meteorological data from weather stations (Figure F. 1).

The monthly temperature distribution is shown below in Figure 43:

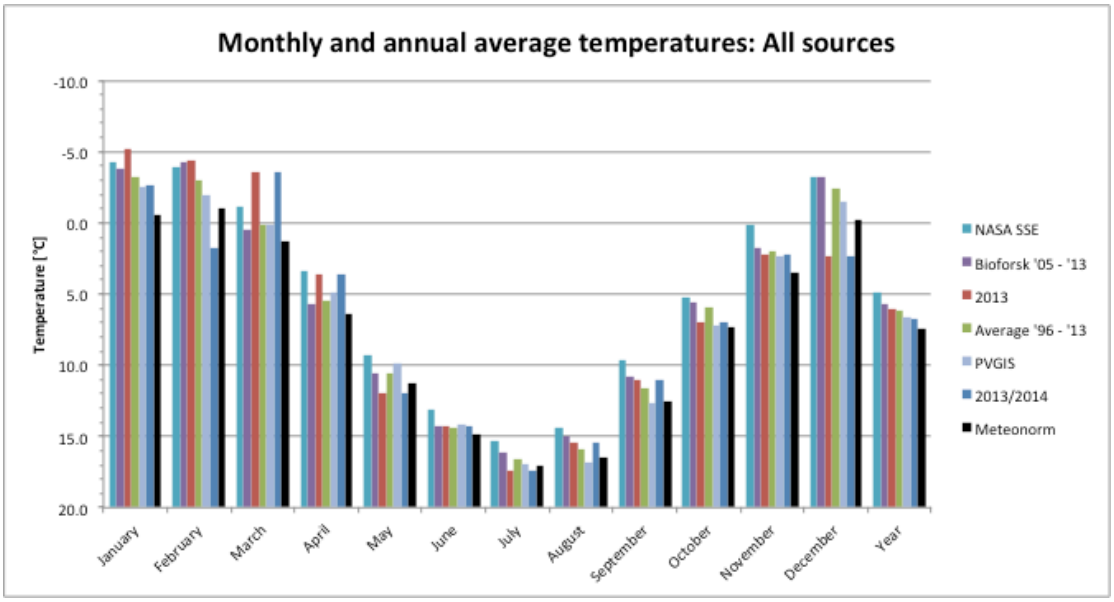

Figure 43: Monthly temperature distribution for all sources evaluated

Note that negative values are upwards in the above figure. Note that the lowest temperatures belong to the sources with highest irradiance.
The RY has some of the highest temperatures.

Wind data generally won't be shown here, as they are less influential in the simulations. More about this in the next subchapter.

The snow cover data from MET is shown below in
Table 9:

Table 9: Snow cover data collected from the MET weather station at Aas

Snow cover data for Aas		
	Mean snow cover [code]	Mean snow cover [%]
Parameter	Integer code	Integer per cent
January	3	75
February	3	75
March	3	75
April	1	25
May	0	0
June	0	0
July	0	0
August	0	0
September	0	0
October	0	0
November	1	25
December	2	50

The table above shows the averaged rounded integer code for the location at Aas. It should be noted that the standard deviance was 1 code unit for all nonzero values. Notice that the three first months of the year shows significant snow cover, December shows a moderate value. April and November show low values.

Table 10 below shows the albedo values found for Aas, one set from the NASA database and another from FAGKLIM. It is apparent that NASA seems to underestimate albedo.

Table 10: Albedo data collected from the NASA SSE database and FAGKLIM

Albedo values for Aas		
	NASA SSE	Average '96 - '13
January	0.18	0.62
February	0.17	0.62
March	0.17	0.51
April	0.13	0.27
May	0.09	0.24
June	0.10	0.23
July	0.14	0.23
August	0.13	0.23
September	0.14	0.24
October	0.11	0.25
November	0.19	0.31
December	0.17	0.48
Annual avg.	0.14	0.35

3.6 Simulations setup and forecast assessment

This subchapter briefly explains the general method used to assess the forecasting accuracy.

3.6.1 The assessment of forecasting accuracy

The basic setup of the simulation process consists of 5 scenarios, or runs.
The data from each meteorological data source will be used as input in PVsyst, and a series of these 5 forecast runs will be conducted.
Each forecast run generates one report in PVsyst, which states the annual yield, the monthly distribution of yield; losses and the performance ratio of the system (see 3.3.3 Simulation results).

When a series of 5 runs has been conducted for each meteorological data source, the forecasted annual yield for each run is compared to the actual annual yield. The state of discrepancy (or bias error) shall be stated for the different runs made, along with the best match to the actual annual inverter output.
The forecasting accuracy should also be stated for the best performing forecast using database data, and the best performing forecast using measured data from weather stations.

When the annual yield has been compared, the analysis aims at comparing forecasted and actual yield on a monthly basis, in order to assess irregularities in the meteorological data used. This then builds the fundament for the discrepancy analysis, which will be explained later.

For last in the analysis, a revised comparison of forecast versus actual yield will be made to adjust for positive mismatching in the array at Aas.
More about this in 3.7.1 System configuration in PVsyst.

3.6.2 The five scenarios

As was explained in the introduction to PVsyst, variations are available to implement different settings. These were used to test how discrepancy evolved as restrictions to the simulation settings were varied.

Five scenarios were chosen to be able to study this evolution of discrepancy:

1. Ideal scenario, only implementing mandatory input (base case)
2. Scenario implementing (1) + the detailed near shading 3D model
3. Scenario implementing (1 ,2) + the module layout
4. Scenario implementing (1, 2, 3) + detailed monthly (heavy) soiling values
5. Scenario implementing (1, 2, 3) + an overall annual soiling value

The ideal scenario is the base case, and is implemented in all consecutive scenarios, as it contains the mandatory input.
The chosen mandatory input is listed in Ch. 3.7.6 Detailed losses - chosen input.

The detailed near shading 3D model was chosen to represent the shading for all the simulations made because it was assumed to be more accurate than a combined far/near shading combination.

3.6.3 The sixth scenario: far/near shading combo

To study the effect of performing a simplified shading analysis or using tools like the Solmetric SUNeye for constructing horizon profiles to use as input in PVsyst, a sixth scenario has been made.
This scenario is supposed to implement the far shading in one step and the near shading in a second step, before implementing the two soiling scenarios, as mentioned in the last section.

An illustration of the course of the five scenarios versus the six is shown below in Figure 44:

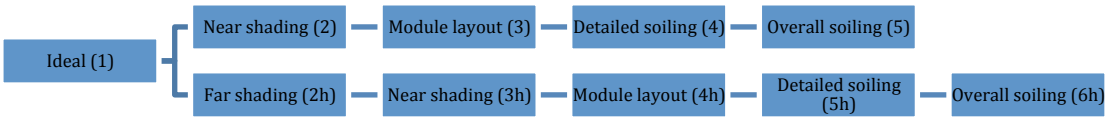

Figure 44: Figure showing the course of simulation including the combined shading scenario

In the figure above, the letter *h* behind each scenario indicates that horizon is included. In the opposite case, the horizon is flat, and only detailed near shading is being used. When comparing the two simulation courses, scenario 2 in the original course is compared to 2h and 3h in the combined course (2 vs. 2h + 3h).

3.7 Simulation settings

The simulation settings chosen as input in PVsyst are presented in this subchapter. A brief explanation will be given of the chosen values used as input into the sections explained under 3.3.2 Project design.

3.7.1 System configuration in PVsyst

Because of the rather complex configuration of the system at Aas, incorporating six different types of panels, some problems were encountered during the configuration of the *system (*3.3.2 Project design*)* in PVsyst.
Firstly, and maybe not surprisingly, the program didn't support the configuration of six different modules within the same string.

As such, the system would have to be modeled as consisting of 9 modules in series, using the weakest panel in the string (PE215AJM).
This because the weakest module would decide the current level of all the modules in reality (see 2.2.1 Module mismatching loss), meaning that choosing another module would overestimate the production.

However, since some of the modules in the string had a higher power rating, their IV-curves consequently also were different, which meant that even in the case of lower current, their output at the MPP of the weak module would still possibly produce more than the weak module. This meant that a forecast would possibly underestimate the actual production. In other words, there would be a positive mismatch in the modeled system configuration.

In order to find out how significant this mismatch was, the IV-curves produced by PVsyst with the one-diode model for all the different panel types were

examined in PVsyst. This way, the current and voltage of the different module types at the MPP of the "weak" module could be noted.
An excerpt from PVsyst showing such an IV-curve for the module type PE240 is shown below in Figure 45:

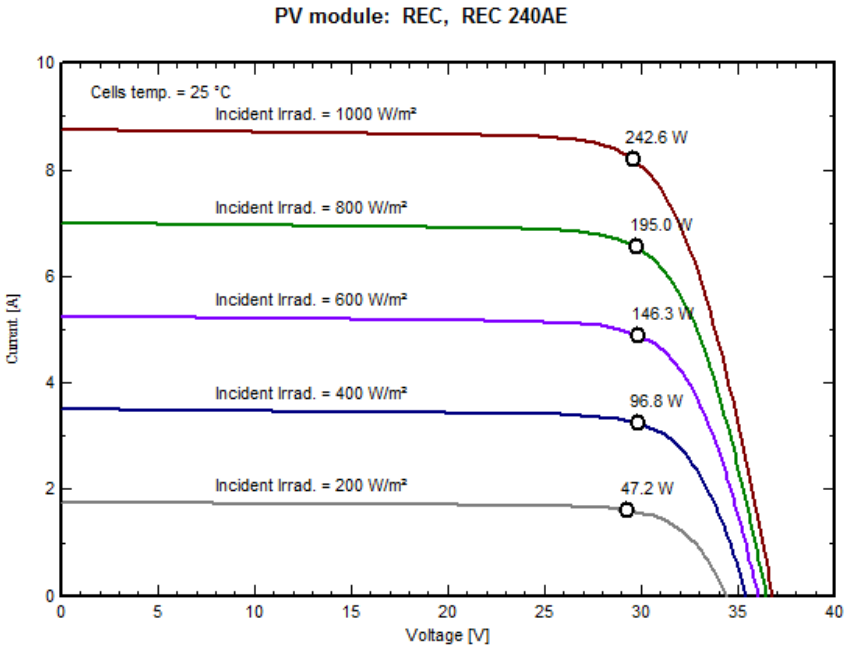

Figure 45: Excerpt from PVsyst showing the IV-curve of the PE240 module

The collected IV-characteristics could then be tabulated in Microsoft Excel, and the power of the different modules at the MPP of the lowest rated module, could be calculated. The result is shown below in Table 11:

Table 11: Table showing the mismatch of the modeled system configuration in PVsyst.

Module type	PE215AJM	PE220 (2007)	PE220 (2008/2010)	PE230	PE235	PE240	Total	Bias error (mean)
Vmpp Pvsyst	28.8	29.0	29.5	30.5	30.5	31.0		
Number of panels	1	1	2	1	1	3	9	
Impp	7.6	7.6	7.6	7.6	7.6	7.6	7.6	
Vmpp tot Pvsyst	7.6	7.6	15.2	7.6	7.6	22.8	68.4	
Pmpp tot PVsyst [W]	219	220	448	232	232	707	2058	-4.3
Pmpp tot PVsyst [kW] sign. fig.	0.2	0.2	0.4	0.2	0.2	0.7	2.1	-4.3
Pmpp tot datasheet [W]	220	220	440	230	235	720	2065	-4.6
Pmpp tot datasheet [kW] sign. Fig.	0.2	0.2	0.4	0.2	0.2	0.7	2.1	-4.6
Pmpp tot sim [W]	219	219	438	219	219	657	1970	-4.4
Pmpp tot datasheet [kW] sign. Fig.	0.2	0.2	0.4	0.2	0.2	0.7	2.0	

In the table, the value of the total collected array power at MPP was also listed according to the datasheet values, in addition to the total array power output at MPP when modeled as the consisting of only the weakest panel.
The result found was that the power output at MPP when using the homogeneous string of weak modules, underestimated the real output at MPP by 4.3% according to the IV-curves in PVsyst, and by 4.6% according to the datasheet values for MPP. The average was 4.4%.

According to formula (2.8), the module efficiency is a function of the P_{MPP}. This means that when faulty simulating the power at MPP with a positive mismatch, the modeled efficiency only makes out 95.6% of the "real" efficiency at MPP. Thus, the forecasted yield could possibly be somewhat underestimated.

Correcting for the positive mismatch is not straightforward. Because the different panels have somewhat different temperature behavior, some stronger modules perform worse in the summer settings, and won't obtain the assumed MPP behavior at the MPP current of the weakest module. Conversely, in cold weather, the module will perform worse than expected due to the weak module limiting the current. However, there is no easy way to foresee these effects, and therefore, a more conservative value of 4% is assumed for the positive mismatch.

Consequently, after formula (2.17a), the yield Y_r of the system will have to be divided by a factor 0.96.

The issue with module mismatch was not the only problem experienced in PVsyst. Also, the inverter at Aas was severely oversized, and upon selection of it in PVsyst, the program refused to perform simulations due to the oversizing - claiming that the inverter voltage threshold would too high for the string configuration. As such, the inverter chosen was the Theia 2.9 He-t, which has about the same efficiency curve as the Theia 4.4 He-t, though with a nominal capacity of 2.9 kW. Therefore, the inverter losses should be expected to be somewhat higher than forecasted, but presumably not more than 1%.

The inverter curve for the Theia 2.9 He-t was sent by producer Eltek Valere by email, and is shown below in Figure 46:

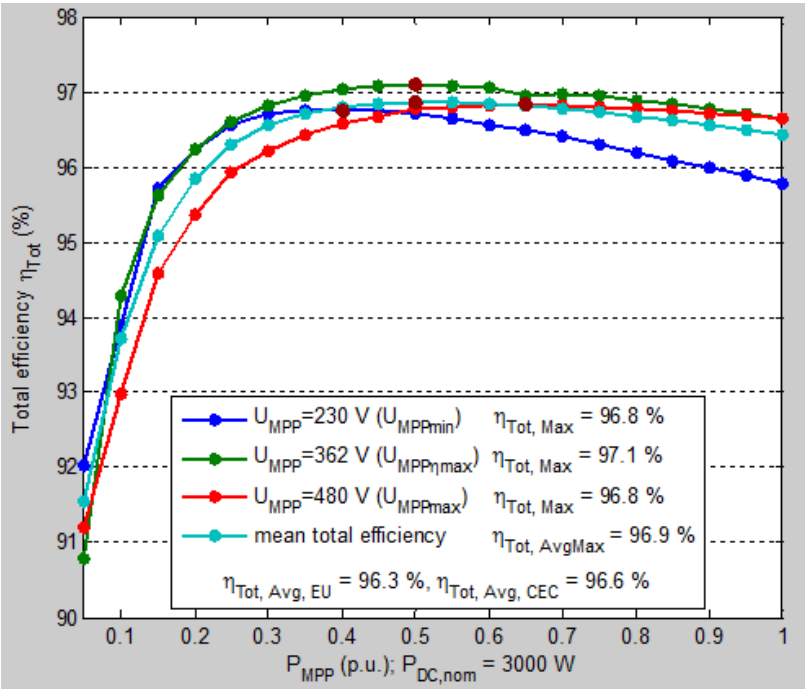

Figure 46: Efficiency curve for Eltek Valere 2.9 He-t string inverter

3.7.2 Shading settings

The construction of the detailed 3D model, used in the investigation of forecasting accuracy, and the simplified 3D model (Figure 31) used in the combined shading scenario are both constructed in the same way in PVsyst. However, the data used to make the models are different.

The simplified model was made using SunEarthTools to measure distances between buildings in the map and their outward dimensions.
In addition, the orientation was measured.

A screenshot showing such a measurement being made is shown below in Figure 47. Notice the coordinate, length and orientation measured in the upper left corner of the figure.

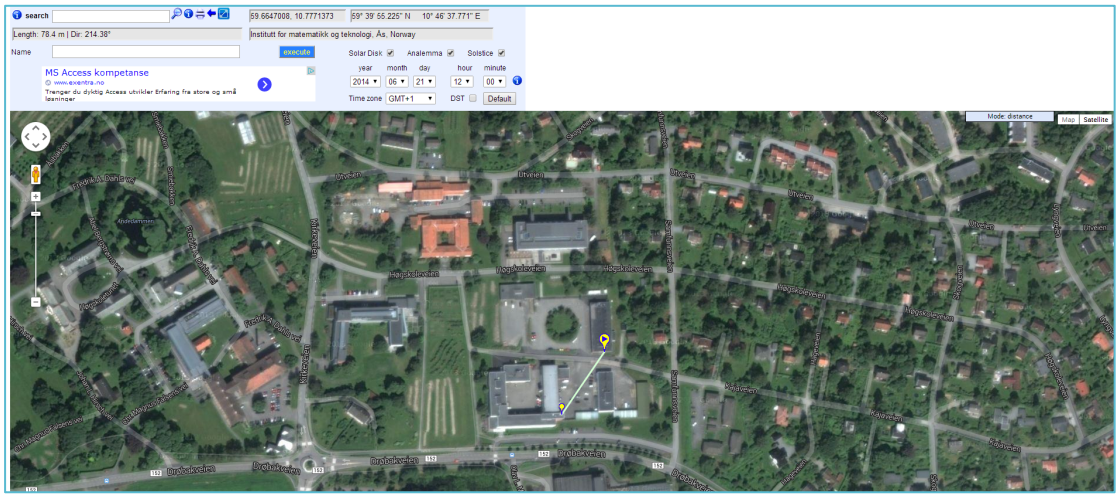

Figure 47: Screenshot of the SunEarthTools measuring mode

The building height of the all shading elements (wing II, Aud Max, student society, trees) and Wing IV was assessed using Theodolite droid in the way explained under the site assessment (Figure 34)

The detailed model is constructed using LiDAR measurements and AutoCAD to make an accurate model. This model consists of nearly 50 shading elements, trees included. The trees were assessed in the 3D environment of global Mapper during the 3D shading scene construction (Figure 36), and will not be listed due to their number and arbitrary shapes. However, a list of the dimensions of the other shading elements used in construction of both the simplified and detailed 3D model is supplied in Table G.1 (Appendix G.1 Simulation settings).

A PVsyst excerpt showing the detailed 3D model is shown below (Figure 48):

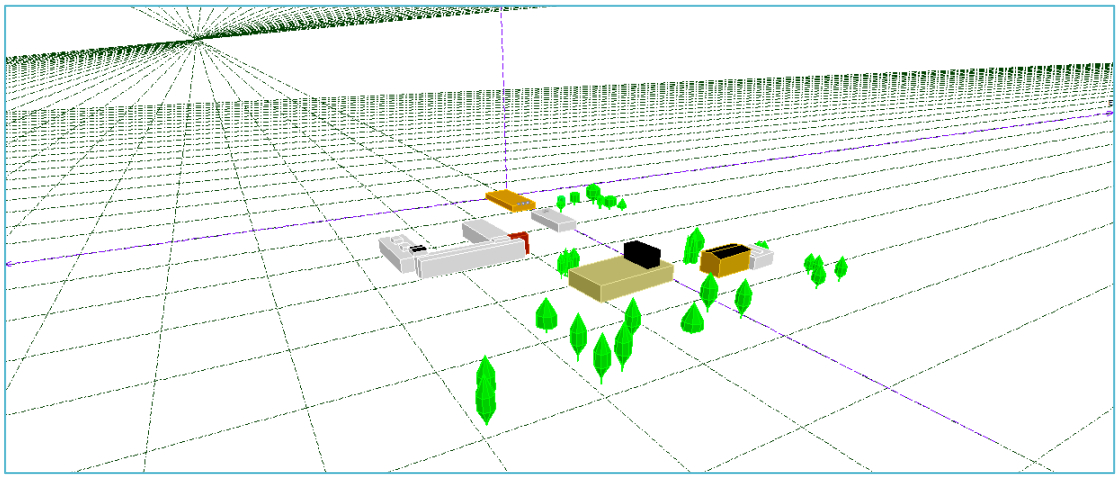

Figure 48: PVsyst excerpt showing the detailed 3D scene at Aas

The horizon construction relied on height measurements made with the Theodolite Droid tool, and of the measured distances between buildings using SunEarthTools. From these measurements, the Pythagorean theorem was used to calculate the sun height in degrees.
By looking at the panoramic horizon photo taken during site assessment, and finding the azimuth location of the different horizon elements in SunEarthTools, the different horizon constituents could be drawn into the sun path diagram for the PV-system site.

The resulting horizon profile is shown beneath in Figure 49:

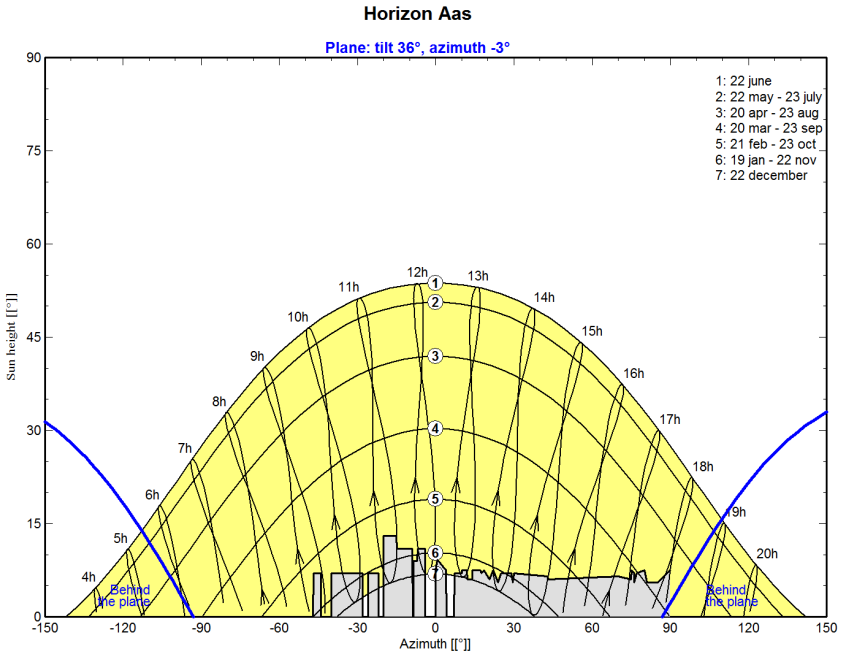

Figure 49: Horizon profile for Aas drawn manually in PVsyst

A PVsyst excerpt showing the displayed horizon profile and the horizon points specified is located in Appendix G.1: Simulation settings (Figure G. 2).
A panoramic photo of the horizon at Aas with the azimuth degree notation of the horizon points of the horizon profile is located in Appendix E: Location specifics: Aas (Figure E. 3).

3.7.3 Albedo test runs

The PVsyst software sets albedo values to 0.20 as default. This value is global and applies to all months. The NASA values for albedo were in this order of magnitude, while the values close to the actual site hauled from FAGKLIM showed values generally much higher. Therefore, some test runs were performed to decide the significance of albedo.

The test runs maintained all the default loss values of the PVsyst program, in order to investigate albedo as an isolated event. The irradiance data chosen were the ones form NASA, as these generally were the highest and could state an upper limit to the impact of albedo.
The test runs were performed for scenario 1 and scenario 5 to see the impact in the most ideal case and a more realistic case.
Three different runs were made for each scenario, one run for each chosen set of albedo values.

The result can be shown below in Table 12:

Table 12: Impact of different albedo values in run 1 and 5.

Impact of different albedo values				
Simulation no.	1	5	Run no.	Albedo values
Yield [kWh/year]	2045	1987	1	NASA
	2055	1994	2	Default
	2067	2001	3	Measured
Discrepancy [%]				
Simulation 1	NASA	Default	Measured	Albedo values
Run no.	1	2	3	
1	0.0	0.5	1.1	NASA
2	-0.5	0.0	0.6	Default
3	-1.1	-0.6	0.0	Measured
Discrepancy [%]				
Simulation 5	NASA	Default	Measured	Albedo values
Run no.	1	2	3	
1	0.0	0.4	0.7	NASA
2	-0.4	0.0	0.4	Default
3	-0.7	-0.3	0.0	Measured

The Table above shows the discrepancy between the different runs made for each scenario. E.g. in scenario 1, the discrepancy between forecasted yield based on NASA albedo values and the forecast based on default values is -0.5%. This indicates that the NASA values underestimate the yield by 0.5% compared to the default values. As can be seen, the largest discrepancy is at -1.1%, though for forecasts based on other sources with lower irradiance levels, this may not be as significant. Especially in a more realistic simulation setting, the discrepancy becomes insignificant, as seen for scenario 5. Therefore, default values were used.

3.7.4 Synthetic hourly generation test

The synthetic hourly data generation in PVsyst allows for choosing different settings for the generation of hourly data. If one only supplies the mandatory weather data, the result is already given, within the stated variation of 0.5 -1.0%. But, if one supplies additional data, the result might change.
Therefore, a test was conducted to see how the data are influenced by the input.

The test was conducted with average 1996 – 2013 data, as the Bioforsk set was the one lacking the diffuse data and the NASA data were interpolated with deemed high inaccuracy. The RY and 2013 series were not considered representable alone for the weather normal at Aas.

The test was conducted according to the following settings (
Table 13):

Table 13: Settings for synthetic hourly generation test

Synthetic hourly generation test settings	
I	Global radiation and temperature data
II	I + Wind data
III	II + diffuse radiation data (uncorrected monthly)
IV	III + diffuse radiation data (corrected monthly)
V	IV + altitude correction

The above table shows the stages in application of restrictions to the data generation in PVsyst. The diffuse data may remain uncorrected or renormalized according to the monthly sum.
The altitude correction was made as an additional measure, as the stated altitude of the PV-system site differed for the weather stations and databases.
The altitude at Aas is stated to be 89 average meters above sea level (AMSL) by FAGKLIM, whereas Bioforsk states it to 94 meters. The weather service YR states the altitude to be at 72 AMSL, referenced by the governmental mapping society [**47**]. The test was conducted for altitudes 72 m, with 89 m for correction.

The results of the test can be seen in Appendix G.9: S. The global irradiance and ambient temperature data supplied don't change in the generation of data, so these are not supplied.
The test shows that supplying diffuse data doesn't give any identifiable change in the generation; the first three settings yield identical results in generation.
The diffuse horizontal irradiation becomes 0.9% higher in both setting IV and V, global irradiation becomes 0.7% lower in setting IV and 2.0% lower in setting V.
Wind data never change, except for setting V, where the change is insignificant.

3.7.5 U-value test runs

The choice of U-values was a little difficult, as several reference values were supplied by PVsyst, depending on location. For free air circulation, the values differed some.

The default value was set at constant, not depending on wind speeds.
In addition, some other values were proposed – some measured on site at solar power plants in Switzerland and others measured by PVsyst users.
The values from solar plants in Switzerland were generally considered to lead to underestimated heat losses, while the user proposed values were for intercontinental climates with higher wind speeds (4 – 5 m/s) [**9**][array thermal losses].

When generating synthetic hourly data, wind speeds didn't seem to change much. Also, the generated synthetic hourly data for Bioforsk showed that wind speeds generated would be relatively independent of the supplied wind speed data (Appendix G.9: Simulation tests and synthetic data - Table G. 39).
It was therefore tempting to choose the constant value (U1).
Though, this was considered to require a test to see how the other U-values would change the forecasted yield.

The test was done with the following U-values (Table 14) in the ideal scenario:

Table 14: The different tested U-values proposed by PVsyst

U-values test, different values		
U-value	U_c [W/m^{2}K]	U_v[W/m^{2}K m/s]
U1	29.0	0.0
U2	25.0	1.2
U3	20.0	6.0

In the above table, U1 is the proposed values for PVsyst for free air circulation, U2 is the PVsyst user proposed values and U3 is the values measured at real PV-systems.

The test results are located in Table G. 40. They show that the difference in applying U1 and U2 give about the same underestimation of the real actual yield in the RY, while U3 underestimates about 2 points-% less. This was assumed to be in accordance with the statement made in the PVsyst help file that the U3 values underestimated heat loss. The proposed U1 value was therefore chosen.

3.7.6 Detailed losses – chosen input

The chosen detailed losses for the simulations in PVsyst were chosen according to considerations made on behalf of values seen implemented in other studies, and own evaluations. The detailed losses chosen are listed below in Table 15:

Table 15: Detailed losses specified in PVsyst, both default and chosen values

Detailed losses in PVsyst		
Factor	Default	Chosen
Ohmic loss [%]	1.5	Calc
Module quality [%]	1.3	1
LID [%]	0	1
Mismatch [%]	1	0
Soiling overall [%]	0	3
Soiling detailed [%]	0	other
IAM loss b_0 value	0.05	0.05
Unavailability	0	0

As can be seen from the table above, only two values were kept the same as the default values in PVsyst.

The Ohmic loss was calculated by the program with formula 2.21 in conjunction with formula 2.22. The cable dimensions found in the site assessment were entered. However, the cable cross-section at Aas of 5 mm^2 wasn't available in PVsyst, and thus a cable cross section of 4 mm^2 was chosen instead.
This would lead to somewhat higher losses than in reality, but the value wasn't deemed to cause significant deviation.

The module linear loss factor read from the datasheets was max 0.7% a year. The module quality loss was therefore considered to be about 1% due to the fact that the modules had about 1.5 years of operation when this thesis was started.

The LID loss was a highly problematic factor to decide. The PVsyst help file proposed a value of 1 - 3% *if* this loss factor was to be implemented.
Studies conducted had seen values in the range 1.3 – 3.9% [**16**], as stated in 2.2.2 Module quality loss. As these losses occur primarily in the first few hundred hours of operation, and that the production at Aas was assessed after about 6 months of intermittent operation, these losses were assumed to be in the lower part of the ranges considered. Also, according to scientists at IFE, the p-Si based modules considered in this thesis are normally less influenced by this effect than m-Si based modules. Consequently, the value was set at 1%.

The overall soiling value of 3% was chosen to be a realistic value for a moderate soiling climate and to present a possibility for comparison to a heavy soiling scenario.
These values are generally difficult to estimate, and are usually different according to location, as stated in 2.2.9 Soiling loss.

Earlier studies have shown annual snow losses at somewhere between 0.3% and 3.3%, with the higher value seen as an extreme. Some other studies have seen lower overall soiling values of 1.5%, with one study claiming 2 – 6% [**16**].
If these losses are supposed to account for the relative proximity of the location to agricultural land, and the relative high number of rainy days in the Norwegian climate, 3% is not considered a farfetched value.
The detailed soiling loss was chosen according to the snow data extracted from Aas. As these data had to be rounded during calculation, many months actually saw higher snow cover values than the ones presented.
The chosen values were therefore considered to be the ones found in the approximated data, seeing that this issue is very difficult to address.

The chosen soling values were (Table 16):

Table 16: Chosen monthly soiling values as input in PVsyst for Aas

Monthly soiling values for Aas [%]	
January	75
February	75
March	75
April	25
May	0
June	0
July	0
August	0
September	0
October	0
November	25
December	50

The soiling value in March is exaggerated in comparison to other reports made, so is the April value, which often would be zero. November values are often also skipped [**48**] [**49**]. Snow tends to slide of modules when some sun is received, but this generally kills much or all of the production when the modules are aligned vertically, as the snow accumulates at the bottom of the module. Therefore, the values observed may not be so wrong, as even small amounts of snow could lead to accumulation. In any case, the point of these values is to make a heavy soiling scenario available for comparison to the overall scenario.

IAM loss values were kept at default as no information of better values could be obtained.

Unavailability losses were not used. Availability seems to be unforeseen and may happen first and foremost in holidays at NULS (NMBU) when no one is tending to the inverter operation. The inverter may then stop feeding the grid.
No maintenance scheme existed for this PV-system, as it was wished to keep the operation similar to that which would be seen by residential housings where maintenance usually is scarce.

3.8 Discrepancy analysis

The discrepancy analysis was performed with the aim of identifying the factors that influence the discrepancy in forecasting and to which degree. This was first and foremost done by looking at the results of the forecasts and trying to explain them by looking into the datasets used as input into PVsyst.

3.8.1 Comparison of losses

The different sources of meteorological data used have different characteristics, especially regarding the essential parameter radiation and temperature.

By looking at the forecasted losses induced in the PV-system, it was attempted to deduce which losses were common among the different forecasts and which losses that differed. The relative size of the different losses was taken into consideration to assess their importance in the forecasted system performance ratio. The reasons for the observed trends in losses among datasets were attempted given and irregularities were attempted explained.

The comparison aimed at identifying which factors were most influential in deciding the accuracy of forecasting, and relating these to the datasets being used.

3.8.2 Loss due to irradiance level; role of diffuse in datasets

As the datasets hauled from FAGKLIM had to be corrected for errors in the diffuse radiation and Bioforsk didn't supply any diffuse data, the role of the diffuse component was evaluated and the diffuse-to-global ratio was investigated. It was attempted to explain some of the differences seen in the losses identified during the comparison of losses, and relate these to forecasting accuracy.

The analysis was aimed at identifying any irregularities in the datasets which gave grounds for drawing conclusions as to the suitability of datasets.
The role of the diffuse in inducing low transposition factors and the connection to the irradiance level of the different sources was attempted established.

3.8.3 Losses due to soiling; relative improvement in accuracy with overall soiling

Due to the highly unreliable effects of soiling and lack of suitable values, it was decided to make an attempt at suggesting such values in order to increase forecasting accuracy.
Common traits of increase or decrease in forecasting accuracy on a monthly basis were attempted identified in order to be able to suggest appropriate soiling values in simulations.

3.8.4 Accuracy of the detailed shading scenario vs. combined shading model

As there was some uncertainty related to the use of a horizon profile when modeling shading in PVsyst, the use of an alternative shading model was attempted and the accuracy of forecasting was compared to that of the detailed 3D model. This was done in order to establish if the amount of work involved in making detailed shading assessments could be justified on a general basis.

3.9 Economical evaluation

This chapter presents the economic evaluations done in the thesis, in addition to establishing the accepted tolerance levels for accuracy.

3.9.1 LCOE

In the same manner as reports of feasibility studies normally present an economical evaluation, it is of interest to present also some numbers for LCOE in this thesis. This is done mainly to give some economic sense to the result of inaccuracies in forecasting. The calculated LCOE will obviously be correlated to the accuracy of forecasting to a high degree, so this shouldn't come as a surprise to the reader. Nevertheless, the usefulness of the result lies in the relative discrepancy between the LCOE calculated on behalf of the actual yield seen in the RY, and that, which is forecasted.

The investment costs used in the project were not collected for the system in the usual way – by contacting a range of suppliers and choosing the cheapest supplier. One Norwegian solar projecting company was contacted for a cost estimate, stating a price of 60000 NOK excluding value added tax (VAT) [**50**]. The VAT in Norway is normally rated at 25% [**51**], which means that for the roughly 2-kWp system at Aas, the price would be about 37500 NOK/kW_p.

In comparison, the system cost of PV-systems in Germany up to a system size of 100 kW_p, was in April 2014 stated at 1400 €/kW_p for a ready-to-use system including installation and projecting costs [**52**].
With an exchange rate of 8.13 NOK/€ [**53**], this gives a price of roughly 11400 NOK/kW_p, which is less than a third of the price in Norway.

A study conducted in 2013 found the total system price for a ready-to-use system in the Norwegian residential market to be 26000 NOK/kW_p including VAT [**48**]. Consequently, this price was used as the valid system price in this thesis.

The chosen values for the LCOE calculations are:

Table 17: Conditions for the calculation of LCOE

LCOE Conditions			
Variable	Symbol	Value	Unit
Project lifetime	N	25	Years
Project cost	C_0	52000	NOK
System capacity	P_{sys}	2.00	kW_p
Operational costs (per year)	AO	1.00	% of C_0
System degradation rate	SDR	0.50	%/year
Discount rate	DR	5.00	%
Residual value	RV	0.00	NOK

Project lifetime is set to 25 years, which is a normal and reasonable assumption for PV-systems as the module datasheets state this guaranteed lifetime.

The project cost is taken as the rough sum of the modeled system size, and for simplicity is kept the same for the forecasted yield adjusted for mismatch.
The operational costs are often stated as 1% of the total system cost, per year, by solar engineering guides in Germany [**4**]. As Germany is a country where photovoltaic is already widely ingrained in society, this is assumed an appropriate value.

The system degradation rate (SDR) is a value subject to much variation. As most modern PV-systems are still first generation systems, their real lifetimes and real system degradation isn't accurately known. Earlier studies conducted have used values of 0.4% [**48**] and 0.5% [**49**], from which the latter has been chosen.

The discount rate used is one termed almost risk free by one other study [**48**]. It seems that many use a discount rate of 6% to incorporate risk, but this rate should be one of the past as new PV-systems become installed and the frequency of the loans taken becomes higher. As such, 5% is chosen.

The residual value is set to zero. In essence, it is not assumed that the system is much worth at the end of its lifetime.

The LCOE will be calculated for both the forecasts based on modeled system capacity and the ones adjusted for positive mismatch.

One study conducted has claimed that grid parity may be achieved in the Norwegian PV residential market in 2019 [**31**]. The LCOE calculated was therefore briefly compared to the spot price at NASDAQ Nordic market for futures in 2018, and the validity of the claim in mentioned study was considered.

3.9.2 Investor risk tolerance (IRT)

The investor risk tolerance (IRT) is one of the essential measures to assess the tolerated inaccuracy of forecasts.

The IRT is subject to the individual investor, and no general level exists. However, within the renewable energy sector, a key range of 6 – 7% IRT is often encountered, although some are fine with risks up to 10% [**2**].

As mentioned earlier in the introduction to PVsyst, investors bring in engineers to confirm production numbers for solar energy systems. This is often done with PVsyst, and as such, the accuracy is important.
Some earlier assessments of the software have stated that the forecasts produced underestimate production by 5 – 9%.
As such, an assessment of forecast accuracy within this range should satisfy both the IRTs stated.

4. Results and Discussion

In this chapter, all results obtained in the simulations are presented.
Every simulation generates a report about four pages depending on the chosen detail of simulation. Presenting these for five simulations, with seven datasets, would require 140 pages of appendices. Thus, these will not be presented.

Instead, the major parameters of interest are extracted from each report and presented in the form of tables and/or figures.
However, also these data make out a substantial amount of information, which may disrupt the fluency of reading. As such, sections may feature the use of precise values or refer to observed trends, found in tables or figures located in the appendix section. The designated appendix will be cited in sections where this applies. Every subchapter ends with a discussion of the presented results.

To ease comprehension, recall that all meteorological data is collated in Appendix F: Meteorological data, so having this readily available is advised.

Also, a revisit of chapter 3.6.2 The five scenarios, may be in order to recall the settings of different simulation runs.

4.1 Annual system performance

This chapter describes the yearly forecast versus the yearly yield, for all runs and all sources evaluated. The overall system performance is presented, along with information about the precision difference between using meteorological data from databases and weather stations. Furthermore, patterns of deviation among datasets, in the discrepancy between forecasted and actual yield, are stated along with the closest match to the actual yield.

4.1.1 Annual forecast vs. annual yield

The forecasted yearly yield for a PV-system depends on many factors, some of which will be dealt with in more detail in the following subchapters.
However, to have a baseline for comparison, it is of interest to know how the forecasted yield differs from the actual yield of the system on a yearly basis.

The forecasted yearly inverter output for the different evaluated sources is compared to the actual inverter output for the year 2013/2014 in Figure 50:

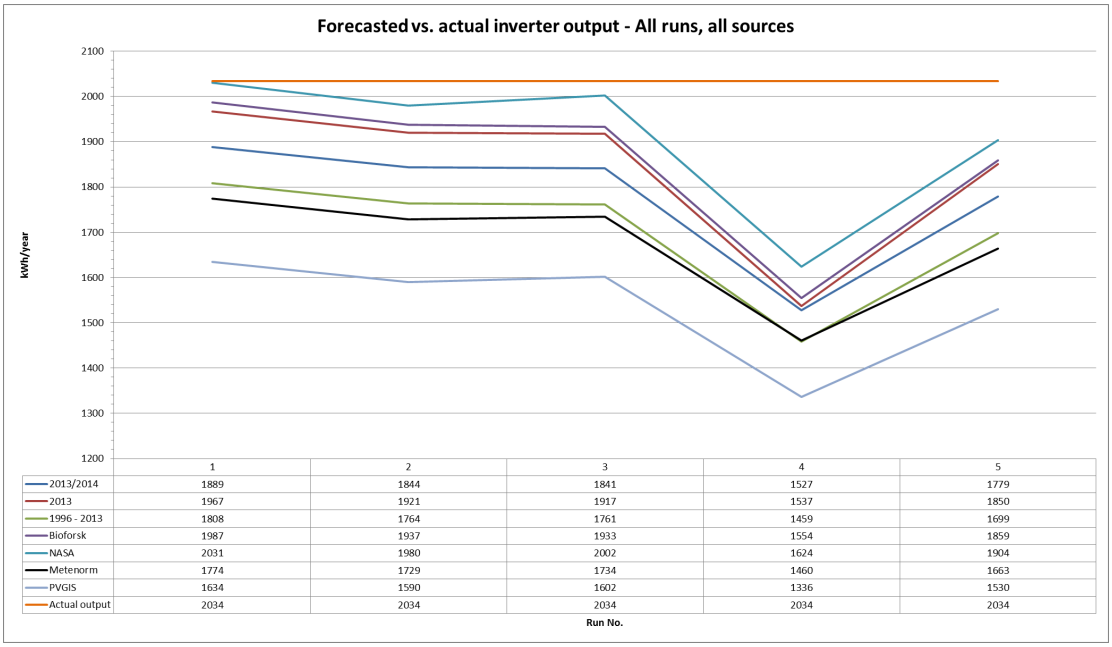

	1	2	3	4	5
2013/2014	1889	1844	1841	1527	1779
2013	1967	1921	1917	1537	1850
1996 - 2013	1808	1764	1761	1459	1699
Bioforsk	1987	1937	1933	1554	1859
NASA	2031	1980	2002	1624	1904
Metenorm	1774	1729	1734	1460	1663
PVGIS	1634	1590	1602	1336	1530
Actual output	2034	2034	2034	2034	2034

Figure 50: Comparison of forecasted and actual inverter output for the PV-system at Aas

As can be seen from the graph the forecasted yield of the system is highest when using meteorological data from NASA as input in PVsyst, this applies for all runs. The Bioforsk forecast comes second, followed closely by 2013 on third, then 2013/2014 (fourth), average 1996 – 2013 (fifth), Meteonorm (sixth) and PVGIS for last (seventh).

In terms of accuracy among forecasts generated from database met-values, NASA comes first, with Meteonorm and PVGIS on a second and third place, respectively.
The most accurate forecasts when using measured data series are obtained by using the Bioforsk met-data, with the 2013 forecast coming second.
The forecast using data from the actual year 2013/2014 comes third, and the average 1996 – 2013 forecast comes on fourth and last place.

The relative change in forecast accuracy can be observed on the slope of the lines. It seems apparent that most forecasts vary in the same manner for the different simulation runs, only exhibiting differences in the detailed soiling scenario (run no. 4). However, upon closer examination, differences may be observed.

The general tendency observed is that the forecasts all are closest to the actual yield in the most ideal case, scenario 1, where only degradation losses and Ohmic losses are included. Thereafter the discrepancy (bias) from actual yield increases when detailed shading is applied in run 2.
This uniformity among the forecasts of all datasets recedes in run 3, when the module layout is incorporated into the simulations.

At this point, the forecasts made with database met-values and measured met values separate in terms of how the discrepancy from actual yield evolves.

The BE of forecasts based on measured met-data continues to increase with simulation run 3 and 4 (detailed soiling), and decreases with run 5 (overall soiling).

In contrast, the database forecasts become increasingly accurate in run 3, though only to a limited extent. Only the NASA forecast gains accuracy of significance, reducing its BE by 1-point percent from 2.6 to 1.6 % (Table G. 6).
After this, the BEs in database forecasts again assumes an increasing behavior with run 4, and a decreasing behavior in run 5.
This is in accordance with the forecasts based on measured met-data.

Other tendencies may also be observed in the measured forecasts.
For example, when studying the slopes from run 3 to 4, the BE increases more for the Bioforsk, 2013 and 1996 - 2013 forecasts, than for the forecast of 2013/2014. This variation appears to continue for the observed decrease in BE from run 4 to 5. The variation of the 2013/2014 forecast in these intervals seems to follow that of the database forecasts, which may appear odd.

The BE , MBE and RMSE of the forecasts for each run can be found beneath in Table 18:

Table 18: BE, MBE and RMSE of all forecasts from all sources

Discrepancy from yield [%] - All runs, all sources										
	2013/2014	2013	1996 - 2013	Bioforsk	NASA	Metenorm	PVGIS	Actual	MBE	RMSE
1	-7.1	-3.3	-11.1	-2.3	-0.2	-12.8	-19.7	0.0	-8.1	10.3
2	-9.3	-5.6	-13.3	-4.7	-2.6	-15.0	-21.8	0.0	-10.3	12.1
3	-9.5	-5.7	-13.4	-5.0	-1.6	-14.7	-21.2	0.0	-10.2	11.9
4	-24.9	-24.4	-28.3	-23.6	-20.2	-28.2	-34.3	0.0	-26.3	26.6
5	-12.5	-9.0	-16.5	-8.6	-6.4	-18.2	-24.8	0.0	-13.7	15.0

As can be seen in the above table, the MBE varies between -8.1% for the most ideal scenario (1), to about -26.3% for the worst scenario (4).
The RMSE is a little higher, being 10.3% the lowest case, compared to 26.6% for the worst scenario.

The highest bias error among all forecasts is experienced with the use of PVGIS data and is -34.4 % for run 4 (detailed soiling), and -19.7% for run 1.
For the most realistic scenario (run 5), the BE is-24.8%.

The lowest bias error was experienced when using NASA data and was -0.2% (match) for run 1 and -20.2% for run 4. Run 5 BE was -6.4%.
Of the forecasts based on measured met-data, the Bioforsk forecasts had a bias error of -2.3% in run 1 and -23.6% in run 4. The run 5 BE was -8.6%.

4.1.2 Discussion of the annual forecast accuracy

The trends in accuracy observed for the different forecasts made may not come as a surprise to most readers. The ranking of sources after amount of annual horizontal global irradiance is the same as that observed for the accuracy of forecasting. This appears logical, as the PV-generator does rely on solar radiation in order to generate electricity. However, the relative accuracy of the forecasts is not linear, as will become clear in later subchapters.

The overall course of the graphs may be expected from the reader.
As the forecasts already in the ideal scenario are below the expected yield, consecutive restrictions will only reduce discrepancy further.

Inducing shading to an ideal scenario will reduce irradiance, and thus yield. Knowing that this shading is applied linearly, without taking the module layout into consideration, the module layout option may at best improve the forecast.
Inducing heavy soiling on the system, will reduce pre-conversion efficiency, and thus reduce yield, leading to a drop in forecast accuracy.
Changing out the heavy soiling - for a more moderate option of overall soiling - will again let the accuracy of forecasts rise, although the accuracy should be lower than in any of the first three runs.

The increasing behavior of the database-graphs in run three, or extra “dipping” and “rise” observed in run 4 and 5, respectively, cannot be easily explained without extra information that will be supplied in consecutive subchapters.

The MBE found for all sources would be too high to satisfy the assumed investor risk tolerance (IRT) of 6 -7%. However, this value disregards the accuracy of individual sources, which may turn out to yield accurate results.

The BE of the different forecasts, for the different sources, may not correlate in an obvious manner.

Table 19 below shows the discrepancy in global irradiance versus the BE in forecast of annual yield, for the different sources of meteorological data:

Table 19: Discrepancy in global irradiance from RY at an annual basis

Global irradiance vs. yield BE -Discrepancy from reference year 2013/2014 [%]							
Source	2013/2014	2013	Average '96 - '13	Bioforsk	NASA SSE	Meteonorm	PVGIS
BE yield	-7.1	-3.3	-11.1	-2.3	-0.2	-12.8	-19.7
Discrepancy Irradiance	0	2.3	-3.5	2.3	5.7	-1.1	-8.7

Taking a look at Table 19 shows that even in the most ideal case, the BE of the NASA forecast is -0.2%, as was mentioned earlier.
This source had a global horizontal irradiance (GH) that was 5.7% higher than that of the reference year (RY), which means that even when incorporating only modest losses, the accuracy of forecast is at match. Most would expect a forecast under such conditions to give an overestimate of the yield.

Evaluating the BE of the best match of forecasts based on measured data, the Bioforsk forecast had a GH 2.3% above that of RY.
Seeing that the GH was 3.4 points-percent lower than the GH of NASA, one could expect the Bioforsk forecast to also have this discrepancy reflected in the yield. This tendency, however, is not observed.

This uncorrelated forecasting becomes even clearer when evaluating the forecast using met-data for the RY of 2013/2014.
The deviance in GH is zero, giving grounds for assuming a forecast unbiased. However, surprisingly, in run 1 its forecast BE is -7.1%.

Knowing that the year 2013 only differs from the RY by the months of January and February, and has a GH 2.3% higher than the RY, with a forecast BE of -3.3%, it dawns that these months may be root of significant error in the forecasts. This will be discussed in the next subchapter.

Continuing to compare differences in irradiance data to the BE in forecasts shows that Meteonorm GH is at -1.1% relative to the RY, with a BE of -12.8% in the ideal run 1. The 1996 – 2013 data series, on the other hand, has a GH -3.5% under the RY, and still yields a forecast BE that is -11.1% in run 1.
Ultimately, when looking at PVGIS, the GH is 8.7% lower than RY, and its BE is -19.7%, meaning that this is the only point where the BEs seems to correlate to differences in yearly irradiance.

The Ohmic losses present in the ideal scenario are constant, so only degradation losses remain as a source of error.
Degradation losses of solar cells are difficult to assess, and determine, so they are subject to assumption in the configuration of PVsyst variations.
If one would subtract these losses (2%), the forecast would be overestimating by the same amount in the ideal case. This would be fine, in an ideal world.

However, when incorporating restrictions to the simulations, one may observe that all forecasts fail to accurately predict the actual yield in run 4, to a significant extent. It therefore seems that this scenario significantly overestimates the soiling amount experienced in reality (More about this in chapter 4.3).

Excluding scenario 4, the only forecasts that would be deemed accurate enough to satisfy IRT in all runs, with the degradation losses subtracted, is the NASA and Bioforsk forecast.
The forecasts using RY data or 2013 data are excluded from this, as they only serve to evaluate the forecasting accuracy of the simulation tool, using the actual reference year data. But, for reference, they both fail to forecast the yield within the stated risk range.

In reality, some degradation will take place. If the fifth scenario is regarded as the most plausible scenario for the system, as many would argue, only the NASA based forecast will have satisfactory accuracy in all instances.

If one would recall the studies saying that PVsyst tend to be conservative in estimations, then bearing in mind that the underestimations have ranged between approximately 5% and 9%, then only some of the forecasts made would fall within this range [**34**] [**38**]. As the studies conducted earlier have no issue of winter soiling, the only relevant comparisons can be made for the overall soiling scenario and the three first scenarios.

Making this comparison, one may find that all sources except PVGIS and Meteonorm yield forecasts within the stated range for run 1.
In run 2, 3 and 5, only the 2013, Bioforsk and NASA forecasts are within the range. That these series are among the most accurate in forecasting yield, may implicate the program is yielding results as expected. If so, then the other sources should be regarded as insufficient for forecasting purposes, which is in accordance with what has already been discussed above.

4.1.3 Annual performance ratio

The PR of the system is as explained in chapter two defined as the ratio of actual yield of the system to that of an ideal system, without losses.

Because this is so, intuitively, many would find it natural to expect a correlation between the annual yield for the system and the size of the PR.
However, the relation between the forecasted or annual yield of a system and its PR may not be that straightforward to deduce. The system producing the most is not necessarily the one operating most efficiently, as will become clear over the course of this analysis.

A comparison of the PRs for the different forecasts made for the PV-system at Aas is shown for all runs in Figure 51 below:

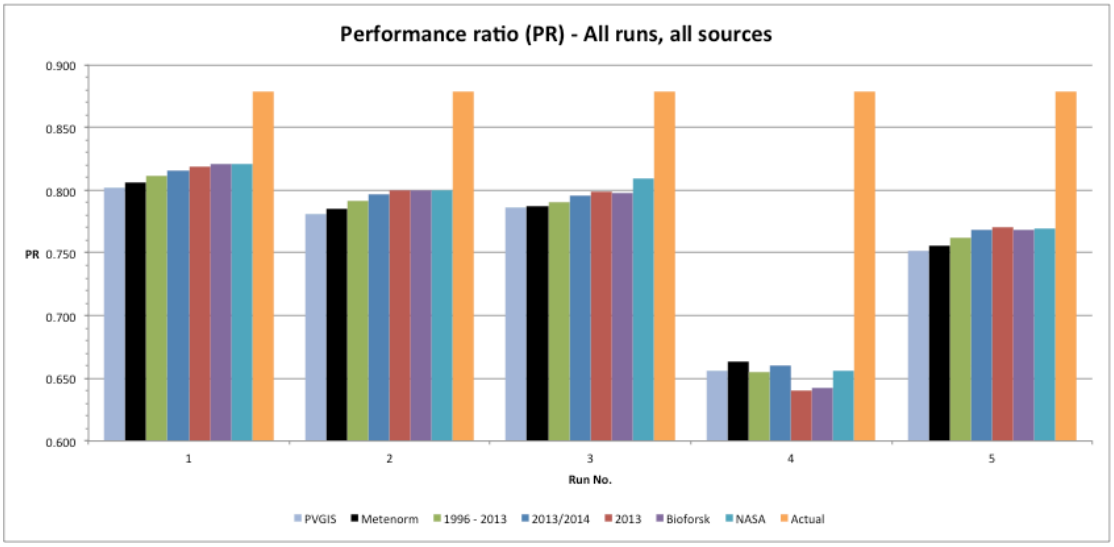

Figure 51: Annual performance ratio for all runs and all sources

Indeed, the graph does illustrate that the performance of the system is well correlated for the three first runs. The order of the system performance over these runs is the same as the general order of the lines for all runs in Figure 50.

The actual system performance is constantly the highest.

The forecasted system performance is best with NASA data, and then performs second best using Bioforsk data, followed by the third best performance using 2013 data. The forecasted system performance then decreases in the order 2013/2014, 1996 - 2013, Meteonorm and PVGIS for last.

Also note how the system performance changes relatively uniformly between run 1 and 2, before it then starts becoming better for the NASA forecast in run 3. Simultaneously, the performance for the Meteonorm and PVGIS forecast become higher, without it really appearing so at first look.
The new observation in this instance is that the performance for the PVGIS forecast apparently increases more, getting more even with the performance of the system with Meteonorm data.

However, for the 4th and 5th run, the correlation seems to be less obvious. Where the order of the most accurate forecasts of annual yield would stay the same, the order of PRs change, and it is different for both the last runs.

In run 4; the system actually performs best when using Meteonorm data.
The system is second best using the 2013/2014 data, and third best using NASA data. The order of performance then decreases in the order 1996 - 2013, PVGIS, Bioforsk and 2013 for last.

In run 5; the forecasted system performance is ordered almost as in the three first runs, only it performs best using 2013 data, second best with NASA data and third best using either Bioforsk or 2013/2014 data (see discussion).

The values of all PRs calculated can be read from Table G. 4 (Appendix G.2: Simulated annual irradiance, yield and PR).
The actual PR is 87.9%, which is a high value for a PV-system (see chapter 2).

The closest match was when using NASA data, with a PR of 82.1% in run 1.
The closest match when using measured data was with Bioforsk data in run 1, the PR was then found to be 82.0%.
The worst PR of 64.0% was encountered when using 2013 data in run 4.
When using databases, the worst PR is 65.6% and was encountered in run 4 by the use of PVGIS data.

If one looks at the variability (SD) of the PR for each run, it can be calculated according to the formulas in 2.5.1 Uncertainty related to the mean.
The value is generally below 1%, which should be considered acceptable.

4.1.4 Discussion of the annual PR

Regarding the performance ratio, some of the discussion related to this measure should be postponed until more information is revealed in later subchapters. Therefore, some questions may be left unanswered until this information is available, as in the last discussion.

As was seen in the results, the way the performance ratio change is relatively homogeneous in the first three runs. Actually, the PR drop is about 2% for the system between run 1 and 2, for all data sources.
This may be attributed to the fact that the shading induced is constant, regardless of the source used. Because the PR is stated according to ideal insolation converted at STC efficiency, without pre-conversion losses, a 2% drop in incident irradiance in plane of array due to shading would cause a similar drop in PR for all forecasts.
The minor differences that exist, although considered insignificant, may most likely be attributed to a higher share of diffuse radiation.

There also is no significant decrease in PR from run 2 to 3, which means that for this particular system configuration, simulating module layout isn't necessary to get an accurate forecast of system PR.
This is in accordance with the trends observed in forecasting.
However, for larger plants and arrays, this particular trend may not be the case. Shading effects are more severe for some configurations than others; the module layout option is made to be able to minimize these.

Seeing that the changes in PR of the three former runs are less important, the discussion may be centered on the events in the last two runs, where the order of efficiency has been rendered.

The trends observed in going from run 3 to 4, may have root in the months of January and February, as mentioned earlier. Looking at the total losses from STC, one may observe that the system has lower losses in run 4 for the forecast based on RY data, than for the forecast based on 2013 data.
As such, the same argument may apply for the PR as it did for yield; something may be off in the two first months of the year.

The performance ratio all the sources are not all that different in run 4, most forecasts yield losses around 34%, give or take a few decimal per cent.
The Bioforsk and 2013 based forecasts yield a poorer system performance than the other five sources; this will be discussed in following chapters.

Run 5 is in accordance with the 4th run; the Bioforsk and NASA data yield forecasts where the system performs worse. This may be attributed to inherent differences between these data and the other data used, and explained later.
The apparent emergence of the 2013 data series as best forecast of system performance shows how the two first months of the year differ from the RY; with heavy soiling, the PR is of the system is worse with 2013 data than with the RY data, a tendency that disappears when heavy soiling is removed.

4.1.5 Section summary: annual data

The BE of the forecasts are not well correlated to the level of irradiance the sources have compared to reference year.
The MBE of all runs were -8.1% for the most ideal scenario with an RMSE of 10.3%. This is unsatisfactory in terms of IRT.
The worst-case scenario MBE was -26.3% with an RMSE of 26.6%.

The most accurate forecasts are produced when using met-data from the NASA SSE database as input in PVsyst, it had a BE of -0.2% in the ideal case, and -20.2% in the worst case scenario.

The second most accurate forecasts are produced when using Bioforsk measured time series as input, giving a BE of -2.3% in the ideal case and –23.6% in the worst-case scenario.

The least accurate forecasts are produced when using PVGIS data, yielding a BE of -19.7% in the ideal case and -24.8% in the most realistic case. Thus, this source cannot satisfy the IRT.

Excluding the worst-case scenario, the forecasts and NASA meteorological data are within the assumed IRT, and Bioforsk satisfies this for the first three scenarios. Both sources yield forecasts in the range of 5 - 9% found in earlier studies.

The RY data fails to yield a satisfactory forecast, differing significantly from the year 2013, which is only different by the months January and February.
These months are assumed to be main source of errors in forecasts.

4.2 System performance on a monthly basis

This chapter goes into detail about the monthly distribution of forecasted versus actual yield, for all runs and all sources evaluated. Patterns of deviation among datasets, in the discrepancy between forecast and actual yield, are stated on a monthly basis. The relative monthly discrepancy from actual yield for months that stand out is stated, along with average monthly and yearly discrepancy.

The tables referred to in this section are located in Appendix G.6: Simulated monthly yield - All sources.

4.2.1 Monthly forecast vs. monthly yield

The monthly distribution of yield may hopefully shed some light onto how the differences in yield on an annual basis are related to the input in meteorological data.

It is first and foremost the amount of inverter output and how it is distributed over the year that is of interest. As was mentioned in the previous subchapter, a suspicion already exists that the months of January and February may be involved in inducing bias errors in the forecasts produced by PVsyst.

The best performing forecasts were made with NASA SSE data, thus the monthly distribution of these data should be studies.

The forecasted monthly distribution of inverter output of the system at Aas using NASA SSE met-data is shown below, in Figure 52:

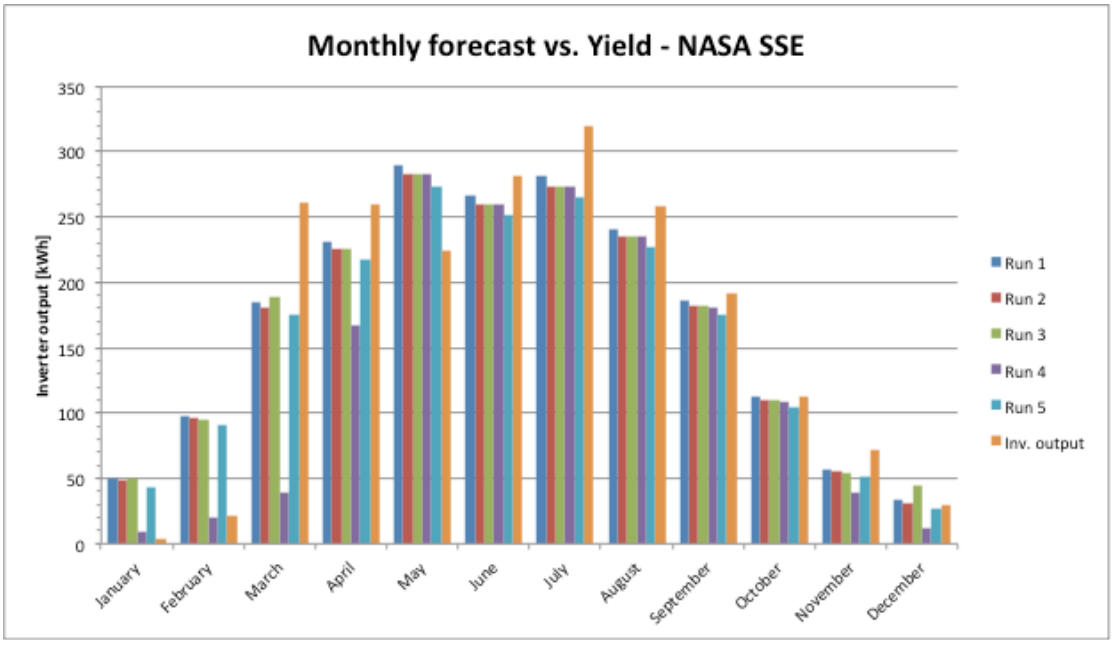

Figure 52: Monthly distribution of forecasted vs. actual inverter output

The monthly distribution shows that the forecasted inverter output is significantly higher for the months January and February, than that of the actual inverter, for all runs except run 4.
In this run the forecast also deviates significantly in March and April, and in November and December.

Excluding run 4, the forecasted output seems to be underestimated for all months except May, where it is significantly overestimated for all runs, and December, where it is overestimated by a little less.
The forecast for run 5 underestimates the inverter output in December.

In order to get a sense of the magnitude of the BE in the forecasts that do well, it may be of help to look at how the data are doing numerically.
The Bioforsk forecasts were doing best of the all forecasts based on measured data, and they bear similarities to the NASA SSE forecasts in terms of how the BE evolved between runs.

Table 20 below shows the BE of all forecasts based on Bioforsk data, along with the MBE and RMSE of all runs on a monthly basis. In addition to the BE of the calendar year, the monthly average BE of each run is shown.
To show the significance of January and February over the year, the yearly and monthly average BE is also calculated excluding these two months.

Table 20: Overview of the BE of the forecasts based on Bioforsk data, including MBE, RMSE

Bioforsk forecasts - annual/sub annual and monthly avg. BE, MBE and RMSE [%]							
Run. No	1	2	3	4	5	MBE	RMSE
January	1692.9	1645.0	1603.4	213.2	1446.8	1320.3	1434.0
February	342.3	333.2	330.9	-11.5	312.8	261.5	295.2
March	-18.7	-20.5	-21.0	-82.7	-23.2	-33.2	41.4
April	-9.4	-11.4	-11.4	-34.8	-14.5	-16.3	18.8
May	20.5	17.5	17.5	17.4	13.8	17.3	17.5
June	1.1	-1.5	-1.5	-1.5	-4.6	-1.6	2.4
July	-19.8	-21.9	-21.9	-21.9	-24.4	-22.0	22.0
August	-16.8	-19.0	-19.0	-19.1	-21.6	-19.1	19.1
September	-9.4	-11.5	-11.6	-12.0	-14.8	-11.9	12.0
October	-10.1	-12.1	-12.6	-13.1	-15.9	-12.8	12.9
November	-36.6	-38.3	-38.9	-57.4	-43.0	-42.8	43.5
December	35.3	29.2	28.8	-50.2	7.7	10.2	33.2
Year	-2.3	-4.7	-5.0	-23.6	-8.6	-8.8	11.7
Year ex. Jan. & Feb.	-8.7	-11.0	-11.2	-24.1	-14.4	-13.9	14.9
Monthly avg.	164.3	157.4	153.6	-6.1	134.9	120.8	162.7
Monthly avg. Ex. Jan. & Feb.	24.3	21.5	21.0	-23.7	16.5	11.9	48.5

From the above table, it can be seen how the forecasts consistently overestimate the inverter output in January and February, giving a MBE of 1320% in January and 262% in February.
May stands out as significantly overestimated, and the same goes for December, although the fourth run shows a significant underestimation.
The MBE of these two months are 17.3% and 10.2%, respectively.

Significant underestimation is seen in March, July, August and November - the MBE of these months are -33.2%, -22.0%, -19.1% and -42.8%, respectively.

The monthly average MBE is at 121%, which is severely high.
Taking a look at run 4 shows that the monthly average is a mere -6.1%, which stands out compared to the rest of the runs.
If the monthly BE is averaged excluding January and February, it is reduced significantly for all runs, except run 4.
Averaging the monthly MBE for all runs excluding January and February shows that it is reduced from the former 121% to less significant 12%.

On an annual basis, the MBE is -8.8%, compared to a BE of -23.6% in run 4.
Excluding January and February, the annual MBE decreases from the former value -8.8% to a more significant -13.9%.
Simultaneously, the BE of run 1 more than triples, while the BE of run 2, 3 and 5 approximately double. In contrast, the BE of run 4 only shows a minor difference, going from -23.6% to -24.1%.

Note that the overestimation made in December, run 5 is, exclusive to the Bioforsk forecast. All forecasts made from other sources show an underestimation at this point.

In order to more closely examine how these trends apply to other sources, it may be regarded sufficient to look at the monthly MBE, in addition to average monthly and annual MBE – both with and without the months of January and February. This is because the trends in monthly BEs are clearly reflected in these values, knowing that the BEs of run 4 will have a smaller influence on the mean.

As was said initially, the Bioforsk forecasts were similar in the evolution of BE over the different scenarios evaluated, to the forecasts of NASA.
The trends observed in the MBE and BEs in the Bioforsk forecasts therefore also apply to the forecasts based on NASA SSE data, though with some differences.
For the NASA forecasts, the trends are a little less pronounced, except for May, where the MBE is 25.7%, and March, where the MBE is -41.0%.
The MBE in January and February is, 1183% and 263%, respectively.
Also, the NASA forecasts don't yield the significant BEs (or MBE) in August.

Considering the 1996 - 2013 series, the forecasts are very similar to the already mentioned trends. The MBE in January and February is third highest of all evaluated sources, being 676% and 186%, respectively and the monthly average BE is higher than for Meteonorm in all instances. This is in accordance with the ranking of the forecasts in terms of accuracy.
April month stands out, having a lower MBE than for NASA forecasts and Bioforsk forecasts, though higher than for Meteonorm forecasts.

The Meteonorm forecasts bare similar trends as the Bioforsk forecasts in all respects only are showing differences in that they significantly underestimate yield in more months of the year. They are consistently underestimating in other words. Also, the MBE in January and February is among the lowest observed, only beat by PVGIS.

The PVGIS forecasts are consistently performing worst in terms of BE, so the MBE and RMSE values they yield are of interest as well. They may be read from an excerpt of the PVGIS BE table x, shown in Table 21 below:

Table 21: Monthly, avg. monthly, annual and sub-annual MBE and RMSE

PVGIS forecasts – annual/sub annual and monthly avg. BE, MBE and RMSE [%]		
Month	MBE	RMSE
January	638.3	704.8
February	143.5	171.3
March	-58.8	60.9
April	-32.5	33.4
May	7.0	7.2
June	-14.5	14.6
July	-27.3	27.3
August	-25.1	25.2
September	-26.5	26.6
October	-32.6	32.6
November	-52.0	52.3
December	-26.4	34.8
Year	-24.4	24.9
Year ex. Jan. & Feb.	-27.2	27.5
Monthly avg.	41.1	99.3
Monthly avg. Ex. Jan. & Feb.	-28.9	31.5

In accordance with the previously presented results, the MBE is significantly higher in January and February.

Most other months are significantly underestimated; the BEs of March and November stand out compared to the rest, being -58.8% and -52.0%, respectively.
The months April and October also shows significant underestimation, though less severe than in the preceding mentioned months.
May is, as in any other case, is overestimated; the MBE is "only" 7 % and the RMSE the lowest for all forecasts produced, among all sources.

Turning to the annual MBE, it may be seen that it decreases slightly when excluding January and February, that is, the RMSE increases.
Simultaneously, the RMSE increases when taking the monthly average for the year, excluding these two months.
This is analog to the trend shown in both Table 20 and Table 21, and for reference, the trend that can be seen in the forecasts based on all sources, except for the RY.

Studying the tables for discrepancy in Appendix G.6: Simulated monthly yield - All sources; it can also be seen that for run 4, the RY is the only data set where

the annual BE of the forecast increases. Going from -24.9% to -24.2% on an annual basis, when excluding January and February, the difference is not all that much – but still apparent.

The pattern of deviance registered in run 4 in Table 20, with a reduced positive BE in January and a slightly, but significant, negative BE in February – is a common pattern of deviation registered among most of the forecasts made.
Only the forecast for the RY shows a different pattern, where both months show a significant negative BE. Actually, the RY forecast has negative BEs for all runs in February. Also, the BE of May is consistently negative, in contrast to all other forecasts.

The MBE of the RY forecast is comparable to that of all other sources, though with the lowest value observed for all sources in January.
In February, the MBE is negative, reflecting the negative value of the BE for February in all runs. For May, the value is also negative, in accordance with what was stated above. All other months, the trend is relatively similar to that described for Bioforsk, with an underestimated July, November and December.

The forecasts based on 2013 data show a trend somewhere in-between that of the reference year and the other sources. The BEs are in accordance with those found for other sources for most of the year, the same is the MBE.
The only real difference is that May is underestimated.

For the forecasts based on both the RY and 2013, it should be noted that March is relatively unbiased, compared to all other forecasts, regardless the source.

4.2.2 Discussion of monthly production data

In order to comment on the most relevant results first, it is of interest to recall the primary problem statement of the thesis: What is the existing discrepancy between forecasted and actual yield?

The last subchapter managed to answer this question and state which of the sources used as input that was most accurate in forecasting: NASA and Bioforsk.

The result in this subchapter shows that the reason why these sources may be so accurate in forecasting is because they overestimate production in months where production is actually low.
This fact is undisputable; taking the monthly average of the BEs shows a lower value when excluding the months with the highest MBE.
Simultaneously, this leads to an expected increase in the annual BE.

In essence, it seems like the actual accuracy of the forecasting isn't at all as high as one would like to believe, which means that the real discrepancy should be even higher.

Many would argue the case that the most important issue when planning a PV-system is that the forecast may satisfy the IRT, which we have found is possible in one case. However, the new information obtained shows that the forecasts

generated may be significantly inaccurate if used for system optimization for parts of the year. This is not a problem necessarily related the simulation tool, but rather a problem related to the input, the meteorological data.

In order to clear up where the data should have been accurate, and where not, it may be necessary to look at the actual RY, to reveal where the irradiance differs. One would expect a clear correlation between the incoming radiation for the different sources and the amount they overestimate in the months that have been mentioned. However, this relation is not so simple as one would expect.

Taking a look at the monthly global irradiance data incident on the horizontal plane (Appendix F: Meteorological data), it may be observed that the RY has lower irradiance in some months than others. This is natural, as not every year is the same, and some months will have more sun than others.

Upon closer examination of the irradiance chart, it is evident that the months of January and February in the RY receive less irradiance than all the other time series. Thus, it may appear logical why these months are overestimated on a general basis.

Especially when considering the average data series, 1996 - 2013, it is obvious that the month of January and February was a month that received little irradiance in the RY. The 2013 time series confirms this, as it shows more incoming irradiance in these months and is closer to the average.
Also note that the Bioforsk time series, which is an average of the nine most recent years, 2005 - 2013, is even higher. The NASA series, in both of these months, is close to the two average series.

Examining the simulated monthly yield for the RY and the BEs, it may be seen that the BE in January is the lowest found in any forecast, although it still does overestimate the inverter output for all runs except run 4.
In this run, the forecast underestimates the yield, which means that soiling apparently was an issue in the RY for January - more about this in the next subchapter.

In February, the trend is one of constant underestimation of yield, a tendency that gets worse in run 4. This seems odd, as it means that the performance of the inverter in the RY was close to 94% in this month. This is not impossible, but definitely unlikely, especially considering the diffuse to global ratio (DGR).
In this case, the solution may actually lie in the DGR, as it was adjusted to make up for un-calibrated measurements, and the correction factor in low irradiance months was told to be inaccurate. If the diffuse correction factor was supposed to be somewhere at 1.05 and was calculated as 1.31, then the direct beam components should have been about 20% higher.

However, how this would influence the output is highly speculative.
It is definitely possible that it would lead to significant improvement in accuracy of the forecast, although unlikely, as the highest amount of radiation is not

incident in this part of the year, giving February a minor influence on the overall performance of the year.

In light of this evidence, it seems that the two first months of 2014 were abnormal in terms of irradiance, and in fact about every other time series showed a more normal irradiance. If these months had been overestimated in the same manner as the other forecasts do, the annual RMSE would increase. The fact that the annual RMSE goes down when January and February is excluded supports this theory.

Using NASA SSE data yields the most accurate annual forecasts, and it therefore is reasonable to expect it to have the highest MBE in January and February - considering that the overestimation of these two months may have been reason for this accuracy. However, as was shown in the results, this is not the case.

Of all the sources, the highest MBE in the forecasted inverter output for January was obtained when using the Bioforsk data.
The fact that NASA is the source receiving the most radiation in this month means that other factors play an influence in determining the forecast.
In February, on the other side, there is a correlation; NASA data shows most irradiance and has the highest MBE, but the difference between the MBE is only about one single percent. Somehow, Bioforsk data tend to overestimate the production by more than NASA data. Albeit the incident radiation in January comes second to NASA, the difference may be considered insignificant.

One proposed mechanism that could be the reason for this is temperature, although the differences between the sets in January and February are minor. Looking at the forecast BEs in these months, one sees that Bioforsk overestimates more in January, though the temperature is higher.
In February, the differences in BE are insignificant - only a tad lower - with a lower temperature. Thus this mechanism is purely speculative at best.
As will be seen in the next subchapter, temperature has a smaller overall impact on the performance this system, but might be a reason for the observed phenomenon.

Another proposed mechanism that may be the reason is the diffuse to global ratio (DGR), which is lower for the Bioforsk data in the months discussed, a subject that will be covered in the next subchapter.

Studying the other sources for these months shows that 2013 had the third highest irradiance, average 1996 - 2013 received fourth most, PVGIS fifth most, with Meteonorm on a sixth place. The ranking of the months in terms of MBE is 2013, average 1996 - 2013, Meteonorm and PVGIS. In addition, the month of February showed the highest MBE for the average 1996 - 2013.
In essence, no reasonable correlation is found between these MBEs and the irradiance data. Another look at DGR may yield a better comprehension.

Continuing this line of though, recall that the only real difference between the RY and the 2013 time series, are these exact months (January and February).

Thus, when looking at the remaining ten months of the year, one may contemplate the two time series as one and the same.

Examining the irradiance chart with this in mind shows that March, April and July receive more irradiance in the RY than in all the other time series.
Hence, in these months, one would expect the forecasts based on all the other time series to underestimate in these months.
Indeed, this is exactly what the data shows.

In the same manner, from the chart one may see that the month of May shows that the RY received less than expected irradiance, which is why this month is consistently standing out as overestimated in the forecasts.

However, the correlation between the sources showing the highest amount of incident irradiance in these months is not well proven. Trying to see how the different sources do correlate to the months of March, April and July shows that the sources correlate in order for March and July, though not for April and May. As such, the way radiance is tied to the forecasted yield seems highly random; which might be acceptable, considering weather is highly unpredictable.

Looking at August may yield answers in what happens that makes NASA data forecast more accurately in this month.
Apparently, it does have the highest amount of irradiance (ex. RY), followed by Bioforsk and the 1996 – 2013 average.
Unfortunately, the correlation is unclear also here; the Bioforsk forecast underestimates more in this month than the average series, albeit the NASA forecast is more accurate in forecasting than the reference year.

The trend in correlation between irradiance and forecast BE is more obvious for NASA and the RY in September, though again shows a deviating behavior when assessing how Bioforsk irradiance is correlated.
The irradiance received by Meteonorm is second highest after NASA, though shows a lower MBE (higher RMSE) than the Bioforsk forecast.

Remembering that the diffuse irradiance of Bioforsk is synthetically generated by PVsyst, it dawns that this factor may indeed be the culprit causing this pattern. Though, as will be seen in the following subchapter, this is no easy argument.

Considering November shows that only NASA overestimates the irradiance in this year, whereas both the averages (1996 - 2013 & Bioforsk), and the other databases, lie significantly lower than the RY in terms of irradiance.
Consequently, November was a good month sun wise, and one would expect well-correlated forecasts for NASA and the RY.
However also here, the BE of both sources is significant - although in the same order of magnitude – both being negative. Consequently, all other time series yield negative forecasts too, indicating a significantly higher system performance in reality than what is reflected in any meteorological data.

December, lastly, does show that the order of irradiance gives a reasonable correlation with forecasted yield, though not for the sources showing the least amount of incoming irradiance in this month: average 1996 – 2013 and Meteonorm. Here the average forecast has a higher December MBE than the Meteonorm forecast, again showing that the relation between irradiance and production is a complex one. Regarding the deviation of Bioforsk for December, this may be related to the DGR, as will be seen in the next subchapter.

The exclusion of the months of January and February may be seen as a necessary approach see what the real BE forecasts should be. Because May and December is insignificant in overestimation, compared to these months, the exclusion of these months is hardly necessary.

4.2.3 Section summary

From the discussion of the monthly data, it seems apparent that excluding January and February does removes a significant source of error in the data, as the yield in these months is consistently overestimated.

The overestimation is in part assumed to be caused by deviation in the meteorological data for the reference year in the months where it applies. Thus, excluding the months gives a more realistic comparison of forecast accuracy, removing errors in data at one hand, and overestimations on the other.

This means that the real RMSE of forecasts should be higher and thus more inaccurate. The most accurate forecasts, based on NASA SSE and Bioforsk data, are as accurate as they are mostly due to a high RMSE in the mentioned months.

This may not be of interest for the general planning of a PV-system on an annual basis, but shows that planning for parts of the year may be considered unsatisfactory.

The correlation between irradiance of individual moths and the BE observed is highly speculative in nature and cannot be well proven.
A source of error for this pattern may be the temperature to a minor degree, albeit more likely the diffuse to global ratio (DGR), which will be discussed in subchapter 4.3.

4.3 Discrepancy analysis

Here, losses are compared for all runs and all sources, particularly looking at losses from irradiance, shading and soiling.
The role of diffuse radiation in irradiance losses is evaluated, and the relative improvement of accuracy in forecasting using overall soiling values is discussed.
Further, the accuracy of the detailed shading scenario is compared to that of the simplified shading scenario, along with shading losses for different runs.
Ultimately, the performance ratio calculated from the losses is compared to that calculated from the yield to establish inaccuracy of rounding significant figures.

4.3.1 Comparison of losses

The different losses induced on a system are of interest to evaluate where the differences in system performance are most obvious. This may give hints as to where to look for deviations between meteorological datasets.

It is already clear which data sources yield the best forecasts, and as all settings are equal for the different sets, the best performing forecasts should stand out in one way or another.
If attention is directed first to the best performing forecasts, which are based on NASA data, this forecast may give information about trends observed.

The losses calculated and presented in each report that follows a simulation run, have been collected and tabulated.
You may find these tables in Appendix G.7: Simulated losses – Tabular presentation of values from reports.
.
Table 22 below shows the table of losses for the forecasts based on NASA met-data – all values are listed in percent. Negative is regarded loss, positive addition.

The transposition surplus (TP) represents the extra amount of radiation received in the plane of the array due to the transposition factor R.
It is the number following the decimal place after the number 1, which indicated a horizontal module. For example, in the case of NASA, R = 1.244.
The TP may vary according to the relative amount of diffuse radiation in a dataset (see 3.3.4 Accuracy of PVsyst).

The importance of the TP mainly lies in our ability to deduct the amount of forecasted ideal radiation incident in the plane of array, being able to compare the influence on performance ratio (PR).

The PR in turn may be calculated by eq. (2.17a), by multiplying the optical efficiency and the relative system efficiency. The respective efficiency is calculated by subtracting the respective loss from the number 100 and dividing on 100.

The listed change in PR is located in the last table row - it shows the difference between the PR calculated from the yearly yield and reference yield.
As may be seen from the table, there is small difference in the two performance ratios, especially in the fourth run, where it is more significant.

Most sources have values for absolute deviation of less than one percent. The only common treat in terms of different PR is in the fourth run, where most data series show absolute deviations upwards of one percent.

Table 22: Comparison of the losses for all forecasts made with the NASA SSE met-data

Forecasted losses [%] - NASA SSE					
Run	1	2	3	4	5
Transposition	24.4	24.4	24.4	24.4	24.4
Near shading	0.0	-2.6	-2.6	-3.2	-3.2
IAM	-3.1	-3.0	-3.0	-2.9	-2.9
Soiling	0.0	0.0	0.0	-15.8	-3.0
Optical loss	-3.1	-5.6	-5.6	-21.9	-9.1
Irradiance	-7.9	-8.1	-8.1	-8.8	-8.4
Module quality/LID	-2.0	-2.0	-2.0	-2.0	-2.0
Module layout	0.0	0.0	-0.1	0.0	0.0
Temperature	-0.4	-0.3	-0.3	-1.1	-0.2
Ohmic	-0.9	-0.9	-0.9	-0.9	-0.8
Inverter	-4.6	-4.6	-3.4	-5.0	-4.7
Total system loss	-15.8	-15.9	-14.8	-17.8	-16.1
PR	81.6	79.4	80.4	64.2	76.3
ΔPR	-0.5	-0.6	-0.5	-1.4	-0.7

From the table above, one may deduct that the transposition surplus (TP) was 24.4% in this case. For reference, the only other time series that showed a higher TP was 2013, with 24.8% and Bioforsk, with 26.2%.

The near shading losses lie at 2.6%, but increase and maintain 0.6% higher for the runs where soiling applies, at 3.2%.
This general trend is observed for all forecasts, regardless the source, with only minor variations. Some sources might yield a value 0.1% lower in the 2nd run, than in the 3rd, but still assume constant values in the two last runs.
The general increase in shading loss with the onset of soiling is not as high as in the NASA case, generally speaking – but generally is about 0.5%.
This variation doesn't appear significant.

One also sees that the IAM losses are relatively constant, for all scenarios.
This trend is observed in all forecasts made, with only minor variations.
The small decrease in IAM loss seen between run 1 and 2, is also a trend that consistently appears among all the forecast – albeit also regarded insignificant.

The soiling losses in the case of NASA forecasts are collectively at 15.8% in run 4. In comparison, the 2013 forecast show the highest soiling losses (17.5%) in run 4, followed by Bioforsk forecasts (17.3%). The PVGIS forecast has the second lowest values (13.9%) and Meteonorm has (13.7%).

In run 5, the soiling value was set, and hence does not change for any forecast made.

In terms of overall optical loss, the NASA forecasts come second only surpassed by Bioforsk (23.6%) and 2013 (23.4%). In comparison, the reference year (RY) has optical losses of 21%, while PVGIS and Meteonorm have 20.2% and 20.0%, respectively.

To look at system losses, it might be interesting looking at another table, to see how it compares to the one of NASA. Taking PVGIS as an example may show how the losses vary. The forecasted losses for PVsyst are shown in Table 23:

Table 23: Comparison of forecasted losses using PVGIS met-data

Forecasted losses [%] - PVGIS					
Run	1	2	3	4	5
Transposition	18.8	18.8	18.8	18.8	18.8
Near shading	0.0	-2.8	-2.8	-3.3	-3.3
IAM	-3.3	-3.1	-3.0	-3.0	-3.0
Soiling	0.0	0.0	0.0	-13.9	-3.0
Optical loss	-3.3	-5.9	-5.8	-20.2	-9.3
Irradiance	-9.1	-9.2	-9.2	-9.8	-9.6
Module quality/LID	-2.0	-2.0	-2.0	-2.0	-2.0
Module layout	0	0	-0.2	0	0
Temperature	-0.7	-0.6	-0.6	-1.4	-0.5
Ohmic	-0.8	-0.8	-0.8	-0.8	-0.8
Inverter	-5.1	-5.2	-4.2	-5.6	-5.2
Total system loss	-17.7	-17.8	-17.0	-19.6	-18.1
PR	79.6	77.4	78.2	64.2	74.3
ΔPR	-0.7	-0.7	-0.5	-1.4	-0.8

One of the apparent trends in this table is how the TP is lower.
Consequently, it appears the diffuse modeling made in PVsyst has a significant impact on the amount of available radiation, and hence, forecasted yield.
Other optical loss factors remain similar as before.

Looking at irradiance losses, one may observe that these are about 1% higher for all runs, compared to those of the NASA forecast. This trend is not one usually seen in the other tables. Meteonorm has losses about 0.5 – 0.7% higher, but most others have losses that are 0.3% higher.

The module quality losses were assumed constant, so these generally won't be commented.

In module layout, we see that there is an insignificant loss in run 3 of 0.2%.

Out of all the forecasts, the only data series failing to show this treat is the RY and 2013 data series. This indicates that module layout will have an effect when simulating systems, albeit insignificant for most practical purposes.

The temperature losses are seemingly constant for all runs, with only minor alterations between runs. Thus, the overall performance doesn't seem to be largely influenced by this parameter. However, it should be noted that the temperature losses are larger than for NASA forecasts, and that Bioforsk forecasts don't show any temperature loss at all, except in run 4.
The temperature losses for Meteonorm are all above 1%, except in run 5.

The trend generally observed is a relatively constant temperature loss over all the runs, regardless of met-data used. Only run 4 and five deviate significantly. Usually, the loss is highest in run 4 and lowest in run 5, of all runs made.
This indicates a general (albeit odd) correlation between soiling and temperature loss; heavy soiling heats the module, while light soiling cools the module.

The Ohmic losses are generally considered insignificant; they never exceed the 1%-barrier for any forecast. This is as expected; the Ohmic losses were calculated from the amount of cabling the system has.

Also inverter losses are generally maintained at a relatively constant level, they usually make out about 5%, give or take a few decimal percent.
These losses generally also increase in run 4, reflecting the lower efficiency in inverters when the load is reduced.
The only significant exception in all of the forecasts made is NASA, which generally has a little lower level of inverter loss.
In run 3 these losses are at 3.4%, which is below 1% of that seen in forecasts based on most other sources, in the same run. However, both Meteonorm and PVGIS forecasts do show the same reduced losses in run 3.

Turning attention to the system loss, PVGIS shows general losses at 17 - 18%, only offset by run 4, where it is closer to 20%.
This level of system loss is the highest among all forecasts.
Interestingly, when looking at the other forecasts, the level of losses is lowest for NASA forecasts, and decreases in the order of the forecasts.
This is in accordance with the trend observed in PR, earlier in
If one would recall the studies saying that PVsyst tend to be conservative in estimations, then bearing in mind that the underestimations have ranged between approximately 5% and 9%, then only some of the forecasts made would fall within this range. As the studies conducted earlier have no issue of winter soiling, the only relevant comparisons can be made for the overall soiling scenario and the three first scenarios.

Making this comparison, one may find that all sources except PVGIS and Meteonorm yield forecasts within the stated range for run 1.
In run 2, 3 and 5, only the 2013, Bioforsk and NASA forecasts are within the range. That these series are among the most accurate in forecasting yield, may

implicate the program is yielding results as expected. If so, then the other sources should be regarded as insufficient for forecasting purposes, which is in accordance with what has already been discussed above.
4.1.3 Annual performance ratio.

Regarding the PR, it is interesting to note, that among all sources, the forecasts made yield approximately the same performance ratios within the same run, when calculating them from the losses. Only minor variations exist; consequently, the 1st run shows PRs of 81% give or take a little.
Also, for run 4, the only sources that really stand out with lower PRs are Bioforsk and 2013, having a value approximately 2 points-percent below that of the rest.

4.3.2 Discussion of losses

Finding PRs different when utilizing an alternative equation may seem strange at first instance, as they really should have been the same.
The first thought that appears in this context goes to significant figures.
In the PVsyst reports, one may see that the figures for yield are rounded, often displaying four significant figures in the loss diagram when stating energy quantities. Also, the efficiency at STC is stated to this extent, so it has two decimals.

If one looks at the loss tables, one may find that as restrictions are applied consecutively in the runs, the number of loss factors increase.
Moreover, the losses are stated to two significant figures.
Thus, if every loss factor is regarded as a single efficiency factor, all of these multiplied may yield high rounding errors, if the loss factors are rounded before every multiplication.

Table 24 below shows a trial calculation in Excel for run 4, multiplying each of the consecutive losses in each group of losses to yield the efficiency.
It is clear from the table that the PR calculated by the column of reduced values, stated to 6 instead of 5 significant figures, gives an error in calculation of 0.714%. Thus, the program does seem to have a built in mechanism for overstating losses.

Nevertheless, the PRs calculated from yield usually do show approximately the same values as the ones displayed in the PVsyst report.
Thus, these may be assumed the correct ones. The results obtained by comparing the values mainly serves the purpose of enlightening planners of the apparent errors in the statement of losses, and maybe also elsewhere.
Attention should therefore be given to detail when planning, as discrepancies of up to two percent hardly can be rendered insignificant.

Table 24: Trial calculation with six significant figures in Excel

	Is [%]	η	Could be	Difference
Run	4	4	4	4
Transposition	24.4	1.2440	1.24351	0.00049
Near shading	-3.2	0.9680	0.96751	0.00049
IAM	-2.9	0.9710	0.97051	0.00049
Soiling	-15.8	0.8420	0.84151	0.00049
Optical loss	-21.9	0.7810	0.79016	-0.00916
Irradiance	-8.8	0.9120	0.91151	0.00049
Module quality/LID	-2.0	0.9800	0.97951	0.00049
Module layout	0.0	1.0000	0.99951	0.00049
Temperature	-1.1	0.9890	0.98851	0.00049
Ohmic	-0.9	0.9910	0.99051	0.00049
Inverter	-5.0	0.9500	0.94951	0.00049
Total system loss	-17.8	0.8220	0.82151	0.00049
PR		0.6420	0.6491	-0.00714

The fact that transposition factors differ significantly may be owed to the inherent diffuse modeling in PVsyst.
The Perez model used for diffuse transposition in these simulations is set as default in version 6 of the program. The PVsyst help file does state that this requires well-measured data with high precision, and that previous versions of the program featured the Hay model, due to higher accuracy. However, recent works of 2011 apparently has given grounds to believe that the Perez model is accurate enough, therefore changing it to default.

The reported MBE of transpositions made validated by real world data, showed values of around 2%. According to the help file, the Perez model usually gives yearly average forecasted values for diffuse up to 2%.
Using real diffuse data as input supposedly will also yield higher accuracy [**9**].

The synthetic hourly data test made during the planning of the simulation runs was based on average 1996 – 2013 data, and it showed that the diffuse horizontal radiation was 0.9%% higher if diffuse data was supplied when generating the hourly data, while global radiation in collector plane was about 0.7% lower.

Indeed, this may be one reason why Bioforsk forecasts get higher transposition factors, seeing that no diffuse data were supplied in this dataset.
More about this is and the role of diffuse radiation in datasets is discussed in the next section of this subchapter.

Turning to near shading, it seems that the variation in the values observed between runs 2/3 and 4/5 are modest enough to be rendered insignificant.

The relative size of these losses also isn't disturbing, making out around three percent on a general basis, although this might be different for other system configurations.

However, it does seem peculiar that the values increase with the onset of soiling. And even more so, why do they stay constant for overall soiling?

One thought goes to diffuse and reflected components of radiation; remembering that these losses apply *before* reaching the module, it seems obvious that if one applies shading, the direct beam component is effectively hindered.
However, this won't necessarily apply to other radiation components.
If then soiling is applied, it may be that the shading loss then increases, as also other radiation is hindered at module level.
Such an explanation makes physical sense, but a contradiction is met in that the loss appears constant for both run 4 and 5 for all forecasts, regardless the source.

More about this will be discussed when evaluating the accuracy of the near shading model versus the combination model, later in this subchapter.

The IAM losses are regarded as constant, as their variation is so small.
Thus, not much space will be offered to this in the discussion, although it is interesting to note that the trend of decreasing IAM loss with consecutive runs stands in contrast to the increasing trend in shading losses.

Considering soiling; it is interesting to see that the soiling losses are different with the same amount of soiling applied, in run 4.
However, the reason for this might simply be that not all radiation in a year arrives at the same time - meaning some sources of meteorological data may have most of their radiation incident in the months where soiling doesn't apply.
Locating the table of monthly vs. yearly radiation in Appendix F: Meteorological data may give some answers (Table F. 2).

The table shows how much the monthly incoming irradiation makes out relative to that of the year as a whole. It can be seen that most sources have a relatively even distribution of incoming radiation over the year.
It comes to mind that the radiation bears striking resemblance to the normal distribution, or the Gauss curve - when looking at Figure F. 1.
This appears logical, considering that weather data is highly random.

As such, there are only minor differences in the incoming irradiation for the months affected by soiling, something that might exclude the distribution as a reason for the appearing differences in soiling loss.

The reader should make a couple of observations though; the months of January and February stand out as receiving about double of what the RY is receiving, in all time series. Also, the months of March and April stand out as receiving more irradiation in the RY. For the months of November and December, there are not such apparent differences.

Recalling the discussion in the last subchapter about monthly distribution, the months of January and February were severely overestimated in all forecasts except the one based on the RY. Because a higher amount of the yearly irradiation arrives in these months, the soiling losses should be higher for the other time-series. This seems to be the case for the 2013 series, which shows 17.3% soiling loss, compared to the 15.2% in the RY.
However, the NASA series has double the amount of irradiation in January and triple the amount in February compared to the RY, with only a little higher soiling loss over the year (15.8%). Thus, the correlation is not at all straightforward to deduce.

On the other hand, the months of March and April were underestimated more by all forecasts, except the one from the RY (and 2013). This may reduce the impact of the soiling a little, not yielding the significant differences one would expect. Nevertheless, in general, these correlations are to weak to conclude anything, and thus should be regarded as speculations.

The irradiance discussions until now have by far dealt with the consequences of the differences in irradiance levels, and it is therefore considered unimportant to elaborate more at this point. Seeing that most forecasts have a relatively constant irradiance loss supports this decision.
One point should be made though; note that low TPs in general induce higher irradiance losses, a result that follows from the nature of DGR, which is discussed in the next section. Also note how irradiance loss increases in run 4; when heavy soiling is induced, the irradiance level reaching the modules will be lower, thus inducing efficiency loss. The fact that the irradiance loss returns to its original level in run 5 confirms this.

To comment on temperature losses, it should be maintained that they generally are insignificant. This is maybe not so strange, considering that Norway is a country with low mean temperatures, also in summer. In addition, the months in the beginning and the end of the year may feature high irradiance levels and low temperatures, which are the optimal conditions of any PV-system.
Such conditions may induce efficiency increase in periods (see eq. 2.15 and 2.17).

Excluding run 4, Bioforsk forecasts have almost no temperature losses, compared to Meteonorm forecasts, which have losses of around 1%.
The difference of these two data sets in terms of temperatures is that Meteonorm has the highest average temperature of the year, while Bioforsk has the second lowest. The NASA forecasts have only a tad higher temperature loss in general than Bioforsk forecasts, with a lower average temperature of the year.
This might be because of a higher amount of incident radiation over the year, which would increase cell temperatures. Studying the other dataset average yearly temperatures and temperature loss, there seems to be good correlation.

The observed phenomenon of higher temperature losses with heavy soiling and lowest losses with overall soiling is not straightforward to deduce.

One may speculate upon the factors that might influence this, though the physical laws governing the heat transport from the modules almost surely don't apply in a computer simulation program.

If they did, one could deduce that because the module gets covered in snow, it would not be able to dispose of heat, with a layer of melted water insulating it from the above snow. At the same time, if it would receive sunlight in parts uncovered by snow, the cell temperature would be increased and lead to losses. However, seeing that soiling losses are considered a constant loss factor in PVsyst, applied *before* the light hits the module, this definitely doesn't apply in the program.

As such, no constructive conclusions may come from discussing this topic, and it is therefore left open.

For last, some words should be said about the inverter losses.
Since these losses are relatively constant in most forecasts produced, the focus may be directed towards the phenomenon of lower losses in the PVGIS, Meteonorm and NASA forecasts in run 3, which are all databases.
These reduced losses may be assumed to follow from the fact that when module layout is applied, PVsyst calculates shading differently. Instead of applying a linear loss according to how much of the module is covered, takes into account the bypass diodes and electrical configuration of modules.
This means that the modules may actually become more efficient, and the inverter will work with a higher load factor, rendering its operation more efficient. Why this only applies to forecasts based on database sets, however, remains a mystery.

Other general factors that are apparent is that all forecasts show higher inverter losses in run 4, only to have them reduced in run 5. This shows that inverter operation is inefficient due to low load, as less radiation reaches the inverter.

Also note, due to the fact that inverter had to be downsized in order to perform simulations, the inverter losses forecasted should be higher than observed here. The extent of these losses is difficult to evaluate without assessing simulation data on an hourly basis, which is a tedious task. On grounds of the fact that the actual inverter output is higher than any of the yielded forecasts, this task is considered unnecessary to complete.

4.3.3 Loss due to irradiance level; role of diffuse in datasets

In former discussions, the diffuse radiation has been subject to constant prejudice as a factor that may explain trends observed. In order to address this subject, it is now time to look at the DGR.

A low DGR is equivalent to a higher share of beam components in the incident radiation. As was explained in chapter 2, as light is attenuated through the atmosphere, it loses energy. Consequently, if a module receives a lot of diffuse (attenuated) light, the chance is high that the energy available in the light spectrum is insufficient to contribute in a significant manner to the photovoltaic

effect. In essence, the PV-generator becomes an absorber of incident energy without being able to utilize it to its full extent.

As such, of two modules receiving the same amount of global radiation, with different DGR, the module receiving the light with a low DGR will generate current more efficiently.

Figure 53 below shows the ratio of diffuse radiation to the global radiation on both a monthly and yearly basis, for all sources evaluated in the thesis.
Note that the graph doesn't show the average values for the year. These would've been somewhat higher, owing to the extreme values in some months of the year.

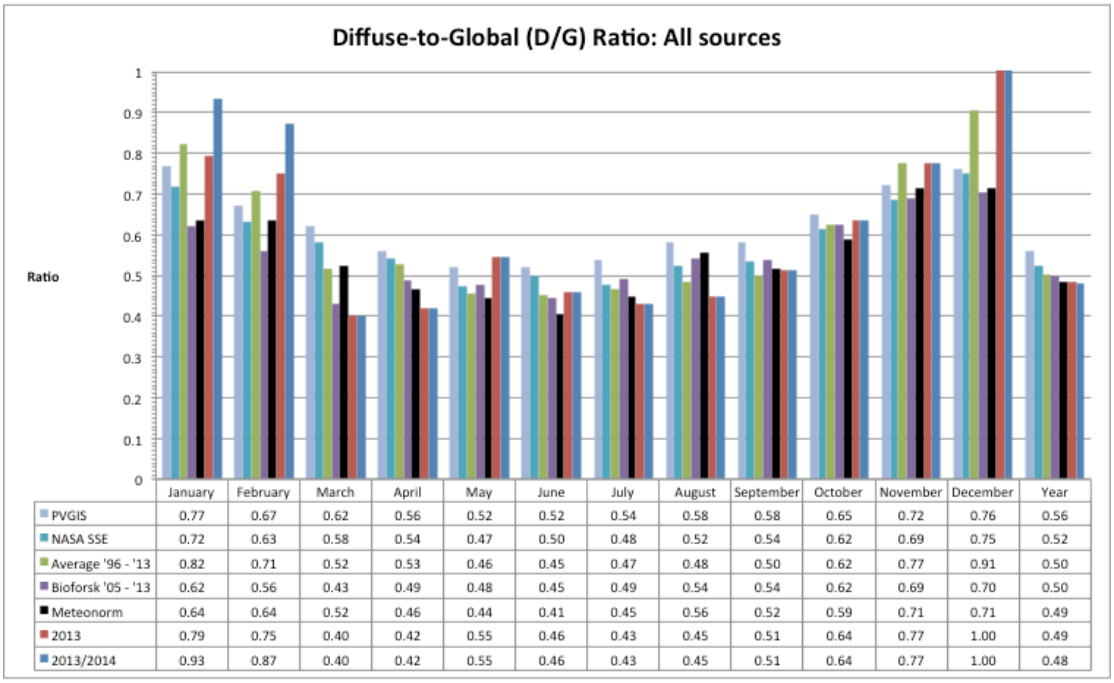

	January	February	March	April	May	June	July	August	September	October	November	December	Year
PVGIS	0.77	0.67	0.62	0.56	0.52	0.52	0.54	0.58	0.58	0.65	0.72	0.76	0.56
NASA SSE	0.72	0.63	0.58	0.54	0.47	0.50	0.48	0.52	0.54	0.62	0.69	0.75	0.52
Average '96 - '13	0.82	0.71	0.52	0.53	0.46	0.45	0.47	0.48	0.50	0.62	0.77	0.91	0.50
Bioforsk '05 - '13	0.62	0.56	0.43	0.49	0.48	0.45	0.49	0.54	0.54	0.62	0.69	0.70	0.50
Meteonorm	0.64	0.64	0.52	0.46	0.44	0.41	0.45	0.56	0.52	0.59	0.71	0.71	0.49
2013	0.79	0.75	0.40	0.42	0.55	0.46	0.43	0.45	0.51	0.64	0.77	1.00	0.49
2013/2014	0.93	0.87	0.40	0.42	0.55	0.46	0.43	0.45	0.51	0.64	0.77	1.00	0.48

Figure 53: Graph showing the diffuse to global ratio of all sources of met-data evaluated

The graph shows how PVGIS, the source yielding the least accurate forecasts, is the source with the highest yearly DGR. NASA comes on a clear second place, followed by the average 1996 - 2013, Bioforsk, Meteonorm, 2013 and last but not least - the RY.

From the chart, one may observe that especially in the winter months January, February, November and December – the DGR of the Bioforsk forecast is significantly lower than in the 2013 case.
For reference, the same also applies in the months January and February when comparing to just about any other source.

For the RY, it seems apparent that in the months of January, February, and December, the DGR is higher than for any other source. This also applies to May. In November, it is about the same as the average 1996 - 2013, but higher than for the other sources. October month is similar for about all sources, and here, the DGR of the RY is the lowest.

4.3.4 Discussion of the role of diffuse radiation in datasets

As was said in the last discussion, Bioforsk is the only dataset, which had no diffuse irradiance data. At the same time, its forecasts yield a higher transposition surplus (TP) than any other source. This, of course may seem like more than a coincidence, and as was mentioned before - the generation of the synthetic data is subject to errors of up to two percent.

From the theory, we know that the transposition factor is dependent on tilt, among other things. When a module is tilted, its diffuse component decreases, and the direct beam components increase. So a high TP is consistent with a low DGR.

If one looks at the TP in the loss diagrams, PVGIS had the lowest values, which corresponds well to the overall high DGRs, both on monthly and annual basis. The second lowest TP is obtained with Meteonorm data; however, this source doesn't show a high DGR. Therefore, one cannot with high certainty say that the DGR is responsible for a high TP in itself.

This might appear logical to most, though not self-evident to all.
One must remember that PVsyst generates the diffuse data on basis of the global irradiance data supplied by the user, and that these diffuse data are lower when no diffuse data are available to correct on an annual basis.
This means that the high values of irradiance in the Bioforsk dataset may be the basis of the high TP, and that the low DGR generated by PVsyst in combination with these values may give the highest TP.

If one look to the 2013 data series, the TP is second highest, and the global irradiance is at the same level as Bioforsk on an annual basis. At the same time, the DGR is the second lowest, thus apparently showing correlation.
NASA has the third highest TP, but the second highest DGR on an annual basis. At the same time, the time series has the highest global irradiance, which may give a high TP despite the high DGR.
Although the average 1996 - 2013 series has a higher annual DGR than the RY, the TP for the two series is about the same - despite that the RY has a higher amount of annual global irradiance. The months of January and February have significantly higher DGR in the RY than in the average, which should be the reason for this.

Following this line of though, the Meteonorm source has a low annual DGR, but also the next lowest annual global irradiance, resulting in the low TP.
Lastly, the PVGIS source has the highest DGR and the lowest annual global resource, which means that it should also have the lowest TP.

In essence, the observed TPs seem to be in accordance with the theory.

Now, in order to say something about the observed RMSEs in January and February, one may use the TP as a tool, knowing how it correlates to the DGR.

The RMSE of Bioforsk is the highest in January and February, and it also has the highest TP and lowest DGR.
The RMSE of the NASA series is second highest in January, and highest in February - but its TP is third highest. This may be assumed to be due to the fact that the irradiance is higher in this series than in the 2013 series for both months. Relative to the Bioforsk series, the higher RMSE in February may be owed to the fact that the difference in DGR between the to series goes down a little compared to what it was in January, making the higher irradiance in the NASA dataset for this month overestimate the production a tad more.

The 2013 series in turn, comes on a third place in terms of RMSE in January, but a fourth place in February - with a second highest TP. As revealed above, this is then most likely due to the fact that is has a higher DGR in these months than NASA and Bioforsk series, though coming third after NASA and Bioforsk series in terms of irradiance.

The average 1996 - 2013 series comes 4th highest with RMSE in the month of January, it has the 4th highest TP and its irradiance in the mentioned month is about 2/3 lower than in the 2013 series.
The DGR is higher in January than for the 2013 series, and the difference in irradiance larger relative to that in February. The higher DGR of the 2013 series in February makes the RMSE of the forecasts based on this series less marked in this month and lower than for the average series.

The Meteonorm series has the 5th highest RMSE in January and February, and its TP is the 6th highest. The irradiance in the months is also the least most overestimated compared to the RY, which makes the correlation a little obscure. However, the DGR is lower in these months than for the PVGIS series, so its safe to assume that this is the reason why the PVGIS series comes in a 6th place in terms of RMSE, despite having a higher irradiance. Also, the TP of PVGIS is at 7th and last place.

Considering the RY in January and February, it may be seen that the RMSE is the lowest observed, though the TP is at the same level as the average 1996 - 2013 series. However, the DGR is the highest of all, and correspondingly the irradiance is actually the lowest of all series for these two months.
Thus, despite high TP, the effect of low irradiance and high DGR combined makes this series overestimate less than it should in January and February.
This indicates that the correction of the diffuse in the RY was indeed a little faulty, a theory supported by the RMSE of the average series.
This in turn also means that the average 1996-2013 series may be a little faulty as well (as RY is a part of it), due to the same correction, though minor as the global has been adjusted upwards in 8 of the years.

Evaluating the above-mentioned relations, one might assume it is safe to conclude that the DGR is indeed the sought after culprit to explain why the yield in the months of January and February are estimated the way they are.

As such, it seems evident that the high MBE in January and February, seen in the last chapter when looking at monthly irradiance and production data, may be correlated to the modeling of diffuse in PVsyst and the DGR in general.

As mentioned in the previous subchapter (4.2.2 Discussion of monthly production data), the correlation between months and DGR may probably also be transferred between other months, with the same level of reasoning as here. Indeed, one could perform the tedious task of correlating all months, but seeing that the months of January and February are the months leading to the highest level of insecurity in the forecasts, these months are the most important ones to assess.

The month of May is overestimated by all other forecasts than those based on RY (and 2013), indicating that this month indeed was weaker than normal irradiance wise. The opposite is true for July - the fact that the RY forecasts do underestimate less, supports this theory.
NASA and Bioforsk forecasts, due to their general overestimation of resource in this month compared to the other months, alone overestimate December. However, November is underestimated in the same manner as forecasts based on all other sources. The RY doesn't deviate at all, but would probably overestimate, considering that the diffuse correction might have been faulty. Still, all other sources underestimate the actual output.

Therefore; removing these months to assess the accuracy of forecasting would yield a "false" improvement of the forecasts; an improvement induced by one self. This is not the same as removing January and February, which lead to an overestimation of yield, an improvement of forecasting, based on existing flaws in the datasets. If one assesses the meteorological data, one finds that most datasets have annual deviations in irradiance well within what would normally be regarded as a normal annual variability. PVGIS stands out as the only source where this doesn't apply. Because January and February months are overestimated, removing them will therefore show their true deviance from the actual RY to a higher degree.

This supports the results found in the last subchapter that removing these months should increase the RMSE of the forecasts. The natural consequence of this would be to reduce the overall distance between the lines seen in Figure 50, chapter 4.2.1 Monthly forecast vs. monthly yield. Such a graph will be shown in the next subchapter.

4.3.5 Losses due to soiling; relative improvement of accuracy with overall soiling

As have been seen so far, the soiling losses induced generally don't improve forecasting accuracy. This leads to one questioning the right amount of soiling. As was mentioned in the theory section, the relation of soiling is not an easy one to deduce, as soiling varies highly from year to year. Also, from the comparison of losses, it could be seen that the soiling is highly variable without giving general correlations between TP. This therefore generally also weakens the expectance of DGR as the culprit of the high variable soiling.

As such, it is of primary interest to investigate how the relative improvement of accuracy develops when soiling is decreased, in order to reveal general patterns of soiling, without focusing too much on values for the actual deviations within individual forecasts.

Figure 54 shows how the forecasts based on NASA SSE met-data perform compared to the actual yield in run 4 and 5.

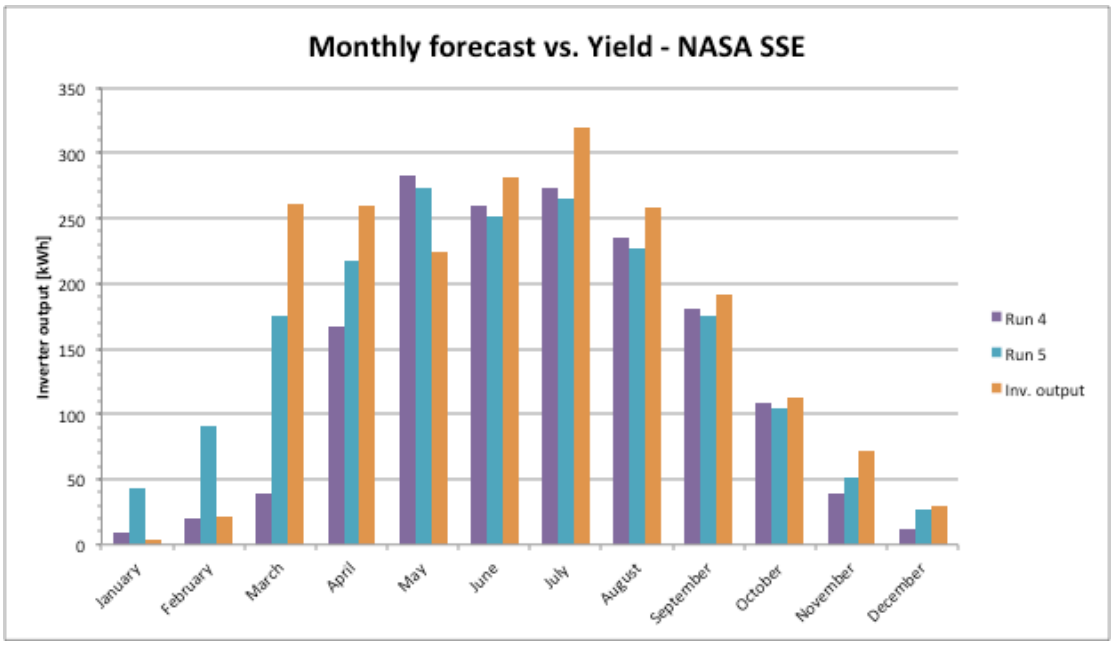

Figure 54: Revised monthly forecast vs. yield for the NASA SSE database

When looking at the above figure, it can be seen that when going from run 4 to run 5, in January and February, the discrepancy between forecasted and actual yield increases.

For the months of March, April and May, this trend is reversed - meaning that implementing lower overall soiling in run 5 decreases the discrepancy.

On the other hand, for the months June to October, the discrepancy goes up from run 4 to run 5.

November and December shows the same tendency as for the months March to May, and the discrepancy goes up from run 4 to run 5,

In order to compare these observations, one may take a look at the tabular representation of the relative increase in discrepancy when going from run 4 to run 5. This way, the trends may also appear more apparent to some readers.

Table 25 shows the BE of the 4th and 5th run of the forecasts made with 2013 met-data. In addition, the discrepancy between BEs for the months is shown, along with the calculated relative discrepancy between the runs.

Table 25: Discrepancy from yield in run 4 and 5, along with absolute and relative discrepancy between runs, for the average 1996 - 2013 forecast.

Forecast, average (1996 - 2013) - Discrepancy: soiling [%]					
Run. No	4	5	Discrepancy	Rel. Discrepancy	Tendency
January	53.4	753.3	699.9	1310.6	UP
February	-31.5	227.5	259.0	622.1	UP
March	-85.1	-32.9	52.3	-61.4	DOWN
April	-42.6	-24.7	17.9	-42.0	DOWN
May	14.5	10.9	3.6	-24.8	DOWN
June	-11.6	-14.4	2.8	23.8	UP
July	-22.3	-24.7	2.4	11.0	UP
August	-15.7	-18.4	2.7	17.1	UP
September	-15.7	-18.4	2.7	17.2	UP
October	-22.6	-25.2	2.6	11.4	UP
November	-64.3	-52.1	12.2	-19.0	DOWN
December	-80.2	-54.3	25.9	-32.3	DOWN
Year	-28.3	-16.5	11.8	-41.7	DOWN
Year ex. Jan. & Feb.	-28.3	-20.4	8.0	-28.1	DOWN

From the table, one may observe in the far right column named "tendency", in which direction the relative discrepancy goes.
The "up" notation shows that the BE increases from run 4 to run 5 for the months January and February, and months June to October.
The "down" notation shows that the BE decrease in the months March to May and November and December.
For the year as a whole, the tendency is a decrease, and the same goes for the year excluding January and February.

The trend shown above in both tabular form and in the monthly distribution of forecasted vs. actual yield is the general trend for all the forecasts.
Though, some exceptions do exist.

The RY forecasts fails to show an upward trend in February, and the downward trend in May. Otherwise the general tendency remains.
For 2013 forecasts, the May tendency is upwards, Otherwise the general tendency remains.
For the Bioforsk forecast, the year excluding January and February shows an upward trend; otherwise, the general tendency applies.

To sum the general results found in soiling patterns for the vertical alignment, the following Table 26 shows how the observed soiling patterns are interpreted:

Table 26: Overview over the interpreted meaning of observed soiling patterns

Soiling tendency - Aas					
Month	Tendency	Meaning	Elaborated	Required soiling level	Recommended value
January	UP	5 too low	More soiling than estimated	Heavy	0.75 - 0.85
February	UP	5 too low	More soiling than estimated	Heavy to moderate	0.5 - 0.7
March	DOWN	4 too high	Less soiling than estimated	Low to none	0.0 - 0.25
April	DOWN	4 too high	Less soiling than estimated	Low to none	0.0 - 0.25
May	DOWN	4 too high	Less soiling than estimated	Low to none	0.0 - 0.25
June	UP	5 too high	Less soiling than estimated	None	0
July	UP	5 too high	Less soiling than estimated	None	0
August	UP	5 too high	Less soiling than estimated	None	0
September	UP	5 too high	Less soiling than estimated	None	0
October	UP	5 too high	Less soiling than estimated	None	0
November	DOWN	4 too high	Less soiling than estimated	None	0
December	DOWN	4 too high	Less soiling than estimated	None	0
Year	DOWN	4 too high	Less soiling than estimated	None	0

Recall that all months except January and February usually are underestimated. Also, May was abnormal in the RY.
Revisiting the soiling values in run 4, it is known that the values were zero between June and October. Thus, considering what the upward and downward tendencies meant in terms of soiling generated the first four columns in the table above.

From the table, up in January and February means that soiling is too low in run 5.
Down in March to April, means that soiling is too high in run 4.
Up in June to October means that 5 is too high, as no soiling is applied in these months in run 4.
Down in November, December and for the Year as a whole, means that the soiling is too high in run 4.

Then, comparing the tables over monthly forecasted yield (Appendix G.6: Simulated monthly yield - All sources) for results between run 3 and run 5, one may observe how the BEs of the months change for the months where run 5 was an improvement over run 4 (March - April, November, December, year).
From this, one may construct the latter two columns.

For the months of January and February, the results were clear: the soiling in January was too low in all instances, the soiling value in February usually led to underestimation in run 4, and the opposite in run 5. Therefore, the soiling value in January has to be high, and in February may be too moderate.

March and April generally saw no improvement from run 3 to 5, but one cannot exclude that this may be the case in certain years. Therefore, the value may be low to none. The same applies for May, as it is unknown how this month will be -

if overall soiling is sufficient or if pollen and dust will come with the onset of spring.

All other months generally saw no improvement by applying soiling at all, also not the year as a whole. Thus, an overall soiling value of zero may be appropriate.

4.3.6 Discussion of soiling patterns

To address the exceptions mentioned in the results; the fact that RY forecasts fail to show an upward trend in February is because February generally is underestimated in these forecasts, as previously shown.

The 2013 forecasts on the other hand, does show this trend.
Knowing that these two data series only differ by the two first months of the year, therefore, it is reasonable to think that this treat is related to the February month being abnormal in the RY.
This reasoning is grounded in how the average series and Bioforsk series perform irradiance wise in these months, representing a "normal" for comparison.

Indeed, comparing to any other source used, they all show the upward trend in the months of January and February.

In the same manner, in the RY (and 2013) forecasts, the month of May is not overestimated, in contrast to all other forecasts.

Regarding the Bioforsk forecast, it has already been shown that this series have a significant bias in the early months of the year - and also in December.
Thus when the heavy soiling is introduced this bias is generally offset.
Owing to the fact that the Bioforsk series have the highest amount of incoming radiation in December, compared to that of other sources, introducing an overall lower soiling value of 3% seems inadequate to offset the bias.
The overall effect is that the December radiation leads to an overestimation of production in run 5, and the relative discrepancy increases if the months of January and February are excluded.

In essence, it is safe to assume that the general tendency observed should be the one observed also in the future - unless the arrangement of the modules is altered.

As was explained in the theory section (2.2.9 Soiling loss), a horizontal arrangement of the modules may significantly lower the influence of soiling due to snow in the winter months of January and February.
If this were to be done, then the forecasted yield would maybe not be so much overestimated. The fact that all forecasts made have a significant amount of bias in these months, with a high MBE, and that they show a reduction in their bias for these months in run 4, supports this theory.

Hence, the supplied interpretation of soiling patterns only applies in the case where the modules are maintained vertical. The whole matter of overestimation due to soiling may be changed considerably, if not avoided altogether, if modules are arranged horizontally both in reality and in the simulation program.

Note that the supplied table is only a suggestion of appropriate values for the site at Aas. The generality cannot be proven, although considering that the condition for weather data to be accepted as representable for a location is that they are measured within a climatic distance of 20 km, one may assume that the soiling pattern would apply to locations within the accepted climatic distance of Aas.

It maybe also goes without saying, but the different sources may still yield bias errors with the suggested values. All factors that may improve the simulations aside, there is a difference in the meteorological data, so one has to assume there will always be variations in the accuracy of a forecast, due to the random nature of weather.

4.3.7 Accuracy of detailed shading vs. shading/horizon combination

One of the essential methodological results was related to the investigation of the accuracy of the detailed shading scenario that was used to construct the near shading scene utilized in all simulation runs 2 - 5.

In order to assess this, it may first be of interest to see how the forecast does compared to the detailed shading scenario, when graphing the annual forecasted yield versus the actual yield.

As the combined scenario consists of six runs, and not five, this comparison in itself is not trivial. Thus, in order to assess this, the near shading and far shading runs may be combined in a presentation, to show how the result differs overall.

Figure 55 below shows how the forecasted inverter outputs of the two different models perform towards the actual inverter output.
The pink graph is the new addition. Note that the other graphs aren't displayed. This is because the combined scenario lies very close to the detailed scenario, thus the other graphs are perceived as being in the way of seeing the trends.

The tabular values of the six runs, and those of the detailed shading scenario referred to here, including all bias errors, losses and the relative increase in accuracy with overall soiling is found in Appendix G.6: Simulated monthly yield - All sources. For reference, the soiling pattern found was consistent with the one found in the previous section.

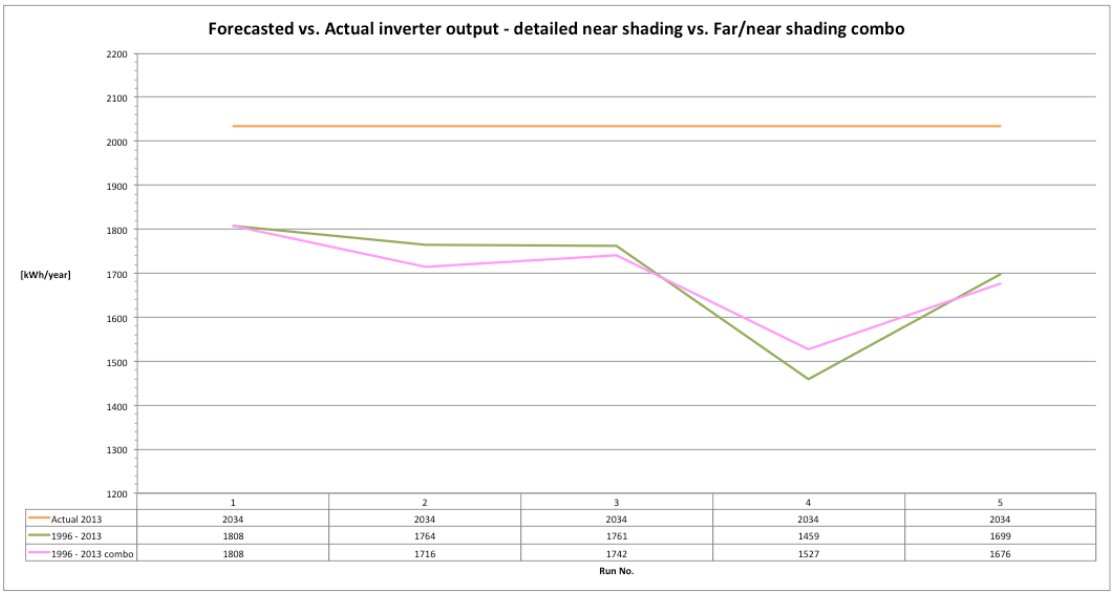

Figure 55: Forecasted vs. actual annual inverter output for the 1996 - 2013 average with combined shading model

Looking at the graph above, it becomes clear that the forecast generated combined model is not very different from the one made with the detailed model. In general, the graph of the combined forecasts lies a little below for all runs, except for run 4. This indicates that it in general is more inaccurate than the detailed near shading model, having higher BEs.

To assess the real difference in using the combined model, it may be useful to look at the monthly distribution of the BEs over the course of the six runs, as the sixth run isn't displayed here. Table 27 shows a comparison of these BEs:

Table 27: BE table for the far/near-shading combo using the average 1996 - 2013 data.

Average 1996 - 2013 far/near shading combo - Discrepancy from yield [%]								
Run. No	1	2	3	4	5	6	MBE	RMSE
January	887.5	644.6	631.9	638.3	56.6	609.5	578.1	630.4
February	251.1	237.9	232.0	234.3	-20.6	221.6	192.7	215.2
March	-28.8	-30.6	-32.0	-31.1	-84.1	-33.7	-40.0	44.6
April	-20.2	-22.1	-23.3	-22.1	-38.9	-25.0	-25.3	26.0
May	17.4	14.5	12.7	14.5	17.6	10.3	14.5	14.7
June	-9.3	-11.6	-13.1	-11.6	-8.3	-14.9	-11.5	11.7
July	-20.3	-22.3	-23.5	-22.2	-21.0	-25.1	-22.4	22.5
August	-13.5	-15.7	-17.0	-15.6	-11.6	-18.8	-15.4	15.5
September	-13.3	-15.5	-16.8	-15.5	-11.0	-18.6	-15.1	15.3
October	-20.1	-22.6	-24.1	-23.4	-13.7	-26.4	-21.7	22.1
November	-47.0	-53.7	-54.5	-53.8	-59.9	-55.6	-54.1	54.2
December	-43.4	-65.9	-66.6	-65.9	-80.6	-67.6	-65.0	65.9
Year	-11.1	-14.2	-15.6	-14.4	-24.9	-17.6	-16.3	16.9
Year ex. Jan. & Feb.	-15.4	-18.0	-19.4	-18.1	-25.1	-21.2	-19.5	19.8
Monthly avg.	78.4	53.1	50.5	52.1	-23.0	46.3	42.9	37.0
Monthly avg. Ex. Jan. & Feb.	-19.8	-24.5	-25.8	-24.7	-31.1	-27.5	-25.6	-26.6

Notice that when looking at the table, Run 1 is the same as for both shading models, and run 2 is far shading, 3 is near shading, 4 is module layout, run 5 is now the heavy soiling scenario, whereas the 6th run is the overall soiling scenario.

From the table, one may observe that the BE of the combined shading model forecasts is lower for the month January than is the case for the detailed near shading model. In the heavy soiling scenario, the difference is minor in January, although a little higher for February - that is, the RMSE has decreased.
The detailed model generally yields a lower MBE for February, but the RMSEs are about the same. For the rest if the year, the RMSEs are very similar.

Note from the table that the MBE and RMSE are also very similar for the year, both with and without January included. The RMSEs are actually a tad lower for the combined scenario at this point. The monthly average BE is generally a little lower in the combines scenario, that is, less positive.
However, in run 5, the values are a little higher, that is, less negative.

Excluding January and February yields a lower average BE in general in the combined shading model, that is, more negative - though also in this case the heavy soiling scenario stands out as showing less negative in average monthly BE in the combined shading model.

The main differences lie in a generally lower BE for most runs and months in the combined model, with the heavy soiling scenario standing out with less bias, a less negative value in run 2 and 5.
This is consistent with that shown in Figure 55.

In terms of losses, the real main difference between the two shading models is that the combined model has a higher combined shading loss (4.2%), with a relatively constant near shading loss with 0.5% and a far shading loss of 3.7%. Interestingly, the far shading loss "jumps" slightly to 3.9% in the heavy soiling scenario, a phenomenon that disappears in the overall soiling scenario.
In comparison, the detailed model has a near shading loss of 2.6% before heavy soiling, and 3.1% after heavy soiling is applied. In the overall soiling scenario, however, this phenomenon is not reversed.

4.3.8 Discussion of shading model accuracy

From the shown results, one can hardly conclude that the tedious task of finding architectural plans, measuring them accurately, and constructing a life-like 3D model for use in PVsyst simulations, is necessary.

The MBE of the months of January and February does reduce, due to the fact that the simplified horizon consistently induces a higher shading loss in PVsyst. However, the accuracy only improves to a small degree.

The combined model generally has about 1% lower BE for most runs, on an annual basis. If one consider run 2 and 3 in the combined model as one, the

annual BE is -15.6%. This is about 2%-points lower than that the equivalent run 2 for the detailed model. The relative difference, therefore, is insignificant.

The fact that the results are so similar over all the runs means that the change in accuracy has no practical meaning, comparing the deviations between the forecasts in terms of accuracy. Only if one would apply the heavy soiling scenario, a real difference may be seen, the BE is the almost 4%-points lower in the combined model than in the detailed model.
But, this can hardly make a difference when the yield already is underestimated by some 28% in the detailed scenario.

If one would consider using the combined model when forecasting with one of the most accurate sources in terms of weather data, lets say NASA, then the difference would be insignificant in the heavy soiling scenario.
In the NASA forecast for run 4, the BE is about -20%, which with 4% added would still yield a BE of -16%.

Subtracting 2%-points from the NASA annual BE in run 2, would render the forecast just accurate enough to make it fall within the IRT.
Consequently, any forecast with soiling values added would render the inaccuracy unacceptable. Therefore, in this case, the difference between the two models does have a practical meaning, as an engineer planning a plant using NASA data, likely could try to apply overall soiling values as a means to assimilate real-world conditions.

However, as has been seen in other reports made before, engineers do try hard to imitate the real world when simulating PV-system performance, applying heavy soiling values [**48**] [**49**]. This means, that most of these are not only underestimating the resource to a high degree and giving very inaccurate forecasts, but also that the application of a simplified model would be almost just as good in terms of forecasting as any detailed 3D model.

Thus, the amount of work invested into constructing 3D scenes, when applying real world conditions, can hardly be justified.

4.3.9 Section summary

In this section, we have studied the forecasted losses and found that PVsyst imprecisely states them, though the program still states PRs precisely.

Irradiance losses seem to be higher for datasets with low TP, this seems related to a high DGR and the general level of irradiance in the dataset, in accordance with theory.

The diffuse modeling in PVsyst, together with generally high irradiance data and missing diffuse data, seems to be the reason why Bioforsk forecasts yield a significant overestimation in January and February months.

The diffuse correction in the RY data seems to be faulty, this seems to yield a poor overall accuracy of the forecasts made, especially for the end of the year.

A soiling pattern has been found for the location at Aas, the validity is assumed to apply within the accepted climatic distance for met-data (20 km).
The pattern shows that a heavy soiling value is necessary for January, a Heavy to moderate value for February, and low to none soiling in March to April.
For the rest of the year, the forecasts are most accurate when omitting soiling totally. An overall soiling value of zero is assumed appropriate to yield more accurate forecasts. The issue of soiling may be reduced, or avoided altogether, by a horizontal arrangement of the module.

A detailed soiling scenario is deemed unnecessary, as the differences in forecast accuracy is only improved little by a detailed shading model. The general accuracy of forecasting should be increased to justify the necessary work that has to be done to construct 3D-models.

4.4 Revised annual forecast vs. annual yield

In this subchapter, the subject of the faulty irradiance in January and February is addressed by excluding the months of January and February from the actual and forecasted yield, to reveal how the accuracy of the forecasts change.
Also, the forecasted yield is adjusted for positive mismatch in the system at Aas, in order to reveal if the forecasts may be rendered sufficiently accurate to satisfy the investor risk tolerance (IRT).

4.4.1 Revised forecast vs. yield and PR – excluding January and February

The tables referenced in this chapter may be located in Appendix G.3: Simulated annual irradiance, yield and PR – Excluding January and February.

So far, January and February have been blamed repeatedly for giving inaccurately high accuracy for the best performing forecasts, based on NASA and Bioforsk data. Also, the Bioforsk data should probably yield a less accurate forecast in these months due to the fact that the diffuse irradiance may be assumed to be too low as a consequence of diffuse modeling in PVsyst.

Furthermore, the RY, 2013 and average 1996 - 2013 series may all have been affected by a faulty correction factor, yielding too high DGRs in these two months.

Therefore, the months of January and February have been removed, both from actual inverter production data and the forecasts, to yield the following revised forecast vs. yield graph, shown in Figure 56:

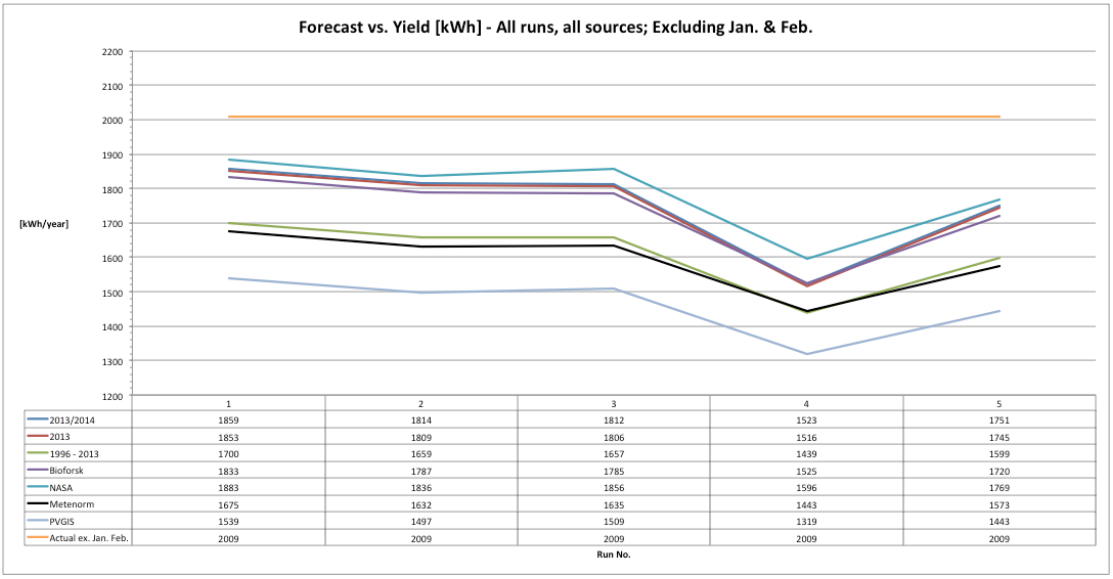

	1	2	3	4	5
2013/2014	1859	1814	1812	1523	1751
2013	1853	1809	1806	1516	1745
1996 - 2013	1700	1659	1657	1439	1599
Bioforsk	1833	1787	1785	1525	1720
NASA	1883	1836	1856	1596	1769
Metenorm	1675	1632	1635	1443	1573
PVGIS	1539	1497	1509	1319	1443
Actual ex. Jan. Feb.	2009	2009	2009	2009	2009

Figure 56: Forecasted vs. actual inverter output when January and February are excluded

The graph shows that the discrepancy indeed does increase between the forecasted yield and the actual yield. The actual annual BE of the different forecasts can be found in Table G. 12.

From the table, one may observe that the BE of the RY has been lowered only insignificantly in all runs, compared to in the original comparison. On the other hand, NASA now has a significant BE in run 1 of -6.3%.
In consecutive runs the BE naturally is higher, being about -20% in run 4 and about -12% in run 5.

The Bioforsk series has had about the same increase in BE, showing -8.7% in the first run, -24.1% in run 4 and -14.4% in run 5.
The BEs of forecasts based on the average 1996 - 2013 series shows lower decrease in accuracy than the well performing forecasts, though higher than the RY and 2013 based forecasts. Other sources show the same trend of lower accuracy, though the inaccuracy in forecasting is generally to high to consider relevant to mention.

Shedding a look on the PR is also of interest, in order to see how the exclusion of the two poor months affects the forecasted system performance. Figure 57 illustrates how the performance ratios distribute.

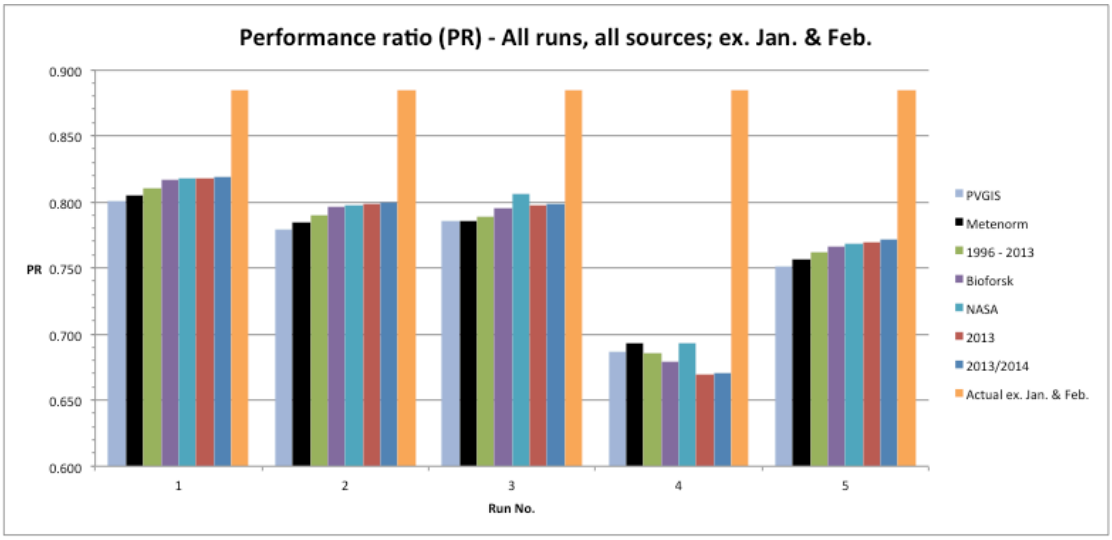

Figure 57: Revised forecasted PR when excluding January and February

From the figure, one may se how the distribution now is almost as in the original comparison, only that the RY and 2013 forecasts now yield the highest PRs in the two first runs, followed by NASA and Bioforsk forecasts. The third run reflects a higher increase in PR for the databases than for other series. In the fourth run, the PRs are showing a decline in the RY and 2013 forecasts, whereas the database forecasts advance. The relative difference in PRs between average 1996 – 2013, and Bioforsk forecasts, decreases compared to the original comparison, whereas Meteonorm gets a higher PR. In run 5, the order of the PRs is back to the same as in run 1.

4.4.2 Discussion of revised forecast vs. yield and PR - ex. January and February

The results in the last subchapter predicted how a new comparison of forecast vs. yield would look as one where the lines were closer together.
The reasoning was a smaller overall difference between the data series, because months that introduced significant error in the datasets would have been removed. Indeed, this trend has been shown in Figure 56.

If one would recall the studies saying that PVsyst tend to be conservative in estimations, then bearing in mind that the underestimations have ranged between approximately 5% and 9%, then only few of the forecasts made would fall within this range [**34**] [**38**]. As the studies conducted earlier have no issue of winter soiling, the only relevant comparisons can be made for the overall scenario and the three first scenarios. Bioforsk forecasts are within the range for the ideal run, but NASA forecasts for the three first runs. All other sources fall outside the stated range.

The forecasts based on NASA and Bioforsk data showed only minor difference in the BE for run 4 after the exclusion of January and February, proving that the soiling factor corrected for the advantage of higher irradiance in the datasets and overestimation.

The RY and 2013 forecasts are identical in the figure, as would be expected, now that the only months separating them have been removed.

Also, one may recognize that the "dips" and "rise" of Bioforsk, 2013 and average 1996 - 2013 series are not anymore as noticeable.
This may be attributed to the fact that the high overestimation in the months removed, earlier would give a significant contribution to accuracy, which would be removed by the fourth run that applied heavy soiling.
If the contributing months are taken away, the remaining contribution over the year is only the one from May and December, as mentioned in the last subchapter. This contribution shows that for example the Bioforsk and average 1996 - 2013 series still have "dips" and "rises", though to a much smaller extent.

The fact that the BE of the RY, 2013 and average series didn't show the same "jumps" in inaccuracy as NASA and Bioforsk when January and February were excluded, confirms that these months were less important to the accuracy of the forecasts.

The observed PRs in Figure 57 show how the exclusion of the poor performing months in the actual inverter production data yielded a higher PR.
Maybe not so strange, considering that soiling may have reduced the performance, and that considering the other months of the year generally are considered better performing.

The fact that RY and 2013 forecast have an increased PR from the exclusion of January and February, similar to that of the actual inverter, shows that these months indeed were abnormal in the sense of production and probably also irradiance. That the PRs of NASA and Bioforsk forecasts decline, shows that the forecasts did have a significant advantage in yielding a high share of production in months that were originally poor. Their decline after removing the months is thus expected.

The increase in PR of the system in database forecasts in run 3 was also seen in the original comparison, although this time it is known that the databases have higher inverter efficiency in this run, one that obviously persists when January and February months are excluded. The same trend explains the reason why the accuracy in forecasting goes up in this run. The reason why it only applies to databases though, is still a mystery.

In the 4th run, the RY forecasts now have lost their advantage of lower overestimation in the 4th run, and thus the PR is lower relative to the PR of the other forecasts than for the original comparison. That the Bioforsk forecast gets a relatively higher PR the months of January and February are excluded can be grounded in the same argument as for the RY. The Bioforsk and NASA PRs became lower in the first runs due to their lost advantage in the two months, which is the same that happens for RY in the fourth run where it had the advantage in the original comparison. Consequently, the Bioforsk and NASA series now yield the advantage in the fourth run, the opposite trend of the original one.

In the fifth run, the trend order of PRs is back to the original in run 1, showing that the advantages the RY forecasts now have gained from excluding January and February have been reassumed.

The overall result when excluding the months of January and February is that the forecasts become more homogeneous and inaccurate in general.
The exclusion shows that the PRs of the best performing forecasts are somewhat overestimated due to the inherent overestimation of resource in the datasets they are based on.

In one sense, it may be comforting that the data series seem more homogeneous, when sources of error are removed, as it shows that there is some sort of consistency among the data.
In another sense, the fact that reliability of forecasts is based on overestimation of certain months may be highly worrying to most engineers, especially those taking pride in working with high precision.

As mentioned before, it would be difficult to accurately simulate for parts of the year if the simulations rely on an overestimation like this.
Even assuming ideal conditions may yield significant errors, which cannot be tolerated by any engineer or investor.
Assuming ideal conditions is often a part of engineering, but if they are necessary to obtain results, even erroneous ones, without placing any requirements to the expertise of the engineer, then one cannot claim a simulation tool to be of use.
The forecasting would then be better left to manual labor by the engineer.

Also the economic consequences of the inaccuracies may be worrying.
If one wants to plan systems for parts of the year, a high bias error has to be assumed, as no source yields satisfactory results in terms of IRT.
The NASA source may at best yield results just within the stated IRT and it is the only source to do so. For a heavy soiling scenario, most forecasts have about the same inaccuracy in forecasting as before the exclusion, which is still regarded too high for any practical purpose.
Moreover, the levelized cost of energy (LCOE) will be significantly offset by factors like this, as high underestimations of yield will give higher prices of electricity. This may render solar power as an alternative power source considered insufficient for most purposes, by many.

4.4.3 Revised forecast vs. yield – adjusted for positive mismatch

So far, no attention has been given to the fact that the forecasts made in PVsyst are based on a system configuration where all modules are assumed to be of the same type. This assumption was necessary to assure that the forecasts didn't overestimate yield. Seeing that the forecasts don't overestimate the yield, one may ponder upon what the real yield could have been.

In chapter three, it was found that the mismatch was about 4 percent, that is, simulated MPP capacity is about 4% lower than what it should be.

If this is applied to the forecasts, the revised forecast vs. yield looks like in the graph shown in Figure 58:

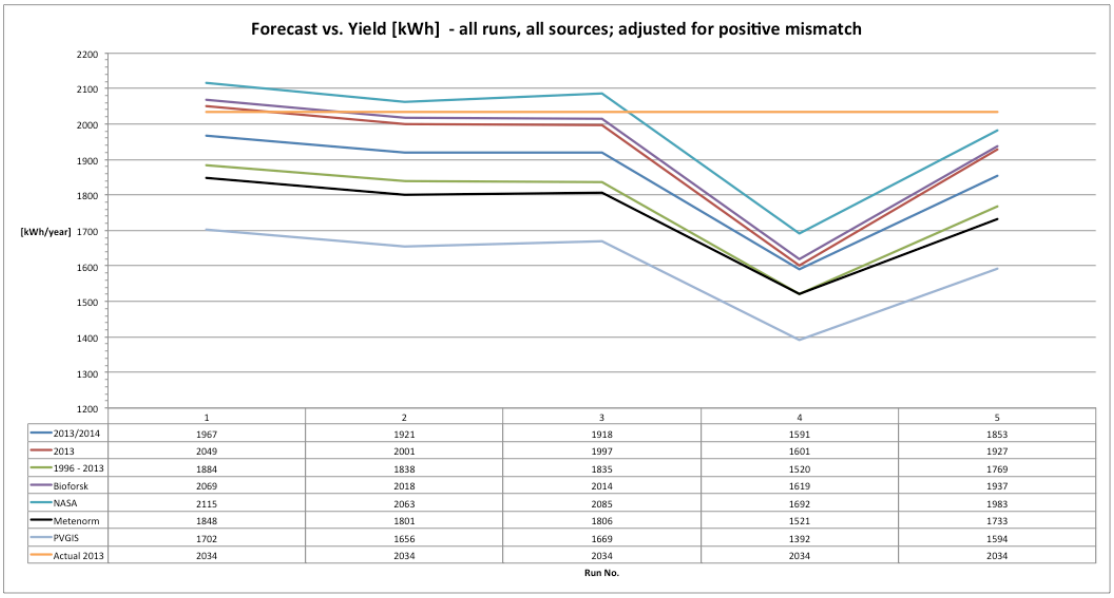

	1	2	3	4	5
2013/2014	1967	1921	1918	1591	1853
2013	2049	2001	1997	1601	1927
1996 - 2013	1884	1838	1835	1520	1769
Bioforsk	2069	2018	2014	1619	1937
NASA	2115	2063	2085	1692	1983
Metenorm	1848	1801	1806	1521	1733
PVGIS	1702	1656	1669	1392	1594
Actual 2013	2034	2034	2034	2034	2034

Figure 58: Forecasted vs. actual yield for all sources when yield is adjusted for mismatch

From the graph, one may observe that the forecasts now are higher, which is as expected. The observed trend is that all forecasts are closer to actual yield, and that the accuracy is higher.
Is seems apparent that the RY and 2013 forecasts now yield satisfactory accuracy in the three first runs, together with the NASA and Bioforsk forecasts.

In the fourth run, the forecasts all seem to be to inaccurate still, and in the fifth run, the NASA, Bioforsk and 2013 forecasts still seem to yield relatively accurately results.

To be able to compare the differences better and get a better sense of the actual the numerical value of the discrepancy from yield is listed below in Table 28.

Table 28: Discrepancy from yield for all forecasts when they are adjusted for positive mismatch

Discrepancy from yield [%] - All runs, all sources; adjusted for positive mismatch										
	2013/2014	2013	1996 - 2013	Bioforsk	NASA	Metenorm	PVGIS	Actual 2013	MBE	RMSE
1	-3.3	0.8	-7.4	1.7	4.0	-9.1	-16.3	0.0	-4.2	7.9
2	-5.6	-1.6	-9.6	-0.8	1.4	-11.5	-18.6	0.0	-6.6	9.3
3	-5.7	-1.8	-9.8	-1.0	2.5	-11.2	-18.0	0.0	-6.4	9.2
4	-21.8	-21.3	-25.3	-20.4	-16.8	-25.2	-31.6	0.0	-23.2	23.6
5	-8.9	-5.2	-13.0	-4.8	-2.5	-14.8	-21.6	0.0	-10.1	11.9

From the table above, one may observe how the NASA forecasts are overestimated by between 4% in the first runs and 2.5% in the third run.
The Bioforsk forecasts are only overestimated in the first run.

In the fifth run, it is apparent that the NASA, Bioforsk and 2013 data series all yield satisfactory accuracy in forecasting, within the assumed investor risk tolerance (IRT) of 6 - 7%. However, in run 4, all sources still fail to yield accurate forecasts, with the best forecast (NASA) around 17% under the yield.

If one disregards which source being used, the MBE shows -4.2% for the first run, this is about half of what it was in the original comparison, being about 4%-points lower. The 2nd and 3rd run lie at just below -10% in the original comparison, which differs from the values now observed by about 4%.
The same is observed for the fifth run, though some deviance is seen in the fourth, where the original value was at about -23%. Disregarding this one standout value, the positive adjustment is well reflected in the MBE.

The PRs of the different sources are excluded as they only show the same order as in the original plot, though somewhat increased.
The general tendency is that the PRs get closer to the original value of the actual system, which should be expected.

4.4.3. Discussion of revised forecasts adjusted for positive mismatch

It should be obvious to most that adjusting yield for positive mismatch is not as trivial as it is shown here. Indeed, this is the reason why the value of 4% was used, instead of the calculated mismatch value, which was a little higher.
In light of this, the accuracy of the revised forecasts should not be taken to be precise, but rather approximate.

However, it should be noted that the curves that are seen in Figure 58 are the ones one would normally expect a simulation program to yield, at least from a physical point of view. When the ideal scenario is used, an overestimation of yield is what most engineers probably would anticipate. As such, this graph, at least in the opinion of the author, seems more credible as the correct representation of the actual system at Aas.

Nevertheless, the result is approximate the same as it was in the original comparison. If one assumes the fifth scenario to be the most realistic one, only two data sources will yield satisfactory results in terms of accuracy: NASA SSE and Bioforsk.

Seeing that engineers tend to try to imitate the real world conditions, and apply heavy soiling values, it should be noted that the accuracy is still unsatisfactory for all practical purposes in run 4. Indeed, one may argue that the soiling values applied in this thesis were somewhat high and extended to apply for longer than the values chosen in other studies - though, such values are highly site specific, and therefore cannot be compared well among different studies.

If one would recall the studies saying that PVsyst tend to be conservative in estimations, then bearing in mind that the underestimations have ranged between approximately 5% and 9%, then only some of the forecasts made would fall within this range [**34**] [**38**]. As the studies conducted earlier have no issue of

winter soiling, the only relevant comparisons can be made for the overall soiling scenario and the three first scenarios.

Making these comparisons would show that most forecasts fall within the range for the first three forecasts, excluding Meteonorm and PVGIS.
If one also assumes that the 1996 - 2013 series is a little faulty due to diffuse correction, then these forecasts are also within the stated range.

However, only the NASA, Bioforsk and 2013 series forecast within this range in the fifth run. As the 2013 series is only included for comparison, then the only forecasts still within the range are the NASA and Bioforsk forecasts.
This supports the general findings that these sources are the most reliable.

4.4.4 Section summary

The overall result when excluding the months of January and February is that the forecasts become more homogeneous and inaccurate in general.
This indicates that the real forecasting accuracy is unsatisfactory in general,

The exclusion shows an insignificant difference in BE for run 4 in forecasts based on NASA and Bioforsk data, while forecasts based on data from other sources generally are affected more. This supports that the overestimation of irradiance in these datasets is the reason for the high accuracy of forecasts based on these sources.

The accuracy of the best performing forecast (NASA) is at -6.3% for the ideal scenario, which is just within the assumed IRT. The NASA forecasts are also the only ones within the range of underestimation found by previous studies, in the three first runs.

Forecasts that are adjusted for positive mismatch show that the Bioforsk and NASA forecasts are the ones generally considered within the IRT and also the stated range of underestimation previously found in other studies.
However, in the heavy soiling scenario, no forecast is satisfactory in terms of accuracy, the most accurate forecast (NASA) underestimating by 17%.

4.5 Economical evaluation

This is the final subchapter of the results, and it will briefly give an overview over the economic consequences induced when underestimating yield.
The levelized cost of energy (LCOE) will be calculated and stated for the original forecasts and for the forecasts adjusted for positive mismatch, to yield a comparison of the differences.

4.5.1 LCOE for all sources according to forecast

The high inaccuracy in forecasting could lead to a significant increase in estimated electricity price for a system.
The actual yield of the system would give an LCOE of 2.07 NOK/kWh, if it were counted as the initial yield of the system.

Underneath, Figure 59 shows how the LCOE is distributed for the different original forecasts for the PV-system at Aas.

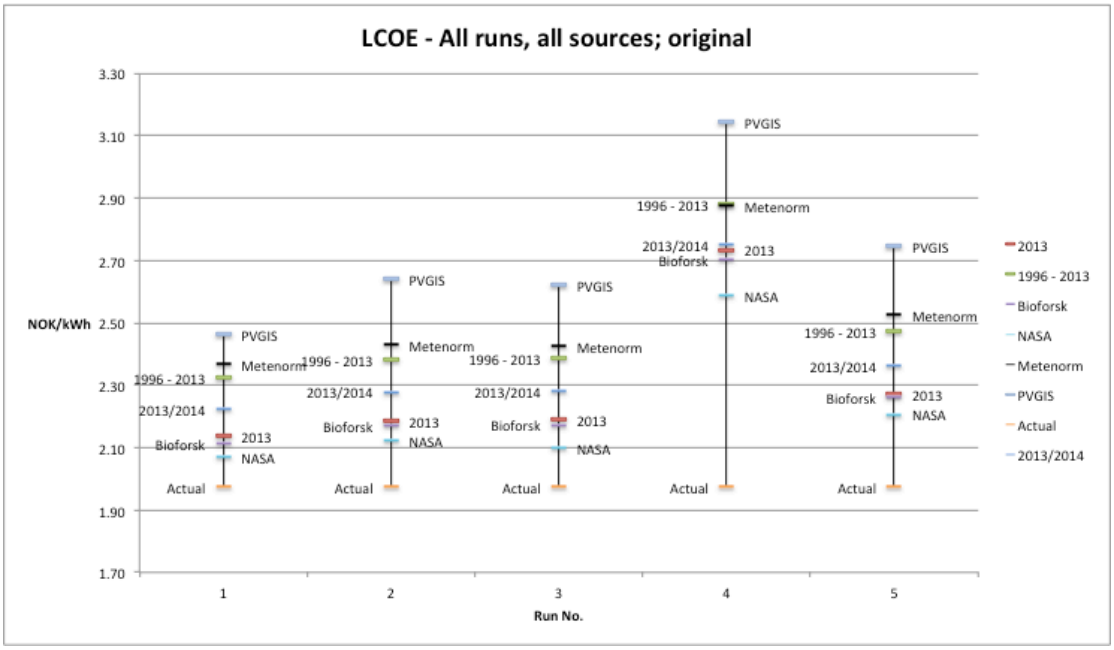

Figure 59: LCOE for the PV-system at Aas with original forecasts

From the above figure, it may be observed that PVGIS consistently has the highest LCOE, which in run 1 is 2.57 (NOK/kWh and in run 4 is 3.15 NOK/kWh. For NASA forecasts, the LCOE is 2.07 and 2.59 NOK/kWh in the same runs, respectively. For Bioforsk forecasts, the LCOE is 0.07 NOK/kWh higher than for the NASA forecasts in run 1, and 0.11 NOK/kWh higher in run 4.

The RY and 2013 forecasts give LCOEs of 2.23 NOK/kWh and 2.14 NOK/kWh, for run 1, and 2.75 NOK/kWh and 2.73 NOK/kWh, in run2, respectively.

For reference, the MBE in the forecasted LCOE is 9.1% for run 1 and about 36% in run 4.

The LCOE will be a little lower when the forecasts are adjusted for positive mismatch, this can be shown below in Figure 60:

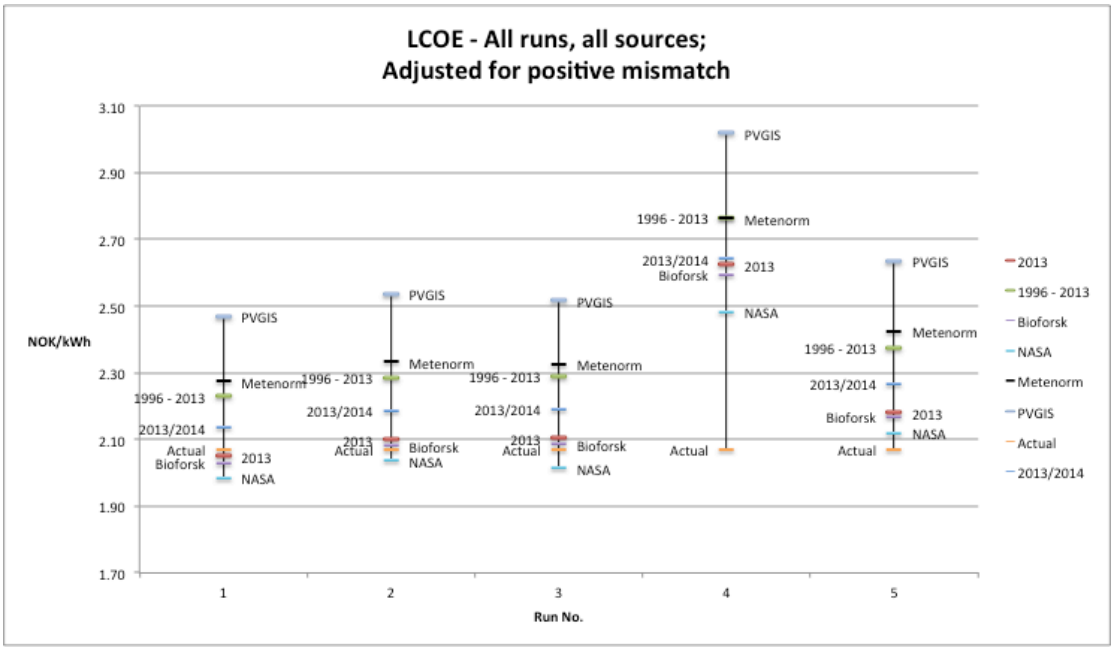

Figure 60: LCOE prices for the PV-system at Aas when forecasts are adjusted for positive mismatch

Note that in the above figure, the vertical axis of the plot has been changed from the previous graph to better display the differences between the LCOE of the different forecasts. The new maximum value is 3.10 NOK/kWh.

As can be seen from the figure, the forecasted LCOEs are now a little lower. The PVGIS forecasts yield a little lower price in the 1st run, with a LCOE of 2.47 NOK/kWh, 0.10 NOK/kWh below the original LCOE. For run 4, this difference is 0.13 NOK/kWh.

For NASA, the new LCOE is 1.99 (-0.08) NOK/kWh and 2.48 (-0.11) NOK/kWh, in the 1st and 4th run, respectively. The parenthesized values are the changes from the original forecasted LCOE.
For Bioforsk forecasts, the new LCOE is 2.03 (-0.08) NOK/kWh and 2.60 (-0.10) NOK/kWh in the 1st and 4th run, respectively.

For the RY and 2013 series, the forecasted LCOEs are 2.14 (-0.09) NOK/kWh and 2.05 (-0.09) NOK/kWh, for run 1, and 2.64 NOK (-0.11) NOK/kWh and 2.62 (-0.11) NOK/kWh, in run 4, respectively.

For reference, the new MBE is 4.8% and about 30% in run 1 and 4, respectively.

4.5.2 Discussion of LCOE

That the observed order of calculated LCOE is the same as that for the forecasts in terms of accuracy should not be a big surprise as they are directly related.

However, that the LCOEs don't maintain the same relative difference to each other may not be as obvious. One must remember that some forecasts showed a different response to restrictions in module layout and soiling, among others. This is rooted in the inherent differences between the meteorological data used as input, and therefore the "dip" and "rise" behavior is reflected in the graphs

between run 3 and 5. The improved database accuracy may be observed by looking closely at run 2 and 3.

In calculating the LCOE, an almost risk free interest of 5% was assumed.
This value may be different in some instances, which is a factor that would have to be counted in for anyone looking to purchase a PV-system, though it's variation is not necessarily very high.
As loans for renewable energy systems (RES) become increasingly usual, one might expect them to receive fair interest rates downwards of the 5% assumed.

The SDR applied is 0.5%, which in general is at the same level as that assumed by other engineers in studies conducted earlier.
However, the issue of SDR is one of higher insecurity, than for the interest rate, which is relatively foreseeable. The SDR, in the first instance, is assumed in addition to the already assumed degradation losses of a module.
This may seem like a double "punishment" when accounting for losses.
It hardly seems justifiable to be so conservative in calculation of prices, as the yield forecasted already is underestimated in most instances.
This is a subject that will be addressed as more PV-systems soon reach the end of their presumed lifespans, when the remaining efficiency of the system may be revealed.

To comment on the results that have been found in numerical form; The LCOE of the actual system is 2.07, this value is only achieved by NASA forecasts in run 1 of the original forecasts. Adjusting for positive mismatch makes this value fall below the actual LCOE, though in run 5, it is very close to the actual LCOE.
If the adjusted yield is regarded more reliable, then NASA will generally yield good accuracy on this level in terms of LCOE. This is as expected from the previous results.
The LCOE of Bioforsk prices generally lie close enough to the actual price also in the ideal scenario, and in run 5 is at 2.17, which also could be accepted by many.
However, the prices yielded by PVGIS, and also Meteonorm for that sake, are too high to be taken as accurate enough.

As have been seen, most forecasts yield an unsatisfactory accuracy in run 4, leading to prices well above the actual LCOE.
This means that for most practical purposes, when trying to simulate the real world by assuming heavy soiling, the LCOE will also be wildly overestimated.
This is in accordance with previously found result.

For last, it may be suitable to comment on grid parity. Studies have estimated that the Norwegian residential market for PV power should reach grid parity within 2019 [**31**]. Currently, the spot price at the NASHDAQ Nordic for 2018 is 0.238 NOK/kWh, rendering it highly unlikely that any grid parity event will be reached in Norway by this time with the LCOE calculated or forecasted in this thesis.

4.5.3 Section summary

This subchapter has shown that the actual LCOE of the system is at 2.07 NOK/kWh, considering the actual yield in the reference year (RY) as the initial yield of the system in the LCOE calculation. This LCOE is forecasted when using NASA SSE data, in the ideal scenario.

The most accurate adjusted forecasts are made by using NASA data - they show a lower than actual LCOE for the three first runs, with a slight overestimation in the fifth run.
The Bioforsk forecasts lead to acceptable forecasted LCOEs in the three first runs as well, though maybe too inaccurate in the fifth run.
No sources yield a satisfactory prediction of LCOE in the heavy soiling scenario when the forecasts are adjusted.

The SDR rate chosen as basis for the comparison is highly questionable, particularly due to the degradation losses already taken into account in the simulations. Actual SDRs for newer systems may be found when these end their assumed lifespans in near future, potentially reducing the LCOE.

The by one study assumed grid parity event for residential households in Norway in 2019 is unlikely to occur, considering the estimated spot price on the NASDAQ Nordic market for 2018 is 0.238 NOK/kWh, which is 1.863 NOK/kWh lower than the current lowest LCOE calculated for the system in this thesis.

5. Conclusions

The meteorological data used in the thesis had large variations.
The NASA and Bioforsk data generally had high values for irradiance and low values of DGR over the year as a whole. The average data series hauled from FAGKLIM generally showed to lower amounts of irradiance, which indicates that the irradiance level may have increased some over the last decade, when considering the high irradiance in Bioforsk data.
PVGIS and Meteonorm data generally are considered to underestimate the solar resource on a yearly basis, though PVGIS is the only source that really shows significantly lower irradiance levels than the RY.

The MBE of forecasting regardless of the source was found to be -8.1% in the best-case scenario with an RMSE of 10.3%.
The MBE of forecasting regardless of source was found to be -26.3% in the worst-case scenario with an RMSE of 26.6%.
When adjusting for positive mismatch, the MBE of the best-case scenario was found to be -4.2% with an RMSE of 7.9%. For the worst-case scenario, the MBE was -23.2% with an RMSE of 23.6%.

The results obtained show that on a general basis, when excluding heavy soiling, only forecasts based on NASA SSE data and Bioforsk measured data fall within a range of underestimation of 5 -9% - found in previously conducted modeling accuracy studies. This also applies when forecasts are adjusted for positive mismatching.

The forecasted yield was found to be most accurately predicted using NASA SSE database met-data. These forecasts matched the actual inverter output in an ideal scenario only incorporating degradation losses of 2% in total.
The bias error (BE) of the forecasts made in other scenarios simulated, all show to fall within an assumed investor risk tolerance (IRT) of 6 - 7%, except for when heavy soiling is applied.
The databases Meteonorm and PVGIS were deemed unsuitable in terms of accuracy of forecasting. The lowest BE obtained with Meteonorm was -12.8% and with PVGIS -19.7%, both in an ideal scenario.

Forecasts based on Bioforsk average data from a measured time series in the vicinity of the PV-system site, generally yielded satisfactory accuracy within the IRT for simulations only incorporating a near shading model and the module layout option in PVsyst. This series yielded the most accurate forecasts from measured data.

The most accurate forecasts based on sources like the NASA SSE and Bioforsk showed that the high forecasting accuracy of *annual* yield is due to much overestimated irradiance in the winter months of January and February.
This theory was supported by the application of heavy soiling values in these months. When the months of January and February were excluded, the forecast BE did not change significantly in the heavy soiling scenario, though did change significantly in other scenarios - particularly for high irradiance sources like NASA SSE and Bioforsk.

This implicated that the use of NASA SSE data and Bioforsk data would yield sufficiently reliable results within the IRT, for the above-mentioned scenarios, only when used for forecasting *annual* yield.

Use of a reference year (RY) time series as meteorological input yielded unsatisfactory results in all simulation scenarios made - the forecast BEs was generally outside the accepted IRT. This is generally believed to be due to faulty data, induced by corrections of the diffuse radiation in the time series after sensor calibration, which led to incorrect diffuse values in months with low light conditions. Using a second time series identical to the RY, where the two first months of the year differed, supported this theory.
The result was that the forecasts based on the second time series was comparable to those based on Bioforsk data, in terms of accuracy in forecasting.

The proofing of data quality by using an elaborated collection of sources for meteorological data is recommended for successfully obtaining accurate forecasting results.

Nonetheless, the results in this thesis cannot generally be owed to differences in the meteorological data, and the simulation software does seem to underestimate the production significantly in most cases.
Therefore, further work should be conducted to investigate methods to obtain more accurate forecasts.

The heavy soiling model generally showed to induce unacceptable inaccuracy in forecasting, the lowest BE was -20.2%, obtained by using NASA SSE data.
In essence, the heavy soiling scenario is a source of significant error in forecasting accuracy and underestimates the available resource and yield.
Soiling losses are generally considered to be the most uncertain factor that influences forecasting.
Evaluating soiling over the different months of the year, soiling values have been suggested to reduce the overall discrepancy between forecasted and actual yield. Heavy soiling values are suggested in January, heavy to moderate in February, low to none for March - April and none for the rest of the year and as an overall value for the year as a whole. These values are assumed valid for locations within a climatic distance of 20 km from Aas.

A horizontal module arrangement is suggested in order to reduce, or avoid altogether, the induced forecasting errors. Other means would be to clean modules regularly; this should be expected feasible for residential and medium sized commercial systems.

Shading losses were generally low and remained relatively constant in all forecasts generated in this thesis. This also applied in the combined shading model, though the losses were about 1 - 1.5% higher than for the detailed scenario. Because the near shading loss in the combined model was almost insignificant, the construction of a detailed 3D shading model was not considered justifiable in terms of work load - a simplified model seems to yield accurate

enough results for most practical purposes. Therefore, using a SUNeye horizon-graphing device may be a good investment.

Excluding soiling scenarios from simulations, the highest losses are due to a low irradiance level, though this is generally at the same level for most sources.
High diffuse-to-global ratio (DGR) in the datasets seem to lead to lower transposition factors when evaluated in conjunction with the irradiance level of the source used. Consequently, the sources with highest DGR often are the ones with highest observed irradiance loss in forecasts.
Also, due to the diffuse modeling in PVsyst, omitting diffuse radiation data may lead to a faulty DGR, with higher simulated beam components and transposition surplus. For higher accuracy, therefore, these data should be supplied.

Inverter losses seem to be relatively constant for all sources, maintaining a value of around 5%. Particularly databases seem to have increased inverter efficiency when applying module layout, due to higher load factors.
The fact that this only applies forecasts based on met-data from databases remains a mystery.

Temperature losses are generally considered insignificant, usually maintaining values below 1%. An unexplainable phenomenon seems to lead to a significant (>1%) temperature loss with heavy soiling applied and a reduced (below ideal scenario) temperature loss with overall soiling applied.

The actual LCOE of the system is 2.07 NOK/kWh. It is considered accurately predicted when using NASA data for forecasting, and to a lesser extent Bioforsk data. Adjusting for positive mismatch in the system configuration under modeling maintains this trend.
A grid parity event is not considered likely to occur in any foreseeable future within the residential PV-market for this particular system.

6. Further work

Regarding meteorological data; databases really should incorporate northern latitudes in their register. The most used existing databases today, and the ones used in this thesis, are usually highly unreliable and only possess data up to about 50 degrees North. Therefore, data has to be interpolated, using weather stations often located well beyond any reasonable climatic distance.
The result can be seen from the Meteonorm and PVGIS forecasting inaccuracies. Work should therefore be conducted to ensure a working database, also for northern latitude above 50 degrees.

One way to achieve sufficient access to meteorological data is to perform so-called distributed measurements. In short, pyrometer and temperature measuring instruments should be distributes widely and equipped with a wireless data-logging device. Most research institutions, schools, universities and other forms of forums established to collect and distribute information should also perform this extra task. The price of instruments is generally lower than the average curriculum for any such institution, with lifespans of several decades and low operating requirements. The advantage will be of public good, and the weather data can also be made available for profit.

Regarding modeling; in this thesis, the use of a 3D model was not justifiable. However, in more demanding shading environments, the 3D model may be.
If this were not the case, than no such option would exist in PVsyst.
As such, the availability of LIDAR measurements should be made more available to engineers intending to plan PV-systems. The commercializing of extended LIDAR measurements, offering database access or the likes to 3D mappings of more or less any area, would be a significant improvement to the engineering society in general. The apparent success of Google street view implicates that such measurements are indeed in the public interest and market ready.

In terms of horizon modeling and PVsyst, it would be interesting to see more studies comparing the SUNeye versus accurate LIDAR modeling in simulation programs. This way, one could conclude which method really would yield the most accurate results. Indeed, if the SUNeye is sufficient for most planning purposes, a significant amount of time and resource may be saved in the planning process of a PV-system.

Regarding modules; studies showing real module deterioration and performance degradation in northern latitudes would be key to exclude overestimation of these factors in simulation tools.

Some producers of solar panels have started looking at the modeled performance of their modules in PVsyst, suggesting alternative ways of planning in PVsyst to get more accurate results - one is Sandia Corporation.
This should be investigated in order to yield results that may be of use to the solar industry in general - especially in Norway, where the market is still underdeveloped.

7. References

[1] Sigurd Øygarden Flæten. (2013, Nov) TU (Teknisk ukeblad). [Online]. http://www.tu.no/kraft/2013/11/20/norsk-solinnstraling-er-opptil-10-prosent-hoyere-enn-tidligere-antatt

[2] Erik S. Marstein, Centre director, Norwegian Centre for Solar Cell Technology, January 2014.

[3] CivicSolar. (2011, October) CivicSolar. [Online]. http://www.civicsolar.com/resource/balance-system-bos-components-solar-pv

[4] German Solar Energy Society, *Planning and installing photovoltaic systems*. Berlin, Gemany: Earthscan, 2008, vol. 2, Several publishers exist.

[5] Frauenhofer ISE. (2013, November) Downloads. [Online]. http://www.ise.fraunhofer.de/de/downloads/pdf-files/aktuelles/photovoltaics-report-in-englischer-sprache.pdf

[6] Christiana Honsberg and Stuart Bowden. (2008, June) PVEDUCATION. [Online]. http://www.pveducation.org/pvcdrom

[7] Dr Rod Nave. (1998, January) HyperPhysics. [Online]. http://hyperphysics.phy-astr.gsu.edu/hbase/solids/band.html

[8] Sandia corporation. (2013, November) PVPerformance: Modeling collaborative. [Online]. http://pvpmc.org/modeling-steps/module-iv-curve/diode-equivalent-circuit-models/

[9] PVsyst. (2013) PVsyst Help. [Online]. http://files.pvsyst.com/help/

[10] PHOTON. (2014, Apr.) Photon. [Online]. http://www.photon.info/photon_lab_modul_temperatur_en.photon?ActiveID=1288

[11] L.A., Krenzinger, A., Prieb, C.W.M Hecktheuer, "Methodology for Photovoltaic Modules Characterization and Shading Effects Analysis," *Journal of the Brazilian Society of Mechanical Sciences*, vol. 24, no. 1, pp. 26-32, Jan. 2002.

[12] Openelectrial. (2013, June) Openelectrical. [Online]. http://www.openelectrical.org/wiki/index.php?title=Photovoltaic_Cell_Model

[13] Roger A., Ventre, Jerry Messenger, *Photovoltaic Systems Engineering*, 2nd ed., Roger A. Messenger, Ed. Boca Raton, Florida, USA: CRC Press LLC, vol. 1.

[14] Detlef Koenemann. (2013, March) Inverter, storage and PV-system technology: Industry guide 2013. [Online]. http://www.pv-system-tech.com/fileadmin/user_upload/2013/pdf/InSyst13_GW-ES.pdf

[15] M., Mikonowicz, A., Kuitche, J. Tamizhmani, "Nameplate, datasheet and sampling requirements of photovoltaic modules," Arizona state university/PowerMark Corp, Arizona, 2012.

[16] Driesse A, Pelland S, Turcotte D, Poissant Y Thevenard D, "Uncertainty in long-term photovoltaic yield predicitons," Varennes Research Center, CanmetENERGY, Varennes, CA, PhD Thesis 2010.

[17] Jr. R.G. Ross, "Design techniques for flat-plate photovoltaic arrays," in *15th Photovoltaic specialists conference*, Orlando, FL, 1981.

[18] Rob W., Pollard, Andrew, Pearce, Joshua M. Andrews, "The Effects of Snowfall on Solar Photovoltaic Performance," *Solar energy*, vol. 92, no. 1, pp. 84-97, June 2013.

[19] Charles A. Landau. (2014, April) Optimal tilt of solar panels. [Online]. http://www.solarpaneltilt.com/

[20] David Wattson. (2010,2014) FT Exploring - science and technology; Solar energy - tilt angle. [Online]. http://www.ftexploring.com/solar-energy/tilt-angle5.htm

[21] Robert A. Rohde. (2009, June) File: Solar spectrum.png. [Online]. http://www.globalwarmingart.com/wiki

[22] National Renewable Energy Laboratory (NREL). (2010, april) NREL. [Online]. http://rredc.nrel.gov/solar/glossary/

[23] Joachim Baumgärtner. (2013) Green Rhino Energy. [Online]. http://www.greenrhinoenergy.com/solar/radiation/tiltedsurface.php

[24] Kipp & Zonen. (2013) Pyranomaters: CMP 3 pyranometer. [Online]. http://www.kippzonen.com/Product/11/CMP-3-Pyranometer#.U14e_vmSyPZ

[25] NMBU Arne Auen Grimenes. (2014, April) FAGKLIM: Om instrumenter og målinger. [Online]. http://www.umb.no/fagklim/artikkel/om-instrumenter-og-malinger

[26] Meteoroloisk institutt (MET). (2014) Meteorologi: Variasjoner og feilkilder. [Online]. http://met.no/

[27] John M. Cimbala. (2011, August) Basic statistics. PDF document.

[28] Gunnar G. Løvås, *Statistikk for universiteter og høyskoler*, 2nd ed., Gunnar G. Løvås, Ed. Oslo, Oslo, Norway: Universitetsforlaget, vol. 1.

[29] Wikimedia Commons Mwtoews. (2007, April) Wikimedia Commons. [Online]. http://commons.wikimedia.org/wiki/File:Standard_deviation_diagram.svg

[30] C.J., Matsura, K. Willmott, "On the use of dimensioned measures of error to evaluate the performance of spatial interpolators," *International Journal of Geographical Information Science*, vol. 20, no. 1, pp. 89-102, 2006.

[31] Ch. , Gerlach, A. Breyer, "GLOBAL OVERVIEW ON GRID-PARITY EVENT DYNAMICS," q-cells, Valencia, Analysis.

[32] Seth B., You, Fengqi, Veselka, Thomas, Velosa, Alfonso Darling, "Assumptions and the levelized cost of energy for photovoltaics," *Energy & Environmental science*, vol. 4, no. 9, pp. 3133-3139, February 2011.

[33] Craig Hunter. (2013, February) Soldier systems. [Online]. http://soldiersystems.net/2013/02/20/tacapps-theodolite-nav-app-adds-geo-datum-pack/

[34] T., Hibberd, B. Yates, "Production modeling for grid tied PV systems," *Solarpro*, vol. III, no. 3.3, pp. 30 -56, April/May 2010.

[35] PVsyst forum. (2014) PVsyst forum. [Online]. http://forum.pvsyst.com/index.php

[36] André Mermoud and Bruno Wittmer. (2014, January) PVsyst user's manual. PDF.

[37] Solmetric Inc. (2011) SunEye 210 Shade Tool. [Online]. http://www.solmetric.com/buy210.html

[38] Rick Ga., Frearson, Lyndon, Rodden, Paul Lee, "An assesment of photovoltaic modelling software using real world performance data," Cat projects, The desert knowledge Australia solar centre (DKASC), Alice Springs, Scientific 2010.

[39] Statens Vegvesen , "Aleer og trerekker i Oslo og Akershus," Vegdirektoratet, Statens Vegvesen Region Øst, UMB, Several cities, Survey ISBN 978-82-7704-117-9, 2009.

[40] Kjeller Vinteknikk (KVT) - Byrkjedal, Øyvind; Løvholm, Anne Line; Sónia, Liléo, "Resource mapping of solar energy, An overview of available data in Norway," Lillestrøm, 2013.

[41] Joint Research Centre. (2012, February) Joint Research Centre, Institute for Energy and Transport (IET) - Solar radiation. [Online]. http://re.jrc.ec.europa.eu/pvgis/solres/solrespvgis.htm#Comparison

[42] Jan Remund, Meteotest, "Quality of Metenorm Version 6.0," Bern, 2008.

[43] NASA. (2013, October) Surface meteorology and Solar energy. [Online]. https://eosweb.larc.nasa.gov/sse/documents/SSE6Methodology.pdf

[44] NASA. (2014, February) Surface meteorology and Solar energy. [Online]. https://eosweb.larc.nasa.gov/cgi-bin/sse/sse.cgi?skip@larc.nasa.gov+s06+s09#s06

[45] Bioforsk. (2014) Landbruksmeteorologisk tjeneste (LMT). [Online]. http://lmt.bioforsk.no/

[46] Norwegian Meteorological Institute (MET). (2014) eKlima. [Online]. http://sharki.oslo.dnmi.no/portal/page?_pageid=73,39035,73_39049&_dad=portal&_schema=PORTAL

[47] MET, NRK. (2014) YR. [Online]. http://www.yr.no/sted/Norge/Akershus/%C3%85s/Orrestien/

[48] Multiconsult, "Kostnadsstudie, Solkraft i Norge 2013," Enova SF, Economical evaluation 125340-RIEn-RAP-001, 2013.

[49] Adreas Madland Størdal, "PV system design and yield simulations for a farm in rygge municipality," Mathematical sciences and technology, NMBU (NULS), Ås, Master Thesis 2013.

[50] Thor Christian Tuv, CEO, FUSEN Solar AS, April 15, 2014.

[51] Skatteetaten. (2014) Merverdiavgift. [Online]. http://www.skatteetaten.no/no/bedrift-og-organisasjon/merverdiavgift/

[52] Photovoltaic-guide. (2014, April) Photovoltaic preis index. [Online]. Photovoltaic-guide.de

[53] Norges Bank. (2014, May) Norges Bankk - Valutakurs for euro. [Online]. http://www.norges-bank.no/no/prisstabilitet/valutakurser/eur/

Appendices

Appendix A: Tools overview
Appendix B: Module labels Aas
Appendix C: Datasheets
Appendix D: Inverter production data
Appendix E: Location specifics: Aas
Appendix F: Meteorological data
Appendix G: Simulated production data
Appendix H: Economical data

Appendix A: Tools overview

The following tools were used in this thesis.
Some are licensed and can only be used as an evaluation version without the purchase of a valid license.

Table A. 1: Overview over tools used in this thesis and their current availability.

List of tools used in thesis				
Name	**Location**	**Platform**	**Application**	**Available online at:**
AutoCAD 2014	PC, IFE	Windows 7 OS	Technical drawing;	http://www.autodesk.no/products/autodesk-autocad/overview
			Measuring buildings and distances	
Global Mapper v15.1	PC, IFE	Windows 7 OS	Accurate topography and geography data	http://www.bluemarblegeo.com/products/global-mapper.php
Google Maps	World wide web	HTML	Find coordinates	www.maps.google.no
Microsoft Excel 2010	PC, IFE	Windows 7 OS	Calculation	www.microsoftstore.com/excel
			Tabulating	
Microsoft Word 2010	PC, IFE	Windows 7 OS	Writing documents	www.microsoftstore.com/word
PVsyst V6.2.2	PC, IFE	Windows 7 OS	Simulations, etc.	www.pvsyst.com
		HTML	Help file	
SunEarthTools	World wide web	HTML	Orientation/azimuth	www.sunearthtools.com
Theodolite Droid V1.0.26	Personal mobile device	Android 2.1 +	Site assessment:	www.majorforms.com
			Measure heights	https://play.google.com/
			Measure distance	
			Measure orientation	
			Find location	

Appendix B: Module labels Aas

Table B. 1: Module labels from the system at Aas

Appendix C: Datasheets

In this appendix, the inverter- and PV-module datasheets follow.
Be aware that all datasheets and contained variables are subject to change without further notice; this standard is custom to most component manufacturers as of today.

Up-to-date specification sheets can be found online at the manufacturer's homepage.

The following sheets are contained:

1. REC SCM210 (PE215AJM); Year 2007
2. REC PE-series; Year 2009, 2010, 2011
3. Eltek Valere, Theia he-t inverters

Module type	REC Solar SCM 210				
	205 Wp	210 Wp	215 Wp	220 Wp	225 Wp
Cell type	Multicrystalline	Multicrystalline	Multicrystalline	Multicrystalline	Multicrystalline
Electrical data					
Nominal Power Pmpp (Wp)	205	210	215	220	225
Power Output Tolerance Pmpp (%)	±5	±5	±5	±5	±5
Maximum Power Voltage Umpp (V)	28.08	28.17	28.27	28.33	28.57
Maximum Power Current Impp (A)	7.33	7.46	7.59	7.71	7.88
Open Circuit Voltage Uoc (V)	36.09	36.26	36.37	36.51	36.65
Short Circuit Current Isc (A)	7.93	8.11	8.21	8.32	8.46
Temperature Coefficient of Pmpp (%/°C)	-0.43	-0.43	-0.43	-0.43	-0.43
Temperature Coefficient of Uoc (mV/°C)	-104	-104	-104	-104	-104
Temperature Coefficient of Isc (mA/°C)	4	4	4	4	4
Cell Efficiency (%)	14.04	14.38	14.72	15.07	15.41
Module Efficiency (%)	12.42	12.73	13.03	13.33	13.64
Diodes (Spelsberg junction box)	3 x 10 A	3 x 10 A	3 x 10 A	3 x 10 A	3 x 10 A
Fill Factor FF (%)	0.72	0.71	0.72	0.72	0.72

Values at Standard Test Conditions STC (Air Mass AM 1.5, Irradiance 1000 W/m^2, Cell temperature 25 °C)

NOCT = 43°C ±2
The NOCT (nominal operating cell temperature) is the cell temperature reached at an irradiance of 800 W/m^2, at an environment temperature of 20 °C and a wind speed of 1 m/s.

Operation limits

Max. System Voltage: 1000 V
Module temperature range: -40...+90 °C
Stormproof: wind speed of 130 km/h (equals 800 Pa) and security factor 3
Mounting: instructions of user manual and mounting system supplier to be followed

Specific Data

Cells
Multicrystalline cells produced by REC ScanCell, 156 mm x 156 mm, full square, 60 per module, optimized for low-light conditions

Module
Front: high-transparency solar glass, with antireflection surface treatment. Transmittance (average): 95.4 % +/-0.5 %
Encapsulation: EVA
Back: Tedlar
Junction box: easy access, 3 bypass diodes
Light anodized aluminum frame

Connection
2 x 0.94 m solar cables with MC-Connectors

REC Solar

Made in Sweden by REC ScanModule AB 2007-02_12
For further information contact your local distributor or visit our web site:

www.recgroup.com

Size and weight	SCM 210
Area (m^2)	1.65
Length (mm)	1665
Width (mm)	991
Thickness with frame (mm)	43
Weight (kg)	22 (approx.)

Certification/Standards

REC Solar Modules are TÜV tested, on IEC 61215 accredited and Safety Class II (TÜV-Spec 931/2.572.9) accredited.

www.tuv.com TÜV TÜV Rheinland Group ID: 0000018680

CE

REC PEAK ENERGY SERIES

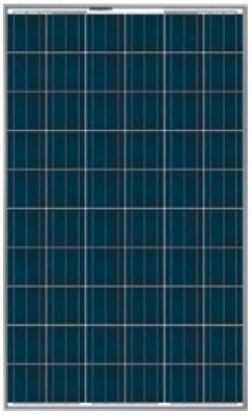

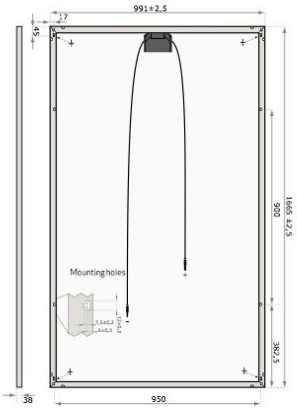

IV CHARACTERISTICS 235W MODULE

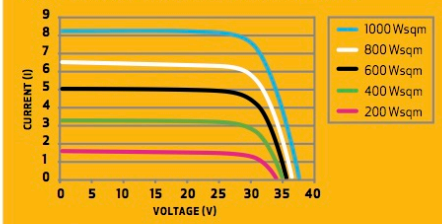

14.2 EFFICIENCY

63 MONTHS WORKMANSHIP WARRANTY

25 YEAR POWER OUTPUT WARRANTY

ELECTRICAL DATA @ STC	REC215PE	REC220PE	REC225PE	REC230PE	REC235PE
Peak Power Watts - P_{MAX} (Wp)	215	220	225	230	235
Watt Class Tolerance - P_{TOL} (W)	0/+5	0/+5	0/+5	0/+5	0/+5
Watt Class Tolerance - P_{TOL} (%)	0/+2	0/+2	0/+2	0/+2	0/+2
Maximum Power Voltage - V_{MPP} (V)	28.3	28.7	29.1	29.4	29.8
Maximum Power Current - I_{MPP} (A)	7.6	7.7	7.7	7.8	7.9
Open Circuit Voltage - V_{OC} (V)	36.3	36.6	36.8	37.1	37.4
Short Circuit Current - I_{SC} (A)	8.1	8.2	8.2	8.3	8.3
Module Efficiency (%)	13.0	13.3	13.6	13.9	14.2

Values at Standard Test Conditions STC (Air Mass AM 1.5, Irradiance 1000 W/m², Cell temperature 25 °C)

GENERAL DATA

Cell Type	60 REC PE multi-crystalline cells 3 strings of 20 cells - 3 by-pass diodes
Glass	High-transparency solar glass with antireflection surface treatment by Sunarc Technology
Back sheet	Double layer high performance polyester
Frame	Anodized aluminium
Cable	Radox 4mm² solar cables, 0.90m +1.20m
Connectors	Radox 4mm² twist locking connector

TEMPERATURE RATINGS (235 W RATED MODULE)

Nominal Operating Cell Temperature (NOCT)	47.9 °C (±2°C)
Temperature Coefficient of P_{MPP}	-0.46 %/°C
Temperature Coefficient of V_{OC}	-0.32 %/°C
Temperature Coefficient of I_{SC}	0.011 %/°C

WARRANTY

10 years limited warranty of 90% power output
25 years limited warranty of 80% power output
63 months workmanship warranty

CERTIFICATION

Certified according to UL1703, IEC 61215 and, IEC 61730

MECHANICAL DATA

Dimensions	1665 x 991 x 38 mm
Area	1.65 m²
Weight	18kg

MAXIMUM RATINGS

Operational Temperature	-40 ... +80°C
Maximum System Voltage	1000V
Maximum Load	551 kg/m² (5400 Pa)
Maximum Wind Speed	197 km/h (safety factor 3)
Max Series Fuse Rating	15A
Max Reverse Current	15A

Note! Specifications subject to change without notice.

REC is a leading vertically integrated player in the solar energy industry. REC is among the world's largest producers of polysilicon and wafers for solar applications, and a rapidly growing manufacturer of solar cells and modules. REC is also engaged in project development activities in selected PV segments. Founded in Norway, REC is an international solar company, employing more than 3,000 people worldwide. REC had revenues in excess of NOK 9 billion in 2009.

Please visit **www.recgroup.com**

March 2010, version A

REC

REC Solar AS
Kjørboveien 29
1329 Sandvika
Norway

www.recgroup.com

REC PEAK ENERGY SERIES

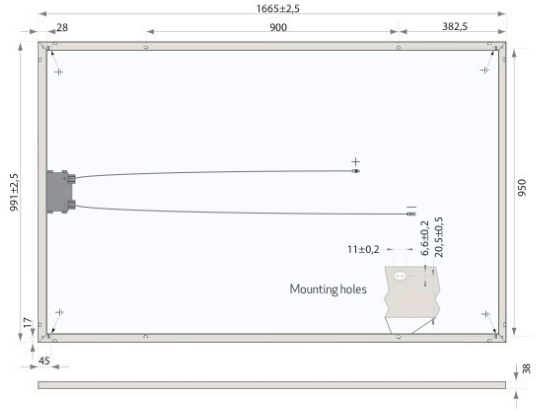

15.1% EFFICIENCY

10 YEAR PRODUCT WARRANTY

25 YEAR LINEAR POWER OUTPUT WARRANTY

TEMPERATURE RATINGS

Nominal Operating Cell Temperature (NOCT)	47.9°C (±2°C)
Temperature Coefficient of P_{MPP}	-0.43 %/°C
Temperature Coefficient of V_{OC}	-0.33 %/°C
Temperature Coefficient of I_{SC}	0.074 %/°C

ELECTRICAL DATA @ STC	REC225PE	REC230PE	REC235PE	REC240PE	REC245PE	REC250PE
Nominal Power - P_{MPP} (Wp)	225	230	235	240	245	250
Watt Class Sorting - (W)	0/+5	0/+5	0/+5	0/+5	0/+5	0/+5
Nominal Power Voltage - V_{MPP} (V)	28.9	29.2	29.6	29.9	30.2	30.5
Nominal Power Current - I_{MPP} (A)	7.79	7.88	7.96	8.04	8.12	8.20
Open Circuit Voltage - V_{OC} (V)	36.2	36.5	36.7	37.0	37.2	37.5
Short Circuit Current - I_{SC} (A)	8.34	8.43	8.51	8.60	8.68	8.76
Module Efficiency (%)	13.6	13.9	14.2	14.5	14.8	15.1

Values at standard test conditions STC (airmass AM 1.5, irradiance 1000 W/m², cell temperature 25°C).
At low irradiance of 200 W/m² (AM 1.5 and cell temperature 25°C) at least 97% of the STC module efficiency will be achieved.

GENERAL DATA

Cell Type	60 REC PE multi-crystalline cells 3 strings of 20 cells - 4 by-pass diodes
Glass	3.2 mm solar glass with anti-reflection surface treatment by Sunarc Technology
Back Sheet	Double layer highly resistant polyester
Frame	Anodized aluminium
Junction box	IP67
Cable	4mm² solar cable, 0.90m +1.20m
Connectors	Hosiden 4mm² (HSC 2009/2010) MC4 connectable

ELECTRICAL DATA @ NOCT	REC225PE	REC230PE	REC235PE	REC240PE	REC245PE	REC250PE
Nominal Power - P_{MPP} (Wp)	167	170	173	176	179	182
Nominal Power Voltage - V_{MPP} (V)	26.6	26.8	27.1	27.3	27.6	27.9
Nominal Power Current - I_{MPP} (A)	6.27	6.33	6.39	6.45	6.51	6.56
Open Circuit Voltage - V_{OC} (V)	33.4	33.6	33.8	34.1	34.3	34.5
Short Circuit Current - I_{SC} (A)	6.79	6.85	6.90	6.96	7.01	7.06

Nominal cell operating temperature NOCT (800 W/m², AM 1.5, windspeed 1 m/s, ambient temperature 20°C).

MAXIMUM RATINGS

Operational Temperature	-40 ... +80°C
Maximum System Voltage	1000V
Maximum Snow Load	550 kg/m² (5400 Pa)
Maximum Wind Load	244 kg/m² (2400 Pa)
Maximum Series Fuse Rating	25A
Maximum Reverse Current	25A

CERTIFICATION

Certified to IEC 61215 & IEC 61730, IEC 62716 (ammonia resistance) & IEC 61701 (salt mist - severity level 6).

PV CYCLE
Member of PV Cycle

WARRANTY

10 year product warranty.
25 year linear power output warranty
(max. degression in performance of 0.7% p.a.).

MECHANICAL DATA

Dimensions	1665 x 991 x 38 mm
Area	1.65 m²
Weight	18 kg

Note! Specifications subject to change without notice.

Rev K - 01.2012

REC is a leading vertically integrated player in the solar energy industry. Ranked among the world's largest producers of polysilicon and wafers for solar applications and a rapidly growing manufacturer of solar cells and modules, REC also engages in project development activities in selected PV segments. Founded in Norway in 1996, REC is an international solar company employing about 4,000 people worldwide with revenues close to EUR 1.7 billion in 2010. Visit www.recgroup.com to learn more about REC.

REC
www.recgroup.com

REC PEAK ENERGY SERIES

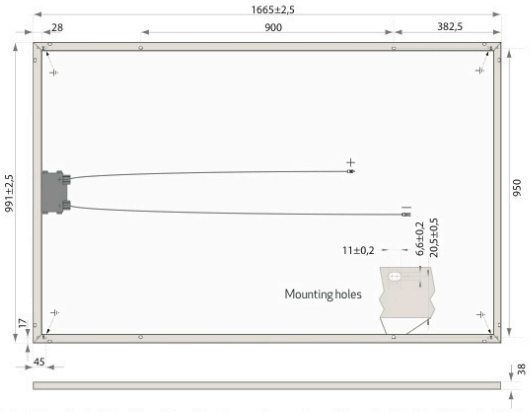

*Diagram indicates Hosiden junction box (Design 2), position and dimensions are the same for modules supplied with Huber & Suhner junction box (Design 1).

ELECTRICAL DATA @ STC	REC235PE	REC240PE	REC245PE	REC250PE	REC255PE	REC260PE
Nominal Power - P_{MPP} (Wp)	235	240	245	250	255	260
Watt Class Sorting - (W)	0/+5	0/+5	0/+5	0/+5	0/+5	0/+5
Nominal Power Voltage - V_{MPP} (V)	29.5	29.7	30.1	30.2	30.5	30.7
Nominal Power Current - I_{MPP} (A)	8.06	8.17	8.23	8.30	8.42	8.50
Open Circuit Voltage - V_{OC} (V)	36.6	36.8	37.1	37.4	37.6	37.8
Short Circuit Current - I_{SC} (A)	8.66	8.75	8.80	8.86	8.95	9.01
Module Efficiency (%)	14.2	14.5	14.8	15.1	15.5	15.8

Analysed data demonstrates that 99.7% of modules produced have current and voltage tolerance of ±3% from nominal values.
Values at standard test conditions STC (airmass AM 1.5, irradiance 1000 W/m², cell temperature 25°C).
At low irradiance of 200 W/m² (AM 1.5 and cell temperature 25°C) at least 97% of the STC module efficiency will be achieved.

ELECTRICAL DATA @ NOCT	REC235PE	REC240PE	REC245PE	REC250PE	REC255PE	REC260PE
Nominal Power - P_{MPP} (Wp)	179	183	187	189	193	197
Nominal Power Voltage - V_{MPP} (V)	27.5	27.7	28.1	28.3	28.5	29.0
Nominal Power Current - I_{MPP} (A)	6.51	6.58	6.64	6.68	6.77	6.81
Open Circuit Voltage - V_{OC} (V)	34.2	34.4	34.7	35.0	35.3	35.7
Short Circuit Current - I_{SC} (A)	6.96	7.03	7.08	7.12	7.21	7.24

Nominal cell operating temperature NOCT (800 W/m², AM 1.5, windspeed 1 m/s, ambient temperature 20°C).

CERTIFICATION

IEC 61215 & IEC 61730, IEC 62716 (ammonia resistance) & IEC 61701 (salt mist - severity level 6).

Member of PV Cycle

WARRANTY

10 year product warranty
25 year linear power output warranty
(max. degression in performance of 0.7% p.a.)

15.8% EFFICIENCY

10 YEAR PRODUCT WARRANTY

25 YEAR LINEAR POWER OUTPUT WARRANTY

TEMPERATURE RATINGS

Nominal Operating Cell Temperature (NOCT)	45.7°C (±2°C)
Temperature Coefficient of P_{MPP}	-0.40 %/°C
Temperature Coefficient of V_{OC}	-0.27 %/°C
Temperature Coefficient of I_{SC}	0.024 %/°C

GENERAL DATA

Cell Type:	60 REC PE multi-crystalline 3 strings of 20 cells
Glass:	3.2 mm solar glass with anti-reflection surface treatment
Back Sheet:	Double layer highly resistant polyester
Frame:	Anodized aluminium (silver)
Junction Box Design 1:	Huber & Suhner: IP67 rated 3 bypass diodes 4 mm² solar cable, 0.9 m + 1.2 m Radox 4 mm², twist lock connectors
Junction Box Design 2:	Hosiden: IP67 rated 4 bypass diodes 4 mm² solar cable, 0.9 m + 1.2 m Hosiden 4 mm² connectors, MC4 connectable

MAXIMUM RATINGS

Operational Temperature:	-40 ... +80°C
Maximum System Voltage:	1000 V
Maximum Snow Load:	550 kg/m² (5400 Pa)
Maximum Wind Load:	244 kg/m² (2400 Pa)
Max Series Fuse Rating:	25 A
Max Reverse Current:	25 A

MECHANICAL DATA

Dimensions:	1665 x 991 x 38 mm
Area:	1.65 m²
Weight:	18 kg

Note! Specifications subject to change without notice.

Rev0 - 10.2012

REC is a leading global provider of solar electricity solutions. With nearly two decades of expertise, we offer sustainable, high-performing products, services and investment opportunities for the solar and electronics industries. Together with our partners, we create value by providing solutions that better meet the world's growing electricity needs. Our 2,400 employees worldwide generated revenues of more than NOK 13 billion in 2011, approximately EUR 1.7 billion. To see more of what REC can offer, visit www.recgroup.com.

REC

www.recgroup.com

MODEL	2.0 HE-t	2.9 HE-t	3.8 HE-t	4.4 HE-t	4.6 HE-t
INPUT DATA					
Nominal DC power	2100 W	3000 W	4000 W	4600 W	4800 W
Max. PV power	2625 W_p	3750 W_p	5000 W_p	5750 W_p	6000 W_p
Max. DC voltage	600 V_{dc}				
Voltage range MPPT	230 to 480 V_{dc}	230 to 480 V_{dc}	230 to 480 V_{dc}	230 to 480 V_{dc}	230 to 480 V_{dc} [1]
Max. input current	9.5 A	13.5 A	18.0 A	21.0 A	21.0 A
Number of PV string inputs	3				
Number of MPP trackers	1				
Input features	Reverse polarity protection, Ground fault monitoring, Integral DC switch disconnector (optional), Integral DC fuses for string inputs (optional), Field configurable for positive or negative grounding, or ungrounded				
OUTPUT DATA					
Nominal output power	2000 W	2900 W	3800 W	4450 W	4600 W
Max apparent power	2000 VA	2900 VA	3800 VA	4450 VA	4600 VA
Nominal AC current	9.0 A	13.0 A	17.0 A	19.5 A	20.0 A
Max. AC current	10.5 A	15.2 A	19.7 A	23.0 A	23.0 A
Mains output voltage	230 Vac (+/-20 %) single or split phase				
Mains frequency	50 Hz / 60 Hz (+/-10 %)				
Cos Phi (power factor)	0.8i to 0.8c selectable				
PERFORMANCE DATA					
Maximum efficiency	97.2 %	97.2 %	97.2 %	97.3 %	97.3 %
CEC efficiency	96.8 %	96.8 %	97.0 %	97.0 %	97.0 %
EU efficiency	96.3 %	96.5 %	96.7 %	96.9 %	96.9 %
Power feed starts at	< 7 W				
Night mode power	< 1 W				
MECHANICAL DATA					
Protection degree (EN 60529)	IP 65				
Dimensions	610 H x 353 W x 154 D mm / 24.02 H x 13.90 W x 6.06 D inches				
Weight	< 19 kg / 42 lbs	< 19 kg / 42 lbs	< 21 kg / 46 lbs	< 21 kg / 46 lbs	< 21 kg / 46 lbs
Cable access	Bottom				
Input cable connection	MC3, MC4, Tyco, Screw terminals, Cable clamp, Others on request				
Output cable connection	Screw terminals, Cable clamp				
DESIGN STANDARDS					
EM compatibility	EN 61000-6-2, EN 61000-6-3				
CE marking	Yes				
Other standards	DIN VDE V 0126-1-1, G83/1, EN 50438, AS 4777, CEI 0-21, EN 61000-3-2, EN 61000-3-3, EN 61000-3-11, EN 61000-3-12, IEC 62109-2, IEC 61727, UTE C 15-712-1, C10/11, VDE AR-N 4105, RD1663, G59/2				
ENVIRONMENTAL DATA					
Operating temperature	- 25 °C to + 65 °C / - 13 to + 149 °F (possible power derating above + 45 °C / + 113 °F)				
Storage temperature	- 30 °C to + 80 °C / - 22 to + 176 °F				
Ventilation	Convection cooling				

ADDITIONAL FEATURES

Topology	High frequency transformer, galvanic isolation
Protection class / Overvoltage category	I / III
Noise Emission	< 37 dB (A)
Communication	Graphical, color display with touch sense buttons, Embedded web-server, Ethernet, CAN and RS485 bus interface, 3x LEDs for visual status indication
Warranty	5 years, 10 years, 15 years, 20 years and 25 years options

1) Output power limitation 230 Vdc to 250 Vdc

EFFICIENCY CURVE THEIA 4.4 HE-t

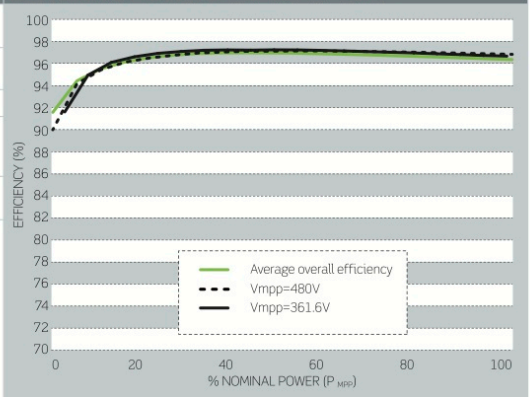

Appendix D: Inverter production data

The inverter log-file will typically display current, voltage and power on both the inverter inlet-side and outlet-side.
In addition, the accumulated energy output for the day, for the month, for the year and total accumulated energy output is shown.

In order to deduce the produced amount of energy, therefore, it was deemed sufficient to look at the total accumulated amount of energy.
However, because the inverter had been in operation for testing at the factory, before delivery to NULS (NMBU), the total energy output was significantly higher than the actual value corresponding to the recent year of production.

On grounds of this, the actual inverter output for twelve months of operation in the above stated period would have to be calculated from the difference in total energy output.

This calculation and the result can be seen in Table D. 1, where end value and initial value refers to the total energy output of the inverter at the end of the month and at the beginning of the month, respectively.
Note that the values shown have been adjusted to display fewer decimal places than in the raw data.

Table D. 1: Calculation of the inverter production for the twelve months considered in this thesis

Inverter output					
Year	Month	End value [MWh]	Initial value [MWh]	Inv. Output [MWh]	Inv. Output [kWh]
2014	January	3.4311	3.4280	0.0031	3.1
2014	February	3.4532	3.4311	0.0220	22.0
2013	March	1.6797	1.4194	0.2604	260.4
2013	April	1.9388	1.6797	0.2590	259.0
2013	May	2.1635	1.9388	0.2248	224.8
2013	June	2.4451	2.1635	0.2816	281.6
2013	July	2.7645	2.4451	0.3194	319.4
2013	August	3.0221	2.7645	0.2576	257.6
2013	September	3.2142	3.0221	0.1921	192.1
2013	October	3.3266	3.2142	0.1123	112.3
2013	November	3.3986	3.3266	0.0721	72.1
2013	December	3.4280	3.3986	0.0293	29.3
	Year	3.4531	1.4193	2.0338	2033.8

Dato/Tid	Input Current (A)	Input Voltage (V)	Input Power (W)	Output Current (A)	Output Voltage (V)	Output Power (W)	Energy Today (Wh)	Energy this Month (kWh)	Energy this Year (kWh)	Energy total (MWh)	Peak Power Today (W)	Innstrålt Effekt (W)
02/20/2013 01:24:00.811 PM	5.882	277.7	1629	6.614	230.5	1525	1364	22.517	55.375	1.371302	1800	10992.9142
02/20/2013 01:25:00.787 PM	5.816	277.9	1618	6.576	230.3	1514	1390	22.543	55.401	1.371328	1800	10933.22751
02/20/2013 01:26:00.794 PM	5.8	278.1	1607	6.525	230.4	1503	1415	22.568	55.426	1.371353	1800	10927.2244
02/20/2013 01:27:00.818 PM	5.752	278.2	1593	6.404	230.3	1475	1440	22.593	55.451	1.371378	1800	10854.58251
02/20/2013 01:28:00.796 PM	5.667	280.4	1578	6.42	230.7	1481	1465	22.618	55.476	1.371403	1800	10668.6055
02/20/2013 01:29:00.817 PM	5.716	276.2	1572	6.367	231.3	1472	1489	22.642	55.5	1.371427	1800	10618.21871
02/20/2013 01:30:00.786 PM	5.647	278.2	1564	6.322	231.6	1464	1514	22.667	55.525	1.371452	1800	10495.54151
02/20/2013 01:31:00.799 PM	5.601	278.2	1553	6.323	231.6	1464	1538	22.691	55.549	1.371476	1800	10410.09204
02/20/2013 01:32:00.828 PM	5.59	278.1	1549	6.259	231.3	1448	1562	22.715	55.573	1.3715	1800	10492.97577
02/20/2013 01:33:00.796 PM	5.57	279.9	1545	6.256	231.2	1447	1586	22.739	55.597	1.371524	1800	10544.80359
02/20/2013 01:34:00.800 PM	5.593	275.7	1538	6.234	231	1440	1610	22.763	55.621	1.371548	1800	10371.17725
02/20/2013 01:35:00.825 PM	5.547	276.2	1526	6.248	230.8	1442	1634	22.787	55.645	1.371572	1800	10417.53618
02/20/2013 01:36:00.790 PM	5.53	273.9	1513	6.146	231.3	1422	1658	22.811	55.669	1.371596	1800	10324.19972
02/20/2013 01:37:00.791 PM	5.471	276.1	1504	6.096	231.2	1409	1681	22.834	55.692	1.371619	1800	10261.91215
02/20/2013 01:38:00.815 PM	5.462	274.3	1490	6.003	230.8	1386	1705	22.858	55.716	1.371643	1800	10204.97396
02/20/2013 01:39:00.792 PM	5.355	277.8	1481	5.95	230.8	1373	1728	22.881	55.739	1.371666	1800	10212.58681
02/20/2013 01:40:00.796 PM	5.404	274.2	1476	5.97	231.6	1383	1751	22.904	55.762	1.371689	1800	10081.19314
02/20/2013 01:41:00.805 PM	5.422	276.1	1491	6.039	231.3	1397	1772	22.925	55.783	1.37171	1800	10161.11046
02/20/2013 01:42:00.793 PM	5.385	275.8	1481	6.004	231.2	1388	1795	22.948	55.806	1.371733	1800	10087.6391
02/20/2013 01:43:00.796 PM	5.424	273.8	1483	6.061	231.5	1403	1818	22.971	55.829	1.371756	1800	10096.01816
02/20/2013 01:44:00.806 PM	5.398	276.2	1484	6.015	231.1	1390	1841	22.994	55.852	1.371779	1800	10169.99563
02/20/2013 01:45:00.795 PM	5.331	278.1	1477	5.968	231.1	1379	1864	23.017	55.875	1.371802	1800	10040.06408
02/20/2013 01:46:00.796 PM	5.368	276.2	1476	5.964	231.7	1382	1887	23.04	55.898	1.371825	1800	10088.01869
02/20/2013 01:47:00.819 PM	5.38	275.7	1471	5.967	230.8	1377	1910	23.063	55.921	1.371848	1800	9951.437321
02/20/2013 01:48:00.796 PM	5.282	272.5	1437	5.867	231	1355	1931	23.084	55.942	1.371869	1800	9860.336212
02/20/2013 01:49:00.796 PM	5.308	274.8	1451	5.898	230.5	1360	1954	23.107	55.965	1.371892	1800	9942.657593
02/20/2013 01:50:00.812 PM	5.272	276.2	1452	5.905	230.2	1359	1976	23.129	55.987	1.371914	1800	9876.138318
02/20/2013 01:51:00.838 PM	5.219	276.3	1437	5.822	231	1345	1999	23.152	56.01	1.371937	1800	9761.713638
02/20/2013 01:52:00.808 PM	5.234	274.7	1431	5.786	231.6	1340	2020	23.173	56.031	1.371958	1800	9689.605985
02/20/2013 01:53:00.793 PM	5.261	272.1	1428	5.774	231.6	1338	2042	23.195	56.053	1.37198	1800	9772.461601
02/20/2013 01:54:00.794 PM	5.215	274.6	1426	5.783	230.8	1335	2065	23.218	56.076	1.372003	1800	9714.911849
02/20/2013 01:55:00.826 PM	5.177	276.4	1426	5.775	231.2	1335	2087	23.24	56.098	1.372025	1800	9666.915061
02/20/2013 01:56:00.796 PM	5.114	278.5	1418	5.75	230.9	1328	2109	23.262	56.12	1.372047	1800	9755.41529
02/20/2013 02:07:00.808 PM	5.003	278.4	1388	5.625	230.7	1297	2351	23.504	56.362	1.372289	1800	9391.446676
02/20/2013 02:10:00.945 PM	4.95	278.5	1373	5.565	230.7	1284	2415	23.568	56.426	1.372353	1800	9241.298552
02/20/2013 02:11:00.791 PM	4.891	280.5	1366	5.513	230.9	1273	2437	23.59	56.448	1.372375	1800	9204.380108
02/20/2013 02:12:00.794 PM	4.917	278.4	1364	5.521	231	1275	2458	23.611	56.469	1.372396	1800	9260.362302
02/20/2013 02:14:00.804 PM	4.873	278.6	1352	5.467	231	1263	2500	23.653	56.511	1.372438	1800	9172.839161
02/20/2013 02:15:00.793 PM	4.863	278.5	1347	5.498	231	1270	2521	23.674	56.532	1.372459	1800	9068.684444

Figure D. 1: Inverter log file excerpt from the Theia 4.4 He-t inverter at Aas.

Appendix E: Location specifics: Aas

Figure E. 3:
Panoramic of site with azimuth degrees as in PVsyst horizon profile

Figure E. 2:
Panoramic of site with designated far/near shading objects

Figure E. 1:
Panoramic of site at Aas for evaluation of surroundings

Appendix F: Meteorological data

This appendix contains all meteorological data evaluated in the thesis. Sub-appendices have been made to ease the browsing for data the user may be interested in or needs to supplement the reading of chapters.

The appendix contents are:

Appendix F.1: Meteorological data from databases

In this sub-appendix, the meteorological data from the three databases used in the thesis are presented as they were received.

The Meteonorm symbols for global and diffuse have been altered to match the denotation used in the thesis, as it more comprehensible.

Note that the data for Aas is presented in $Wh/m_2/day$, which is irradiation, not irradiance. The values used in this thesis are irradiance, meaning that the data have been converted into W by dividing by 24 hours.

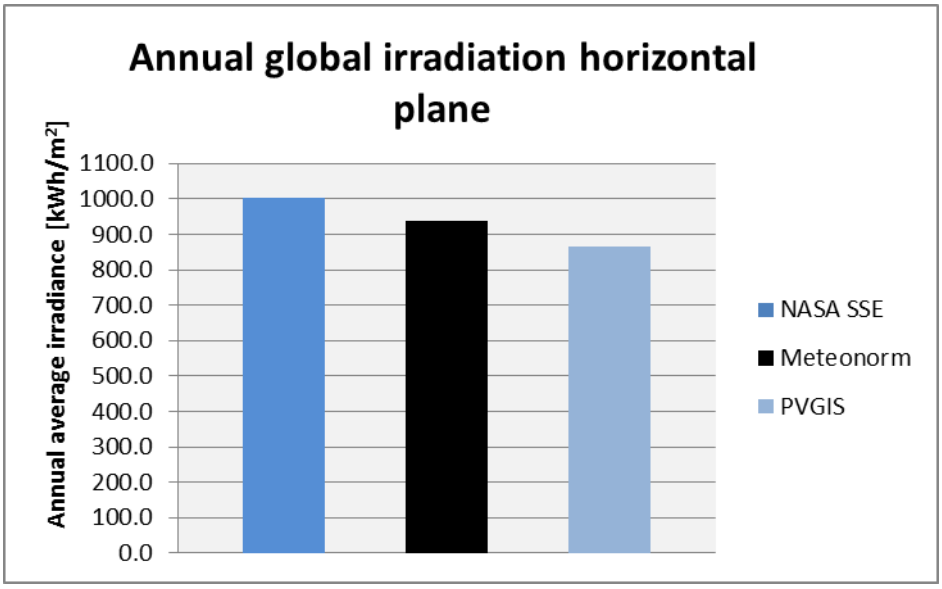

Table F. 1: Annual global horizontal irradiation at Aas for the databases NASA SSE, PVGIS and Meteonorm

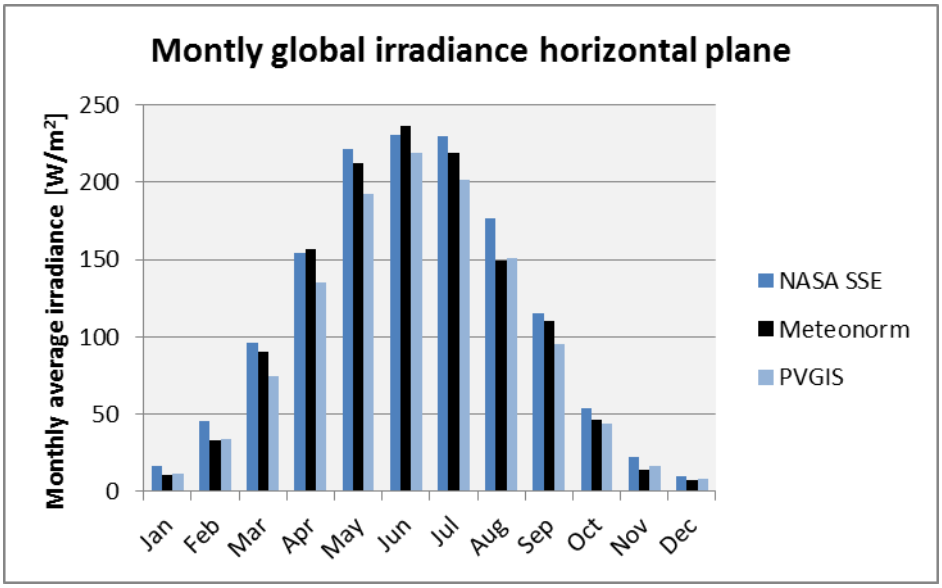

Table F. 2: Monthly distribution of global horizontal irradiance at Aas for the databases NASA SSE, PVGIS and Meteonorm

Table F. 3: The meteorological data hauled from the NASA SSE site for the location at Aas

NASA meteorological data for Aas				
	Global horizontal insolation	Diffuse horizontal insolation	Temperature [°C]	Wind speed [m/s]
Jan	16	12	-4.3	4.4
Feb	45	29	-3.9	4.0
Mar	96	56	-1.1	4.0
Apr	154	83	3.4	3.9
May	222	105	9.3	3.7
Jun	231	115	13.1	3.5
Jul	230	110	15.3	3.5
Aug	176	93	14.4	3.5
Sep	115	62	9.7	3.9
Oct	54	33	5.3	4.2
Nov	23	15	0.1	4.2
Dec	10	8	-3.3	4.3
Annual [W/m2]	114	60	5	4

Table F. 4: The meteorological data hauled from the PVGIS database for the location at Aas

PVGIS meteorological data for Aas				
	Glob [Wh/m^2/d]	D/G	Diff [Wh/m2/d]	Temperature 24h avg. [°C]
Jan	274	0.77	211	-2.5
Feb	813	0.67	545	-2
Mar	1790	0.62	1110	0.1
Apr	3240	0.56	1814	4.9
May	4620	0.52	2402	9.9
Jun	5260	0.52	2735	14.1
Jul	4840	0.54	2614	16.9
Aug	3630	0.58	2105	16.8
Sep	2280	0.58	1322	12.6
Oct	1050	0.65	683	7.2
Nov	404	0.72	291	2.3
Dec	195	0.76	148	-1.5
Year	2370	0.56	1327	6.6

Table F. 5: The meteorological data acquired from Meteonorm, together with uncertainty of measurements and interpolation stations

Month	G_G [W/m2]	G_D [W/m2]	T_a [°C]	Wind speed [m/s]
Jan	11	7	-0.6	4.2
Feb	33	21	-1	3.9
Mar	90	47	1.3	3.8
Apr	157	73	6.4	3.9
May	212	94	11.3	3.8
Jun	236	96	14.8	3.7
Jul	219	98	17.1	3.4
Aug	149	83	16.5	3.5
Sep	110	57	12.5	3.9
Oct	46	27	7.3	3.8
Nov	14	10	3.5	4.1
Dec	7	5	-0.2	3.9
Year	107	52	7.4	3.8
G_G: Use of precalculated radiation map based on satellite and ground information due to low density of network.				
Nearest 3 stations: Ta: Oslo-Blindern (29 km), RYGGE (NOR-AFB) (35 km), OSEBERG (46 km)				
Uncertainty of yearly values: G_G = 6%, G_B = 11 %, T_a = 0.8 °C				
Trend of G_G / decade = 2.1%				
Variability of G_G / year = 4.5%				

Appendix F.2: Meteorological data from weather stations

In this sub-appendix the measured weather data used in this thesis is presented.

The evaluation of which datasets to use, included making an overview of the closest stations to site. Fortunately, NULS (NMBU) conducted meteorological measurements themselves, making the choice of weather data quite simple. However, snow data had to be extracted from the MET collection online.

Soeraasfeltet weather station is marked in the Google Maps screenshot below (Table F. 6), showing the relative location of the weather stations used in this thesis to the PV-system site (Wing IV).

Table F. 6: Screenshot from Google Maps showing the location of Soeraasfeltet weather station

Table F. 7 on the next page shows an overview over all the weather stations in the vicinity of the PV-system site.
All stations listed are held at the same location, at Soeraasfeltet, shown above.
All relevant spatial information is stated; site coordinates in decimal format, AMSL and distance to site.
The parameters measured are also stated, along with the available temporal resolution and the length of the time series.
The primary data chosen are marked in red.

Table F. 7: Overview of information about the weather stations at Aas

Considered weather stations for site at Aas																
Data for site	**AMSL [m]**	**Lat.**	**Long.**	**Weather station**	**Data source**	**AMSL [m]**	**Lat.**	**Long.**	**Distance to site [km]**	**Climatic distance**	**Relevant parameter**	**Temporal resolution**	**Time from**	**Time to**	**Time interval**	**Time since last measurement**
Aas	101	59.659	10.780	Aas	Biofors k	94	59.605	10.820	1	1	Air temperature	Hourly/Daily/ Monthly	1/1/2005	5/6/2014	9 years, 4 months, 5 days	0 years, 0 months, 0 days
											Albedo	Hourly/Daily/ Monthly	1/1/2005	5/6/2014	9 years, 4 months, 5 days	0 years, 0 months, 0 days
											Global radiation	Hourly/Daily/ Monthly	1/2/2005	5/6/2014	9 years, 4 months, 4 days	0 years, 0 months, 0 days
											Wind speed (2 MAGL)	Hourly/Daily/ Monthly	1/1/2005	5/6/2014	9 years, 4 months, 5 days	0 years, 0 months, 0 days
Aas	101	59.659	10.780	Aas	NMBU/ NULS	89	59.605	10.820	1	1	Air temperature	Hourly/Daily/ Monthly	1/1/1990	5/6/2014	24 years, 4 months, 5 days	0 years, 0 months, 0 days
											Albedo	Hourly/Daily/ Monthly	1/1/1990	5/6/2014	24 years, 4 months, 5 days	0 years, 0 months, 0 days
											Diffuse radiation	Hourly/Daily/ Monthly	1/1/1990	5/6/2014	24 years, 4 months, 5 days	0 years, 0 months, 0 days
											Global radiation	Hourly/Daily/ Monthly	1/1/1990	5/6/2014	24 years, 4 months, 5 days	0 years, 0 months, 0 days
											Wind speed (10 MAGL)	Hourly/Daily/ Monthly	1/1/1990	5/6/2014	24 years, 4 months, 5 days	0 years, 0 months, 0 days
Aas	101	59.659	10.780	Aas	MET	89	59.605	10.820	1	1	Air temperature	Hourly/Daily/ Monthly	6/17/1988	5/6/2014	25 years, 10 months, 19 days	0 years, 0 months, 0 days
											Diffuse radiation	Hourly	1/1/1990	12/31/2008	18 years, 11 months, 30 days	5 years, 4 months, 5 days
											Global radiation	Hourly	1/1/1990	12/31/2008	18 years, 11 months, 30 days	5 years, 4 months, 5 days
											Snow cover	Hourly/Daily/ Monthly	01/02/1897	4/30/1988	91 years, 3 months, 27 days	26 years, 0 months, 6 days
											Wind speed (10 MAGL)	Hourly/Daily/ Monthly	6/17/1988	12/31/2008	20 years, 6 months, 14 days	5 years, 4 months, 5 days
Primary data / chosen data																

Table F. 8: Overview over the weather data from the FAGKLIM service at NULS (NMBU) and Bioforsk

Meteorological data from the FAGKLIM service at NULS (NMBU) and Bioforsk																
	2013/2014				2013				Average '96 - '13				Bioforsk '05 - '13			
Month	Glob [W/m^2]	Diff [W/m^2]	Temperature [°C]	Wind [m/s]	Glob [W/m^2]	Diff [W/m^2]	Temperature [°C]	Wind [m/s]	Glob [W/m2]	Diff [W/m2]	Temperature [°C]	Wind [m/s]	Glob [W/m^2]	Diff [W/m^2]	Temperature [°C]	Wind [m/s]
January	7.7	7.2	-2.6	3.0	14.9	11.8	-5.2	2.5	12.7	10.4	-3.3	2.5	16.2	10.1	-3.8	1.7
February	17.6	15.4	1.7	3.4	40.0	30.0	-4.4	2.0	38.6	27.3	-3.1	2.6	41.7	23.3	-4.2	1.6
March	119.3	47.7	-3.6	2.3	119.3	47.7	-3.6	2.3	95.0	49.1	0.1	2.5	101.9	43.8	0.5	1.8
April	162.4	68.4	3.6	3.4	162.4	68.4	3.6	3.4	140.1	73.7	5.4	2.7	156.3	76.0	5.7	2.0
May	169.0	92.3	12.0	3.7	169.0	92.3	12.0	3.7	199.7	91.1	10.6	2.9	207.2	98.7	10.6	2.1
June	227.9	105.1	14.2	4.5	227.9	105.1	14.2	4.5	223.0	100.8	14.3	2.9	240.7	107.2	14.3	1.9
July	236.8	101.8	17.4	4.0	236.8	101.8	17.4	4.0	208.4	97.0	16.6	2.6	209.5	102.6	16.1	1.8
August	174.1	78.3	15.4	4.0	174.1	78.3	15.4	4.0	162.6	78.5	15.9	2.6	163.2	88.6	14.9	1.6
September	106.9	54.9	11.0	3.7	106.9	54.9	11.0	3.7	104.1	52.0	11.6	2.6	108.8	58.6	10.8	1.9
October	46.2	29.4	6.9	4.4	46.2	29.4	6.9	4.4	44.8	27.9	6.0	2.6	49.8	31.0	5.6	1.8
November	22.2	17.2	2.2	4.5	22.2	17.2	2.2	4.5	16.0	12.4	2.0	2.8	18.5	12.7	1.7	1.8
December	7.9	7.9	2.3	4.1	7.9	7.9	2.3	4.1	7.4	6.7	-2.4	2.9	10.4	7.3	-3.2	1.7
Year	108.2	52.1	6.7	3.7	110.6	53.7	6.0	3.6	104.4	52.3	6.1	2.7	110.7	55.1	5.7	1.7

Table F. 9: Monthly average irradiance values calculated from raw data from FAGKLIM , adjusted for diffuse and global measurement errors

Monthly average irradiance data based on different periods - comparison due to irregularities													
1990 - 2013							1996 - 2013						
	Glob [W/m^2]	Avg. dev. [%]	Std. dev. [%]	Diff [W/m^2]	Avg. dev. [%]	Std. dev. [%]		Glob [W/m^2]	Avg. dev. [%]	Std. dev. [%]	Diff [W/m^2]	Avg. dev. [%]	Std. dev. [%]
January	13.0	13.1	16.1	10.7	12.1	16.2	**January**	12.7	12.1	14.9	10.4	9.3	14.5
February	37.7	11.1	15.7	27.0	12.4	15.7	**February**	38.6	9.3	12.6	27.3	11.7	14.9
March	92.5	11.4	14.4	49.7	9.3	12.2	**March**	95.0	10.0	12.8	49.1	9.0	12.8
April	139.4	12.2	14.6	76.1	8.9	12.9	**April**	140.1	14.3	16.4	73.7	7.4	10.5
May	205.2	10.1	11.7	95.1	10.4	14.1	**May**	199.7	10.5	11.8	91.1	8.0	11.1
June	220.2	8.6	11.1	106.6	13.1	20.8	**June**	223.0	7.4	9.9	100.8	7.9	9.5
July	209.9	9.7	11.9	102.0	11.4	15.2	**July**	208.4	9.8	11.7	97.0	8.3	10.4
August	161.2	8.1	12.9	77.1	9.0	15.4	**August**	162.6	6.1	7.1	78.5	6.3	10.5
September	102.9	9.2	11.4	52.9	10.9	13.6	**September**	104.1	8.8	10.9	52.0	10.3	13.8
October	44.1	13.8	17.8	28.0	6.2	7.5	**October**	44.8	15.0	19.5	27.9	6.4	7.8
November	16.1	19.6	23.9	12.6	15.0	18.6	**November**	16.0	19.1	23.3	12.4	12.7	16.5
December	7.7	14.1	21.0	7.0	13.8	19.8	**December**	7.4	11.9	17.7	6.7	12.1	16.7
Year	104.2	3.3	4.3	53.7	6.8	10.0	**Year**	104.4	3.0	4.0	52.3	5.5	8.0

Table F. 10: Comparison of wind speeds for data from FAGKLIM for different periods

Average monthly wind speeds - comparison of time periods due to irregularities						
	1990 - 2013			1996 - 2013		
	Avg.	Avg. dev. [%]	Std. dev. [%]	Avg.	Avg. dev. [%]	Std. dev. [%]
January	2.59	19.7	24.7	2.53	17.8	23.2
February	2.73	21.0	27.1	2.57	18.1	22.7
March	2.76	19.5	26.6	2.54	15.7	18.9
April	2.83	11.6	14.5	2.72	9.9	13.8
May	2.90	9.6	13.8	2.86	9.7	13.4
June	2.85	11.1	16.3	2.85	12.0	17.8
July	2.61	13.0	16.9	2.60	14.0	18.5
August	2.51	16.0	27.0	2.60	15.9	23.0
September	2.58	18.7	26.6	2.63	15.9	18.7
October	2.49	19.2	30.8	2.57	16.8	23.9
November	2.60	22.6	32.0	2.78	17.9	23.2
December	2.63	22.7	32.0	2.85	18.1	22.6
Year	2.67	7.8	12.2	2.7	6.5	10.2

Table F. 11: Comparison of temperatures for data from FAGKLIM for different periods

Temperature 1990 - 2013				1996 - 2013		
	Avg.	Avg. dev. [%]	Std. dev. [%]	Avg.	Avg. dev. [%]	Std. dev. [%]
January	-2.9	69.0	89.5	-3.3	57.6	78.5
February	-2.7	102.7	124.9	-3.1	78.0	96.0
March	0.5	335.6	458.3	0.1	1762.5	2327.4
April	5.4	20.3	23.7	5.4	21.1	24.9
May	10.8	9.8	12.0	10.6	9.7	11.2
June	14.3	6.7	8.4	14.3	6.0	7.0
July	16.6	6.1	7.9	16.6	5.8	7.3
August	15.7	6.9	9.7	15.9	7.2	9.6
September	11.5	8.7	10.4	11.6	8.8	10.7
October	6.0	25.2	31.9	6.0	24.8	30.5
November	1.6	133.6	168.5	2.0	96.8	123.0
December	-2.1	129.8	167.5	-2.4	116.6	146.3
Year	6.2	10.1	14.2	6.2	9.9	14.2

Table F. 12: Comparison of publication irradiance values and raw values for FAGKLIM 2012

2012 Publication data				2012 Raw data and discrepancy from publication values			
From publication	Glob [MJ/m^2]	Diff [MJ/m2]		Raw data	Glob [W/m^2]	Diff [W/m^2]	Corrected Diff [W/m^2]
January	35	25.5		January	12.9	9.2	12.1
February	102.3	64		February	41.6	21.4	28.1
March	277.9	113.5		March	106.6	33.5	43.9
April	319.2	173.2		April	126.6	55.9	73.3
May	592.2	241.7		May	227.5	72.1	94.4
June	539.7	273.6		June	214.3	86.0	112.6
July	475.3	279		July	182.6	85.8	112.4
August	437.1	204.7		August	167.9	60.9	79.7
September	288.8	119.2		September	114.5	37.1	48.6
October	123.1	66.3		October	46.9	20.8	27.3
November	34.3	30.4		November	13.1	10.4	13.6
December	23.3	17.3		December	8.4	5.3	6.9
Year	3248.2	1608.4		Year	105.3	41.5	54.4
Converted to power				**Discrepancy from publication [%]**			
From publication	Glob [W/m2]	Diff [W/m2]		Raw data	Glob	Diff	Corrected diff
January	13.1	9.5		January	-1.2	-3.1	26.9
February	40.8	25.5		February	1.9	-16.2	9.8
March	103.8	42.4		March	2.8	-21.0	3.5
April	123.1	66.8		April	2.8	-16.3	9.7
May	221.1	90.2		May	2.9	-20.1	4.7
June	208.2	105.6		June	2.9	-18.5	6.7
July	177.5	104.2		July	2.9	-17.6	7.9
August	163.2	76.4		August	2.9	-20.4	4.3
September	111.4	46.0		September	2.8	-19.3	5.7
October	46.0	24.8		October	2.1	-15.9	10.2
November	13.2	11.7		November	-0.7	-11.6	15.8
December	8.7	6.5		December	-3.2	-18.5	6.8
Year	102.7	50.9		Year	2.5	-18.3	7.0

Table F. 13: Global irradiance values for all evaluated sources

Global irradiance values all evaluated sources [W/m^2]							
	2013/2014	2013	Average '96 - '13	Bioforsk	NASA SSE	Meteonorm	PVGIS
January	7.7	14.9	12.7	16.2	16.3	11.0	11.4
February	17.6	40.0	38.6	41.7	45.4	33.0	33.9
Mars	119.3	119.3	95.0	101.9	96.3	90.0	74.6
April	162.4	162.4	140.1	156.3	154.2	157.0	135.0
Mai	169.0	169.0	199.7	207.2	221.7	212.0	192.5
June	227.9	227.9	223.0	240.7	230.8	236.0	219.2
July	236.8	236.8	208.4	209.5	229.6	219.0	201.7
August	174.1	174.1	162.6	163.2	176.3	149.0	151.3
September	106.9	106.9	104.1	108.8	115.0	110.0	95.0
October	46.2	46.2	44.8	49.8	54.2	46.0	43.8
November	22.2	22.2	16.0	18.5	22.5	14.0	16.8
December	7.9	7.9	7.4	10.4	10.0	7.0	8.1
Year	108.2	110.6	104.4	110.7	114.3	107.0	98.8

Table F. 14: Discrepancy in global irradiance from reference year 2013/2014

Discrepancy from reference year 2013/2014 [%]							
	2013/2014	2013	Average '96 - '13	Bioforsk	NASA SSE	Meteonorm	PVGIS
January	0	93.1	64.3	110.4	111.0	42.8	48.2
February	0	127.6	119.6	137.1	158.4	87.8	92.7
Mars	0	0.0	-20.4	-14.6	-19.3	-24.6	-37.5
April	0	0.0	-13.8	-3.8	-5.1	-3.4	-16.9
Mai	0	0.0	18.2	22.6	31.2	25.5	13.9
June	0	0.0	-2.2	5.6	1.3	3.5	-3.9
July	0	0.0	-12.0	-11.5	-3.0	-7.5	-14.8
August	0	0.0	-6.6	-6.2	1.3	-14.4	-13.1
September	0	0.0	-2.6	1.8	7.6	2.9	-11.1
October	0	0.0	-3.0	7.8	17.3	-0.4	-5.2
November	0	0.0	-28.1	-16.7	1.2	-37.0	-24.3
December	0	0.0	-5.8	32.6	27.3	-10.9	3.5
Year	0	2.3	-3.5	2.3	5.7	-1.1	-8.7

Table F. 15: Relative share of yearly irradiation per month

Relative share of yearly radiation [%]							
	2013/2014	2013	Average '96 - '13	Bioforsk	NASA SSE	Meteonorm	PVGIS
January	0.6	1.1	1.0	1.2	1.2	0.9	1.0
February	1.2	2.8	2.8	2.9	3.0	2.4	2.6
Mars	9.4	9.2	7.7	7.8	7.1	7.1	6.4
April	12.3	12.1	11.0	11.6	11.1	12.1	11.2
Mai	13.3	13.0	16.3	15.9	16.5	16.8	16.6
June	17.3	16.9	17.6	17.9	16.6	18.1	18.2
July	18.6	18.2	17.0	16.1	17.1	17.4	17.3
August	13.7	13.4	13.2	12.5	13.1	11.8	13.0
September	8.1	7.9	8.2	8.1	8.3	8.4	7.9
October	3.6	3.5	3.6	3.8	4.0	3.7	3.8
November	1.7	1.7	1.3	1.4	1.6	1.1	1.4
December	0.6	0.6	0.6	0.8	0.7	0.6	0.7
Year	100.0	100.0	100.0	100.0	100.0	100.0	100.0

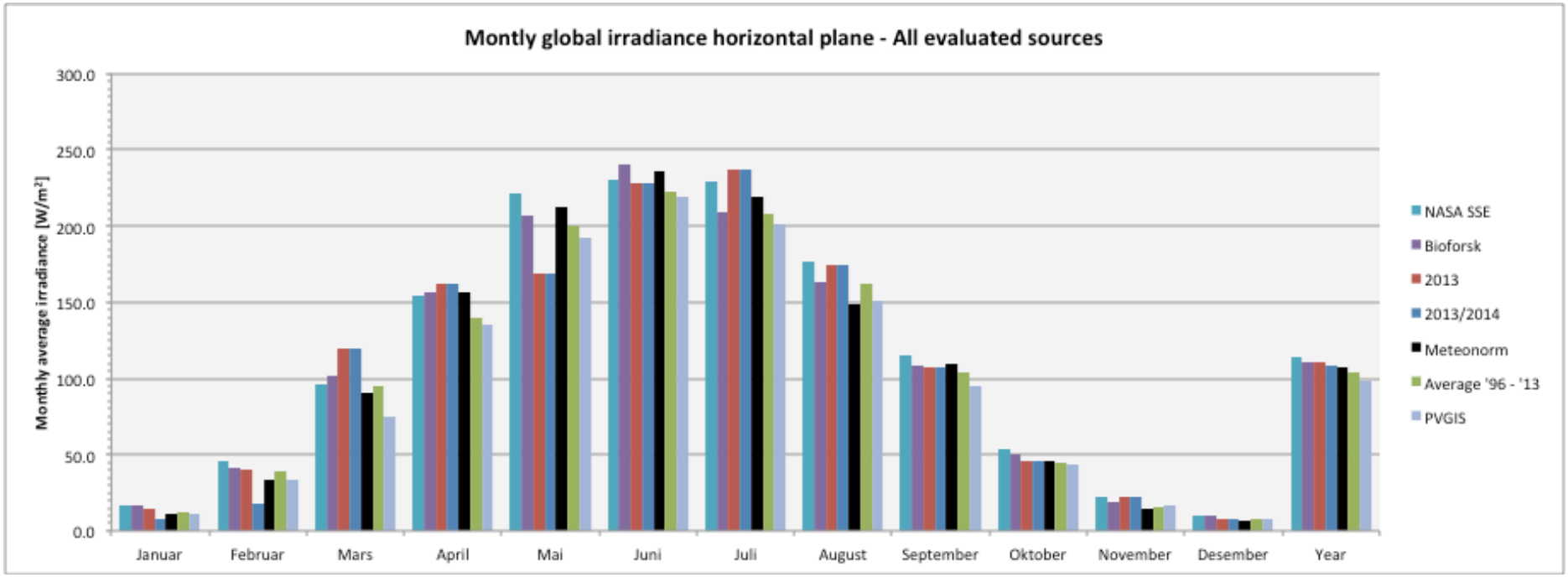

Figure F. 1: Monthly distribution of global irradiance on the horizontal plane for all sources evaluated

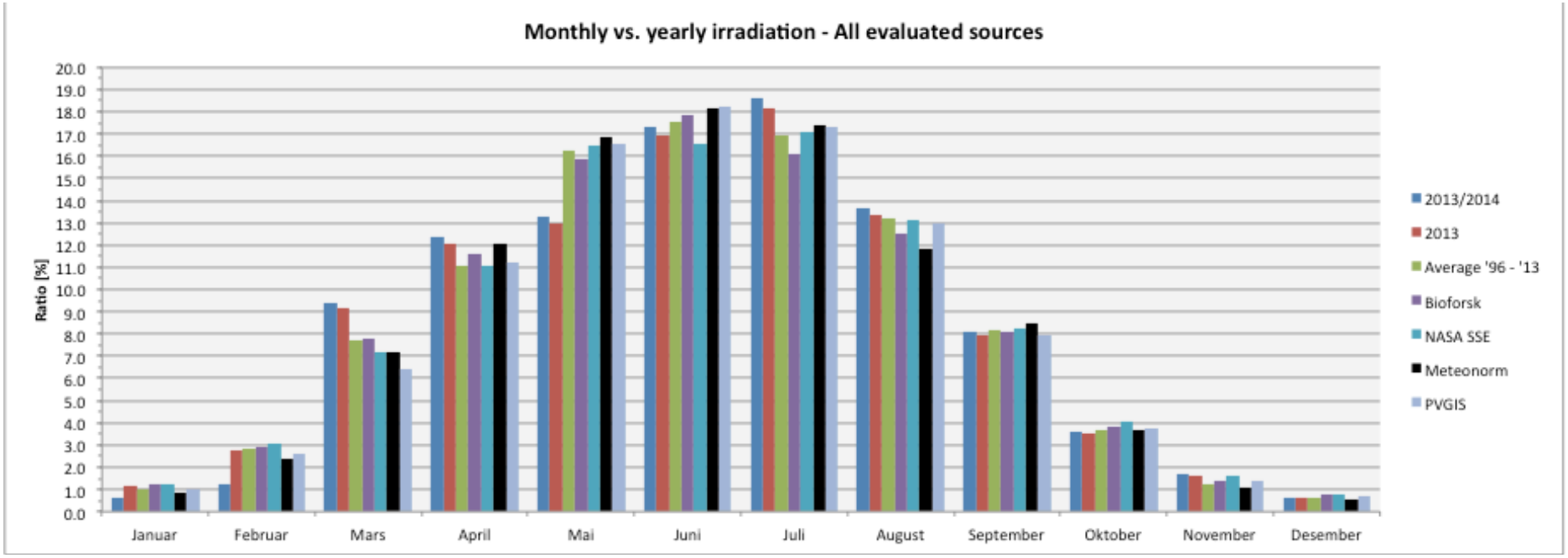

Figure F. 2: Monthly distribution of the yearly incoming irradiation relative to the yearly sum

Appendix G: Simulated production data

This appendix contains all values from the simulations in PVsyst.
The data is ordered in sub-appendices, their contents are:

Appendix G.1: Simulation settings
Appendix G.2: Simulated annual irradiance, yield and PR
Appendix G.3: Simulated annual irradiance, yield and PR – Excluding January and February
Appendix G.4: Simulated yield and PR, adjusted for positive mismatch
Appendix G.5: Simulated yield and PR, adjusted for positive mismatch - Excluding January and February
Appendix G.6: Simulated monthly yield - All sources
Appendix G.7: Simulated losses – Tabular presentation of values from reports
Appendix G.8: Graphical presentation of simulated data
Appendix G.9: Simulation tests and synthetic data

Appendix G.1: Simulation settings

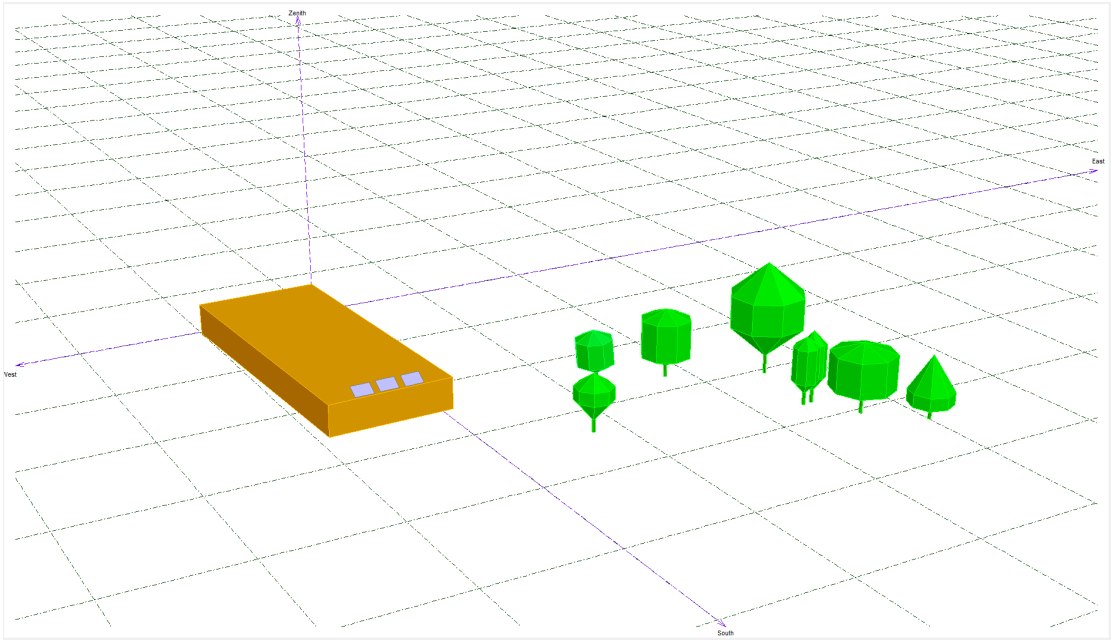

Figure G. 1: Simplified near shading 3D model of the PV-system site at Aas

Table G. 1: Shading elements used in the near shading 3D model constructions

Shading elements								
Building no.	Name	Object type	Length L [m]	Width [m]	Height [m]	MSL [m]	MGD [m]	Azimuth [°]
1	Aud max 1	Building	52.8	28.6	9.4	96.4	-0.8	-95
2	Aud max 2	Roof object	20	9.5	9.1	105.8	8.6	-5
3	Samfunnet 1	Building	26	14	11.6	99	1.8	-95
4	Samfunnet 2	Building	17.8	17.8	7.7	99	1.8	-95
5	Samfunnet 3 & 4	Roof object	12	2.6	1.5	106.7	9.5	-5
6	TF1.0	Building	67.2	6.2	11.3	96.4	-0.8	-92
6	TF1.1	Building	60	5.6	11.3	96.4	-0.8	-92
7	TF1.3	Building	13.4	5.6	13.1	96.4	-0.8	-92
8	TF1.4	Roof object	10.9	5.4	2	107.7	10.5	-92
9	TF2	Building	50.2	15.9	10.8	96.2	-1	-2
10	TF3.0	Building	40	15.8	6.5	96.4	-0.8	-2
11	TF3.1	Roof object	5	1.5	1.5	102.9	5.7	-92
12	TF4	Building	49.5	20	5.3	97.2	0	-2
13	TF1.2	Building	45.3	16.6	9.2	97.5	0.3	-2
14	TF3.2	Roof object	8.2	5.4	2.7	106.7	9.5	-2
15	TF3.3	Roof object	8.2	5.4	2.7	106.7	9.5	-2
16	TF3.4	Roof object	8.5	10.3	2.8	106.7	9.5	-2

PVSYST V6.19		31/03/14 11h06

:

Horizon Aas

File aas_Project.VC3 of 28/03/14 15h33

Geographical Site	**Ås**		Country	**Norway**	
Situation		Latitude	59.7°N	Longitude	10.8°E
Time defined as		Legal Time	Time zone UT+1	Altitude	287 m
Horizon		Average Height	6.5°	Diffuse Factor	0.96
		Albedo Factor	100 %	Albedo Fraction	0.69

Height [°]	0.0	7.0	7.0	0.0	7.0	7.0	0.0	0.0	7.0	0.0	0.0	13.0	13.0	11.0
Azimuth [°]	-47	-47	-44	-44	-40	-28	-28	-26	-26	-22	-20	-20	-15	-15
Height [°]	11.0	0.0	0.0	9.0	9.0	11.0	11.0	0.0	0.0	7.5	9.2	7.5	0.0	0.0
Azimuth [°]	-9	-9	-9	-8	-7	-7	-4	-4	-0	0	0	4	4	7
Height [°]	7.0	7.0	7.5	7.5	6.0	6.0	7.5	7.5	7.0	7.5	6.0	7.5	5.5	7.0
Azimuth [°]	7	10	10	12	12	14	14	17	17	18	21	22	24	25
Height [°]	7.0	5.5	7.0	6.5	6.0	6.5	6.0	7.5	7.0	7.0	7.5	5.5	5.5	7.5
Azimuth [°]	29	30	30	43	43	70	75	75	76	77	80	81	85	90

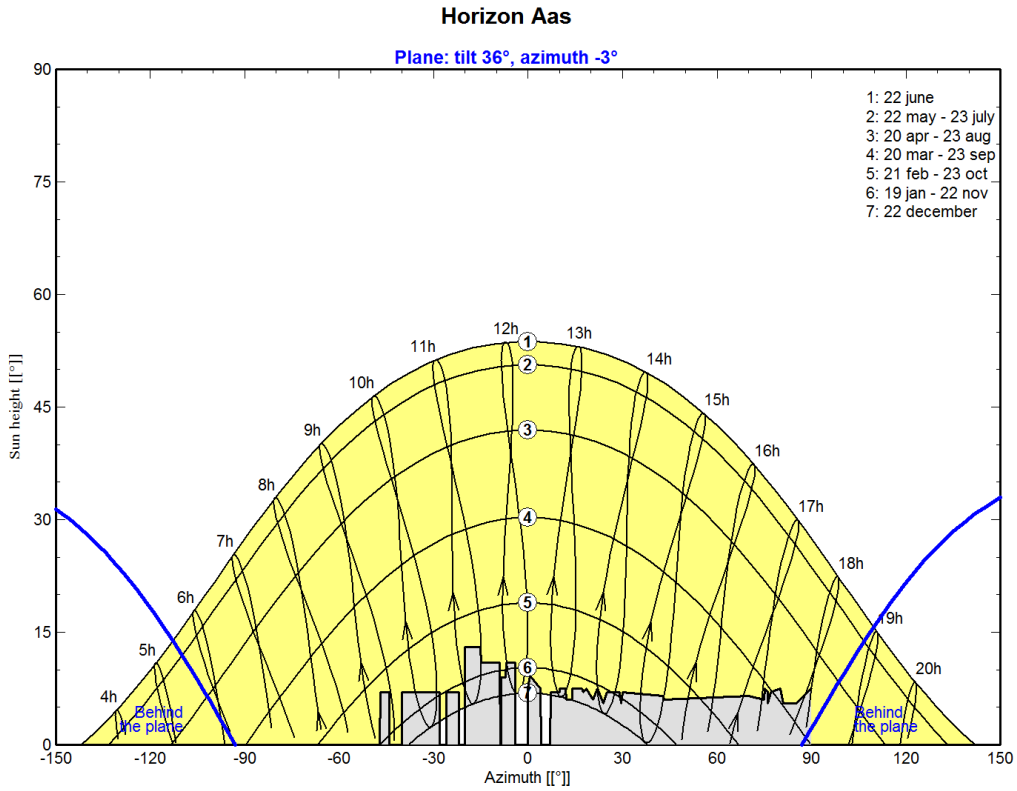

Figure G. 2: Horizon profile for Aas including azimuth notation.

The above figure can be compared to Figure E. 3 (Appendix E: Location specifics: Aas).

Appendix G.2: Simulated annual irradiance, yield and PR

Table G. 2: Annual incident radiation (H), ideal yield (Y_i) and transposition factor R at STC.

Incident radiation and ideal yield at STC							
	2013/2014	2013	1996 - 2013	Bioforsk	NASA	Metenorm	PVGIS
H [kWh/m^2]	952	972	917	970	1005	919	867
R	1.229	1.248	1.228	1.262	1.244	1.210	1.187
H_{inc} [kWh/m^2]	1170	1214	1126	1224	1251	1112	1029
Yi [kWh]	2315	2401	2228	2422	2474	2201	2036

Table G. 3: Forecast vs. yield for all runs and all evaluated sources

Forecast VS Yield [kWh] - All runs, all sources								
	2013/2014	2013	1996 - 2013	Bioforsk	NASA	Metenorm	PVGIS	Actual
1	1889	1967	1808	1987	2031	1774	1634	2034
2	1844	1921	1764	1937	1980	1729	1590	2034
3	1841	1917	1761	1933	2002	1734	1602	2034
4	1527	1537	1459	1554	1624	1460	1336	2034
5	1779	1850	1699	1859	1904	1663	1530	2034

Table G. 4: Calculated system performance ratio for all runs and all sources

Performance ratio - All runs, all sources								
	2013/2014	2013	1996 - 2013	Bioforsk	NASA	Metenorm	PVGIS	Actual
1	0.816	0.819	0.812	0.820	0.821	0.806	0.802	0.879
2	0.797	0.800	0.792	0.800	0.800	0.785	0.781	0.879
3	0.796	0.798	0.790	0.798	0.809	0.788	0.787	0.879
4	0.660	0.640	0.655	0.642	0.656	0.663	0.656	0.879
5	0.768	0.771	0.762	0.768	0.769	0.756	0.751	0.879

Table G. 5. Calculated total system loss due to operation at non-STC conditions

Total losses from STC - All runs, all sources [%]								
	2013/2014	2013	1996 - 2013	Bioforsk	NASA	Metenorm	PVGIS	Actual
1	18.4	18.1	18.8	18.0	17.9	19.4	19.8	12.1
2	20.3	20.0	20.8	20.0	20.0	21.5	21.9	12.1
3	20.4	20.2	21.0	20.2	19.1	21.2	21.3	12.1
4	34.0	36.0	34.5	35.8	34.4	33.7	34.4	12.1
5	23.2	22.9	23.8	23.2	23.1	24.4	24.9	12.1

Table G. 6: Calculated bias error of all runs and all sources plus MBE and RMSE for each run.

Discrepancy from yield [%] - All runs, all sources										
	2013/2014	2013	1996 - 2013	Bioforsk	NASA	Metenorm	PVGIS	Actual	MBE	RMSE
1	-7.1	-3.3	-11.1	-2.3	-0.2	-12.8	-19.7	0.0	-8.1	10.3
2	-9.3	-5.6	-13.3	-4.7	-2.6	-15.0	-21.8	0.0	-10.3	12.1
3	-9.5	-5.7	-13.4	-5.0	-1.6	-14.7	-21.2	0.0	-10.2	11.9
4	-24.9	-24.4	-28.3	-23.6	-20.2	-28.2	-34.3	0.0	-26.3	26.6
5	-12.5	-9.0	-16.5	-8.6	-6.4	-18.2	-24.8	0.0	-13.7	15.0

Table G. 7: Relative increase in discrepancy between runs for all sources and all simulation runs

Relative increase in discrepancy between runs [%] - All runs, all sources								
	2013/2014	2013	1996 - 2013	Bioforsk	NASA	Metenorm	PVGIS	Actual
1	0.0	0.0	0.0	0.0	0.0	0.0	0.0	0.0
2	30.9	69.9	19.6	104.2	1579.8	17.6	11.1	0.0
3	1.3	2.8	1.0	4.6	-40.7	-1.8	-2.7	0.0
4	163.4	326.3	111.0	375.8	1184.8	91.2	61.5	0.0
5	-49.7	-63.0	-41.7	-63.6	-68.3	-35.4	-27.8	0.0

Appendix G.3: Simulated annual irradiance, yield and PR – Excluding January and February

Table G. 8: Incident radiation (H), ideal yield (Y_i) and transposition factor R at STC - ex. Jan. & Feb.

Incident radiation and ideal yield at STC [kWh/m^2] - ex. Jan. & Feb.							
	2013/2014	2013	1996 - 2013	Bioforsk	NASA	Metenorm	PVGIS
H	935	935	882	929	962	887	835
R	1.228	1.225	1.203	1.220	1.209	1.186	1.163
H inc	1147	1145	1061	1134	1163	1051	971
Yi	2270	2266	2099	2244	2302	2080	1922

Table G. 9: Forecast vs. yield for all runs and all evaluated sources – ex. Jan. & Feb.

Forecast VS Yield [kWh] - Excluding Jan. & Feb.								
	2013/2014	2013	1996 - 2013	Bioforsk	NASA	Metenorm	PVGIS	Actual ex. Jan. Feb.
1	1859	1853	1700	1832.9	1883	1675	1539	2009
2	1814	1809	1659	1787.3	1836	1632	1497	2009
3	1812	1806	1657	1784.5	1856	1635	1509	2009
4	1523	1516	1439	1524.9	1596	1443	1319	2009
5	1751	1745	1599	1720.1	1769	1573	1443	2009

Table G. 10: Calculated system performance ratio for all runs and all sources

Performance ratio - All runs, all sources; excluding Jan. & Feb.								
	2013/2014	2013	1996 - 2013	Bioforsk	NASA	Metenorm	PVGIS	Actual
1	0.819	0.818	0.810	0.817	0.818	0.805	0.801	0.885
2	0.799	0.798	0.790	0.797	0.797	0.785	0.779	0.885
3	0.798	0.797	0.789	0.795	0.806	0.786	0.785	0.885
4	0.671	0.669	0.686	0.680	0.693	0.693	0.686	0.885
5	0.771	0.770	0.762	0.767	0.768	0.756	0.751	0.885

Table G. 11: Calculated total system loss due to operation at non-STC conditions

Total losses from STC [%] - All runs, all sources; ex. Jan. & Feb.								
	2013/2014	2013	1996 - 2013	Bioforsk	NASA	Metenorm	PVGIS	Actual
1	18.1	18.2	19.0	18.3	18.2	19.5	19.9	11.5
2	20.1	20.2	21.0	20.3	20.3	21.5	22.1	11.5
3	20.2	20.3	21.1	20.5	19.4	21.4	21.5	11.5
4	32.9	33.1	31.4	32.0	30.7	30.7	31.4	11.5
5	22.9	23.0	23.8	23.3	23.2	24.4	24.9	11.5

Table G. 12: Calculated bias error of all runs and sources, plus MBE and RMSE for each run – excluding January & February.

Discrepancy from yield - Excluding January & February										
	2013/2014	2013	1996 - 2013	Bioforsk	NASA	Metenorm	PVGIS	Actual output ex. Jan. Feb.	MBE	RMSE
1	-7.5	-7.8	-15.4	-8.7	-6.3	-16.6	-23.4	0.0	-12.2	13.6
2	-9.7	-10.0	-17.4	-11.0	-8.6	-18.7	-25.5	0.0	-14.4	15.5
3	-9.8	-10.1	-17.5	-11.2	-7.6	-18.6	-24.9	0.0	-14.2	15.4
4	-24.2	-24.5	-28.3	-24.1	-20.5	-28.2	-34.3	0.0	-26.3	26.6
5	-12.8	-13.1	-20.4	-14.4	-11.9	-21.7	-28.1	0.0	-17.5	18.4

Table G. 13: Relative increase in discrepancy between simulation runs - ex. Jan. and Feb.

Relative increase in discrepancy between runs [%] - All runs, all sources: ex. Jan. & Feb.								
	2013/2014	2013	1996 - 2013	Bioforsk	NASA	Metenorm	PVGIS	Actual
1	0.0	0.0	0.0	0.0	0.0	0.0	0.0	0.0
2	29.4	28.1	13.5	25.9	37.6	12.9	8.9	0.0
3	1.2	1.3	0.5	1.3	-11.7	-0.6	-2.2	0.0
4	147.3	143.3	61.9	115.8	170.4	51.3	37.9	0.0
5	-47.0	-46.4	-28.1	-40.4	-41.9	-23.1	-18.0	0.0

Appendix G.4: Simulated yield and PR, adjusted for positive mismatch

Table G. 14: Forecasted vs. actual yield adjusted for 4% mismatch

Forecast VS Yield [kWh] - All runs, all sources; adjusted for positive mismatch								
	2013/2014	2013	1996 - 2013	Bioforsk	NASA	Metenorm	PVGIS	Actual 2013
1	1967	2049	1884	2069	2115	1848	1702	2034
2	1921	2001	1838	2018	2063	1801	1656	2034
3	1918	1997	1835	2014	2085	1806	1669	2034
4	1591	1601	1520	1619	1692	1521	1392	2034
5	1853	1927	1769	1937	1983	1733	1594	2034

Table G. 15: Forecasted performance ratio when yield has been adjusted for mismatch

Performance ratio - All runs, all sources; adjusted for positive mismatch								
	2013/2014	2013	1996 - 2013	Bioforsk	NASA	Metenorm	PVGIS	Actual
1	0.850	0.853	0.845	0.855	0.855	0.840	0.836	0.879
2	0.830	0.833	0.825	0.833	0.834	0.818	0.813	0.879
3	0.829	0.832	0.823	0.832	0.843	0.821	0.819	0.879
4	0.687	0.667	0.682	0.669	0.684	0.691	0.683	0.879
5	0.801	0.803	0.794	0.800	0.801	0.787	0.783	0.879

Table G. 16: Calculated total system loss from PR, adjusted for positive mismatch

Total losses from STC [%] - All runs, all sources; adjusted for positive mismatch								
	2013/2014	2013	1996 - 2013	Bioforsk	NASA	Metenorm	PVGIS	Actual
1	15.0	14.7	15.5	14.5	14.5	16.0	16.4	12.1
2	17.0	16.7	17.5	16.7	16.6	18.2	18.7	12.1
3	17.1	16.8	17.7	16.8	15.7	17.9	18.1	12.1
4	31.3	33.3	31.8	33.1	31.6	30.9	31.7	12.1
5	19.9	19.7	20.6	20.0	19.9	21.3	21.7	12.1

Table G. 17: Discrepancy from yield for all runs and all sources when adjusted for positive mismatch

Discrepancy from yield [%] - All runs, all sources; adjusted for positive mismatch										
	2013/2014	2013	1996 - 2013	Bioforsk	NASA	Metenorm	PVGIS	Actual 2013	MBE	RMSE
1	-3.3	0.8	-7.4	1.7	4.0	-9.1	-16.3	0.0	-4.2	7.9
2	-5.6	-1.6	-9.6	-0.8	1.4	-11.5	-18.6	0.0	-6.6	9.3
3	-5.7	-1.8	-9.8	-1.0	2.5	-11.2	-18.0	0.0	-6.4	9.2
4	-21.8	-21.3	-25.3	-20.4	-16.8	-25.2	-31.6	0.0	-23.2	23.6
5	-8.9	-5.2	-13.0	-4.8	-2.5	-14.8	-21.6	0.0	-10.1	11.9

Appendix G.5: Simulated yield and PR, adjusted for positive mismatch - Excluding January and February

Table G. 18: Forecasted vs. actual annual yield, all runs and sources - adjusted for positive mismatch

Forecast VS Yield [kWh] - All runs, all sources; adjusted for positive mismatch - Excluding Jan. & Feb.								
	2013/2014	2097	1996 - 2013	Bioforsk	NASA	Metenorm	PVGIS	Actual ex. Jan. Feb.
1	1936	1930	1771	1909	1961	1745	1603	2009
2	1890	1884	1728	1862	1912	1700	1560	2009
3	1888	1881	1726	1859	1933	1703	1572	2009
4	1586	1579	1499	1588	1662	1503	1374	2009
5	1824	1817	1666	1792	1843	1639	1503	2009

Table G. 19: Forecasted vs. actual PR, all runs and sources - adjusted for positive mismatch

Performance ratio - All runs, all sources								
	2013/2014	2013	1996 - 2013	Bioforsk	NASA	Metenorm	PVGIS	Actual
1	0.853	0.852	0.844	0.851	0.852	0.839	0.834	0.868
2	0.833	0.832	0.823	0.830	0.831	0.817	0.812	0.868
3	0.832	0.830	0.822	0.828	0.840	0.818	0.818	0.868
4	0.699	0.697	0.714	0.708	0.722	0.722	0.715	0.868
5	0.804	0.802	0.794	0.799	0.800	0.788	0.782	0.868

Table G. 20: Total system loss calculated from PR - adjusted for positive mismatch

Total losses from STC [%] - All runs, all sources								
	2013/2014	2013	1996 - 2013	Bioforsk	NASA	Metenorm	PVGIS	Actual
1	14.7	14.8	15.6	14.9	14.8	16.1	16.6	13.2
2	16.7	16.8	17.7	17.0	16.9	18.3	18.8	13.2
3	16.8	17.0	17.8	17.2	16.0	18.2	18.2	13.2
4	30.1	30.3	28.6	29.2	27.8	27.8	28.5	13.2
5	19.6	19.8	20.6	20.1	20.0	21.2	21.8	13.2

Table G. 21: Discrepancy from yield for all runs and all sources when adjusted for positive mismatch

Discrepancy from yield [%] - All runs, all sources										
	2013/2014	2013	1996 - 2013	Bioforsk	NASA	Metenorm	PVGIS	Actual 2013	MBE	RMSE
1	-3.6	-3.9	-11.8	-4.9	-2.3	-13.1	-20.2	0.0	-8.6	11.4
2	-5.9	-6.2	-14.0	-7.3	-4.8	-15.4	-22.3	0.0	-10.8	13.4
3	-6.0	-6.3	-14.1	-7.5	-3.7	-15.2	-21.8	0.0	-10.7	13.2
4	-21.0	-21.4	-25.4	-20.9	-17.2	-25.2	-31.6	0.0	-23.2	24.6
5	-9.2	-9.5	-17.1	-10.8	-8.3	-18.4	-25.2	0.0	-14.1	16.2

Appendix G.6: Simulated monthly yield - All sources

Table G. 22: Monthly forecast vs. yield NASA SSE forecasts

Forecast vs. Monthly yield [kWh] - NASA SSE					
Run. No	1	2	3	4	5
January	49.7	48.4	50.6	8.6	43.4
February	97.8	95.8	95.3	19.4	91.5
March	185.1	180.5	189.3	38.6	174.7
April	231.1	225.8	225.7	166.4	218
May	290.2	282.8	282.7	282.7	273.9
June	266.9	259.8	259.8	259.7	251.6
July	280.8	273.7	273.6	273.6	265.1
August	241.1	235.3	235.2	234.9	227.5
September	186	181.9	181.8	180.9	175.2
October	112.1	109.7	109.4	108.5	105.1
November	56.3	54.9	54.4	38.7	51.7
December	33.4	31.4	44.1	11.9	26.2
Year	2030.6	1980	2001.9	1623.9	1903.8
Year ex. Jan. & Feb.	1883	1835.8	1856	1595.9	1769

Table G. 23 : Forecast discrepancy from actual monthly yield, NASA SSE

Discrepancy from actual monthly yield [%] - NASA SSE							
Run. No	1	2	3	4	5	MBE	RMSE
January	1488.4	1446.8	1517.1	174.8	1287.0	1182.8	1288.2
February	343.6	334.5	332.3	-12.0	315.0	262.7	296.6
March	-28.9	-30.7	-27.3	-85.2	-32.9	-41.0	46.6
April	-10.8	-12.8	-12.9	-35.8	-15.8	-17.6	19.9
May	29.1	25.8	25.8	25.8	21.9	25.7	25.8
June	-5.2	-7.7	-7.7	-7.8	-10.7	-7.8	8.0
July	-12.1	-14.3	-14.3	-14.3	-17.0	-14.4	14.5
August	-6.4	-8.6	-8.7	-8.8	-11.7	-8.8	9.0
September	-3.2	-5.3	-5.4	-5.8	-8.8	-5.7	6.0
October	-0.2	-2.3	-2.6	-3.4	-6.4	-3.0	3.6
November	-21.9	-23.8	-24.5	-46.3	-28.3	-29.0	30.3
December	13.8	7.0	50.3	-59.4	-10.7	0.2	35.8
Year	-0.2	-2.6	-1.6	-20.2	-6.4	-6.2	9.6
Year ex. Jan. & Feb.	-6.3	-8.6	-7.6	-20.5	-11.9	-11.0	12.1
Monthly avg.	148.9	142.4	151.8	-6.5	123.5	112.0	148.7
Monthly avg. Ex. Jan. & Feb.	-4.6	-7.3	-2.7	-24.1	-12.0	-10.1	20.0

Table G. 24: Monthly forecast vs. actual yield Meteonorm

Forecast vs. Monthly yield [kWh] - Meteonorm					
Run. No	1	2	3	4	5
January	29.5	28.3	29.2	4.7	25.5
February	69.7	68	70.4	13.2	64.7
March	145.5	141.3	144.4	29.5	136.7
April	198.8	193.7	193.7	142.2	187
May	268.7	261.8	261.7	261.7	253.5
June	260.1	253.4	253.3	253.2	245.3
July	257.3	250.7	250.6	250.5	242.7
August	221.1	215.7	215.7	215.3	208.5
September	166.2	162.5	162.4	161.5	156.4
October	98.8	96.8	96.1	95.5	92.4
November	39.4	38.2	37.3	26.5	35.4
December	19.1	18	19.3	6.6	15.3
Year	1774.2	1728.5	1733.9	1460.4	1663.4
Year ex. Jan. & Feb.	1675	1632.1	1634.5	1442.5	1573.2

Table G. 25: Forecast discrepancy from actual monthly yield, Meteonorm data

Discrepancy from monthly yield [%] - Meteonorm							
Run. No	1	2	3	4	5	MBE	RMSE
January	842.8	804.4	833.2	50.2	715.0	649.1	716.3
February	216.2	208.4	219.3	-40.1	193.5	159.5	188.3
March	-44.1	-45.7	-44.5	-88.7	-47.5	-54.1	56.8
April	-23.3	-25.2	-25.2	-45.1	-27.8	-29.3	30.4
May	19.6	16.5	16.4	16.4	12.8	16.3	16.5
June	-7.6	-10.0	-10.1	-10.1	-12.9	-10.1	10.3
July	-19.4	-21.5	-21.5	-21.6	-24.0	-21.6	21.7
August	-14.2	-16.3	-16.3	-16.4	-19.1	-16.4	16.5
September	-13.5	-15.4	-15.5	-15.9	-18.6	-15.8	15.9
October	-12.0	-13.8	-14.5	-15.0	-17.7	-14.6	14.7
November	-45.3	-47.0	-48.2	-63.2	-50.9	-50.9	51.3
December	-34.9	-38.6	-34.2	-77.5	-47.9	-46.6	49.4
Year	-12.8	-15.0	-14.7	-28.2	-18.2	-17.8	18.6
Year ex. Jan. & Feb.	-16.6	-18.7	-18.6	-28.2	-21.7	-20.8	21.2
Monthly avg.	72.0	66.3	69.9	-27.2	54.6	47.1	99.0
Monthly avg. Ex. Jan. & Feb.	-19.5	-21.7	-21.4	-33.7	-25.4	-24.3	28.3

Table G. 26: Monthly forecast vs. actual yield PVGIS

Forecast vs. Monthly yield [kWh] - PVGIS					
Run. No	1	2	3	4	5
January	28.9	27.8	29.0	4.6	25.2
February	66	64.4	64.0	12.5	61.5
March	130.1	126.3	132.3	25.5	122.2
April	189.4	184.5	187.0	135.5	178.3
May	247.2	240.7	240.6	240.6	233
June	247.8	240.9	240.8	240.8	233.2
July	239	232.4	232.3	232.3	224.9
August	198.2	193.2	193.1	192.9	186.8
September	145.2	141.7	141.7	140.9	136.4
October	78	76.2	76.0	75.5	73
November	38.4	37.3	36.7	25.9	34.8
December	25.7	24.2	28.2	9.2	20.7
Year	1634.1	1589.7	1601.8	1336	1530
Year ex. Jan. & Feb.	1539	1497.4	1508.7	1319.1	1443.3

Table G. 27. : Forecast discrepancy from actual monthly yield, PVGIS data

Discrepancy from yield [%]							
Run. No	1	2	3	4	5	MBE	RMSE
January	823.6	788.5	826.8	47.0	705.4	638.3	704.8
February	199.4	192.1	190.3	-43.3	179.0	143.5	171.3
March	-50.0	-51.5	-49.2	-90.2	-53.1	-58.8	60.9
April	-26.9	-28.8	-27.8	-47.7	-31.2	-32.5	33.4
May	10.0	7.1	7.0	7.0	3.7	7.0	7.2
June	-12.0	-14.5	-14.5	-14.5	-17.2	-14.5	14.6
July	-25.2	-27.2	-27.3	-27.3	-29.6	-27.3	27.3
August	-23.1	-25.0	-25.0	-25.1	-27.5	-25.1	25.2
September	-24.4	-26.2	-26.2	-26.7	-29.0	-26.5	26.6
October	-30.6	-32.2	-32.3	-32.8	-35.0	-32.6	32.6
November	-46.7	-48.2	-49.1	-64.1	-51.7	-52.0	52.3
December	-12.4	-17.5	-3.9	-68.6	-29.4	-26.4	34.8
Year	-19.7	-21.8	-21.2	-34.3	-24.8	-24.4	24.9
Year ex. Jan. & Feb.	-23.4	-25.5	-24.9	-34.3	-28.1	-27.2	27.5
Monthly avg.	65.1	59.7	64.1	-32.2	48.7	41.1	99.3
Monthly avg. Ex. Jan. & Feb.	-24.1	-26.4	-24.8	-39.0	-30.0	-28.9	31.5

Table G. 28: Monthly forecast vs. actual yield average 1996 - 2013 from FAGKLIM

Forecast vs. Monthly yield [kWh]- - Average 1996 - 2013					
Run. No	1	2	3	4	5
January	30.9	29.8	29.2	4.8	26.7
February	77.4	75.7	75.1	15.1	72.2
March	185.5	180.7	180.2	38.7	174.8
April	206.8	202	201.9	148.6	195
May	263.9	257.5	257.4	257.4	249.3
June	255.5	248.9	248.8	248.8	241
July	254.5	248.3	248.2	248.2	240.4
August	222.8	217.4	217.4	217.2	210.3
September	166.6	162.9	162.9	161.9	156.7
October	89.8	87.7	87.1	86.9	84
November	38.2	37.3	37.1	25.7	34.5
December	16.6	16	16	5.8	13.4
Year	1808.4	1764.2	1761.4	1458.9	1698.5
Year ex. Jan. & Feb.	1700.2	1658.7	1657	1439.2	1599.4
Monthly avg.	150.7	147.0	146.8	121.6	141.5
Monthly avg. Ex. Jan. & Feb.	170.0	165.9	165.7	143.9	159.9

Table G. 29: Forecast discrepancy from actual monthly yield, average 1996 - 2013 from FAGKLIM

Discrepancy from monthly yield [%] - average 1996 - 2013							
Run. No	1	2	3	4	5	MBE	RMSE
January	887.5	852.4	833.2	53.4	753.3	676.0	745.5
February	251.1	243.4	240.7	-31.5	227.5	186.2	215.8
March	-28.8	-30.6	-30.8	-85.1	-32.9	-41.6	47.0
April	-20.2	-22.0	-22.1	-42.6	-24.7	-26.3	27.6
May	17.4	14.6	14.5	14.5	10.9	14.4	14.5
June	-9.3	-11.6	-11.6	-11.6	-14.4	-11.7	11.8
July	-20.3	-22.3	-22.3	-22.3	-24.7	-22.4	22.4
August	-13.5	-15.6	-15.6	-15.7	-18.4	-15.7	15.8
September	-13.3	-15.2	-15.2	-15.7	-18.4	-15.6	15.7
October	-20.1	-21.9	-22.5	-22.6	-25.2	-22.5	22.5
November	-47.0	-48.2	-48.5	-64.3	-52.1	-52.0	52.4
December	-43.4	-45.5	-45.5	-80.2	-54.3	-53.8	55.5
Year	-11.1	-13.3	-13.4	-28.3	-16.5	-16.5	17.6
Year ex. Jan. & Feb.	-15.4	-17.4	-17.5	-28.3	-20.4	-19.8	20.3
Monthly avg.	78.4	73.1	71.2	-27.0	60.5	51.2	103.9
Monthly avg. Ex. Jan. & Feb.	-19.8	-21.8	-22.0	-34.6	-25.4	-24.7	28.5

Table G. 30: Forecasted vs. actual monthly yield, RY data from FAGKLIM

Forecast vs. Monthly yield [kWh]- Measured values 2013/2014					
Run. No	1	2	3	4	5
January	10.5	10.1	10.1	1.5	9.3
February	19.9	19.2	19.2	2.8	18.3
March	262.5	256.3	255.1	56.9	248.2
April	252	246.7	246.6	181.8	238
May	209.7	203.8	203.7	203.7	197.2
June	266.4	259.5	259.4	259.4	251.3
July	290.9	283.9	283.9	283.8	275
August	238.9	233.5	233.4	233.1	225.8
September	178	174.4	174.3	173.3	167.9
October	91.8	89.9	89.7	88.8	86
November	52.6	51.2	50.8	36.3	48.4
December	15.7	15.2	15.2	5.5	13.3
Year	1888.7	1843.8	1841.4	1527.1	1778.7
Year ex. Jan. & Feb.	1858.5	1814.4	1812.1	1522.6	1751.1

Table G. 31: Forecast discrepancy from actual monthly yield, RY data from FAGKLIM

Discrepancy from monthly yield [%] - 2013/2014							
Run. No	1	2	3	4	5	MBE	RMSE
January	235.6	222.8	222.8	-52.1	197.2	165.3	198.2
February	-9.7	-12.9	-12.9	-87.3	-17.0	-28.0	40.8
March	0.8	-1.6	-2.0	-78.1	-4.7	-17.1	35.0
April	-2.7	-4.8	-4.8	-29.8	-8.1	-10.0	14.2
May	-6.7	-9.3	-9.4	-9.4	-12.3	-9.4	9.6
June	-5.4	-7.8	-7.9	-7.9	-10.8	-8.0	8.1
July	-8.9	-11.1	-11.1	-11.2	-13.9	-11.2	11.4
August	-7.2	-9.3	-9.4	-9.5	-12.3	-9.6	9.7
September	-7.4	-9.2	-9.3	-9.8	-12.6	-9.7	9.8
October	-18.3	-20.0	-20.1	-21.0	-23.4	-20.6	20.6
November	-27.0	-29.0	-29.5	-49.6	-32.8	-33.6	34.6
December	-46.5	-48.2	-48.2	-81.3	-54.7	-55.8	57.3
Year	-7.1	-9.3	-9.5	-24.9	-12.5	-12.7	14.2
Year ex. Jan. & Feb.	-7.5	-9.7	-9.8	-24.2	-12.8	-12.8	14.1
Monthly avg.	8.0	5.0	4.8	-37.2	-0.4	-4.0	37.4
Monthly avg. Ex. Jan. & Feb.	-12.9	-15.0	-15.2	-30.8	-18.6	-18.5	21.0

Table G. 32: forecasted vs. actual monthly yield, Measured 2013 data from FAGKLIM

Forecast vs. actual Yield - Measured values 2013					
Run. No	1	2	3	4	5
January	38.9	37.8	37.3	6.5	34.8
February	75.7	73.9	73.8	14.5	70.8
March	261.7	256.1	255.1	56.8	247.9
April	252.9	247.8	247.7	182.6	238.9
May	211	205.1	205	205	198.5
June	267.1	260.2	260.1	260.1	251.9
July	292.5	285.4	285.3	285.3	276.4
August	237.4	232	231.9	231.6	224.4
September	169.3	165.6	165.5	164.3	159.1
October	91.6	89.3	88.5	88	85.1
November	53.8	52.5	52.4	36.9	49.3
December	15.2	14.7	14.7	5.6	13.1
Year	1967.1	1920.5	1917.3	1537.2	1850.2
Year ex. Jan. & Feb.	1852.5	1808.7	1806.2	1516.2	1744.6

Table G. 33: Forecast discrepancy from actual monthly yield, Measured 2013 data from FAGKLIM

Discrepancy from monthly yield [%] - Measure values 2013							
Run. No	1	2	3	4	5	MBE	RMSE
January	1143.2	1108.1	1092.1	107.7	1012.2	892.6	976.1
February	243.4	235.2	234.8	-34.2	221.1	180.1	209.6
March	0.5	-1.6	-2.0	-78.2	-4.8	-17.2	35.1
April	-2.4	-4.3	-4.4	-29.5	-7.8	-9.7	14.0
May	-6.1	-8.7	-8.8	-8.8	-11.7	-8.8	9.0
June	-5.2	-7.6	-7.6	-7.6	-10.5	-7.7	7.9
July	-8.4	-10.7	-10.7	-10.7	-13.5	-10.8	10.9
August	-7.8	-9.9	-10.0	-10.1	-12.9	-10.1	10.3
September	-11.9	-13.8	-13.9	-14.5	-17.2	-14.2	14.3
October	-18.5	-20.5	-21.2	-21.7	-24.2	-21.2	21.3
November	-25.3	-27.1	-27.3	-48.8	-31.6	-32.0	33.2
December	-48.2	-49.9	-49.9	-80.9	-55.3	-56.8	58.2
Year	-3.3	-5.6	-5.7	-24.4	-9.0	-9.6	12.3
Year ex. Jan. & Feb.	-7.8	-10.0	-10.1	-24.5	-13.1	-13.1	14.4
Monthly avg.	104.4	99.1	97.6	-19.8	87.0	73.7	116.6
Monthly avg. Ex. Jan. & Feb.	-13.3	-15.4	-15.6	-31.1	-19.0	-18.9	21.4

Appendix G.7: Simulated losses – Tabular presentation of values from reports

Table G. 34: Losses of forecasts based on measured data

2013/2014							2013					
Run	1	2	3	4	5		**Run**	1	2	3	4	5
Transposition	22.9	22.9	22.9	22.9	22.9		**Transposition**	24.8	24.8	24.8	24.8	24.8
Near shading	0	-2.5	-2.6	-2.9	-2.9		**Near shading**	0	-2.5	-2.5	-3	-3
IAM	-3.2	-2.9	-2.9	-2.9	-2.9		**IAM**	-3.1	-2.9	-2.9	-2.9	-2.9
Soiling	0	0	0	-15.2	-3		**Soiling**	0	0	0	-17.5	-3
Optical loss	-3.2	-5.4	-5.5	-21	-8.8		**Optical loss**	-3.1	-5.4	-5.4	-23.4	-8.9
Irradiance	-7.8	-8	-8	-8.9	-8.3		**Irradiance**	-8	-8.1	-8.1	-9.2	-8.4
Module quality/LID	-2	-2	-2	-2	-2		**Module quality/LID**	-2	-2	-2	-2	-2
Module layout	0	0	0	0	0		**Module layout**	0	0	-0.1	0	0
Temperature	-0.9	-0.8	-0.8	-1.4	-0.6		**Temperature**	-0.5	-0.4	-0.4	-1.2	-0.2
Ohmic	-0.9	-0.9	-0.9	-0.8	-0.9		**Ohmic**	-0.9	-0.9	-0.9	-0.8	-0.8
Inverter	-4.7	-4.7	-4.8	-5	-4.9		**Inverter**	-4.6	-4.7	-4.7	-5.2	-4.7
System loss	-16.3	-16.4	-16.5	-18.1	-16.7		**System loss**	-16	-16.1	-16.2	-18.4	-16.1
PR	81.0	79.1	78.9	64.7	76.0		**PR**	81.4	79.4	79.3	62.5	76.4
ΔPR	-0.6	-0.6	-0.7	-1.3	-0.9		**ΔPR**	-0.5	-0.6	-0.6	-1.5	-0.6
Average 1996 - 2013							**Bioforsk 2005 - 2013**					
Run	1	2	3	4	5		**Run**	1	2	3	4	5
Transposition	22.8	22.8	22.8	22.8	22.8		**Transposition**	26.2	26.2	26.2	26.2	26.2
Near shading	0	-2.6	-2.6	-3.1	-3.1		**Near shading**	0	-2.6	-2.6	-3.4	-3.4
IAM	-3.2	-2.9	-2.9	-2.9	-2.9		**IAM**	-3.1	-2.9	-2.9	-2.9	-2.9
Soiling	0	0	0	-15.2	-3		**Soiling**	0	0	0	-17.3	-3
Optical loss	-3.2	-5.5	-5.5	-21.2	-9		**Optical loss**	-3.1	-5.5	-5.5	-23.6	-9.3
Irradiance	-8.3	-8.5	-8.5	-9.2	-8.8		**Irradiance**	-8.2	-8.4	-8.4	-9.3	-8.7
Module quality/LID	-2	-2	-2	-2	-2		**Module quality/LID**	-2	-2	-2	-2	-2
Module layout	0	0	0	0	0		**Module layout**	0	0	-0.2	0	0
Temperature	-0.8	-0.7	-0.7	-1.4	-0.5		**Temperature**	-0.1	0	0	-0.8	0.1
Ohmic	-0.9	-0.9	-0.9	-0.8	-0.8		**Ohmic**	-0.8	-0.8	-0.8	-0.8	-0.8
Inverter	-4.8	-4.9	-4.9	-5.2	-5		**Inverter**	-4.6	-4.7	-4.7	-5.1	-4.7
Total system loss	-16.8	-17	-17	-18.6	-17.1		**Total system loss**	-15.7	-15.9	-16.1	-18	-16.1
PR	80.5	78.4	78.4	64.1	75.4		**PR**	81.7	79.5	79.3	62.6	76.1
ΔPR	-0.6	-0.7	-0.6	-1.3	-0.8		**ΔPR**	-0.4	-0.5	-0.5	-1.5	-0.7

Table G. 35: Losses of forecasts based on databases

NASA SSE							PVGIS					
Run	1	2	3	4	5		Run	1	2	3	4	5
Transposition	24.4	24.4	24.4	24.4	24.4		Transposition	18.8	18.8	18.8	18.8	18.8
Near shading	0.0	-2.6	-2.6	-3.2	-3.2		Near shading	0.0	-2.8	-2.8	-3.3	-3.3
IAM	-3.1	-3.0	-3.0	-2.9	-2.9		IAM	-3.3	-3.1	-3.0	-3.0	-3.0
Soiling	0.0	0.0	0.0	-15.8	-3.0		Soiling	0.0	0.0	0.0	-13.9	-3.0
Optical loss	-3.1	-5.6	-5.6	-21.9	-9.1		**Optical loss**	-3.3	-5.9	-5.8	-20.2	-9.3
Irradiance	-7.9	-8.1	-8.1	-8.8	-8.4		Irradiance	-9.1	-9.2	-9.2	-9.8	-9.6
Module quality/LID	-2.0	-2.0	-2.0	-2.0	-2.0		Module quality/LID	-2.0	-2.0	-2.0	-2.0	-2.0
Module layout	0.0	0.0	-0.1	0.0	0.0		Module layout	0	0	-0.2	0	0
Temperature	-0.4	-0.3	-0.3	-1.1	-0.2		Temperature	-0.7	-0.6	-0.6	-1.4	-0.5
Ohmic	-0.9	-0.9	-0.9	-0.9	-0.8		Ohmic	-0.8	-0.8	-0.8	-0.8	-0.8
Inverter	-4.6	-4.6	-3.4	-5.0	-4.7		Inverter	-5.1	-5.2	-4.2	-5.6	-5.2
Total system loss	-15.8	-15.9	-14.8	-17.8	-16.1		**Total system loss**	-17.7	-17.8	-17.0	-19.6	-18.1
PR	81.0	79.1	78.9	64.7	76.0		PR	81.0	79.1	78.9	64.7	76.0
ΔPR	-1.1	-0.9	-2.0	-0.9	-0.9		ΔPR	0.8	1.0	0.2	-0.9	0.9

Meteonorm					
Run	1	2	3	4	5
Transposition	21.0	21.0	21.0	21.0	21.0
Near shading	0.0	-2.7	-2.7	-3.3	-3.3
IAM	-3.3	-3.0	-3.0	-3.0	-3.0
Soiling	0.0	0.0	0.0	-13.7	-3.0
Optical loss	-3.3	-5.7	-5.7	-20.0	-9.3
Irradiance	-8.6	-8.7	-8.7	-9.3	-9.0
Module quality/LID	-2.0	-2.0	-2.0	-2.0	-2.0
Module layout	0	0	-0.2	0	0
Temperature	-1.1	-1.0	-1.0	-1.6	-0.8
Ohmic	-0.8	-0.8	-0.8	-0.8	-0.8
Inverter	-4.9	-5.0	-4.4	-5.2	-5.0
Total system loss	-17.4	-17.5	-17.1	-18.9	-17.6
PR	81.0	79.1	78.9	64.7	76.0
ΔPR	0.4	0.6	0.1	-1.6	0.4

Appendix G.8: Graphical presentation of simulated data

This appendix presents the graphical appearance of simulated data.
An example of a report from PVsyst is shown on the next page. It shows the forecast from the combined far/near-shading scenario in order to illustrate all parts that may bee seen in a report. Some reports may have fewer elements than this report, and others may have more, depending on the amount of information wanted by the user. The shortest report usually consists of four pages.

Because seven sources were used, with each five runs, in addition to the combined scenario shown here, the total number of reports would be 40.
This generally means that at least 160 report pages could be expected, which is the reason why only one is shown here.

The first report page shows which synthetic file the user has chosen, the location coordinates and name, along with chosen variant and date.
If a general albedo value is applied, then this is shown, if another is applied or the values are specified monthly, then these are shown.

Otherwise the chosen system configuration and components are listed, along with current, voltage and power characteristics.
In addition, the chosen detailed loss factors are listed, along with the loss they induce in the forecast.

The second page shows the sun path including horizon profile for the project site, along with the values for sun height and azimuth specified by the user.
This page is omitted if no horizon is applied, and only near shading is used.

The third page shows the near shading 3D model, along with an iso-shadings diagram that gives the user an idea of how the near shading elements induce shading losses. The lines in the diagram show the shading loss induced for the different times of the year.

The fourth page shows the forecasted yield, performance ratio and specific yield of the system. In addition, the synthetic data are shown - irradiance data, grid injection at monthly basis, and so on. This page is normally the most important one, together with the losses diagram.

The fifth page shows a loss diagram. The first section is termed optical losses, or pre-conversion losses, and includes IAM losses, soiling and the shading loss.
The second section shows array losses. The third section shows inverter losses.
The combined array and inverter losses are termed total system loss in this thesis.

Grid-Connected System: Simulation parameters

Project :	**Grid-Connected Project at Ås**			
Geographical Site	**Ås**		Country	**Norway**
Situation	Latitude	59.7°N	Longitude	10.8°E
Time defined as	Legal Time	Time zone UT+1	Altitude	72 m
	Albedo	0.20		
Meteo data:	**Ås**	Synthetic - Measured 1996 - 2013 All parameters - Alternati		

Simulation variant :	**aas with horizon, shading, module layout and overall soiling**			
	Simulation date	09/04/14 20h24		

Simulation parameters

Collector Plane Orientation	Tilt	36°	Azimuth	-2°
Models used	Transposition	Perez	Diffuse	Erbs, Meteonorm
Horizon	Average Height	6.5°		
Near Shadings	Detailed electrical calculations	(acc. to module layout)		

PV Array Characteristics

PV module	Si-poly	Model	**REC PE215AJM**	
		Manufacturer	REC	
Number of PV modules		In series	9 modules	In parallel 1 strings
Total number of PV modules		Nb. modules	9	Unit Nom. Power 220 Wp
Array global power		Nominal (STC)	**1980 Wp**	At operating cond. 1792 Wp (45°C)
Array operating characteristics (50°C)		U mpp	245 V	I mpp 7.3 A
Total area		Module area	**14.9 m²**	
Inverter		Model	**Theia 2.9 HE-t**	
		Manufacturer	Eltek Valere	
Characteristics		Operating Voltage	230-480 V	Unit Nom. Power 2.90 kW AC

PV Array loss factors

Array Soiling Losses			Loss Fraction	3.0 %
Thermal Loss factor	Uc (const)	29.0 W/m²K	Uv (wind)	0.0 W/m²K / m/s
Wiring Ohmic Loss	Global array res.	363 mOhm	Loss Fraction	1.0 % at STC
Serie Diode Loss	Voltage Drop	0.7 V	Loss Fraction	0.3 % at STC
LID - Light Induced Degradation			Loss Fraction	1.0 %
Module Quality Loss			Loss Fraction	1.0 %
Module Mismatch Losses			Loss Fraction	0.0 % at MPP
Incidence effect, ASHRAE parametrization	IAM =	1 - bo (1/cos i - 1)	bo Param.	0.05

User's needs : Unlimited load (grid)

Grid-Connected System: Horizon definition

Project : **Grid-Connected Project at Ås**

Simulation variant : **aas with horizon, shading, module layout and overall soiling**

Main system parameters	System type	**Grid-Connected**		
Horizon	Average Height	6.5°		
Near Shadings	Detailed electrical calculations	(acc. to module layout)		
PV Field Orientation	tilt	36°	azimuth	-2°
PV modules	Model	REC PE215AJM	Pnom	220 Wp
PV Array	Nb. of modules	9	Pnom total	**1980 Wp**
Inverter	Model	Theia 2.9 HE-t	Pnom	2900 W ac
User's needs	Unlimited load (grid)			

Horizon

Average Height	6.5°	Diffuse Factor	0.95
Albedo Factor	100 %	Albedo Fraction	0.67

Height [°]	0.0	7.0	7.0	0.0	7.0	7.0	0.0	0.0	7.0	0.0	0.0	13.0	13.0	11.0
Azimuth [°]	-47	-47	-44	-44	-40	-28	-28	-26	-26	-22	-20	-20	-15	-15
Height [°]	11.0	0.0	0.0	9.0	9.0	11.0	11.0	0.0	0.0	7.5	9.2	7.5	0.0	0.0
Azimuth [°]	-9	-9	-9	-8	-7	-7	-4	-4	-0	0	0	4	4	7
Height [°]	7.0	7.0	7.5	7.5	6.0	6.0	7.5	7.5	7.0	7.5	6.0	7.5	5.5	7.0
Azimuth [°]	7	10	10	12	12	14	14	17	17	18	21	22	24	25
Height [°]	7.0	5.5	7.0	6.5	6.0	6.5	6.0	7.5	7.0	7.0	7.5	5.5	5.5	7.5
Azimuth [°]	29	30	30	43	43	70	75	75	76	77	80	81	85	90

Horizon Aas

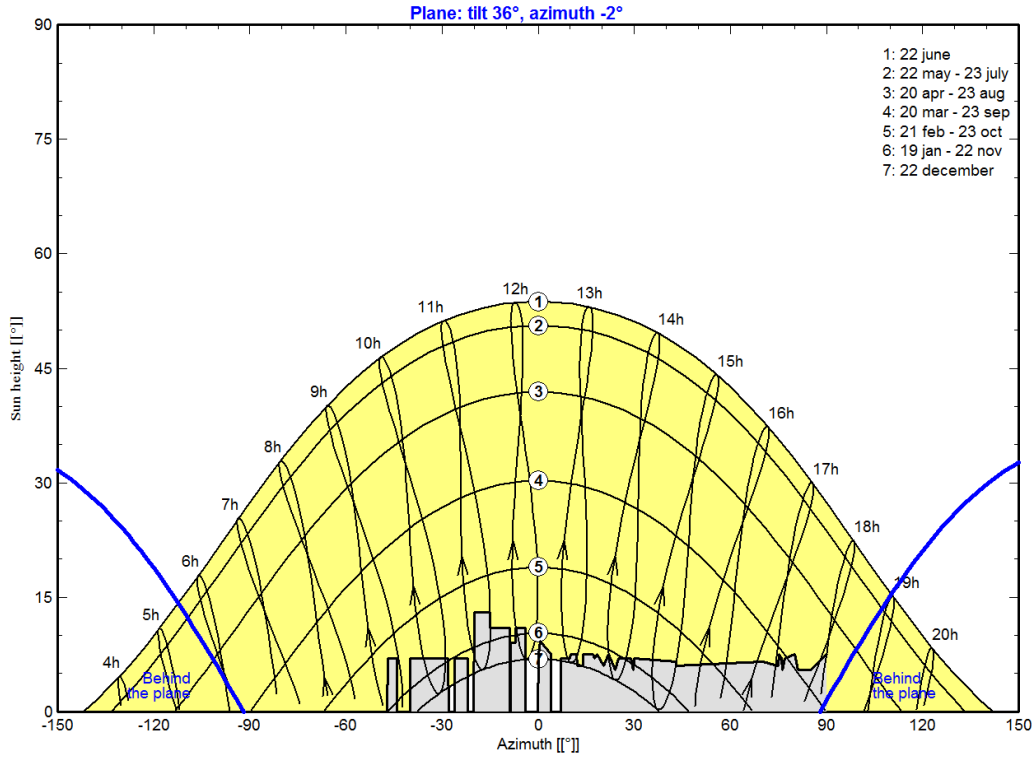

Grid-Connected System: Near shading definition

Project : **Grid-Connected Project at Ås**

Simulation variant : **aas with horizon, shading, module layout and overall soiling**

Main system parameters	System type	**Grid-Connected**		
Horizon	Average Height	6.5°		
Near Shadings	Detailed electrical calculations	(acc. to module layout)		
PV Field Orientation	tilt	36°	azimuth	-2°
PV modules	Model	REC PE215AJM	Pnom	220 Wp
PV Array	Nb. of modules	9	Pnom total	**1980 Wp**
Inverter	Model	Theia 2.9 HE-t	Pnom	2900 W ac
User's needs	Unlimited load (grid)			

Perspective of the PV-field and surrounding shading scene

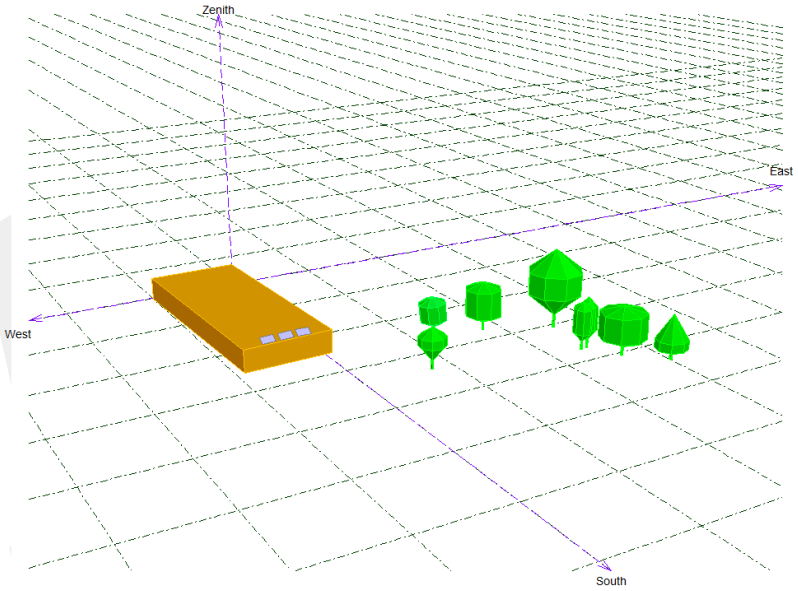

Iso-shadings diagram

Grid-Connected Project at Ås

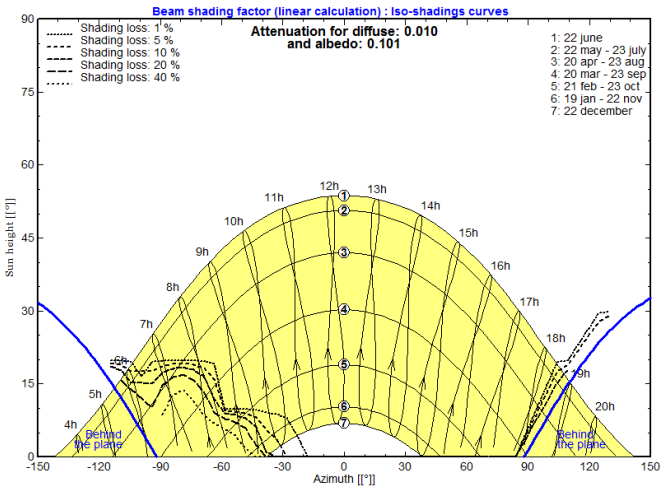

Grid-Connected System: Main results

Project : **Grid-Connected Project at Ås**

Simulation variant : **aas with horizon, shading, module layout and overall soiling**

Main system parameters	System type	**Grid-Connected**		
Horizon	Average Height	6.5°		
Near Shadings	Detailed electrical calculations	(acc. to module layout)		
PV Field Orientation	tilt	36°	azimuth	-2°
PV modules	Model	REC PE215AJM	Pnom	220 Wp
PV Array	Nb. of modules	9	Pnom total	**1980 Wp**
Inverter	Model	Theia 2.9 HE-t	Pnom	2900 W ac
User's needs	Unlimited load (grid)			

Main simulation results

System Production	**Produced Energy**	**1785 kWh/year**	Specific prod.	901 kWh/kWp/year
	Performance Ratio PR	75.3 %		

Normalized productions (per installed kWp): Nominal power 1980 Wp

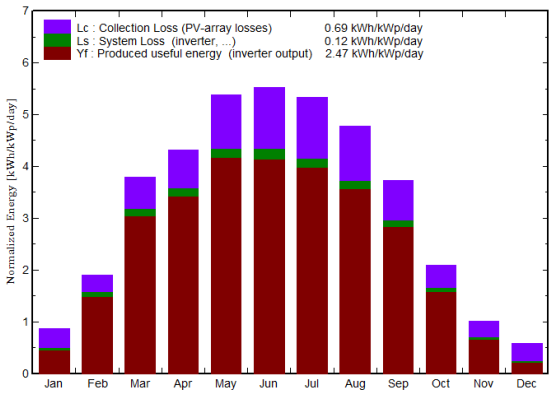

Performance Ratio PR

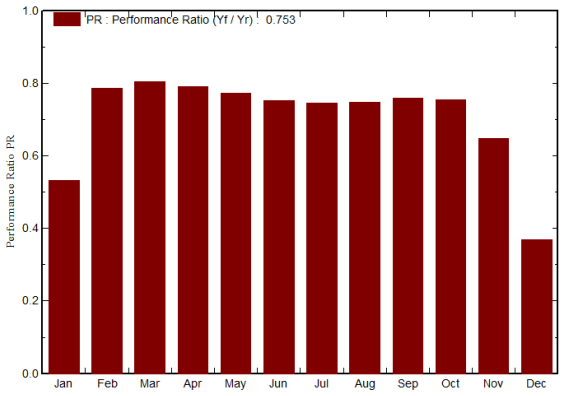

aas with horizon, shading, module layout and overall soiling

Balances and main results

	GlobHor kWh/m²	T Amb °C	GlobInc kWh/m²	GlobEff kWh/m²	EArray kWh	E_Grid kWh	EffArrR %	EffSysR %
January	9.4	-3.30	26.8	18.0	30.9	28.3	7.79	7.11
February	25.9	-3.10	53.2	47.8	87.3	82.9	11.05	10.48
March	70.7	0.10	117.4	106.7	195.3	187.1	11.21	10.73
April	100.9	5.40	129.5	119.1	212.6	203.2	11.05	10.56
May	148.6	10.60	167.0	153.3	267.4	255.8	10.78	10.32
June	160.6	14.30	165.6	151.5	258.0	246.5	10.49	10.03
July	155.0	16.60	165.4	151.7	255.7	244.2	10.41	9.94
August	121.0	15.90	147.9	135.7	229.2	219.3	10.44	9.99
September	75.0	11.60	112.1	102.7	176.4	168.6	10.60	10.13
October	33.3	6.00	64.8	58.7	102.1	96.8	10.61	10.06
November	11.5	2.00	30.4	24.2	42.1	39.0	9.32	8.64
December	5.5	-2.40	17.8	9.1	15.1	13.0	5.73	4.94
Year	917.4	6.19	1197.7	1078.5	1872.2	1784.7	10.53	10.03

Legends:

GlobHor	Horizontal global irradiation	EArray	Effective energy at the output of the array
T Amb	Ambient Temperature	E_Grid	Energy injected into grid
GlobInc	Global incident in coll. plane	EffArrR	Effic. Eout array / rough area
GlobEff	Effective Global, corr. for IAM and shadings	EffSysR	Effic. Eout system / rough area

Grid-Connected System: Loss diagram

Project : **Grid-Connected Project at Ås**

Simulation variant : **aas with horizon, shading, module layout and overall soiling**

Main system parameters	System type	**Grid-Connected**		
Horizon	Average Height	6.5°		
Near Shadings	Detailed electrical calculations	(acc. to module layout)		
PV Field Orientation	tilt	36°	azimuth	-2°
PV modules	Model	REC PE215AJM	Pnom	220 Wp
PV Array	Nb. of modules	9	Pnom total	**1980 Wp**
Inverter	Model	Theia 2.9 HE-t	Pnom	2900 W ac
User's needs	Unlimited load (grid)			

Loss diagram over the whole year

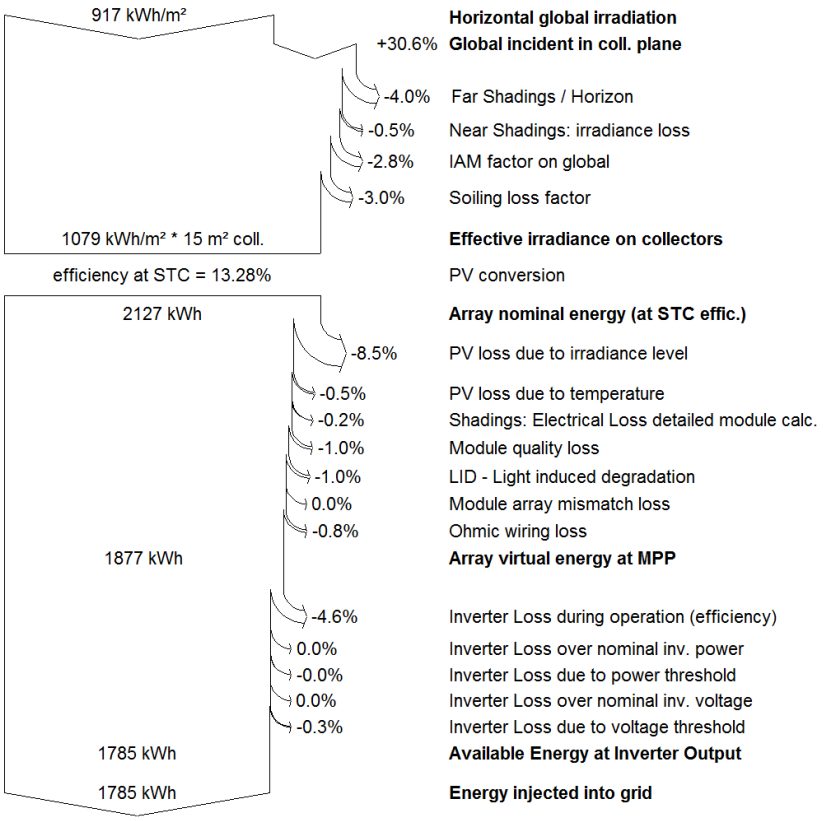

Appendix G.9: Simulation tests and synthetic data

Table G. 36: Results for diffuse irradiation from the synthetic hourly generation test

Generation test - Diffuse horizontal irradiation [kWh/m^2]					
	I	II	III	IV	V
January	6.9	6.9	6.9	7.7	7.7
February	15.2	15.2	15.2	18.4	18.4
March	34.6	34.6	34.6	36.5	36.5
April	46.1	46.1	46.1	53.1	53.1
May	75.9	75.9	75.9	67.8	67.8
June	74.7	74.7	74.7	72.6	72.6
July	61.8	61.8	61.8	72.2	72.2
August	66.5	66.5	66.5	58.4	58.4
September	39.9	39.9	39.9	37.4	37.4
October	20.9	20.9	20.9	20.8	20.8
November	7.6	7.6	7.6	8.9	8.9
December	4.4	4.4	4.4	5.0	5.0
Year	454.5	454.5	454.5	458.7	458.7
Discrepancy from I [%]				0.9	0.9

Table G. 37: Results for global irradiation from the synthetic hourly generation test

Generation test - Global irradiation in collector plane [kWh/m^2]					
	I	II	III	IV	V
January	21.8	21.8	21.8	19.5	19.5
February	50.4	50.4	50.4	45.7	45.7
March	110.4	110.4	110.4	108.7	108.8
April	126.9	126.9	126.9	124.8	120.4
May	161.2	161.2	161.2	163.3	160.3
June	161.9	161.9	161.9	162.4	164.4
July	163.9	163.9	163.9	163.0	161.7
August	139.0	139.0	139.0	142.5	142.2
September	102.6	102.6	102.6	104.9	102.2
October	55.4	55.4	55.4	55.7	53.6
November	27.6	27.6	27.6	24.4	21.9
December	13.4	13.4	13.4	11.2	11.0
Year	1134.5	1134.5	1134.5	1126.2	1111.7
Discrepancy from I [%]				-0.7	-2.0

Table G. 38: Results for wind speed from the synthetic hourly generation test

Generation test - Wind speed [m/s]					
	I	II	III	IV	V
January	3.7	3.7	3.7	3.7	3.5
February	4.0	4.0	4.0	4.0	3.9
March	3.8	3.8	3.8	3.8	3.7
April	3.9	3.9	3.9	3.9	3.7
May	3.7	3.7	3.7	3.7	3.6
June	3.7	3.7	3.7	3.7	3.6
July	3.3	3.3	3.3	3.3	3.2
August	3.4	3.4	3.4	3.4	3.3
September	3.7	3.7	3.7	3.7	3.5
October	3.7	3.7	3.7	3.7	3.6
November	3.9	3.9	3.9	3.9	3.7
December	3.8	3.8	3.8	3.8	3.6
Year	3.7	3.7	3.7	3.7	3.6

Table G. 39: Synthetic hourly data generated for Bioforsk

Synthetic data					
Aas, (Lat. 59.7 − N, long. 10.8 − E, alt. 94 m)					
Bioforsk 2005 – 2013 Synthetic					
Meteo for Aas, Reference year					
Interval beginning	GlobHor	DiffHor	GlobInc	T Amb	WindVel
	$MJ/m^2.mth$	$MJ/m^2.mth$	$MJ/m^2.mth$	°C	m/s
Jan-90	43.4	27.0	109.5	-3.8	3.8
Feb-90	100.8	56.3	190.3	-4.2	4.2
Mar-90	272.8	117.2	423.3	0.5	3.9
Apr-90	405.0	196.9	500.3	5.7	3.9
May-90	554.9	264.3	604.2	10.6	3.8
Jun-90	624.0	277.9	652.5	14.3	3.8
Jul-90	561.1	274.9	595.9	16.1	3.3
Aug-90	437.1	237.2	492.9	14.9	3.5
Sep-90	282.0	151.8	378.7	10.8	3.7
Oct-90	133.3	83.1	212.5	5.6	3.9
Nov-90	48.0	33.0	95.8	1.7	4.0
Dec-90	27.9	19.6	78.9	-3.2	3.9
Year 90	3490.3	1739.2	4334.9	5.8	3.8

Table G. 40: Results from the U-values tests

Forecast vs Yield - Ideal scenario with different U values					
Run. No	1	2	3		Inv. Output [kWh]
January	30.9	30.9	31.1		3.1
February	77.4	77.4	78.3		22.0
March	185.5	186.3	190.2		260.4
April	206.8	207.5	212.2		259.0
May	263.9	264.5	270.5		224.8
June	255.5	255.9	261.8		281.6
July	254.5	254.4	259.5		319.4
August	222.8	223	227.3		257.6
September	166.6	166.9	170.2		192.1
October	89.8	89.8	91		112.3
November	38.2	38.2	38.6		72.1
December	16.6	16.6	16.7		29.3
Year	1808.4	1811.3	1847.3		2033.8
Year ex. Jan. & Feb.	1700.2	1703.1	1738		2008.6
Discrepancy from yield [%]					
Run. No	1	2	3	MBE	RMSE
January	887.5	887.5	893.9	889.7	889.7
February	251.1	251.1	255.2	252.4	252.5
March	-28.8	-28.5	-27.0	-28.1	28.1
April	-20.2	-19.9	-18.1	-19.4	19.4
May	17.4	17.7	20.4	18.5	18.5
June	-9.3	-9.1	-7.0	-8.5	8.5
July	-20.3	-20.4	-18.8	-19.8	19.8
August	-13.5	-13.4	-11.8	-12.9	12.9
September	-13.3	-13.1	-11.4	-12.6	12.6
October	-20.1	-20.1	-19.0	-19.7	19.7
November	-47.0	-47.0	-46.4	-46.8	46.8
December	-43.4	-43.4	-43.1	-43.3	43.3
Year	-11.1	-10.9	-9.2	-10.4	10.4
Year ex. Jan. & Feb.	-15.4	-15.2	-13.5	-14.7	14.7
Monthly avg.	78.4	78.5	80.6	79.1	114.3
Monthly avg. Ex. Jan. & Feb.	-19.8	-19.7	-18.2	-19.3	23.0

Appendix H: Economical data

Table H. 1: LCOE for all runs and sources according to the original forecast

LCOE - All runs, all sources										
	2013/2014	2013	1996 - 2013	Bioforsk	NASA	Metenorm	PVGIS	Actual	MBE [%]	RMSE [%]
1	2.23	2.14	2.32	2.12	2.07	2.37	2.57	2.07	9.1	12.7
2	2.28	2.19	2.38	2.17	2.12	2.43	2.64	2.07	11.9	15.1
3	2.28	2.19	2.39	2.17	2.10	2.42	2.62	2.07	11.7	14.8
4	2.75	2.73	2.88	2.70	2.59	2.88	3.15	2.07	35.9	37.3
5	2.36	2.27	2.47	2.26	2.21	2.53	2.75	2.07	16.3	19.0

Table H. 2: LCOE for all runs and sources with forecasts adjusted for positive mismatch

LCOE [NOK/kWh] - All runs, all sources; adjusted for positive mismatch										
	2013/2014	2013	1996 - 2013	Bioforsk	NASA	Metenorm	PVGIS	Actual	MBE [%]	RMSE [%]
1	2.14	2.05	2.23	2.03	1.99	2.27	2.47	2.07	4.8	9.6
2	2.19	2.10	2.29	2.08	2.04	2.33	2.54	2.07	7.4	11.5
3	2.19	2.10	2.29	2.09	2.02	2.33	2.52	2.07	7.2	11.2
4	2.64	2.62	2.76	2.60	2.48	2.76	3.02	2.07	30.4	31.9
5	2.27	2.18	2.38	2.17	2.12	2.43	2.64	2.07	11.7	14.8

Norges miljø- og
biovitenskapelige
universitet

Postboks 5003
NO-1432 Ås
67 23 00 00
www.nmbu.no